MOLECULAR PATHOGENESIS OF PNEUMOCOCCUS: 2nd Edition

EDITED BY: Guangchun Bai and Jorge Eugenio Vidal

PUBLISHED IN: Frontiers in Cellular and Infection Microbiology

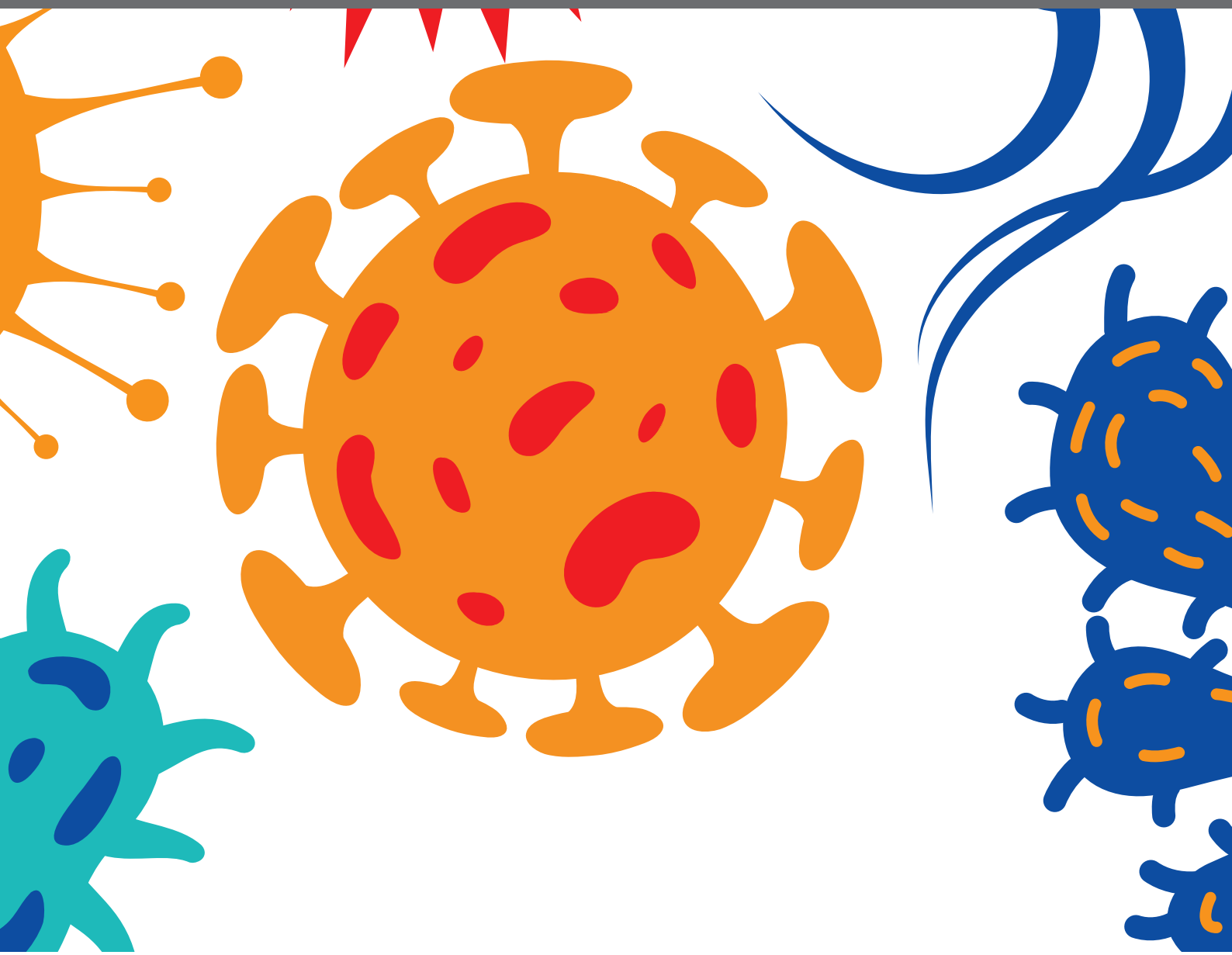

frontiers Research Topics

frontiers

ISSN 1664-8714
ISBN 978-2-88974-939-3
DOI 10.3389/978-2-88974-939-3

About Frontiers

Frontiers is more than just an open-access publisher of scholarly articles: it is a pioneering approach to the world of academia, radically improving the way scholarly research is managed. The grand vision of Frontiers is a world where all people have an equal opportunity to seek, share and generate knowledge. Frontiers provides immediate and permanent online open access to all its publications, but this alone is not enough to realize our grand goals.

Frontiers Journal Series

The Frontiers Journal Series is a multi-tier and interdisciplinary set of open-access, online journals, promising a paradigm shift from the current review, selection and dissemination processes in academic publishing. All Frontiers journals are driven by researchers for researchers; therefore, they constitute a service to the scholarly community. At the same time, the Frontiers Journal Series operates on a revolutionary invention, the tiered publishing system, initially addressing specific communities of scholars, and gradually climbing up to broader public understanding, thus serving the interests of the lay society, too.

Dedication to Quality

Each Frontiers article is a landmark of the highest quality, thanks to genuinely collaborative interactions between authors and review editors, who include some of the world's best academicians. Research must be certified by peers before entering a stream of knowledge that may eventually reach the public - and shape society; therefore, Frontiers only applies the most rigorous and unbiased reviews.
Frontiers revolutionizes research publishing by freely delivering the most outstanding research, evaluated with no bias from both the academic and social point of view. By applying the most advanced information technologies, Frontiers is catapulting scholarly publishing into a new generation.

What are Frontiers Research Topics?

Frontiers Research Topics are very popular trademarks of the Frontiers Journals Series: they are collections of at least ten articles, all centered on a particular subject. With their unique mix of varied contributions from Original Research to Review Articles, Frontiers Research Topics unify the most influential researchers, the latest key findings and historical advances in a hot research area! Find out more on how to host your own Frontiers Research Topic or contribute to one as an author by contacting the Frontiers Editorial Office: frontiersin.org/about/contact

MOLECULAR PATHOGENESIS OF PNEUMOCOCCUS:
2nd Edition

Topic Editors:
Guangchun Bai, Albany Medical College, United States
Jorge Eugenio Vidal, University of Mississippi Medical Center, United States

Publisher's note: In this 2nd edition, the following article has been added: Simmons SR, Tchalla EYI, Bhalla M and Bou Ghanem EN (2022) The Age-Driven Decline in Neutrophil Function Contributes to the Reduced Efficacy of the Pneumococcal Conjugate Vaccine in Old Hosts. Front. Cell. Infect. Microbiol. 12:849224. doi: 10.3389/fcimb.2022.849224

Citation: Bai, G., Vidal, J. E., eds. (2023). Molecular Pathogenesis of Pneumococcus: 2nd Edition. Lausanne: Frontiers Media SA. doi: 10.3389/978-2-88974-939-3

Table of Contents

frontiers in Cellular and Infection Microbiology

EDITORIAL
published: 11 July 2017
doi: 10.3389/fcimb.2017.00310

Editorial: Molecular Pathogenesis of Pneumococcus

Guangchun Bai[1]* *and Jorge E. Vidal*[2,3]

[1] Department of Immunology and Microbial Disease, Albany Medical College, Albany, NY, United States, [2] Hubert Department of Global Health, Rollins School of Public Health, Emory University, Atlanta, GA, United States, [3] Emory Antibiotic Resistance Center, School of Medicine, Emory University, Atlanta, GA, United States

Keywords: ***Streptococcus pneumoniae*, pathogenesis, gene regulation, biofilm, co-infection, drug resistance, microbial, macrophages**

Editorial on the Research Topic

Molecular Pathogenesis of Pneumococcus

Streptococcus pneumoniae has been for decades the number one bacterial killer of children worldwide, but it is also a commensal of the human nasopharynx during childhood. Although vaccination with pneumococcal conjugate vaccines has helped decrease the burden of pneumococcal disease (PD), mortality caused by this pathogen remains high. The introduction of pneumococcal vaccines has also created a niche for vaccine-escape serotypes. Moreover, the rise of multidrug-resistant clones around the world has posed a serious threat in recent years. A better understanding of pneumococcal biology and pathogenesis is needed to further reduce the burden of PD. In the current research topic, nine papers were published for this perspective.

Complex molecules of human epithelia, including the human upper and lower airways, contain N-acetylglucosamine (NAG) that can be metabolized by pneumococcus to survive and persist during colonization, and succeed during pathogenesis. Afzal et al. investigated the transcriptome of the pneumococcal strain D39 growing in media with NAG as a sole source of carbohydrates, and demonstrated upregulated transcription of operons involved in NAG uptake. They confirmed that *nagA* and *nagB* are essential for the growth of pneumococcus in the presence of NAG and found that NagR regulates genes involved in the metabolism of NAG (Afzal et al.).

Phosphorus and metal ions are essential nutrients for all living organisms (Porcheron et al., 2013). Most bacteria encode a single Pst transporter for the uptake of inorganic phosphate (Pi). However, Zheng et al. demonstrated that *S. pneumoniae* possesses two distinct Pst transporters, Pst1 and Pst2. Interestingly, Pi uptake by these two Pst proteins can be compensated by a Na^+/Pi co-transporter, NptA, in non-encapsulated *S. pneumoniae* (NESp) strains. In contrast, either Pst1 or Pst2 is needed for the growth of encapsulated strains. The Pi uptake transporters in *S. pneumoniae* are tightly controlled by two transcription factors, PhoU1 and PhoU2, to maintain high Pi transport in different Pi availability, which is required for optimal capsule biosynthesis (Zheng et al.).

It is known that AdcR-regulated genes play a role in pneumococcal pathogenesis. Manzoor et al. found that a number of genes belonging to the AdcR and the PsaR regulons are highly upregulated in the presence of Ni^{2+}, suggesting the importance of Ni^{2+} in pneumococcal virulence. Additionally, most bacteria have developed strategies for iron acquisition from the host hemoglobulin (Hb) or heme (Andrews et al., 2003). *S. pneumoniae* Spbhp-37 is a cell surface protein and has an high affinity with Hb. The expression of Spbhp-37 is upregulated when *S. pneumoniae* is grown in media where Hb is provided as the sole iron source (Romero-Espejel et al.). Therefore, Spbhp-37 might be essential for *S. pneumoniae* to establish an infection in the host.

Another surface protein of *S. pneumoniae*, pneumococcal surface protein K (PspK), is known to increase colonization and virulence by NESp during otitis media (OM) episodes

OPEN ACCESS

Edited by:
Lorenza Putignani, Bambino Gesù Ospedale Pediatrico (IRCCS), Italy

Reviewed by:
Stephen Peter Kidd, University of Adelaide, Australia

***Correspondence:**
Guangchun Bai
baig@mail.amc.edu

Received: *29 January 2017*
Accepted: *23 June 2017*
Published: *11 July 2017*

Citation:
Bai G and Vidal JE (2017) Editorial: Molecular Pathogenesis of Pneumococcus. Front. Cell. Infect. Microbiol. 7:310. doi: 10.3389/fcimb.2017.00310

(Keller et al., 2014). Therefore, PspK is considered as a NESp-specific virulence factor. Interestingly, it was demonstrated that expression of *pspK* in an encapsulated pneumococcal strain significantly increased adhesion and invasion of human epithelial cells. Additionally, Murine colonization was increased when a capsule mutant expressed *pspK* (Keller et al.). These findings indicate that PspK plays distinct roles in pathogenesis between encapsulated *S. pneumoniae* and NESp.

It is known that macrophages play an essential role in the recognition and clearance of bacterial infections by either innate immunity or present antigen to establish acquired immunity. Phosphoinositide 3-kinase (PI3K) is an essential regulator for Fcγ and CR-mediated phagocytosis (Cox et al., 1999). Protein kinase B (Akt or PKB) is one of the major signal transducers and is a downstream target of PI3K (Alessi et al., 1997). By using immuno-fluorescence microscopy, antibiotic protection assays, and addition of inhibitors of central host cell kinase, new evidence showed that PI3K and Akt play an important role in uptake and killing of *S. pneumoniae* by human THP-1 macrophages, which is independent of Fcγ or CR-mediated phagocytosis pathways (Kohler et al.).

Through investigating interactions between pneumococcal biofilms and biofilms produced by other human pathogens, Khan et al. discovered that pneumococcal strains produce a factor(s) that efficiently eradicates, i.e., within hours, *Staphylococcus aureus* biofilms including those produced by methicillin-resistant *S. aureus* (MRSA) strains. Eradication was more efficient when *S. pneumoniae* and *S. aureus* had direct contact, which mimicked the condition that the strains would naturally encounter on the human upper airways. Physical-mediated killing did not require production of hydrogen peroxide since a *S. pneumoniae* mutant in *spxB* gene, encoding for an enzyme involved in production of H_2O_2, was able to eradicate *S. aureus* biofilms. Authors hypothesized that research on factors allowing eradication of *S. aureus* will provide alternative therapeutics for *S. aureus* infections (Khan et al.).

Influenza pandemics and seasonal outbreaks have enhanced susceptibility to secondary infection with *S. pneumoniae*. Boianelli et al. developed a computational approach to evaluate the efficacy of treatment with Oseltamivir for flu infection and secondary pneumococcal pneumonia. Their mathematical algorithms revealed that increasing the recommended dose (i.e., 75 mg) to 150 mg, or 300 mg, almost doubles the effect of Oseltamivir against secondary bacterial infection. Other aspects of the treatment were also evaluated using their computational approach. Overall, their study warrants clinical trials to determine the efficacy of treatment regimens with Oseltamivir against lethality of secondary pneumococcal infection post influenza (Boianelli et al.).

Macrolides inhibit bacterial protein synthesis by binding to the large 50S ribosomal subunit (Schroeder and Stephens). These antibiotics have been extensively used for treatment of pneumococcal infection, which raises a strong selective pressure contributing to the expansion of macrolide-resistant *S. pneumoniae*. Macrolide resistance in *S. pneumoniae* is predominantly due to ribosomal methylation by the gene product encoded by *erm*(*B*) and macrolide efflux by a two-component efflux pump encoded by *mef* (*E*)/*mel* (Schroeder and Stephens). Current pneumococcal vaccines are effective in reducing macrolide resistance caused by vaccine serotypes. On the other hand, "serotype replacement" post vaccination might lead to macrolide resistance in new serotypes, which remains a public health concern.

AUTHOR CONTRIBUTIONS

All authors listed have made a substantial, direct and intellectual contribution to the work, and approved it for publication.

FUNDING

GB is partly supported by grants of R56AI122763 and R35HL135756 from the National Institutes of Health (NIH). JEV is in part supported by an NIH grant 5R21AI112768-02. The content is solely the responsibility of the authors and does not necessarily represent the official view of the NIH.

REFERENCES

Alessi, D. R., James, S. R., Downes, C. P., Holmes, A. B., Gaffney, P. R., Reese, C. B., et al. (1997). Characterization of a 3-phosphoinositide-dependent protein kinase which phosphorylates and activates protein kinase Balpha. *Curr. Biol.* 7, 261–269. doi: 10.1016/S0960-9822(06)00122-9

Andrews, S. C., Robinson, A. K., and Rodriguez-Quinones, F. (2003). Bacterial iron homeostasis. *FEMS Microbiol. Rev.* 27, 215–237. doi: 10.1016/S0168-6445(03)00055-X

Cox, D., Tseng, C. C., Bjekic, G., and Greenberg, S. (1999). A requirement for phosphatidylinositol 3-kinase in pseudopod extension. *J. Biol. Chem.* 274, 1240–1247. doi: 10.1074/jbc.274.3.1240

Keller, L. E., Friley, J., Dixit, C., Nahm, M. H., and McDaniel, L. S. (2014). Nonencapsulated *Streptococcus pneumoniae* cause acute otitis media in the chinchilla that is enhanced by pneumococcal surface protein K. *Open Forum Infect Dis* 1:ofu037. doi: 10.1093/ofid/ofu037

Porcheron, G., Garenaux, A., Proulx, J., Sabri, M., and Dozois, C. M. (2013). Iron, copper, zinc, and manganese transport and regulation in pathogenic Enterobacteria: correlations between strains, site of infection and the relative importance of the different metal transport systems for virulence. *Front. Cell. Infect. Microbiol.* 3:90. doi: 10.3389/fcimb.2013.00090

Conflict of Interest Statement: The authors declare that the research was conducted in the absence of any commercial or financial relationships that could be construed as a potential conflict of interest.

frontiers in Cellular and Infection Microbiology

ORIGINAL RESEARCH
published: 08 December 2015
doi: 10.3389/fcimb.2015.00091

The Regulation of the AdcR Regulon in *Streptococcus pneumoniae* Depends Both on Zn^{2+}- and Ni^{2+}-Availability

Irfan Manzoor[1,2†], *Sulman Shafeeq*[1,3†], *Muhammad Afzal*[1,2] *and Oscar P. Kuipers*[1*]

[1] Department of Molecular Genetics, Groningen Biomolecular Sciences and Biotechnology Institute, University of Groningen, Groningen, Netherlands, [2] Department of Bioinformatics and Biotechnology, Government College University Faisalabad, Faisalabad, Pakistan, [3] Department of Microbiology, Tumor and Cell Biology, Karolinska Institutet, Stockholm, Sweden

By using a transcriptomic approach, we have elucidated the effect of Ni^{2+} on the global gene expression of *S. pneumoniae* D39 by identifying several differentially expressed genes/operons in the presence of a high extracellular concentration of Ni^{2+}. The genes belonging to the AdcR regulon (*adcRCBA*, *adcAII-phtD, phtA*, *phtB*, and *phtE*) and the PsaR regulon (*pcpA*, *prtA*, and *psaBCA*) were highly upregulated in the presence of Ni^{2+}. We have further studied the role of Ni^{2+} in the regulation of the AdcR regulon by using ICP-MS analysis, electrophoretic mobility shift assays and transcriptional *lacZ*-reporter studies, and demonstrate that Ni^{2+} is directly involved in the derepression of the AdcR regulon *via* the Zn^{2+}-dependent repressor AdcR, and has an opposite effect on the expression of the AdcR regulon compared to Zn^{2+}.

Keywords: metal homeostasis, pneumococcus, nickel, zinc, AdcR, Pht family proteins, AdcR regulon, PsaR regulon

OPEN ACCESS

Edited by:
Jorge Eugenio Vidal, Emory University, USA

Reviewed by:
Hilde De Reuse, Institut Pasteur, France
Stephen Peter Kidd, University of Adelaide, Australia

***Correspondence:**
Oscar P. Kuipers
o.p.kuipers@rug.nl

[†] These authors have contributed equally to this work.

Received: *27 August 2015*
Accepted: *17 November 2015*
Published: *08 December 2015*

Citation:
Manzoor I, Shafeeq S, Afzal M and Kuipers OP (2015) The Regulation of the AdcR Regulon in Streptococcus pneumoniae Depends Both on Zn^{2+}- and Ni^{2+}-Availability. Front. Cell. Infect. Microbiol. 5:91. doi: 10.3389/fcimb.2015.00091

INTRODUCTION

In bacteria, the transition metal ions play an important role in the proper functioning of many enzymes, transporters, and transcriptional regulators. Transition metal ions are the prerequisite for the proper bacterial growth at low concentrations, but metal ions can be lethal at higher concentrations (Blencowe and Morby, 2003; Finney and O'Halloran, 2003; Moore and Helmann, 2005; Ge et al., 2012). Therefore, proper homeostasis of metal ions is very important for the survival of bacteria, which is maintained by the dedicated metal transport- and efflux-systems (Tottey et al., 2008; Waldron and Robinson, 2009; Lisher et al., 2013). These systems are tightly regulated by metal-responsive transcriptional regulators to ensure the proper functioning of the cell by maintaining the minimum levels of metal ions inside the cell.

Streptococcus pneumoniae is one of the most common human pathogens that reside asymptomatically in the human nasopharynx (Mitchell, 2003). However, it may occasionally translocate to the lungs, the eustachian tube, the blood, and the nervous system, causing pneumoniae, otitis media, bacteremia, and meningitis, respectively (Obaro and Adegbola, 2002; Bogaert et al., 2004). During translocation from the nasopharynx to other infection sites, *S. pneumoniae* may encounter different environmental conditions including varying metal ions concentrations, which might affect the expression of different genes including virulence genes (Gupta et al., 2009; Shafeeq et al., 2011b, 2013; Plumptre et al., 2014a). However, the exact conditions that *S. pneumoniae* might face during infections, are poorly understood.

The role of manganese (Mn^{2+}), zinc (Zn^{2+}), copper (Cu^{2+}), iron (Fe^{2+}), cobalt (Co^{2+}), and cadmium (Cd^{2+}) on the gene regulation of *S. pneumoniae* have already been established and several metal-specific acquisition- and efflux-systems have been characterized. These systems include AdcRCBA (the Zn^{2+}-uptake system), CzcD (the Zn^{2+}-efflux system), PsaBCA (the Mn^{2+}-uptake system), MntE (the Mn^{2+}-efflux system), the *cop* operon (the Cu^{2+}-efflux system), and PiaABCD, PiuBCDA, and PitADBC (the Fe^{2+}- and Fe^{3+}-uptake systems) (Kloosterman et al., 2007, 2008; Hendriksen et al., 2009; Rosch et al., 2009; Bayle et al., 2011; Shafeeq et al., 2011a, 2013; Manzoor et al., 2015c). These systems have further been shown to be regulated by metal-specific transcriptional regulators in *S. pneumoniae*. The Zn^{2+}-uptake system (AdcRCBA) is repressed by transcriptional regulator AdcR in the presence of Zn^{2+} (Shafeeq et al., 2011a). Similarly, the *psaBCA* operon encoding Mn^{2+}-uptake system are repressed by transcriptional regulator PsaR in the presence of Mn^{2+} (Johnston et al., 2006; Kloosterman et al., 2008), whereas, this PsaR-mediated repression is relieved by the addition of Zn^{2+}, Co^{2+}, Cd^{2+}, or Ni^{2+} (Kloosterman et al., 2008; Jacobsen et al., 2011; Begg et al., 2015; Manzoor et al., 2015a,b,c).

Ni^{2+} is an essential micronutrient for certain bacteria, due to its role in various cellular processes like methane formation, hydrolysis of urea, and consumption of molecular hydrogen (Chen and Burne, 2003; Mulrooney and Hausinger, 2003; Rodionov et al., 2006; Anwar et al., 2007). In *Escherichia coli*, the *nik* operon (*nikABCDE*) involved in the transport of Ni^{2+} is shown to regulate by transcriptional regulator NikR (De Pina et al., 1999). Moreover, the expression of NmtA, an ATP-dependent transporter involved in the efflux of Ni^{2+} and Co^{2+}, is tightly regulated by Ni^{2+}-responsive transcriptional regulator NmtR in *Mycobacterium tuberculosis* (Cavet et al., 2002). Ni^{2+} is also shown to regulate the expression of urease activity in *Streptococcus salivarius* and *Helicobacter pylori* (van Vliet et al., 2001; Chen and Burne, 2003). The amount of Ni^{2+} in the human blood is estimated to be 0.83 ng ml^{-1} (Alimonti et al., 2005) and it is likely that *S. pneumoniae* may encounter Ni^{2+} during infection in blood. So far, very little is known about the impact of Ni^{2+} on the global gene expression of *S. pneumoniae*. Previously, the role of Ni^{2+} in the regulation of the Zn^{2+}-efflux system *czcD* was reported (Kloosterman et al., 2007). It was shown that the SczA-mediated expression of *czcD* was highly increased in the presence of Zn^{2+}, Co^{2+}, or Ni^{2+} (Kloosterman et al., 2007). Moreover, a number of proteins and motif with Co^{2+}- and Ni^{2+}-binding capacity has been identified by Immobilized metal affinity column (IMAC) and LTQ-Orbitrap mass spectrometry (MS) that have diverse functions in the *S. pneumoniae* (Sun et al., 2013). In a recent study, we demonstrated the role of Ni^{2+} in regulation of the PsaR regulon and showed that Ni^{2+} not only alleviates the Mn^{2+}-dependent binding of PsaR to the promoter regions of the PsaR regulon genes, but also cause Mn^{2+} deficiency possibly by blocking Mn^{2+}-uptake *via* PsaA, hence leading to the high expression of the PsaR regulon in the presence of Ni^{2+} (Manzoor et al., 2015b).

In this current study, we used a transcriptomic analysis approach for the identification of differentially expressed genes/operons in response to high extracellular Ni^{2+} in *S. pneumoniae*. The expression of genes belonging to the AdcR regulon and the PsaR regulon was highly upregulated in the presence of Ni^{2+}. We further studied the role of Ni^{2+} in the AdcR-mediated regulation of the *adcRCBA*, *adcAII-phtD*, *phtA*, *phtB*, and *phtE* by using transcriptional *lacZ*-reporter studies, inductively coupled plasma-mass spectrometry (ICP-MS) analysis and electrophoretic mobility shift assays (EMSAs), and showed that Ni^{2+} and Zn^{2+} play an opposite role in the regulation of the *adcRCBA*, *adcAII-phtD*, *phtA*, *phtB*, and *phtE*.

MATERIALS AND METHODS

Bacterial Strains and Media

Bacterial strains used in this study are listed in **Table 1**. Growth of bacteria and DNA manipulation were performed as described (Shafeeq et al., 2011a; Manzoor et al., 2015a). All experiments in this study were performed in chemically defined medium (CDM).

TABLE 1 | List of strains and plasmids used in this study.

Strain/plasmid	Description	Source
S. pneumoniae		
D39	Serotype 2 strain, *cps 2*	Laboratory of P. Hermans
SS200	D39 Δ*adcR*; Ery^R	Shafeeq et al., 2011a
IM404	D39 Δ*bgaA*::P*czcD-lacZ*; Tet^R	Manzoor et al., 2015a
IM501	D39 Δ*bgaA*::P*adcR-lacZ*; Tet^R	This study
IM502	D39 Δ*bgaA*::P*adcAII-lacZ*; Tet^R	This study
IM503	D39 Δ*bgaA*::P*phtA-lacZ*; Tet^R	This study
IM504	D39 Δ*bgaA*::P*phtB-lacZ*; Tet^R	This study
IM505	D39 Δ*bgaA*::P*phtE-lacZ*; Tet^R	This study
IM551	SS200 Δ*bgaA*::P*adcR-lacZ*; Tet^R	This study
IM552	SS200 Δ*bgaA*::P*adcAII-lacZ*; Tet^R	This study
IM553	SS200 Δ*bgaA*::P*phtA-lacZ*; Tet^R	This study
IM554	SS200 Δ*bgaA*::P*phtB-lacZ*; Tet^R	This study
IM555	SS200 Δ*bgaA*::P*phtE-lacZ*; Tet^R	This study
E. coli		
EC1000	Km^R; MC1000 derivative carrying a single copy of the pWV1 *repA* gene in *glgB*	Laboratory collection
Plasmids		
pPP2	Amp^R Tet^R; promoterless *lacZ* For replacement of *bgaA* with promoter *lacZ*-fusion. Derivative of pPP1	Halfmann et al., 2007
pIM501	pPP2 P*adcR-lacZ*	This study
pIM502	pPP2 P*adcAII-lacZ*	This study
pIM503	pPP2 P*phtA-lacZ*	This study
pIM504	pPP2 P*phtB-lacZ*	This study
pIM505	pPP2 P*phtE-lacZ*	This study
SS107	pNZ8048 carrying strep-tagged AdcR downstream of PnisA	Shafeeq et al., 2011a

TABLE 2 | List of primers used in this study.

Name	Nucleotide sequence (5′→3′)	Restriction site
Padcr-F	CGGAATTCTTTTTCAGCAAAGATTGGG	EcoRI
Padcr-R	CGGGATCCCTTTCCTTTTAGACTTCTC	BamHI
PadcAII-F	CGGAATTCCTTCACTTATGGCTATAAGC	EcoRI
PadcAII-R	CGGGATCCAAAGAAAGACACTTAACAGG	BamHI
PphtA-F	CGGAATTCTGAACTTCAAAAAGAATACG	EcoRI
PphtA-R	CGGGATCCCTTAAAATCAAAGCTGCCGC	BamHI
PphtB-F	GCATGAATTCGGCAGAAGCAGAAAAATTAC	EcoRI
PphtB-R	CGATGGATCCAAGTGTAGCTACTGACC	BamHI
PphtE-F	CGGAATTCAGAAGTAGATAGTCTCTTGG	EcoRI
PphtE-R	CGGGATCCACGATAACAGCTGATCCAGC	BamHI

Salts of metal ion $ZnSO_4.7H_2O$ and $NiSO_4.6H_2O$ were used as specified in the Results section. Primers used in this study are based on the genome sequence of *S. pneumoniae* D39 and are listed in **Table 2**.

DNA Microarray and Data Analysis

For microarray analysis in response to Ni^{2+}, *S. pneumoniae* D39 wild-type was grown in two biological replicates in CDM with and without the addition of 0.5 mM $NiSO_4.6H_2O$. To analyze the impact of *adcR* deletion on the transcirptome of *S. pneumoniae* in the presence of Ni^{2+}, D39 wild-type and Δ*adcR* (SS200) (Shafeeq et al., 2011a) were grown in two biological replicates in CDM with 0.3 mM of $NiSO_4.6H_2O$. All other procedures regarding microarray experiments and data analysis were done as described before (Shafeeq et al., 2011b; Afzal et al., 2015). For the identification of differentially expressed genes a Bayesian $p < 0.001$ and a fold change cut-off of 2 was applied. The DNA microarray data have been submitted to gene expression omnibus (GEO) database under the accession number GSE73852.

Construction of Transcriptional *lacZ*-fusions and β-galactosidase Assays

Chromosomal transcriptional *lacZ*-fusions to the promoter regions of *adcR*, *adcAII*, *phtA*, *phtB*, and *phtE* were constructed in plasmid pPP2 (Halfmann et al., 2007) with the primer pairs listed in **Table 2**, resulting in pIM501-505. These plasmids were introduced into D39 wild-type and Δ*adcR* (SS200) (Shafeeq et al., 2011a) resulting in strains IM501-505 and IM551-554, respectively. All plasmids were checked for the presence of correct insert by means of PCR and DNA sequencing. For β-galactosidase activity, the derivatives of *S. pneumoniae* were grown in triplicate in CDM supplemented with different metal ion concentrations (w/v) mentioned in the Results and harvested at the mid-exponential growth phase. The β-galactosidase activity was measured as described before (Kloosterman et al., 2006). Standard deviations were calculated from three independent replicates of each sample.

Inductively Coupled Plasma-mass Spectrometry (ICP-MS) Analysis

To determine the cell-associated concentration of metal ions, an ICP-MS analysis was performed on the cells grown in triplicates in CDM with and without the addition of 0.5 mM Ni^{2+} till the mid-exponential growth phase. Cell cultures were centrifuged at 4°C and washed twice with overnight Chelex (Sigma) treated phosphate-buffered saline (PBS) with 1 mM nitrilotriacetic acid. Cells were dried overnight in a Speedvac at room temperature. The dried cells were dissolved in 2.5% nitric acid (Ultrapure, Sigma Aldrich) and lysed at 95°C for 10 min by vigorous vortexing after each 30 s. The lysed cell samples were used for ICP-MS analysis as described (Jacobsen et al., 2011). Metal ion concentrations were expressed as μ g g^{-1} dry weight of cells.

Overexpression and Purification of Strep-tagged AdcR

The nisin-inducible (NICE) expression system (Kuipers et al., 1998) in *Lactococcus lactis* strain NZ9000 was used for the overexpression of C-terminally Strep-tagged AdcR (Shafeeq et al., 2011a). Cells were grown until an OD_{600} of 0.4 in 1 L culture followed by the induction with 10 ng ml^{-1} nisin. The purification of AdcR-Strep tag was performed using the Streptactin column from IBA according to the supplier's instructions (www.iba-go.com). The purified protein was eluted in buffers without EDTA and stored at a concentration of 0.5 mg/ml in the elution buffer (100 mM Tris-HCl [pH 8], 150 mM NaCl, 2.5 mM desthiobiotin, and 1 mM β-mercaptoethanol) with 10% glycerol at −80°C.

Electrophoretic Mobility Shift Assays

Electrophoretic mobility shift assays (EMSAs) were performed as described (Kloosterman et al., 2008). In short, PCR products of the promoter regions of *adcR*, *adcAII*, *phtA*, *phtB*, and *pcpA* were labeled with [γ-^{33}P] ATP. All the EMSAs were performed with 5000 cpm of [γ-^{33}P] ATP-labeled PCR products in buffer containing 20 mM Tris-HCL (pH 8.0), 5 mM $MgCl_2$, 8.7% (w/v) glycerol, 62.5 mM KCl, 25 μg/ml bovine serum albumin and 25 μg/ml poly (dI-dC). Various metal ions were added in concentrations as described in the Results section. Reactions were incubated at 30°C for 30 min before loading on gels. Gels were run in 1 M Tris-borate buffer (pH 8.3) at 95 V for 90 min.

RESULTS

Identification of Ni^{2+}-dependent Genes in *S. pneumoniae*

To investigate the impact of Ni^{2+} on the transcriptome of *S. pneumoniae*, a DNA microarray-based comparison of D39 wild-type grown in CDM with 0.5 mM Ni^{2+} to the same strain grown in CDM with 0 mM Ni^{2+} was performed. **Table 3** summarizes the list of differentially expressed genes in the presence of 0.5 mM Ni^{2+}. The PsaR regulon consisting of the operon *psaBCA* (encoding Mn^{2+}-dependent ABC transporters, PsaBCA), *pcpA* (encoding a choline binding protein, PcpA), and *prtA* (encoding a serine protease PrtA) were highly upregulated in the presence of

TABLE 3 | Summary of transcriptome comparison of *S. pneumoniae* D39 wild-type grown in CDM plus 0.5 mM Ni^{2+} to CDM plus 0 mM Ni^{2+}.

Gene tag[a]	Function[b]	Ratio[c]	*P*-value
SPD0475	CAAX amino terminal protease family protein	5.39	1.48E−11
SPD0526	Fructose-1,6-bisphosphate aldolase, class II	3.07	1.93E−13
SPD0558	Cell wall-associated serine protease, PrtA	9.67	2.92E−13
SPD0738	Cytidine deaminase	21.92	6.05E−07
SPD0888	Adhesion lipoprotein, AdcAII (LmB)	2.07	7.08E−07
SPD0889	Pneumococcal histidine triad protein D, PhtD	2.06	5.81E−10
SPD0890	Pneumococcal histidine triad protein E, PhtE	7.13	2.81E−05
SPD1038	Pneumococcal histidine triad protein A, PhtA	12.54	2.00E−14
SPD1078	L-lactate dehydrogenase	4.21	2.04E−14
SPD1138	Heat shock protein, HtpX	3.61	9.44E−05
SPD1360	Hypothetical protein	7.29	1.15E−10
SPD1402	Non-heme iron-containing ferritin, DpR	2.65	2.10E−11
SPD1461	Manganese ABC transporter, ATP-binding protein, PsaB	11.90	5.33E−15
SPD1462	Manganese ABC transporter, permease protein, PsaC	10.71	5.26E−14
SPD1464	Thiol peroxidase	2.13	8.68E−10
SPD1632	Hypothetical protein	2.32	3.47E−05
SPD1633	Galactose-1-phosphate uridylyl transferase, GalT	2.68	7.81E−06
SPD1634	Galactokinase, GalK	4.13	1.29E−08
SPD1635	Galactose operon repressor, GalR	5.00	4.27E−07
SPD1636	Alcohol dehydrogenase, zinc-containing, AdhB	35.69	0.00E+00
SPD1637	Transcriptional regulator, MerR family	38.25	0.00E+00
SPD1638	Cation efflux system protein, CzcD	77.89	5.55E−15
SPD1651	Iron-compound ABC transporter, ATP-binding protein	−3.91	1.27E−13
SPD1652	Iron-compound ABC transporter, iron-compound-binding protein	−3.73	4.57E−12
SPD1965	Choline binding protein, PcpA	2.80	8.16E−04
SPD1997	Zinc ABC transporter, zinc-binding lipoprotein, AdcA	3.91	1.14E−12
SPD1998	Zinc ABC transporter, permease protein, AdcB	2.00	2.47E−04
SPD1999	Zinc ABC transporter, ATP-binding protein, AdcC	4.17	1.29E−13
SPD2000	*adc* operon repressor, AdcR	3.88	2.46E−11

[a] *Gene numbers refer to D39 locus tags.*
[b] *D39 annotation/TIGR4 annotation (Hoskins et al., 2001; Lanie et al., 2007).*
[c] *Ratios >2.0 or <2.0 (wild-type + 0.5 mM Ni^{2+}/wild-type + 0 mM Ni^{2+}).*

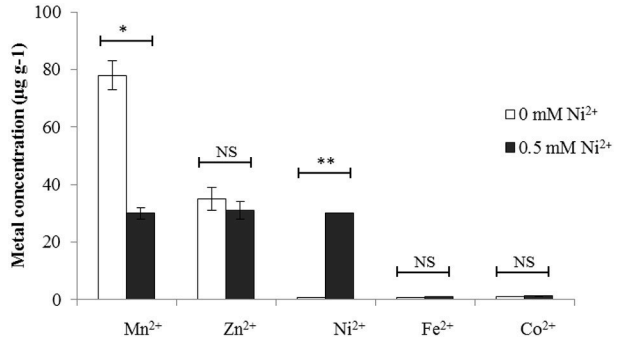

FIGURE 1 | Cell-associated metal ion concentrations (expressed ug g^{-1}) of *S. pneumoniae* D39 wild-type when grown in CDM with either 0 mM or 0.5 mM Ni^{2+}. The statistical significance of the differences in the mean metal ion concentrations was determined by One-way ANOVA (NS not significant, $^{*}P < 0.05$, and $^{**}P < 0.001$).

Ni^{2+}. The Ni^{2+}-dependent upregulation of the PsaR regulon in the presence of Ni^{2+} is consistent with our recent study, where we have explored the Ni^{2+}-dependent regulation of the PsaR regulon in more details (Manzoor et al., 2015b). Expression of a gene cluster including the cation efflux system gene *czcD*, the MerR family transcriptional regulator, and the Zn^{2+}-containing alcohol dehydrogenase *adhB* was increased more than 35-fold in the presence of Ni^{2+}. The cation efflux system CzcD was shown to protect *S. pneumoniae* against the intracellular Zn^{2+}-stress (Kloosterman et al., 2007). A novel TetR family transcriptional regulator SczA has been shown to activate the expression of *czcD* in the presence of Zn^{2+}, Co^{2+}, or Ni^{2+} (Kloosterman et al., 2007). Therefore, the upregulation of *czcD* in our transcriptomic analysis is consistent with the finding presented in previous study (Kloosterman et al., 2007). Furthermore, genes encoding a heat shock protein (HtpX) and a Dpr homolog (spd_1402) were also differentially expressed. The Dpr protein has been shown to protect bacterial cells from oxidative stress (Pulliainen et al., 2003).

The genes belonging to the AdcR regulon were also upregulated in the presence of Ni^{2+}. The expression of the *adc* operon was 4-fold upregulated. The expression of *adcAII-phtD* operon was upregulated 2-fold. The expression of other genes encoding for Pht family proteins (PhtA and PhtE), was upregulated more then 7-fold. Previously, it was shown that the expression of the AdcR regulon is repressed by the transcriptional regulator AdcR in the presence of Zn^{2+} (Shafeeq et al., 2011a). Transcriptome data was further validated by qRT-PCR analysis (Supplementary data: Table S1). Upregulation of the AdcR regulon in the presence of Ni^{2+} might also indicate the putative role of Ni^{2+} in the regulation of the AdcR regulon by the transcriptional regulator AdcR. Therefore, we decided to further explore the role of Ni^{2+} in the regulation of the AdcR regulon and to determine the intracellular concentrations of metal ions in *S. pneumoniae* D39 grown in the presence of either 0.5 mM Ni^{2+} or 0 mM Ni^{2+} in CDM.

S. pneumoniae Accumulates More Ni^{2+} When Grown in the Presence of 0.5 mM Ni^{2+}

To investigate whether the observed transcriptomic responses correlated with high cell-associated concentration of Ni^{2+}, we performed an ICP-MS analysis on the same conditions used for performing the transcriptome analysis, i.e., cells grown either in the presence of 0.5 mM Ni^{2+} or 0 mM Ni^{2+} in CDM. Our

ICP-MS data revealed that the cells grown in the presence of 0.5 mM Ni^{2+} accumulate 30-fold more cell-associated Ni^{2+} compared to the cells grown in 0 mM Ni^{2+} (30 $\mu g\ g^{-l}$ dry mass of cells vs. $<1\ \mu g\ g^{-l}$ dry mass of cells) (**Figure 1**). Moreover, 2.6-fold decrease in the cell-associated concentration of Mn^{2+} was observed. The cell-associated concentration of other metal ions was not changed in the presence of 0.5 mM Ni^{2+} compared to 0 mM Ni^{2+}. Therefore, it is likely that the transcriptomic changes observed in the presence of 0.5 M Ni^{2+} are due to the high intracellular concentration of Ni^{2+}.

Ni^{2+}-dependent Expression of the AdcR Regulon

To explore the transcriptional regulation of the genes/operons belonging to the AdcR regulon (*adcRCBA*, *adcAII-phtD*, *phtA*, *phtB*, and *phtE*) found in our microarray analysis, transcriptional *lacZ*-fusions were constructed to the promoter regions of *adcR*, *adcAII*, *phtA*, *phtB*, and *phtE* in plasmid pPP2 (Halfmann et al., 2007) and transferred to *S. pneumoniae* D39 wild-type. The expression of P*adcR-lacZ*, P*adcAII-lacZ*, P*phtA-lacZ*, P*phtB-lacZ*, and P*phtE-lacZ* was measured in CDM and CDM-Zn^{2+} (Zn^{2+} depleted medium) with the addition of 0, 0.1, 0.3, or 0.5 mM Ni^{2+}. As AdcR represses the expression of the AdcR regulon in the presence of Zn^{2+}, we also used Zn^{2+}-depleted medium (CDM-Zn^{2+}). β-galactosidase activity (Miller Units) showed that the elevated concentration of Ni^{2+} led to the high expression of all these promoters in CDM and CDM-Zn^{2+} (**Figures 2A,B**). However, the expression of these promoters was much higher in CDM-Zn^{2+} compared to CDM. The full CDM contains minor amounts of Zn^{2+} (around 883 $\mu g\ l^{-1}$) (Manzoor et al., 2015a), which could explain the lower expression of these promoters in CDM compared to CDM-Zn^{2+}. This data not only suggests the role of Ni^{2+} in the regulation of the *adcRCBA*, *adcAII-phtD*, *phtA*, *phtB*, and *phtE*, but also indicate the ability of Ni^{2+} to derepress the Zn^{2+}-dependent repression of these genes.

Opposite Effect of Zn^{2+} and Ni^{2+} on the Expression of the AdcR Regulon

β-galactosidase activities shown above indicate that Ni^{2+} might compete with Zn^{2+} and that both metal ions have opposite effects

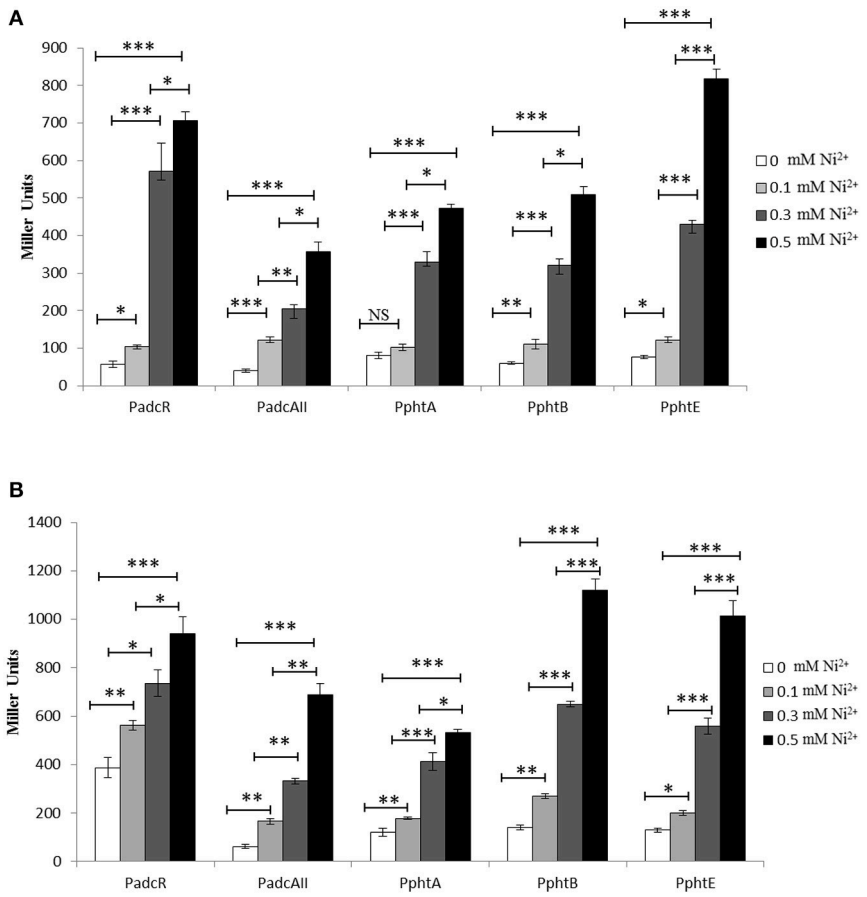

FIGURE 2 | Expression level (in Miller units) of the D39 wild-type containing transcriptional *lacZ*-fusions to P*adcR*, P*adcAII*, P*phtA*, P*phtB*, and P*phtE*, grown in CDM (A) and CDM-Zn^{2+} (Zn^{2+}-depleted medium) (B) with different added concentrations of Ni^{2+}. Standard deviation of three independent replications is indicated with error bars. Statistical significance of the differences in the expression levels was determined by One-way ANOVA (NS, not significant, $^{*}P < 0.05$, $^{**}P < 0.001$, and $^{***}P < 0.0001$).

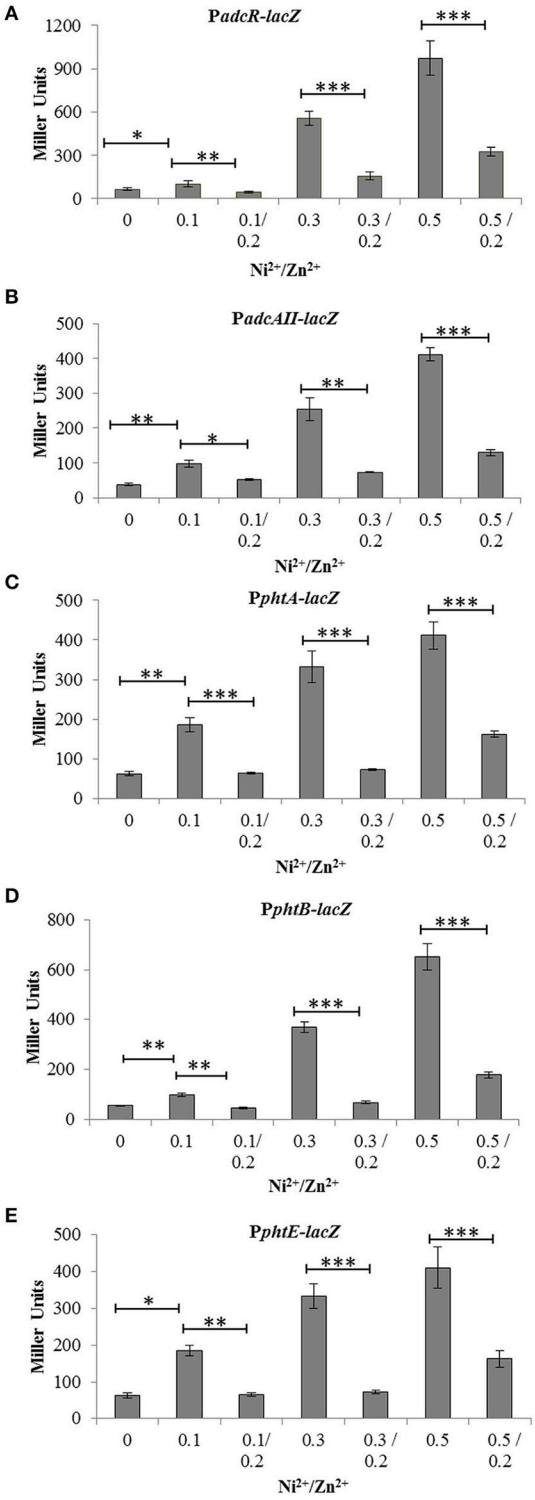

FIGURE 3 | Expression level (in Miller units) of the D39 wild-type containing transcriptional *lacZ*-fusions to P*adcR* (A), P*adcAII* (B), P*phtA* (C), P*phtB* (D), and P*phtE* (E), grown in CDM with or without addition of different concentrations of Ni^{2+} and Zn^{2+}. Standard deviation of three independent replications is indicated with error bars. Statistical significance of the differences in the expression levels was determined by One-way ANOVA (*$P < 0.05$, **$P < 0.001$, and ***$P < 0.0001$).

on the expression of the *adcRCBA*, *adcAII-phtD*, *phtA*, *phtB*, and *phtE*. In order to study the interplay of Ni^{2+} and Zn^{2+} in the regulation of *adcRCBA*, *adcAII-phtD*, *phtA*, *phtB*, and *phtE* in more details, we performed β-galactosidase assays with P*adcR-lacZ*, P*adcAII-lacZ*, P*phtA-lacZ*, P*phtB-lacZ*, and P*phtE-lacZ* in CDM with the addition of varying concentrations of Ni^{2+} and Zn^{2+} together. β-galactosidase data (Miller Units) showed that addition of Zn^{2+} in the medium leads to the repression of P*adcR-lacZ*, P*adcAII-lacZ*, P*phtA-lacZ*, P*phtB-lacZ*, and P*phtE-lacZ*, even in the presence of Ni^{2+}. However, repression caused by Zn^{2+} was much weaker at higher concentrations of Ni^{2+} (**Figures 3A–E**). This data confirm that Ni^{2+} and Zn^{2+} have an opposite effects on the expression of *adcRCBA*, *adcAII-phtD*, *phtA*, *phtB*, and *phtE*, where Zn^{2+} represses and Ni^{2+} derepresses the expression of these genes.

Role of the Transcriptional Regulator AdcR in the Ni^{2+}-dependent Expression of the AdcR Regulon

Previously, it has been shown that the transcriptional regulator AdcR represses the expression of *adcRCBA*, *adcAII-phtD*, *phtA*, *phtB*, and *phtE* in the presence of Zn^{2+} (Shafeeq et al., 2011a). In this study, our transcriptomic analysis and transcriptional *lacZ*-reporter data indicate that Ni^{2+} derepresses the expression of these genes. To identify whether the transcriptional regulator AdcR is also responsible for the Ni^{2+}-dependent expression of *adcRCBA*, *adcAII-phtD*, *phtA*, *phtB*, and *phtE*, we have transformed P*adcR-lacZ*, P*adcAII-lacZ*, P*phtA-lacZ*, P*phtB-lacZ*, and P*phtE-lacZ* into the *adcR* mutant (SS200) and performed β-galactosidase assays. β-galactosidase data revealed that the deletion of *adcR* leads to increase expression of P*adcR-lacZ*, P*adcAII-lacZ*, P*phtA-lacZ*, P*phtB-lacZ*, and P*phtE-lacZ* even in the absence of Ni^{2+} (**Figure 4**). Upregulation of these transcriptional *lacZ*-fusions in the *adcR* mutant indicates that Ni^{2+}-dependent expression of *adcRCBA*, *adcAII-phtD*, *phtA*, *phtB*, and *phtE* is mediated by transcriptional regulator AdcR.

To elucidate the Ni^{2+}-dependent role of AdcR in more details and find more targets of AdcR in the presence of Ni^{2+}, microarray comparison of the *adcR* mutant with D39 wild-type was performed in CDM with 0.3 mM Ni^{2+}. As expected, the expression of genes belonging to the AdcR regulon was highly upregulated (**Table 4**), except for the *adc* operon, which was downregulated in our transcriptome analysis (**Table 4**). For creating an *adcR* mutant in previous study, an erythromycin-resistance gene cassette was used to replace the *adcR* gene (Shafeeq et al., 2011a). Therefore, downregulation of the *adc* operon might be due to the polar effect of *adcR* deletion on the downstream genes of *adcR* (Shafeeq et al., 2011a). We further validated our DNA microarray data by qRT-PCR. qRT-PCR data is also in agreement with our transcriptome data (Supplementary data: Table S2).

Binding of AdcR to Its Target Is Zn^{2+}-and Ni^{2+}-dependent

To study the direct interaction of AdcR with the promoter regions of the genes belonging to the AdcR regulon in the

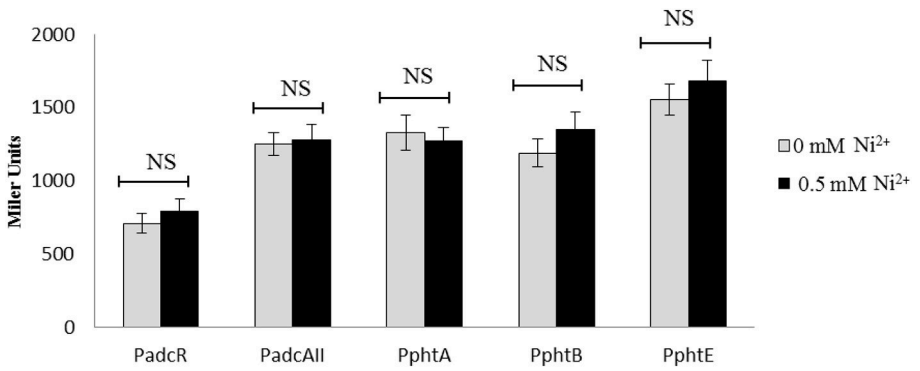

FIGURE 4 | Expression level (in Miller units) of the *adcR* mutant containing transcriptional *lacZ*-fusions to P*adcR*, P*adcAII*, P*phtA*, P*phtB*, and P*phtE* grown in CDM with or without addition of 0.5 mM Ni^{2+}. Standard deviation of three independent replications is indicated with error bars. Statistical significance of the differences in the expression levels was determined by One-way ANOVA (NS, not significant).

TABLE 4 | Summary of transcriptome comparison of *S. pneumoniae* D39 wild-type with Δ*adcR* (SS200) grown in CDM with 0.3 mM Ni^{2+}.

Gene tag[a]	Function[b]	Ratio[c]	*P*-value
SPD0126	Pneumococcal surface protein A, PhpA	2.29	1.35E−05
SPD0277	6- phospho-beta-glucosidase, CelA	12.36	2.28E−13
SPD0278	Hypothetical protein	6.67	1.12E−09
SPD0279	PTS system, IIB component, CelB	7.82	3.99E−09
SPD0280	Transcriptional regulator, CelR	10.24	2.71E−12
SPD0281	PTS system, IIA component, CelC	4.80	1.75E−07
SPD0282	Hypothetical protein	6.8	6.87E−10
SPD0283	PTS system, IIC component, CelD	7.10	8.67E−09
SPD0308	ATP-dependent Clp protease, ATP-binding subunit, ClpL	4.21	5.54E−10
SPD0888	Adhesion lipoprotein, AdcAII (LmB)	1.65	3.39E−04
SPD0889	Pneumococcal histidine triad protein D, PhtD	3.51	1.21E−08
SPD0893	Hypothetical protein	3.51	8.62E−07
SPD1038	Pneumococcal histidine triad protein A, PhtA	5.59	8.67E−09
SPD1514	ABC transporter, ATP-binding protein	−3.35	4.04E−08
SPD1515	Hypothetical protein	−4.06	4.50E−09
SPD1516	Hypothetical protein	−4.57	3.25E−09
SPD1997	Zinc ABC transporter, zinc-binding lipoprotein, AdcA	−18.45	4.07E−13
SPD1998	Zinc ABC transporter, permease protein, AdcB	−2.71	1.29E−04
SPD1999	Zinc ABC transporter, ATP-binding protein, AdcC	−10.76	3.21E−12
SPD2000	*adc* operon repressor, AdcR	−15.29	7.99E−11
SPD2001	Hypothetical protein	−25.05	1.31E−12

[a] *Gene numbers refer to D39 locus tags.*
[b] *D39 annotation/TIGR4 annotation (Hoskins et al., 2001; Lanie et al., 2007).*
[c] *Ratios >2.0 or <2.0 (SS200 + 0.3 mM Ni^{2+}/wild-type + 0.3 mM Ni^{2+}).*

presence of Ni^{2+}, we performed EMSAs with purified Strep-tagged AdcR (Ad-Strep tag) and ^{33}P-labeled promoters of *adcR*, *adcAII*, *phtA*, *phtB*, and *pcpA*. To prevent the interference of metal ions with Ad-Strep tag, all the experiments were performed in EDTA free gels and buffers. The *pcpA* promoter region was taken as a negative control. Ad-Strep tag was unable to shift the promoter regions of *adcR*, *adcAII*, *phtA*, and *phtB* in the absence of metal ions (Lane 2 in **Figure 5**). However, the addition of 0.2 mM Zn^{2+} led to the binding of Ad-Strep tag to the promoter regions of *adcR*, *adcAII*, *phtA*, and *phtB* (Lane 3 in **Figures 5A–D**), which is consistent with our previous study (Shafeeq et al., 2011a). Interestingly, 0.2 and 0.4 mM Ni^{2+} were unable to stimulate the binding of Ad-Strep tag with the promoter regions of *adcR*, *adcAII*, *phtA*, and *phtB* (Lane 4 and 5 in **Figures 5A–D**). In our transcriptome data mentioned above, Ni^{2+} showed a derepressive effect on the expression of the AdcR regulon. Therefore, we also decided to check the interaction of Ad-Strep tag with the promoter regions of *adcR*, *adcAII*, *phtA*, and *phtB* in the presence of both Zn^{2+} and Ni^{2+} together. The Zn^{2+}-dependent interaction of AdcR with these promoters in the presence of 0.2 mM Zn^{2+} was alleviated with the addition of 0.2 mM or 0.4 mM Ni^{2+} (Lane 6 and 7 in **Figures 5A–D**). Under the same conditions, we did not see any band shift with the promoter region of *pcpA* as a negative control (**Figure 5E**). Thus, this data indicates that Zn^{2+} and Ni^{2+} have an opposite effects on the interaction of AdcR with the promoter regions of *adcR*, *adcAII*, *phtA*, and *phtB*.

Effect of Ni^{2+}on SczA-mediated Expression of the Zn^{2+}-efflux system *czcD*

To investigate the regulation of *czcD* in the presence of Ni^{2+}, we studied the transcriptional response of P*czcD-lacZ* grown in complete CDM with the addition of different concentrations of Ni^{2+}. β-galactosidase assays showed that P*czcD-lacZ* responded to Ni^{2+} and its expression was highly increased with an increasing concentration of Ni^{2+} (**Figure 6**). This data is in agreement with our transcriptomic data mentioned above and suggests the putative role of CzcD in Ni^{2+} homeostasis.

DISCUSSION

Transition metal ions such as Mn^{2+}, Zn^{2+}, Cu^{2+}, Fe^{2+}, Co^{2+}, and Cd^{2+} have been shown to play a pivotal role in the

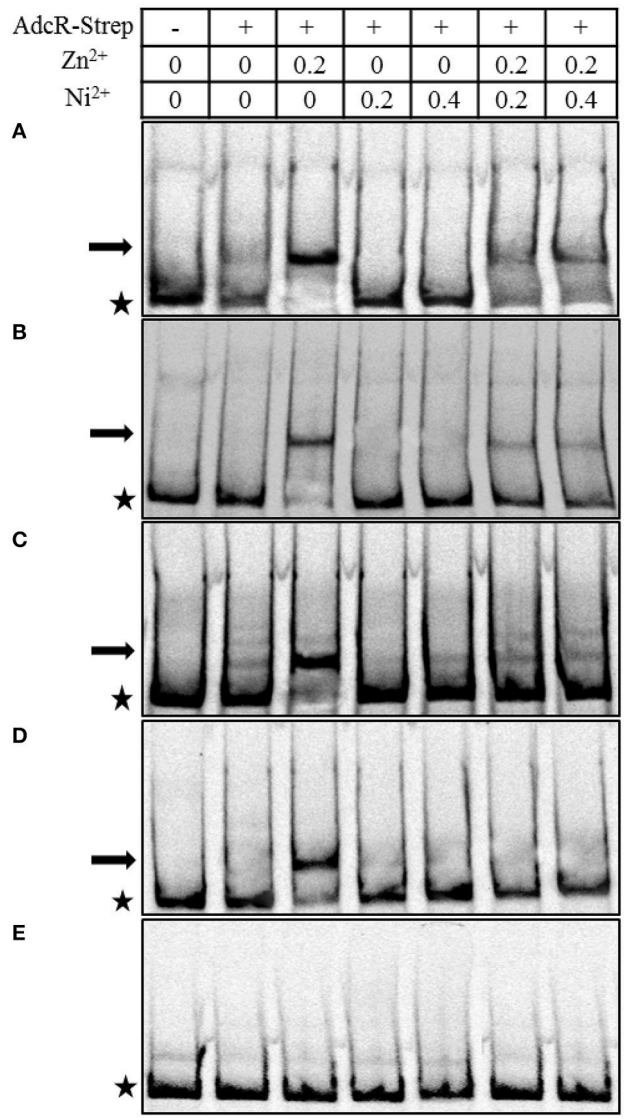

FIGURE 5 | *In vitro* interaction of Ad-Strep tag with the promoter regions of *adcR* (A), *adcAII* (B), *phtA* (C), *phtB* (D), and *pcpA* (E). Ad-Strep was added at a concentration of 30 nM as indicated above panel, while lane 1 is without added protein. Arrows indicate the position of shifted probe and asterisks indicate the position of free probe. 0.2 mM Zn^{2+} was added in lanes 3, 6, and 7. Whereas, Ni^{2+} was added at the concentration of 0.2 mM in lane 4 and 6, and 0.4 mM in lanes 5 and 7.

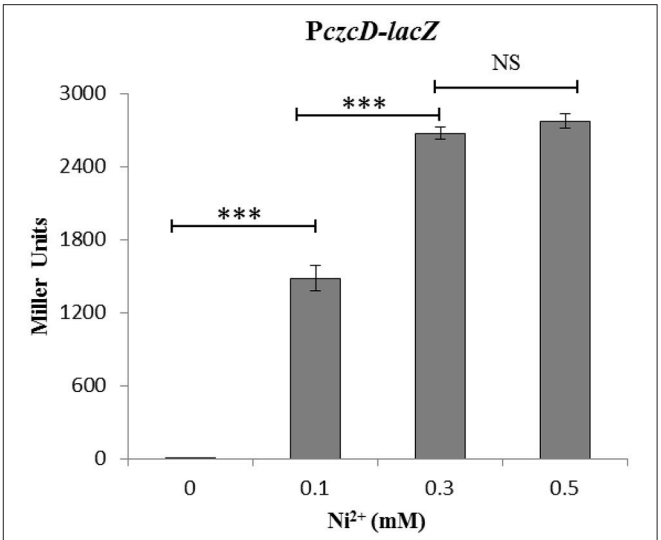

FIGURE 6 | Expression level (miller units) of the D39 wild-type containing transcriptional *lacZ*-fusion to P*czcD* grown in CDM with different added concentrations of Ni^{2+}. Standard deviation of three independent replications is indicated with error bars. Statistical significance of the differences in the expression levels was determined by One-way ANOVA (NS, not significant and ***$P < 0.0001$).

metabolism and virulence of *S. pneumoniae* (Brown et al., 2001; Kloosterman et al., 2008; Shafeeq et al., 2011b; Begg et al., 2015). However, the role of Ni^{2+} on the global gene expression of *S. pneumoniae* has not been studied before. In this study, we analyze the transcriptome changes in *S. pneumoniae* D39 wild-type in response to high Ni^{2+} concentration. The expression of a number of important genes and operons with diverse functions, including the AdcR regulon (*adcRCBA*, *adcAII-phtD, phtA*, *phtB*, and *phtE*), the PsaR regulon (*pcpA*, *prtA*, and *psaBCA*) regulon, and the Zn^{2+}-efflux system *czcD* were significantly altered in the presence of Ni^{2+}. We further studied the role of Ni^{2+} in the regulation of the AdcR regulon and demonstrated that Ni^{2+} plays an opposite role compared to Zn^{2+} in the regulation of the AdcR regulon.

The AdcR regulon consists of *adcRCBA*, *adcAII-phtD*, *phtA*, *phtB*, *phtE*, and *adhC* in *S. pneumoniae*. The *adc* operon (*adcRCBA*) is involved in Zn^{2+} acquisition, and encodes for a Zn^{2+}-responsive MarR family transcriptional regulator, AdcR, two ABC transporter proteins AdcC and AdcB, and an extracellular Zn^{2+}-binding protein AdcA (Dintilhac et al., 1997; Dintilhac and Claverys, 1997; Bayle et al., 2011). The *adcAII* gene encodes an adhesion lipoprotein which has an overlapping specificity with AdcA for Zn^{2+} (Bayle et al., 2011). AdcAII belongs to the LraI-lipoprotein family and is organized in an operon with a *phtD* gene encoding pneumococcal histidine triade protein precursor D (PhtD). *phtA*, *phtB*, and *phtE* encodes for pneumococcal histidine triade protein A, B, and E, respectively. Recent studies have demonstrated the role of the PhT family proteins (PhtA, PhtB, PhtE, and PhtD) in intracellular Zn^{2+} acquisition and pathogenesis in *S. pneumoniae* (Hava and Camilli, 2002; Ogunniyi et al., 2009; Plumptre et al., 2014b). The *adhC* gene encodes for a Zn^{2+}-containing alcohol dehydrogenase. Previously, it was demonstrated that the expression of *adcRCBA*, *adcAII-phtD*, *phtA*, *phtB*, and *phtE* is repressed, while the expression of *adhC* is activated by the transcriptional regulator AdcR in the presence of Zn^{2+} (Shafeeq et al., 2011a). Here, we show that Ni^{2+} also plays a role in the regulation of *adcRCBA*, *adcAII-phtD*, *phtA*, *phtB*, and *phtE*. Our β-galactosidase assays showed that the expression of *adcRCBA*, *adcAII-phtD*, *phtA*, *phtB*, and *phtE* was increased with increasing concentrations of Ni^{2+}. However, we did not find any significant

change in the expression of *adhC* in our both transcriptome analysis performed in this study. This might exclude the role of Ni^{2+} in the AdcR mediated regulation of *adhC*.

High concentrations of Ni^{2+} can be very toxic for bacteria (Macomber and Hausinger, 2011). Therefore, bacteria must limit the toxic amount of Ni^{2+} to perform normal cellular functions. In many bacteria, CDF-family efflux pumps help to maintain proper concentrations of heavy metals in the cell. For example, in *Bacillus subtilis*, the CzcD heavy metal efflux pump is involved in the homeostasis of Zn^{2+}, Co^{2+}, Cu^{2+}, and Ni^{2+}, and is regulated by CzrA (Moore et al., 2005). It is also important to note that the expression of *czcD* is highly upregulated in our transcriptome analysis in response to Ni^{2+}. Expression of *czcD* is regulated by the TetR family transcriptional regulator SczA in the presence of Zn^{2+}, Co^{2+}, or Ni^{2+} (Kloosterman et al., 2007). Moreover, Zn^{2+}, Co^{2+}, or Ni^{2+} has been shown to stimulate the binding of SczA to the promoter region of *czcD* (Kloosterman et al., 2007). In this study, we further confirmed the expression of *czcD* in the presence of Ni^{2+} by transcriptional *lacZ*-reporter study with P*czcD-lacZ* and our results are consistent with a previous study (Kloosterman et al., 2007).

The PsaR regulon consists of *psaBCA*, *pcpA*, and *prtA* that encodes for the Mn^{2+} uptake system (PsaBCA), a choline binding protein (PcpA), and a serine protease (PrtA), respectively. The expression of the PsaR regulon is shown to be repressed by the DtxR family transcriptional regulator PsaR in the presence of Mn^{2+} (Johnston et al., 2006). Notably, Zn^{2+} and Co^{2+} can bind with PsaR to relieve the Mn^{2+}-dependent repression of the PsaR regulon (Kloosterman et al., 2008; Manzoor et al., 2015a). Recently, we have studied the regulation of the PsaR regulon in the presence of Ni^{2+} and demonstrated that like Zn^{2+} and Co^{2+}, Ni^{2+} also has the ability to derepress the Mn^{2+}-dependent repression of the PsaR regulon, and that high concentrations of Ni^{2+} leads to cell-associated Mn^{2+} deficiency (Manzoor et al., 2015b). In this study, we have also observed the significant upregulation of the PsaR regulon in our transcriptome analysis performed in the presence of Ni^{2+} (**Table 3**). Upregulation of the PsaR regulon in our transcriptome further verifies our previous results (Manzoor et al., 2015b). Moreover, we have also observed the cell-associated deficiency of Mn^{2+} in our ICP-MS analysis performed in this study (**Figure 1**), which is also in consistent with our previous results (Manzoor et al., 2015b).

The interplay, or competition, of metal ions plays an important role in the regulation of metal responsive genes. In *S. pneumoniae*, competition of Mn^{2+} with Zn^{2+}, Co^{2+}, or Ni^{2+} in the regulation of the PsaR regulon by transcriptional regulator PsaR has already extensively been studied (Kloosterman et al., 2008; Manzoor et al., 2015a,b). Similarly, the interplay of Cu^{2+} and Zn^{2+} in the regulation of *cop* operon by transcriptional regulator CopY was studied before, where Cu^{2+} induces and Zn^{2+} represses the CopY-mediated expression of *cop* operon (Shafeeq et al., 2011b). Here, we elaborated for the first time the interplay of Ni^{2+} and Zn^{2+} in the regulation of genes belonging to the AdcR regulon. Our *lacZ*-reporter studies determined the ability of Ni^{2+}, in derepressing the Zn^{2+}-dependent repression of *adcRCBA*, *adcAII-phtD*, *phtA*, *phtB*, and *phtE*. Our *in vitro* data showed that the Zn^{2+}-dependent binding of AdcR to the promoter regions of the genes belonging to the AdcR regulon was alleviated by the addition of Ni^{2+}. Recently, it has been shown that Cd^{2+}-uptake reduces the accumulation of cell-associated Mn^{2+} and Zn^{2+} (Begg et al., 2015). Our ICP-MS comparison of cells grown in CDM with 0.5 mM to 0 mM Ni^{2+} has not shown any difference in the concentration of Zn^{2+} or other metal ions, which also indicates the direct role of Ni^{2+} in the regulation of *adcRCBA*, *adcAII-phtD*, *phtA*, *phtB*, and *phtE*. Moreover, the role of genes belonging to the AdcR regulon in the pathogenesis of *S. pneumoniae* has already been demonstrated, which also suggests the important role of Ni^{2+} in pneumococcal virulence.

SUPPLEMENTARY MATERIAL

The Supplementary Material for this article can be found online at: http://journal.frontiersin.org/article/10.3389/fcimb.2015.00091

REFERENCES

Afzal, M., Manzoor, I., and Kuipers, O. P. (2015). A fast and reliable pipeline for bacterial transcriptome analysis case study: serine-dependent gene regulation in *Streptococcus pneumoniae*. *J. Vis. Exp.* e52649. doi: 10.3791/52649

Alimonti, A., Bocca, B., Mannella, E., Petrucci, F., Zennaro, F., Cotichini, R., et al. (2005). Assessment of reference values for selected elements in a healthy urban population. *Ann. Ist. Super. Sanità* 41, 181–187.

Anwar, H. A., Aldam, C. H., Visuvanathan, S., and Hart, A. J. (2007). The effect of metal ions in solution on bacterial growth compared with wear particles from hip replacements. *J. Bone Joint Surg. Br.* 89-B, 1655–1659. doi: 10.1302/0301-620X.89B12.19714

Bayle, L., Chimalapati, S., Schoehn, G., Brown, J., Vernet, T., and Durmort, C. (2011). Zinc uptake by *Streptococcus pneumoniae* depends on both AdcA and AdcAII and is essential for normal bacterial morphology and virulence. *Mol. Microbiol.* 82, 904–916. doi: 10.1111/j.1365-2958.2011.07862.x

Begg, S. L., Eijkelkamp, B. A., Luo, Z., Couñago, R. M., Morey, J. R., Maher, M. J., et al. (2015). Dysregulation of transition metal ion homeostasis is the molecular basis for cadmium toxicity in *Streptococcus pneumoniae*. *Nat. Commun.* 6:6418. doi: 10.1038/ncomms7418

Blencowe, D. K., and Morby, A. P. (2003). Zn(II) metabolism in prokaryotes. *FEMS Microbiol. Rev.* 27, 291–311. doi: 10.1016/S0168-6445(03)00041-X

Bogaert, D., De Groot, R., and Hermans, P. W. M. (2004). *Streptococcus pneumoniae* colonisation: the key to pneumococcal disease. *Lancet Infect. Dis.* 4, 144–154. doi: 10.1016/S1473-3099(04)00938-7

Brown, J. S., Gilliland, S. M., and Holden, D. W. (2001). A *Streptococcus pneumoniae* pathogenicity island encoding an ABC transporter involved in iron uptake and virulence. *Mol. Microbiol.* 40, 572–585. doi: 10.1046/j.1365-2958.2001.02414.x

Cavet, J. S., Meng, W., Pennella, M. A., Appelhoff, R. J., Giedroc, D. P., and Robinson, N. J. (2002). A nickel-cobalt-sensing ArsR-SmtB family repressor. Contributions of cytosol and effector binding sites to metal selectivity. *J. Biol. Chem.* 277, 38441–38448. doi: 10.1074/jbc.M207677200

Chen, Y.-Y. M., and Burne, R. A. (2003). Identification and characterization of the nickel uptake system for urease biogenesis in Streptococcus salivarius 57.I. *J. Bacteriol.* 185, 6773–6779. doi: 10.1128/JB.185.23.6773-6779.2003

De Pina, K., Desjardin, V., Mandrand-Berthelot, M. A., Giordano, G., and Wu, L. F. (1999). Isolation and characterization of the nikR gene encoding a nickel-responsive regulator in *Escherichia coli*. *J. Bacteriol.* 181, 670–674.

Dintilhac, A., Alloing, G., Granadel, C., and Claverys, J. P. (1997). Competence and virulence of *Streptococcus pneumoniae*: Adc and PsaA mutants exhibit a requirement for Zn and Mn resulting from inactivation of putative ABC metal permeases. *Mol. Microbiol.* 25, 727–739. doi: 10.1046/j.1365-2958.1997.5111879.x

Dintilhac, A., and Claverys, J. P. (1997). The adc locus, which affects competence for genetic transformation in *Streptococcus pneumoniae*, encodes an ABC transporter with a putative lipoprotein homologous to a family of streptococcal adhesins. *Res. Microbiol.* 148, 119–131. doi: 10.1016/S0923-2508(97)87643-7

Finney, L. A., and O'Halloran, T. V. (2003). Transition metal speciation in the cell: insights from the chemistry of metal ion receptors. *Science* 300, 931–936. doi: 10.1126/science.1085049

Ge, R., Chen, Z., and Zhou, Q. (2012). The actions of bismuth in the treatment of Helicobacter pylori infections: an update. *Met. Integr. Biometal Sci.* 4, 239–243. doi: 10.1039/c2mt00180b

Gupta, R., Shah, P., and Swiatlo, E. (2009). Differential gene expression in *Streptococcus pneumoniae* in response to various iron sources. *Microb. Pathog.* 47, 101–109. doi: 10.1016/j.micpath.2009.05.003

Halfmann, A., Hakenbeck, R., and Brückner, R. (2007). A new integrative reporter plasmid for *Streptococcus pneumoniae*. *FEMS Microbiol. Lett.* 268, 217–224. doi: 10.1111/j.1574-6968.2006.00584.x

Hava, D. L., and Camilli, A. (2002). Large-scale identification of serotype 4 *Streptococcus pneumoniae* virulence factors. *Mol. Microbiol.* 45, 1389–1406. doi: 10.1046/j.1365-2958.2002.03106.x

Hendriksen, W. T., Bootsma, H. J., van Diepen, A., Estevão, S., Kuipers, O. P., de Groot, R., et al. (2009). Strain-specific impact of PsaR of *Streptococcus pneumoniae* on global gene expression and virulence. *Microbiol. Read. Engl.* 155, 1569–1579. doi: 10.1099/mic.0.025072-0

Hoskins, J., Alborn, W. E. Jr., Arnold, J., Blaszczak, L. C., Burgett, S., DeHoff, B. S., et al. (2001). Genome of the bacterium *Streptococcus pneumoniae* strain R6. *J. Bacteriol.* 183, 5709–5717. doi: 10.1128/JB.183.19.5709-5717.2001

Jacobsen, F. E., Kazmierczak, K. M., Lisher, J. P., Winkler, M. E., and Giedroc, D. P. (2011). Interplay between manganese and zinc homeostasis in the human pathogen *Streptococcus pneumoniae*. *Met. Integr. Biometal Sci.* 3, 38–41. doi: 10.1039/C0MT00050G

Johnston, J. W., Briles, D. E., Myers, L. E., and Hollingshead, S. K. (2006). Mn^{2+}-dependent regulation of multiple genes in *Streptococcus pneumoniae* through PsaR and the resultant impact on virulence. *Infect. Immun.* 74, 1171–1180. doi: 10.1128/IAI.74.2.1171-1180.2006

Kloosterman, T. G., Hendriksen, W. T., Bijlsma, J. J. E., Bootsma, H. J., van Hijum, S. A. F. T., Kok, J., et al. (2006). Regulation of glutamine and glutamate metabolism by GlnR and GlnA in *Streptococcus pneumoniae*. *J. Biol. Chem.* 281, 25097–25109. doi: 10.1074/jbc.M601661200

Kloosterman, T. G., van der Kooi-Pol, M. M., Bijlsma, J. J. E., and Kuipers, O. P. (2007). The novel transcriptional regulator SczA mediates protection against Zn^{2+} stress by activation of the Zn^{2+}-resistance gene czcD in *Streptococcus pneumoniae*. *Mol. Microbiol.* 65, 1049–1063. doi: 10.1111/j.1365-2958.2007.05849.x

Kloosterman, T. G., Witwicki, R. M., van der Kooi-Pol, M. M., Bijlsma, J. J. E., and Kuipers, O. P. (2008). Opposite effects of Mn^{2+} and Zn^{2+} on PsaR-mediated expression of the virulence genes pcpA, prtA, and psaBCA of *Streptococcus pneumoniae*. *J. Bacteriol.* 190, 5382–5393. doi: 10.1128/JB.00307-08

Kuipers, O. P., de Ruyter, P. G. G., Kleerebezem, M., and de Vos, W. M. (1998). Quorum sensing-controlled gene expression in lactic acid bacteria. *J. Biotechnol.* 64, 15–21. doi: 10.1016/S0168-1656(98)00100-X

Lanie, J. A., Ng, W.-L., Kazmierczak, K. M., Andrzejewski, T. M., Davidsen, T. M., Wayne, K. J., et al. (2007). Genome sequence of Avery's virulent serotype 2 strain D39 of *Streptococcus pneumoniae* and comparison with that of unencapsulated laboratory strain R6. *J. Bacteriol.* 189, 38–51. doi: 10.1128/JB.01148-06

Lisher, J. P., Higgins, K. A., Maroney, M. J., and Giedroc, D. P. (2013). Physical Characterization of the manganese-sensing pneumococcal surface antigen repressor from *Streptococcus pneumoniae*. *Biochemistry (Mosc.)* 52, 7689–7701. doi: 10.1021/bi401132w

Macomber, L., and Hausinger, R. P. (2011). Mechanisms of nickel toxicity in microorganisms. *Met. Integr. Biometal Sci.* 3, 1153–1162. doi: 10.1039/c1mt00063b

Manzoor, I., Shafeeq, S., Kloosterman, T. G., and Kuipers, O. P. (2015a). Co^{2+}-dependent gene expression in *Streptococcus pneumoniae*: opposite effect of Mn^{2+} and Co^{2+} on the expression of the virulence genes psaBCA, pcpA and prtA. *Microb. Physiol. Metab.* 6, 748. doi: 10.3389/fmicb.2015.00748

Manzoor, I., Shafeeq, S., and Kuipers, O. P. (2015b). Ni^{2+}-dependent and PsaR-mediated regulation of the virulence genes pcpA, psaBCA and prtA in *Streptococcus pneumoniae*. *PLoS ONE* 10:e0142839. doi: 10.1371/journal.pone.0142839

Manzoor, I., Shafeeq, S., and Kuipers, O. P. (2015c). Transcriptome analysis of *Streptococcus pneumoniae* D39 in the presence of cobalt. *Genomics Data* 6, 151–153. doi: 10.1016/j.gdata.2015.08.033

Mitchell, T. J. (2003). The pathogenesis of streptococcal infections: from tooth decay to meningitis. *Nat. Rev. Microbiol.* 1, 219–230. doi: 10.1038/nrmicro771

Moore, C. M., Gaballa, A., Hui, M., Ye, R. W., and Helmann, J. D. (2005). Genetic and physiological responses of *Bacillus subtilis* to metal ion stress. *Mol. Microbiol.* 57, 27–40. doi: 10.1111/j.1365-2958.2005.04642.x

Moore, C. M., and Helmann, J. D. (2005). Metal ion homeostasis in *Bacillus subtilis*. *Curr. Opin. Microbiol.* 8, 188–195. doi: 10.1016/j.mib.2005.02.007

Mulrooney, S. B., and Hausinger, R. P. (2003). Nickel uptake and utilization by microorganisms. *FEMS Microbiol. Rev.* 27, 239–261. doi: 10.1016/S0168-6445(03)00042-1

Obaro, S., and Adegbola, R. (2002). The pneumococcus: carriage, disease and conjugate vaccines. *J. Med. Microbiol.* 51, 98–104. doi: 10.1099/0022-1317-51-2-98

Ogunniyi, A. D., Grabowicz, M., Mahdi, L. K., Cook, J., Gordon, D. L., Sadlon, T. A., et al. (2009). Pneumococcal histidine triad proteins are regulated by the Zn^{2+}-dependent repressor AdcR and inhibit complement deposition through the recruitment of complement factor H. *FASEB J.* 23, 731–738. doi: 10.1096/fj.08-119537

Plumptre, C. D., Eijkelkamp, B. A., Morey, J. R., Behr, F., Couñago, R. M., Ogunniyi, A. D., et al. (2014a). AdcA and AdcAII employ distinct zinc acquisition mechanisms and contribute additively to zinc homeostasis in *Streptococcus pneumoniae*. *Mol. Microbiol.* 91, 834–851. doi: 10.1111/mmi.12504

Plumptre, C. D., Hughes, C. E., Harvey, R. M., Eijkelkamp, B. A., McDevitt, C. A., and Paton, J. C. (2014b). Overlapping Functionality of the Pht Proteins in Zinc Homeostasis of Streptococcus pneumoniae. *Infect. Immun.* 82, 4315–4324. doi: 10.1128/IAI.02155-14

Pulliainen, A. T., Haataja, S., Kähkönen, S., and Finne, J. (2003). Molecular basis of H2O2 resistance mediated by Streptococcal Dpr. Demonstration of the functional involvement of the putative ferroxidase center by site-directed mutagenesis in Streptococcus suis. *J. Biol. Chem.* 278, 7996–8005. doi: 10.1074/jbc.M210174200

Rodionov, D. A., Hebbeln, P., Gelfand, M. S., and Eitinger, T. (2006). Comparative and functional genomic analysis of prokaryotic nickel and cobalt uptake transporters: evidence for a novel group of ATP-binding cassette transporters. *J. Bacteriol.* 188, 317–327. doi: 10.1128/JB.188.1.317-327.2006

Rosch, J. W., Gao, G., Ridout, G., Wang, Y.-D., and Tuomanen, E. I. (2009). Role of the manganese efflux system mntE for signalling and pathogenesis in *Streptococcus pneumoniae*. *Mol. Microbiol.* 72, 12–25. doi: 10.1111/j.1365-2958.2009.06638.x

Shafeeq, S., Kloosterman, T. G., and Kuipers, O. P. (2011a). Transcriptional response of *Streptococcus pneumoniae* to Zn^{2+}) limitation and the repressor/activator function of AdcR. *Met. Integr. Biometal Sci.* 3, 609–618. doi: 10.1039/c1mt00030f

Shafeeq, S., Kuipers, O. P., and Kloosterman, T. G. (2013). The role of zinc in the interplay between pathogenic streptococci and their hosts. *Mol. Microbiol.* 88, 1047–1057. doi: 10.1111/mmi.12256

Shafeeq, S., Yesilkaya, H., Kloosterman, T. G., Narayanan, G., Wandel, M., Andrew, P. W., et al. (2011b). The cop operon is required for copper homeostasis and contributes to virulence in *Streptococcus pneumoniae*. *Mol. Microbiol.* 81, 1255–1270. doi: 10.1111/j.1365-2958.2011.07758.x

Sun, X., Yu, G., Xu, Q., Li, N., Xiao, C., Yin, X., et al. (2013). Putative cobalt- and nickel-binding proteins and motifs in *Streptococcus pneumoniae*. *Met. Integr. Biometal Sci.* 5, 928–935. doi: 10.1039/c3mt00126a

Tottey, S., Waldron, K. J., Firbank, S. J., Reale, B., Bessant, C., Sato, K., et al. (2008). Protein-folding location can regulate manganese-binding versus copper- or zinc-binding. *Nature* 455, 1138–1142. doi: 10.1038/nature07340

van Vliet, A. H. M., Kuipers, E. J., Waidner, B., Davies, B. J., de Vries, N., Penn, C. W., et al. (2001). Nickel-responsive induction of urease expression inhelicobacter pylori is mediated at the transcriptional level. *Infect. Immun.* 69, 4891–4897. doi: 10.1128/IAI.69.8.4891-4897.2001

Waldron, K. J., and Robinson, N. J. (2009). How do bacterial cells ensure that metalloproteins get the correct metal? *Nat. Rev. Microbiol.* 7, 25–35. doi: 10.1038/nrmicro2057

Conflict of Interest Statement: The authors declare that the research was conducted in the absence of any commercial or financial relationships that could be construed as a potential conflict of interest.

frontiers in Cellular and Infection Microbiology

ORIGINAL RESEARCH
published: 26 April 2016
doi: 10.3389/fcimb.2016.00048

Induction of Central Host Signaling Kinases during Pneumococcal Infection of Human THP-1 Cells

Thomas P. Kohler, Annemarie Scholz, Delia Kiachludis and Sven Hammerschmidt*

Department Genetics of Microorganisms, Interfaculty Institute for Genetics and Functional Genomics, Ernst-Moritz-Arndt Universität Greifswald, Greifswald, Germany

Streptococcus pneumoniae is a widespread colonizer of the mucosal epithelia of the upper respiratory tract of human. However, pneumococci are also responsible for numerous local as well as severe systemic infections, especially in children under the age of five and the elderly. Under certain conditions, pneumococci are able to conquer the epithelial barrier, which can lead to a dissemination of the bacteria into underlying tissues and the bloodstream. Here, specialized macrophages represent an essential part of the innate immune system against bacterial intruders. Recognition of the bacteria through different receptors on the surface of macrophages leads thereby to an uptake and elimination of bacteria. Accompanied cytokine release triggers the migration of leukocytes from peripheral blood to the site of infection, where monocytes differentiate into mature macrophages. The rearrangement of the actin cytoskeleton during phagocytosis, resulting in the engulfment of bacteria, is thereby tightly regulated by receptor-mediated phosphorylation cascades of different protein kinases. The molecular cellular processes including the modulation of central protein kinases are only partially solved. In this study, the human monocytic THP-1 cell line was used as a model system to examine the activation of Fcγ and complement receptor-independent signal cascades during infection with *S. pneumoniae*. Pneumococci cultured either in chemically defined or complex medium showed no significant differences in pneumococcal phagocytosis by phorbol 12-myristate 13-acetate (PMA) differentiated THP-1 cells. Double immuno-fluorescence microscopy and antibiotic protection assays demonstrated a time-dependent uptake and killing of *S. pneumoniae* 35A inside of macrophages. Infections of THP-1 cells in the presence of specific pharmacological inhibitors revealed a crucial role of actin polymerization and importance of the phosphoinositide 3-kinase (PI3K) and Protein kinase B (Akt) as well during bacterial uptake. The participation of essential host cell signaling kinases in pneumococcal phagocytosis was deciphered for the kinase Akt, ERK1/2, and p38 and phosphoimmunoblots showed an increased phosphorylation and thus activation upon infection with pneumococci. Taken together, this study deciphers host cell kinases in innate immune cells that are induced upon infection with pneumococci and interfere with bacterial clearance after phagocytosis.

Keywords: *Streptococcus pneumoniae*, phagocytosis, THP-1 cells, cell signaling, p38, Akt, PI3K, ERK1/2

OPEN ACCESS

Edited by:
Guangchun Bai,
Albany Medical College, USA

Reviewed by:
Kishore Alugupalli,
Thomas Jefferson University, USA
Glen C. Ulett,
Griffith University, Australia
Jose Yuste,
Instituto de Salud Carlos III, Spain

****Correspondence:***
Thomas P. Kohler
kohlert@uni-greifswald.de

Received: *25 January 2016*
Accepted: *13 April 2016*
Published: *26 April 2016*

Citation:
Kohler TP, Scholz A, Kiachludis D and Hammerschmidt S (2016) Induction of Central Host Signaling Kinases during Pneumococcal Infection of Human THP-1 Cells. Front. Cell. Infect. Microbiol. 6:48. doi: 10.3389/fcimb.2016.00048

INTRODUCTION

Streptococcus pneumoniae is a common colonizer of the upper respiratory tract of human, with increased colonization rates in children and the elderly (Garenne et al., 1992; Bogaert et al., 2004b; Hussain et al., 2005). Beside its role as a harmless colonizer, pneumococci are also a common cause of otitis media, pneumonia, meningitis and sepsis, especially in children under the age of 5 years (Bogaert et al., 2004a; Sleeman et al., 2006). *S. pneumoniae* possesses a wide variety of virulence factors to colonize the host, invade into tissues and to evade the human immune system (Jonsson et al., 1985; Gamez and Hammerschmidt, 2012; Voss et al., 2012). The epithelia of the upper respiratory tract of human represent thereby a physical barrier which needs to be conquered in the process of invasive pneumococcal diseases. Pneumococci therefore release amongst others pneumolysin, neuraminidase, and hyaluronidase to the environment, leading to disruption of connective tissues and extracellular matrices, promoting dissemination of the bacteria into underlying tissues, and the blood system (Kelly and Jedrzejas, 2000; Feldman et al., 2007; Trappetti et al., 2009; Mitchell and Mitchell, 2010). In this scenario, phagocytic cells play an essential role in the recognition and clearance of bacterial infections (van Furth and Cohn, 1968; van Furth et al., 1972). Macrophages represent an important link between the innate and the acquired immune system due to the possibility to phagocytose and digest bacteria and to present part fragments of processed bacteria in association with major histocompatibility complex (MHC) class I or II to T-cells (Greenberg and Grinstein, 2002). Bacterial recognition and uptake by macrophages can be initiated by the activation of different surface receptors. Fc receptor-mediated phagocytosis is initiated by recognition of immunoglobulin G (IgG) opsonized microorganisms. Here, members of the Fcγ receptor family are able to recognize and bind the constant Fc region of IgG molecules that opsonize pathogenic microorganisms (Gomez et al., 1994; Ravetch, 1997). Microorganisms can also be opsonized for complement receptor-mediated phagocytosis by proteins of the complement system, like C3b or C4b, resulting from cleavage of complement factors (Ghiran et al., 2000).

Besides recognition of opsonized microorganisms, cells of the innate immune system have the capability to sense bacteria directly via their target specific molecular structures, the so called pathogen-associated molecular patterns (PAMPs) via pattern recognition receptors (PRRs). These receptors are located on the surface of host cells, intracellularly and are also be secreted (Janeway and Medzhitov, 2002; Iwasaki and Medzhitov, 2015). For the recognition of pneumococci various PRRs have been described, including the C-reactive protein (CRP), members of the toll-like receptor family (TLRs), Nod proteins, the LPS binding protein (LBP), and CD14 (Mold et al., 2002; Weber et al., 2003; Currie et al., 2004; Echchannaoui et al., 2005; Malley et al., 2005). Furthermore, the C-type lectin SIGN-R1 and the scavenger receptor MARCO, both expressed by macrophages, have been described as PRRs important for the recognition of pneumococci (Arredouani et al., 2004; Kang et al., 2004).

However, recognition of bacteria via PAMPs and sensing of opsonized bacteria leads to the initiation of signal transduction cascades catalyzed by different protein kinases ending up in the activation of proteins involved in actin remodeling and therefore phagocytosis (Freeman and Grinstein, 2014). Nevertheless, the molecular process of actin remodeling during phagocytosis is only partially understood and best studied in Fcγ and complement-3 receptor-(CR3) mediated phagocytosis.

The signaling network of protein kinases involved in phagocytosis is rather complex and dependent from the activated surface receptors and cross-talk between different signaling pathways.

Members of the phosphoinositide-3-kinase (PI3K) family are essential for many cellular processes by transducing outside-inside signaling. Amongst others, this signaling leads to the activation of downstream effector pathways, including the reorganization of the cytoskeleton via exchange factors that regulate the small GTPase Rac and activation of the protein kinase C (PKC) as well as the serine/threonine protein kinase B (PKB/Akt) (Hawkins et al., 1995; Katso et al., 2001; Engelman et al., 2006). Moreover, experiments with pharmacological inhibitors of the PI3K (Wortmannin and LY294002) revealed also an essential role in FCγ and complement receptor-mediated phagocytosis (Cox et al., 1999; Aderem, 2003). Blocking of the PI3K leads not to an inhibition of opsonized particle binding or initial actin polymerization but seems to be required for membrane extension and fusion during engulfment (Araki et al., 1996; Cox et al., 1999).

Another important component of intracellular signaling processes is the protein kinase B (Akt), a serine/threonine (Ser/Thr) protein kinase involved in a wide variety of signaling pathways concerning such as cell growth, survival, or cellular metabolism (del Peso et al., 1997; Wullschleger et al., 2006; Manning and Cantley, 2007). Akt is an important downstream target of the PI3K, and represents therefore a mediator of the PI3K activity, as shown for example by blocking Akt activation using the PI3K inhibitor Wortmannin (James et al., 1996). Also, Akt was further shown to be activated during the process of Fcγ receptor-mediated phagocytosis (Ganesan et al., 2004).

A third protein family widely involved in cellular signal transduction pathways is the mitogen-activated protein kinase (MAPK) family. These kinases are also Ser/Thr protein kinases converting extracellular stimuli into a cellular response and they are involved in many physiological processes (Widmann et al., 1999). Examples for conventional MAPKs are the two MAPK isoforms ERK1 and ERK2 which can be activated by a number of different growth factors such as platelet-derived growth factor (PDGF) and epidermal growth factor (EGF) as well as in response to insulin, ligand binding on heteromeric G-protein coupled receptors (GPCR), cytokines, osmotic stress, and microtubule disorganization (Boulton et al., 1990; Raman et al., 2007).

ERK1/2 was shown to be activated during the process of Fcγ-mediated phagocytosis (Karimi and Lennartz, 1998; Fitzer-Attas et al., 2000). Interestingly, ERK1/2 was shown to be inhibited in the early phase of CR3-dependent bacterial phagocytosis as shown by infection of human macrophages with *Francisella tullarensis* (Dai et al., 2013).

The p38 kinases are a further sub-group of the MAPK family, which includes the p38 α, β, γ, and δ kinases. The p38 kinases are highly activated by cytokines and environmental stress and were shown to be critical for the regulation of immune and inflammatory processes (Cuenda and Rousseau, 2007). Bacterial binding to various TLRs initiates bacterial phagocytosis via signaling cascades involving amongst others p38 (Doyle et al., 2004).

A widely-used model cell line for the analysis of macrophage/pathogen interactions are the human monocytic THP-1 cells. The addition of phorbol 12-myristate 13-acetate (PMA) to the growth medium leads to the differentiation of monocytes into macrophage-like phagocytic cells. Due to their availability of Fc receptors, C3b receptors and various pattern recognition receptors, as well as the lack of surface and cytoplasmatic immunoglobulins, THP-1 cells can be used for immunocytochemical studies (Tsuchiya et al., 1980; Matsumoto et al., 1990).

In this study, the human pathogen *S. pneumoniae* and human THP-1cells were used to evaluate the role of the bacterial growth medium on phagocytosis, to study the time-dependent uptake of pneumococci and to visualize the intracellular fate over time within the macrophages. On the other hand Fcγ- and CR-independent signaling mechanisms during phagocytosis of *S. pneumoniae* in differentiated THP-1 cells were analyzed. Therefore, infection experiments in the presence of pharmacological inhibitors of actin polymerization, PI3K and Akt were carried out. Furthermore, cell lysates from different time points of infected THP-1 cells were analyzed by immunoblot analysis to identify the participation of important cellular protein kinases involved in cell signaling during pneumococcal phagocytosis.

MATERIALS AND METHODS

Bacterial Strains, Media, and Culture Conditions

Streptococcus pneumoniae NCTC 10319 (serotype 35A, low encapsulated) (Pracht et al., 2005) was grown in complex medium Todd-Hewitt broth (Oxoid) supplemented with 0.5% yeast extract (THY), defined chemical medium RPMI modified ($RPMI_{mod}$) (Schulz et al., 2014), or on blood agar plates (Oxoid) at 37°C and 5% CO_2.

Bacterial Growth Curves

Bacteria were plated from cryo cultures on blood agar (Columbia agar with sheep blood, Oxoid) and incubated at 37°C and 5% CO_2. THY medium or $RPMI_{mod}$ (40 ml in polypropylene tubes) was inoculated with freshly grown bacteria to an initial OD_{600} = 0.1–0.15 and incubated without agitation in a water bath at 37°C. Growth was monitored at appropriate time points by measuring absorbance at OD_{600} (BioPhotometer, Eppendorf).

Phagocytosis Experiments

Monocytic THP-1 cells were seeded in 24-well plates (2×10^5 cells per well in RPMI-1640 supplemented with 10% heat inactivated FCS in a volume of 1 ml) and differentiation was stimulated by the addition of 200 nmol/ml phorbol 12-myristate 13-acetate (PMA) (Sigma-Aldrich). Prior to infection THP-1 cells were incubated for 72 h at 37°C and 5% CO_2. Pneumococci cultured in $RPMI_{mod}$ to mid-log phase (OD_{600} = 0.35–0.45), were centrifuged and washed with infection medium (RPMI-1640, PAA) containing 1% heat inactivated fetal bovine serum (Gibco).

THP-1 cells were infected with *S. pneumoniae* using a multiplicity of infection (MOI) of 50 bacteria per phagocyte at 37°C and 5% CO_2 in infection medium. Bacteria were slightly centrifuged (2 min, 200 × g) onto the cells to initiate a simultaneous contact with phagocytes. Post infection, phagocytes were washed with infection medium and subsequently incubated with Penicillin G (100 units/ml, Sigma-Aldrich) and Gentamicin (0.1 mg/ml, Sigma-Aldrich) for 1 h at 37°C and 5% CO_2. After washing, the phagocytes were lysed using a 1% saponin solution. The colony forming units (cfu) of released intracellular pneumococci was determined by plating the bacteria in appropriate dilutions on blood agar plates (Hermans et al., 2006; Noske et al., 2009; Hartel et al., 2011).

Phagocytosis was also analyzed in the presence of the pharmacological inhibitors of PI3-kinase (Wortmannin, 50 nM and LY294002 50 μM, ENZO Life Sciences), Akt kinase (Akt-inhibitor VIII, 2.5 and 5 μM, Calbiochem), and actin polymerization (Cytochalasin D, 0.125 and 0.25 μM, ENZO Life Sciences).

Double Immunofluorescence Staining

Pneumococci attached to or phagocytosed by PMA-differentiated THP-1 cells were visualized by double immunofluorescence microscopy (DIF). Therefore, THP-1 cells (2×10^5) were seeded on sterile glass cover slips (12 mm, Hartenstein) and cultured at 37°C and 5% CO_2, 72 h prior to the infection (in the presence of 200 nmol/ml PMA) and infected as described above. Post-infection, THP-1 cells were washed with infection medium to remove unbound bacteria and then fixed with 1% paraformaldehyde (Roth). After blocking with 5% bovine serum albumin (BSA, Roth), extracellular bacteria were stained using a polyclonal anti-pneumococcal serum (1:200) and secondary goat anti-rabbit IgG coupled to Alexa-Fluor-488 (1:500, Abcam). Intracellular pneumococci were stained with Alexa-Fluor-568 goat anti-rabbit IgG (1:500, Abcam) after permeabilization of the THP-1 cells with 0.1% Triton-X-100 (Sigma) (10 min, room temperature) and pneumococcal antiserum as primary antibody (1:200). For the statistical analysis 100 cells per experiment and time point were analyzed for the number of intracellular bacteria.

SDS-Page and Immunoblotting

To analyze the phosphorylation status of selected host kinases during pneumococcal infection, cell lysates were prepared as followed. THP-1 cells (1×10^6) cells were seeded in 6-well plates in a volume of 2 ml/well. Cells were infected as described above and infection was stopped at different time-points by washing cells with ice-cold infection medium, following cell disruption by the addition of Triton-X-100 lysis buffer (10 mM TRIS, 100 mM NaCl, 1 mM EDTA, 1 mM EGTA, 1 mM NaF, 20 mM $Na_4P_2O_7$, 2 mM Na_3VO_4, 0.1% SDS, 1% Triton-X-100,

10% glycerin, 0.5% sodium deoxycholate) supplemented with a protease inhibitor (Complete®, Roche). Afterwards, plates were incubated on ice for 10 min followed by sonication (2 × 30 s). After centrifugation (18,234 × g, 10 min, 4°C) protein concentration of the supernatant was determined using the Bradford assay (Sigma) and stored at −20°C. Cell lysates (50 µg/sample) were separated by sodium dodecyl sulfate polyacrylamide gel electrophoresis (SDS-PAGE) on 12% gels. Proteins were transferred on a nitrocellulose membrane (GE Healthcare) by semi-dry blotting. After transfer, the membrane was blocked overnight at 4°C in TBS + 5% skim milk (Roth). Immunodetection was carried out using specific primary and horse radish peroxidase-(HRP)-conjugated secondary antibodies (listed in **Table 1**). A primary antibody against glycerinaldehyde-3-phosphate dehydrogenase (GAPDH) was used as a loading control. Luminol was used as substrate for HRP. Detection was carried out using a chemiluminescence-detecting camera (ChemoCam, INTAS).

Statistics and Quantitative Analysis of Immunoblots

All data are reported as the mean ± SD. Statistical analysis was performed with unpaired, two-tailed Student's *t*-test using GraphPad Prism® software v5.01. In all analyzes a $p < 0.05$ was considered statistically significant.

The image processing program ImageJ was used for quantificational analysis of immunoblots by densitometry (Girish and Vijayalakshmi, 2004; Schneider et al., 2012).

RESULTS

Influence of Bacterial Growth Medium on Pneumococcal Phagocytosis by THP-1 Cells

To assess the impact of the bacterial growth medium on pneumococcal phagocytosis by PMA-differentiated THP-1 cells, *S. pneumoniae* were grown in complex medium (THY) or chemically defined medium ($RPMI_{mod}$)prior to infection. The growth curves of *S. pneumoniae* in the different growth media (**Figure 1A**) showed a delayed growth in the chemically defined medium in comparison to the complex medium, which is probably due to the high adaptation of pneumococci to the overall nutrient availability in $RPMI_{mod}$. In consequence, pneumococci cultured in THY showed an earlier achievement of the stationary phase and a higher optical density.

Pneumococci used in infection assays were harvested from the exponential growth phase (OD_{600} = 0.35–0.45). PMA-differentiated THP-1 cells were infected for 1 h. The number of recovered intracellular surviving bacteria was determined by the antibiotic protection assay. The results revealed no significant influence of the bacterial growth medium on pneumococcal uptake by PMA-differentiated THP-1 (**Figures 1B,C**).

Kinetics of *S. pneumoniae* Phagocytosis by THP-1 Cells

In the results of the antibiotic protection assay a time-dependent increase of phagocytized pneumococci could be observed over time without saturation 90 min post infection (**Figure 2A**). In the complementary infection assay, adherent extracellular, and ingested intracellular pneumococci were visualized and illustrated using DIF-staining. Similar to the antibiotic protection assay, an increase of intracellular bacteria was monitored over time as shown by representative microscopic images (**Figure 2B**). The enumeration of intracellular bacteria in 100 infected THP-1 cells using immunofluorescence microscopy confirmed the results of the antibiotic protection assay. This approach also demonstrated a time-dependent increase of intracellular bacteria upon increasing infection times, without reaching saturation 90 min post-infection (**Figure 2C**).

Intracellular Fate of Phagocytized Pneumococci

The intracellular fate of *S. pneumoniae* after phagocytosis was analyzed in a time-dependent manner post-infection of THP-1 cells. Extracellular bacteria were killed after infection by the addition of antibiotics. The intracellular number of recovered, viable bacteria was determined after lysis of the THP-1 cells and plating of the bacteria on blood agar plates. The THP-1 cells

TABLE 1 | Antibodies used in this study.

Antibody	Dilution	MW [kDa]	Source	Company
Akt Antibody	1:500	60	Rabbit	Cell Signaling (#9272)
Phospho-Akt (Ser473)	1:500	60	Rabbit	Cell Signaling (#9271)
GAPDH polyclonal antibody	1:50,000	36	Goat	Abnova (#PAB6637)
p44/42 MAPK (ERK1/2) (137F5)	1:1000	42, 44	Rabbit	Cell Signaling (#4695)
Phospho-p44/42 MAPK (ERK1/2) (Thr202/Tyr204)	1:1000	42, 44	Rabbit	Cell Signaling (#9101)
P38 MAPK	1:1000	43	Rabbit	Cell Signaling (#9212)
Phospho-p38 MAPK (Thr180/Tyr182)	1:1000	43	Rabbit	Cell Signaling (#4511)
Goat Anti-Rabbit IgG (H+L) (Clone: pAb)-HRPO	1:500–1:2500	None	Goat	Dianova (#111-035-045)
Polyclonal Rabbit Anti-Goat IgG/HRP	1:2000	None	Rabbit	Dako (#P044901-2)
Goat Anti-Rabbit IgG H&L (Alexa Fluor® 488)	1:500	None	Goat	Abcam (#ab150077)
Goat Anti-Rabbit IgG H&L (Alexa Fluor® 568)	1:500	None	Goat	Abcam (#ab175471)

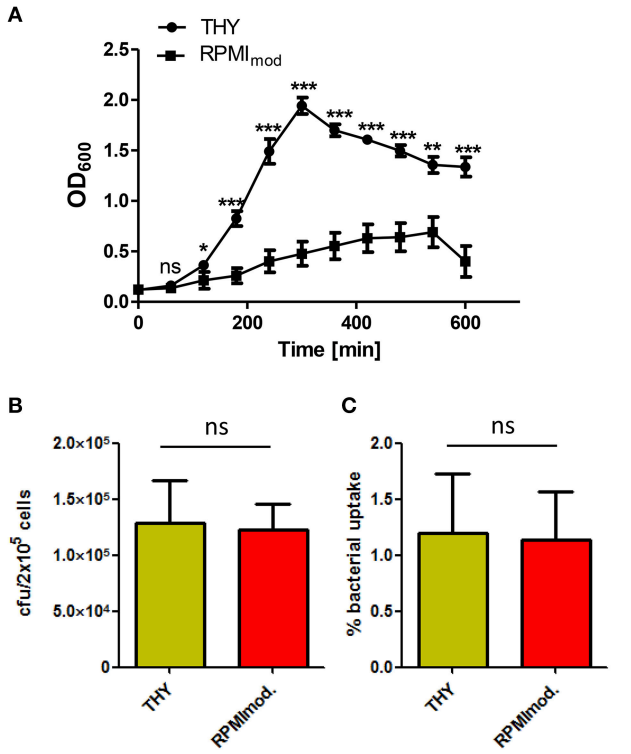

FIGURE 1 | Influence of the cultivation medium on pneumococcal phagocytosis. (A) Growth curves of *S. pneumoniae* 35A grown in complex medium (THY) or chemically defined medium (RPMI$_{mod.}$). The significance of the THY-medium is based on the difference to RPMI$_{mod}$. **(B,C)** Phagocytosis of *S. pneumoniae* 35A after growth in THY or RPMI$_{mod}$. PMA-differentiated THP-1 cells (2×10^5) were infected (30 min) with a pneumococcal MOI of 50 at 37°C and 5% CO_2. After infection, extracellular pneumococci were killed by the addition of Gentamycin and Penicillin G (incubation at 37°C and 5% CO_2 for 1 h). The number of intracellular bacteria was determined by plating cell lysates on blood agar and visualized as recovered cfu **(A)** or % bacterial uptake of the infection dose **(B)**. Values represent means ± SD of at least three independent experiments. ns = not significant, $p > 0.5$; *$p < 0.05$; **$p < 0.01$; ***$p < 0.001$.

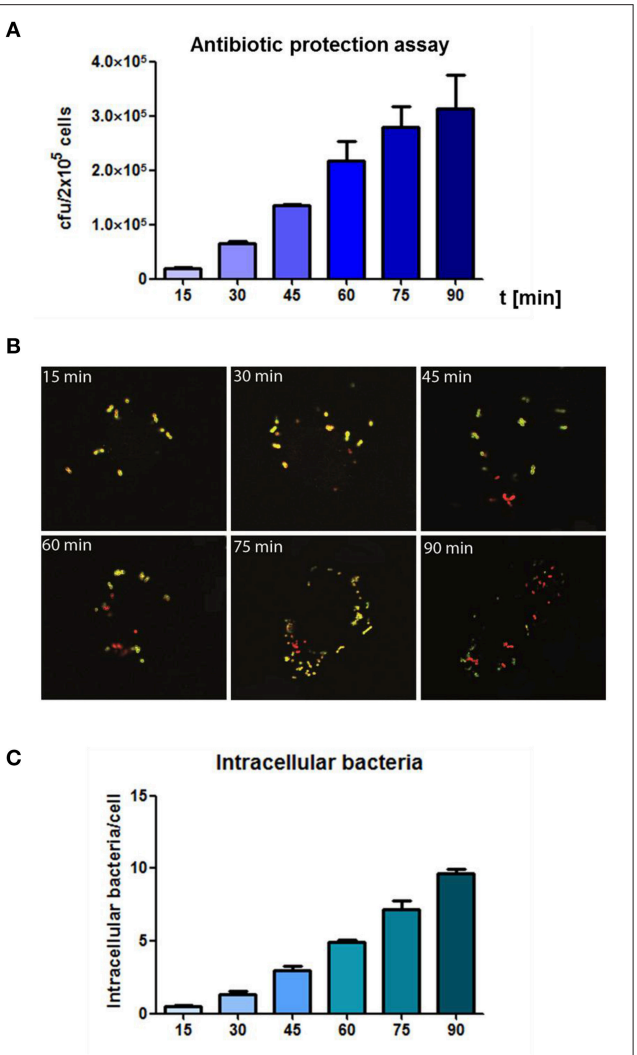

FIGURE 2 | Analysis of the time-dependent phagocytosis of *S. pneumoniae*. (A) Antibiotic protection assay: PMA-differentiated THP-1 cells (2×10^5) were infected with exponential grown *S. pneumoniae* 35A (MOI = 50). The infection was stopped at different time points (15–90 min) by adding of Penicillin G and Gentamicin. Intracellular recovered viable pneumococci were quantified after plating cell lysates on blood agar and enumeration of cfu. **(B)** Double immunofluorescence staining of THP-1 cells at different time-points of infection. Extracellular bacteria were stained using polyclonal anti-pneumococcal antiserum and Alexa-Fluor-488 labeled secondary antibody (green) and after permeabilization of cells with 0.1% Triton-X 100 intracellular bacteria (red) were stained using a polyclonal anti-pneumococcal antiserum and secondary Alexa-568-labeled antibody. **(C)** Intracellular pneumococci of 100 infected THP-1 cells on microscopic slides were counted (double immunofluorescence microscopy) at different time points of infection. Values represent means ± SD of at least three independent experiments.

showed a continuous killing of the engulfed pneumococci during the evaluation period as determined by a constant decrease of bacterial cfu over time (**Figure 3A**). Similar, the DIF-staining and fluorescence microscopy confirmed the results of the antibiotic protection assay (**Figures 3B,C**). Representative images and numbers of intracellular bacteria within infected THP-1 cells confirmed the decrease of intracellular pneumococci over the observed time period. Taken together, these results revealed an effective time-dependent intracellular killing of phagocytized pneumococci by THP-1 cells.

Inhibition of Pneumococcal Phagocytosis by Inhibitors of Central Host Cell Kinases

Phagocytosis and hence, the rearrangement of the host cell cytoskeleton requires most likely bacterial binding to cell surface receptors, followed by cell signaling through different protein kinases and finally activation of proteins involved in the reorganization of the cytoskeleton. To demonstrate the influence of actin polymerization during phagocytosis, infection experiments were carried out in the presence of Cytochalasin D (CytoD), a potent inhibitor of actin polymerization. PMA-differentiated THP-1 cells were infected with *S. pneumoniae* 35A in the presence of different concentrations of CytoD. DIF-staining and immunofluorescence microscopy were applied to visualize the effect of CytoD on the phagocytosis rate. The

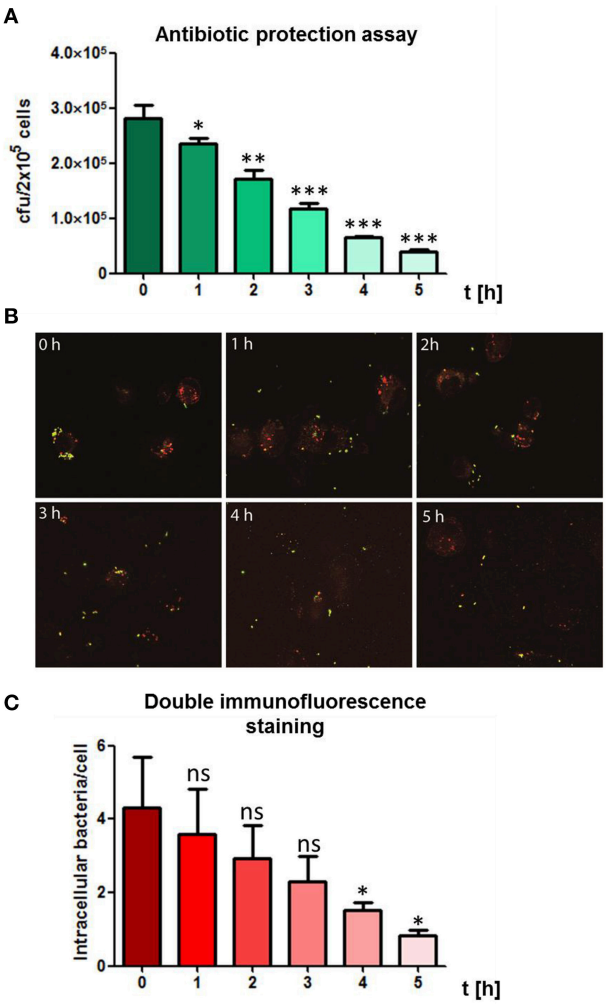

FIGURE 3 | Time-dependent killing of intracellular pneumococci. (A) To visualize the bacterial fate of intracellular bacteria, PMA-differentiated THP-1 cells (2×10^5) were infected with exponential grown *S. pneumoniae* 35A (MOI = 50) for 60 min at 37°C and 5% CO_2. Post infection, extracellular pneumococci were killed by the addition of Gentamycin and Penicillin and subsequently cells were incubated in infection medium. Living intracellular bacteria were quantified by plating cell lysates at different time points post-infection on blood agar. **(B)** Double immunofluorescence staining of infected THP-1 cells at different time-points post infection. Extracellular pneumococci appear in green and intracellular in red. **(C)** Intracellular pneumococci of 100 infected THP-1 cells on microscopic slides were counted after DIF-staining at different time points post-infection. Values represent means ± SD of at least three independent experiments. ns = not significant, $p > 0.5$; *$p < 0.05$; **$p < 0.01$; ***$p < 0.001$.

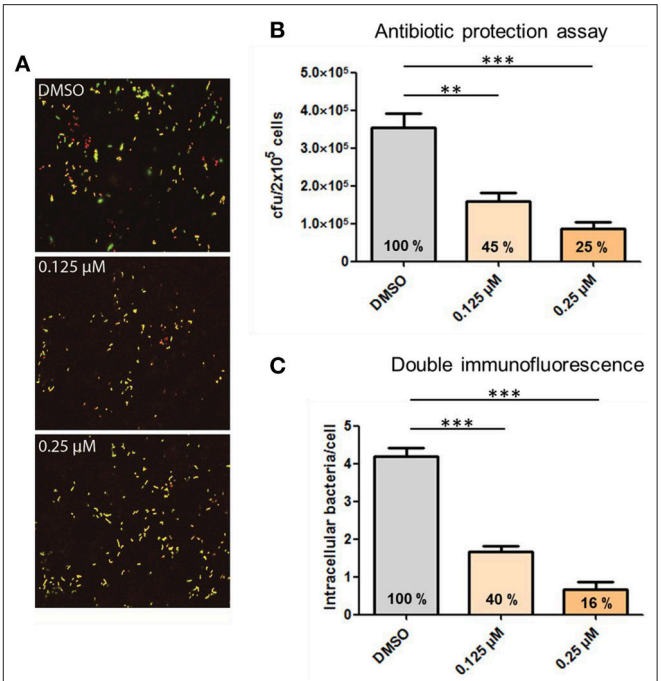

FIGURE 4 | Influence of the actin polymerization on pneumococcal phagocytosis. PMA-differentiated THP-1 cells (2×10^5) were infected for 1 h with exponentially grown *S. pneumoniae* 35A (MOI = 50) in the presence of the actin polymerization inhibitor Cytochalasin D (0.125, 0.25 µM). **(A)** Double immunofluorescence staining of THP-1 cells. Extracellular pneumococci appear in green and intracellular in red. **(B)** The number of intracellular recovered and surviving pneumococci cfu was determined using the antibiotic protection assay. **(C)** Intracellular pneumococci of 100 infected THP-1 cells on microscopic slides were enumerated after DIF-staining. Values represent means ± SD of at least three independent experiments. **$p < 0.01$; ***$p < 0.001$.

addition of increasing concentrations of CytoD resulted in a dose-dependent decline of intracellular pneumococci within the infected THP-1 cells (**Figure 4A**). To quantify ingested bacteria the number of intracellular bacteria was enumerated in infected cells by DIF-staining and subsequent immunofluorescence microscopy (**Figure 4C**). A significant, dose-dependent effect of CytoD on the phagocytosis rate (reduction of intracellular bacteria to 40 and 16%) was visible. These results were confirmed with an antibiotic protection assay where the amount of living extracellular bacteria significantly declined dose-dependently (45 and 25%) with increasing concentrations of CytoD (**Figure 4B**).

This experimental approach was further chosen to analyze the role of the protein kinases PI3K and Akt in the process of pneumococcal phagocytosis by THP-1 cells. The presence of the PI3K inhibitors Wortmannin and LY294002 resulted in a significant inhibition of pneumococcal uptake after 1 h of infection. The microscopic images of the DIF-stained infections (**Figure 5A**) and counted bacteria within the THP-1 cells (**Figure 5C**) showed a significant decrease of intracellular bacteria (33 and 30%) compared to the control cells treated only with DMSO. These results were comparable to the results obtained in the complementary antibiotic protection assay (**Figure 5B**). To analyze the role of the protein kinase Akt, different concentrations of the Akt inhibitor VIII were used during pneumococcal infection of THP-1 cells. The results of the antibiotic protection assay (**Figure 6A**) in the presence of Akt inhibitor VIII revealed a dose-dependent decrease of viable intracellular pneumococci (66 and 39%) with increasing concentrations of the inhibitor. Taken together, these results reflect the essential role of actin polymerization and the involvement of the protein kinases PI3K and Akt in the Fcγ

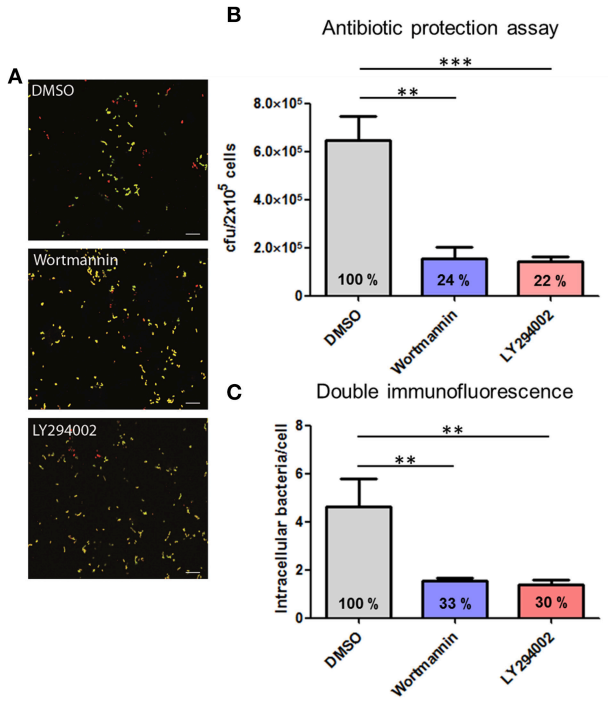

FIGURE 5 | Influence of the pharmacological inhibitors Wortmannin and LY294002 of the PI3K on pneumococcal phagocytosis. PMA-differentiated THP-1 cells (2×10^5) were infected for 1 h with exponential grown *S. pneumoniae* 35A in the presence or absence of the PI3K inhibitor Wortmannin (50 nM) or LY294002 (50 μM). **(A)** Double immunofluorescence staining of THP-1 cells. Extracellular pneumococci appear in green and intracellular in red. **(B)** Intracellular cfu was determined by the antibiotic protection assay and intracellular cfu was determined by plating cell lysates on blood agar. **(C)** Intracellular pneumococci of 100 infected THP-1 cells on microscopic slides were counted after DIF-staining. Values represent means ± SD of at least three independent experiments. $^{**}p < 0.01$; $^{***}p < 0.001$.

and CR-independent phagocytosis of *S. pneumoniae* through PMA-differentiated THP-1 cells.

Time-Dependent Phosphorylation of Selected Protein Kinases during Bacterial Phagocytosis

To evaluate the involvement and time-dependent phosphorylation of various protein kinases during pneumococcal infection, PMA-differentiated THP-1 cells were infected with *S. pneumoniae* for different time periods. Cell lysates were used for SDS-PAGE and immunoblot analysis with specific antibodies against phosphorylated and non-phosphorylated forms of different protein kinases (**Table 1**). The inhibition of Akt in the presence of Akt inhibitor VIII was already demonstrated to be involved in pneumococcal uptake as shown by an antibiotic protection assay (**Figure 6A**). The immunoblots of Akt/pAkt indicated an increase in Akt phosphorylation 10 min post infection with the highest amount after 20 min (**Figure 6B**). A densitometric approach was chosen to quantify the obtained results from the immunoblot. The analysis reflects thereby the observed increase of the phosphorylated form of Akt as shown in **Figures 6 C,D**. Moreover, the phosphorylation of the MAPKs ERK1/2 and p38 during pneumococcal uptake was analyzed (**Figure 7**). Here the amount of phosphorylated ERK1/2 (pERK1/2) starts to increase 20 min post-infection, whereas the amount of phosphorylated p38 (pp38) increases already after 5 min post-infection.

DISCUSSION

The innate immune system comprises an enormous arsenal of defense strategies to recognize and eliminate foreign microbes, colonizing or invading the human body. These include amongst others physical barriers like epithelia and mucus, secreted enzymes, antimicrobial peptides, and phagocytes (Someya et al., 2013; Sperandio et al., 2015). A critical function of the immune system is the detection and elimination of invading microbes in normally sterile compartments of the human body. In such a case, professional phagocytes recognize microbes amongst others via PRRs, triggering intracellular signal cascades leading in the end to engulfment and elimination of foreign intruders (Silva, 2010).

In this study, we investigated the interaction of pneumococci with macrophage-like, PMA-differentiated THP-1 cells in the absence of human antibodies or complement. This approach allowed us to analyze the host cell response independently of Fcγ or CR-mediated phagocytosis pathways.

Pneumococci have to adapt to various environmental conditions, including nutrient availability, during colonization of mucosal surfaces in humans and invasive infections. Changes in the nutrient composition or availability results in an alteration of intracellular metabolites, influencing regulatory networks and as a consequence gene expression and protein production (Orihuela et al., 2004; Tang, 2011; Schulz and Hammerschmidt, 2013). Pneumococcal growth in a chemically defined medium reflects much more the *in vivo* situation, in which certain nutrients and/or carbon sources are limited. As shown in the pneumococcal growth curves (**Figure 1A**), growth was indeed affected due to the limitation of several nutrients. Interestingly, no difference in bacterial uptake through THP-1 cells could be observed using chemically defined ($RPMI_{mod}$) or complex medium (THY). This indicates that the composition of surface-exposed bacterial structures necessary for the recognition and uptake of *S. pneumonia* by THP-1 cells are not substantially changed or reduced due to the composition of the chosen growth media.

Kinetics of pneumococcal phagocytosis by THP-1 cells were analyzed by DIF-staining and subsequent fluorescence microscopy. With this approach, all intracellular bacteria can be visualized, while no differentiation between living and non-viable bacteria is possible. First intracellular pneumococci within THP-1 cells were detected after 15–30 min of infection. The monitored pneumococcal internalization happened in the same time-frame as carried out with other bacteria like *S. aureus* and THP-1 cells (Miller et al., 2011). A saturation in pneumococcal uptake was not observed within the analyzed time period (15–90 min), suggesting a higher capacity of THP-1 cells to take up bacteria.

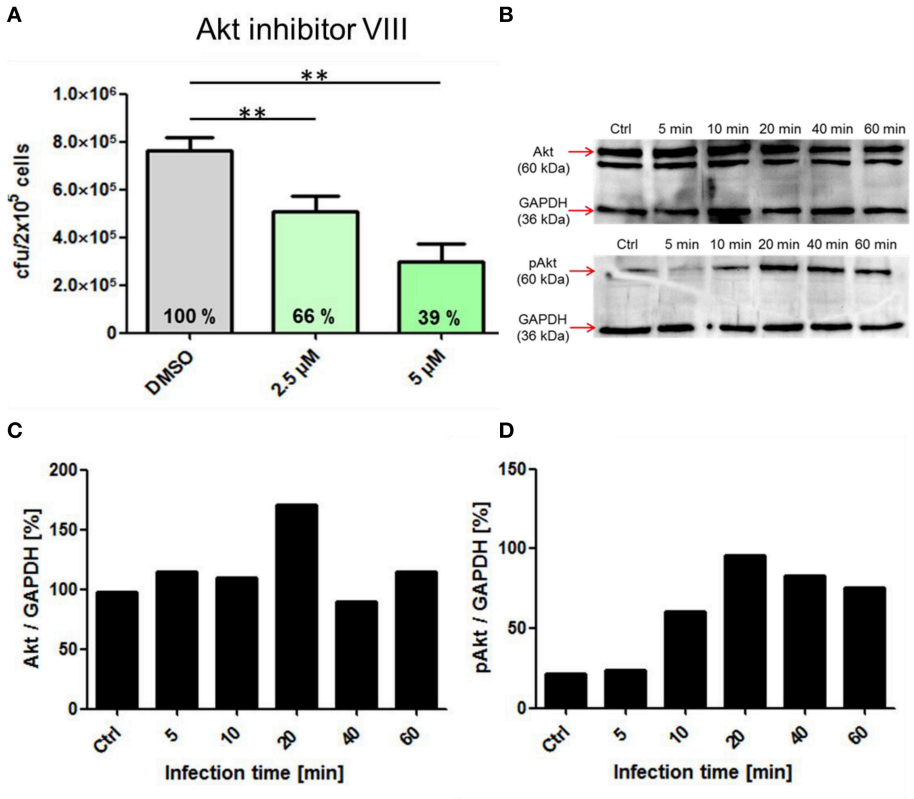

FIGURE 6 | Influence of the pharmacological Inhibitor Akt inhibitor VIII on pneumococcal phagocytosis and cell signaling. (A) Intracellular cfu was determined after infection of PMA-differentiated THP-cells (2×10^5) with *S. pneumoniae* 35A in the presence of Akt inhibitor VIII (2.5, 5 μM or DMSO as control) using the antibiotic protection assay and subsequent plating of bacteria on blood agar. **(B)** Immunoblot analysis of total Akt and pAkt. Cell lysates of different time points post-infection (5 to 60 min, Ctrl = uninfected cells) separated using SDS-PAGE and immunoblot analysis. GAPDH was used as a loading control. **(C,D)** Densitometric quantification of total Akt and pAkt in relation to GAPDH by ImageJ. Values of **Figure 4A** represent means ± SD of at least three independent experiments. $^{**}p < 0.01$.

A major virulence factor of *S. pneumoniae* is the polysaccharide capsule protecting the bacteria from phagocytosis (Wood et al., 1946). In our experimental approach, the low encapsulated strain 35A was chosen to facilitate recognition of surface exposed PAMPs by macrophage PRRs. Intracellular killing of bacteria in macrophages takes place in the phagolysosome via proteases, antimicrobial peptides and reactive oxygen and nitrogen species (Garin et al., 2001). Whereas, several bacterial species evolved strategies to survive or escape from phagolysosomes, such mechanisms are unknown for pneumococci. However, it was shown that during pneumococcal phagocytosis by dendritic cells, a minor proportion of the pneumococci escape from the intracellular vacuoles and resides in the cytosol (Noske et al., 2009). The reason or mechanisms for the pneumococcal escape from phagosomes is unknown. For experiments regarding the intracellular fate of the phagocytized pneumococci during infection, one time point was chosen. Pneumococci phagocytized after 1 h of infection were nearly completely killed within 5 h post-infection in a time-dependent manner, demonstrating the inability of *S. pneumoniae* 35A to survive within the macrophages. However, a minor amount of remaining intracellular pneumococcal cfu 5 h post-infection could be explained with the outbreak of some of the pneumococci from macrophage phagosomes into the cytoplasm.

The participation of the actin machinery and central cellular protein kinases involved in intracellular signaling pathways was analyzed by pneumococcal infection assays in the presence of specific pharmacological inhibitors and immunoblot analysis of THP-1 cell lysates from different time points of infection. The engulfment of pneumococci into phagosomes requires the recognition of the bacteria via surface receptors on THP1-cells, activation of signal cascades and in the end remodeling of the cytoskeleton. The inhibition of actin polymerization by Cytochalasin D during phagocytosis leads in the conducted experiments to a dose-dependent reduction of pneumococcal uptake up to 75%. These results underline the essential function of cytoskeleton rearrangement in pneumococcal phagocytosis by PMA-differentiated THP-1 cells.

The PI3K is an essential regulator of phagocytosis as shown for Fcγ and CR-mediated phagocytosis (Araki et al., 1996; Cox et al., 1999). The enzyme catalyzes after activation the phosphorylation of phosphatidylinositol 4,5-bisphosphate (PIP2) to phosphatidylinositol 3,4,5-trisphosphate (PIP3) (Domin and Waterfield, 1997). PIP3 was shown to be a key player in signaling

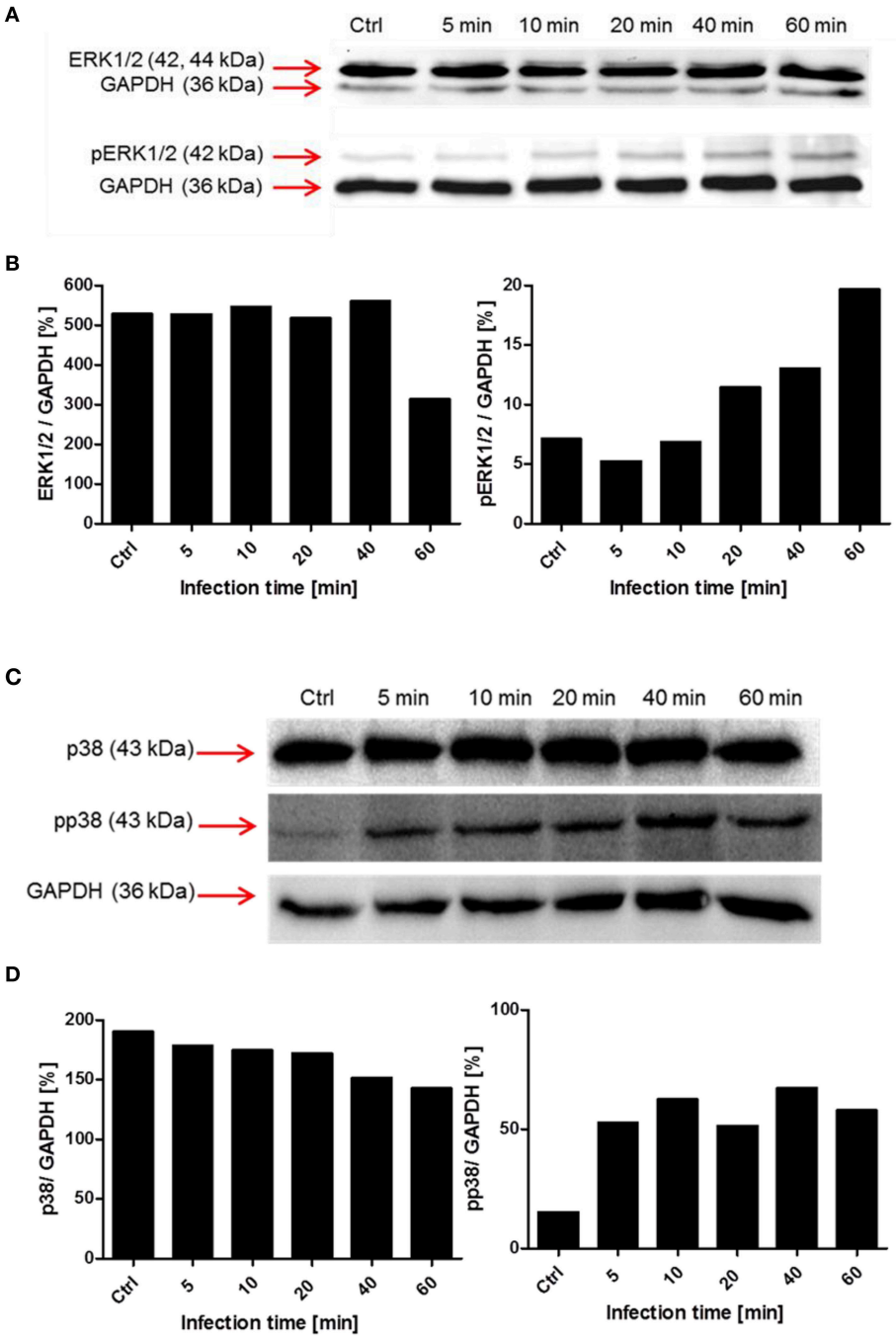

FIGURE 7 | Time-dependent phosphorylation of mitogen-activated protein kinases during pneumococcal uptake. Cell lysates of different time points post-infection (5–60 min, Ctrl = uninfected cells) were analyzed using SDS-PAGE and subsequent immunoblot analysis (antibodies used are listed in **Table 1**). GAPDH was used as a loading control. **(A,B)** Immunoblot analysis and densitometric analysis of ERK1/2 and phosphorylated ERK1/2 (pERK1/2) **(C,D)** Immunoblot and densitometric analysis of p38 and phosphorylated p38 (pp38).

pathways controlling phagocytosis (Gerisch et al., 2009). The activation of the PI3K can, besides others, also occur via PRRs as shown for various TLRs (Arbibe et al., 2000; Monick et al., 2001). Also in our experiments, using non-opsonized pneumococci, inhibition of the PI3K by the pharmacological inhibitors Wortmannin or LY294002 leads to strong decrease in pneumococcal phagocytosis. The protein kinase B (Akt) is one of the major signal transducers, activated by PIP3 of the PI3K (Chan et al., 1999). After 10 min of pneumococcal infection, the amount of phosphorylated Akt started to increase, with a maximum

20 min post-infection (**Figure 4B**). Inhibition of Akt by Akt inhibitor VIII led to a dose-dependent decrease of phagocytized pneumococci within the THP-1 cells. First intracellular bacteria where observed after 15–30 min after infection, which is in concert with the activation of Akt after 10 min, which in turn leads to activation of proteins involved in cytoskeleton rearrangement and therefore engulfment of the pneumococci.

Besides the activation of the PI3K and Akt, we were interested in the activation of the mitogen activated kinases ERK1/2 and p38. The infection of THP-1 cells with *S. pneumoniae* resulted in an increase of pERK1/2 20 min post-infection, without saturation after 60 min. The downstream substrates of ERK1/2 includes amongst others transcription factors, kinases, and cytoskeletal proteins (Yoon and Seger, 2006) involved in proliferation, differentiation, and activation of macrophages (Rao, 2001). Further investigations are needed here, especially with a focus on the role of ERK1/2 in the induction of cytokines during phagocytosis. The second MAPK we focused on is p38. This kinase was shown to be activated by several external stimuli like TNF-α, heat, osmotic shock, or growth factors (Freshney et al., 1994; Rouse et al., 1994). Doyle et al. proposed a model in which the activation of TLRs in macrophages leads amongst others to the activation of p38 resulting in the upregulation of scavenger receptors like MARCO and therefore enhanced phagocytosis (Doyle et al., 2004). In our experiments, the phosphorylation of p38 started within the first 5 min post-infection indicating an important role in the early phase of pneumococcal phagocytosis.

The activation of the aforementioned kinases during pneumococcal infection seems not to be restricted to professional phagocytes. Pneumococci were shown to interact with the cellular polymeric immunoglobulin receptor (pIgR) of respiratory epithelial cells via the pneumococcal surface protein C (PspC). The modulated signaling cascades resulting in uptake of the bacteria involves amongst others the PI3K, Akt, and the MAPKs ERK1/2 (Agarwal and Hammerschmidt, 2009; Agarwal et al., 2010). Furthermore, pneumococci were shown to be taken up by human epithelial pharyngeal cells (Detroit 562) exploiting vitronectin as a bridging molecule to interact with $\alpha_v\beta_3$ integrins. In addition to the integrin linked kinase (ILK) the PI3K plays an essential role in pneumococcal endocytosis via the vitronectin mechanism (Bergmann et al., 2009).

The analysis of further signaling cascades like the JNK, Src, and focal adhesion kinases is necessary to gain deeper insights into signaling events triggered by pneumococci during phagocytosis.

Moreover, pneumococcal infection of macrophages was shown to contribute to apoptosis (Ulett and Adderson, 2006). Therefore, it could be of great interest to analyze the participation of pneumococcal triggered cell signaling pathways on the induction of apoptosis.

Taken together, we used the model of PMA-differentiated THP-1 cells to characterize the interaction of *S. pneumoniae* with professional phagocytes. The relevance of the bacterial growth medium on phagocytosis as well as the time-dependent uptake and killing was demonstrated. Furthermore, insights into cell signaling processes during bacterial uptake were deciphered by using pharmacological inhibitors and performing immunoblot analysis.

AUTHOR CONTRIBUTIONS

TK was writing the paper and performed experiments. TK was the supervisor of AS. AS executed experiments, DK executed experiments, SH was writing the paper, supervisor of DK, project leader.

ACKNOWLEDGMENTS

We thank Peggy Stremlow for excellent technical assistance. This work was supported by Deutsche Forschungsgemeinschaft Grant DFG HA 3125/4-2.

REFERENCES

Aderem, A. (2003). Phagocytosis and the inflammatory response. *J. Infect. Dis.*187(Suppl. 2), S340–S345. doi: 10.1086/374747

Agarwal, V., Asmat, T. M., Dierdorf, N. I., Hauck, C. R., and Hammerschmidt, S. (2010). Polymeric immunoglobulin receptor-mediated invasion of *Streptococcus pneumoniae* into host cells requires a coordinate signaling of SRC family of protein-tyrosine kinases, ERK, and c-Jun N-terminal kinase. *J. Biol. Chem.* 285, 35615–35623. doi: 10.1074/jbc.M110.172999

Agarwal, V., and Hammerschmidt, S. (2009). Cdc42 and the phosphatidylinositol 3-kinase-Akt pathway are essential for PspC-mediated internalization of pneumococci by respiratory epithelial cells. *J. Biol. Chem.* 284, 19427–19436. doi: 10.1074/jbc.M109.003442

Araki, N., Johnson, M. T., and Swanson, J. A. (1996). A role for phosphoinositide 3-kinase in the completion of macropinocytosis and phagocytosis by macrophages. *J. Cell Biol.* 135, 1249–1260. doi: 10.1083/jcb.135.5.1249

Arbibe, L., Mira, J. P., Teusch, N., Kline, L., Guha, M., Mackman, N., et al. (2000). Toll-like receptor 2-mediated NF-kappa B activation requires a Rac1-dependent pathway. *Nat. Immunol.* 1, 533–540. doi: 10.1038/82797

Arredouani, M., Yang, Z., Ning, Y., Qin, G., Soininen, R., Tryggvason, K., et al. (2004). The scavenger receptor MARCO is required for lung defense against pneumococcal pneumonia and inhaled particles. *J. Exp. Med.* 200, 267–272. doi: 10.1084/jem.20040731

Bergmann, S., Lang, A., Rohde, M., Agarwal, V., Rennemeier, C., Grashoff, C., et al. (2009). Integrin-linked kinase is required for vitronectin-mediated internalization of *Streptococcus pneumoniae* by host cells. *J. Cell Sci.* 122, 256–267. doi: 10.1242/jcs.035600

Bogaert, D., De Groot, R., and Hermans, P. W. (2004a). *Streptococcus pneumoniae* colonisation: the key to pneumococcal disease. *Lancet Infect. Dis.* 4, 144–154. doi: 10.1016/S1473-3099(04)00938-7

Bogaert, D., van Belkum, A., Sluijter, M., Luijendijk, A., de Groot, R., Rumke, H. C., et al. (2004b). Colonisation by *Streptococcus pneumoniae* and *Staphylococcus aureus* in healthy children. *Lancet* 363, 1871–1872. doi: 10.1016/S0140-6736(04)16357-5

Boulton, T. G., Yancopoulos, G. D., Gregory, J. S., Slaughter, C., Moomaw, C., Hsu, J., et al. (1990). An insulin-stimulated protein kinase similar to yeast kinases involved in cell cycle control. *Science* 249, 64–67. doi: 10.1126/science.2164259

Chan, T. O., Rittenhouse, S. E., and Tsichlis, P. N. (1999). AKT/PKB and other D3 phosphoinositide-regulated kinases: kinase activation by phosphoinositide-dependent phosphorylation. *Annu. Rev. Biochem.* 68, 965–1014. doi: 10.1146/annurev.biochem.68.1.965

Cox, D., Tseng, C. C., Bjekic, G., and Greenberg, S. (1999). A requirement for phosphatidylinositol 3-kinase in pseudopod extension. *J. Biol. Chem.* 274, 1240–1247. doi: 10.1074/jbc.274.3.1240

Cuenda, A., and Rousseau, S. (2007). p38 MAP-kinases pathway regulation, function and role in human diseases. *Biochim. Biophys. Acta* 1773, 1358–1375. doi: 10.1016/j.bbamcr.2007.03.010

Currie, A. J., Davidson, D. J., Reid, G. S., Bharya, S., MacDonald, K. L., Devon, R. S., et al. (2004). Primary immunodeficiency to pneumococcal infection due to a defect in Toll-like receptor signaling. *J. Pediatr.* 144, 512–518. doi: 10.1016/j.jpeds.2003.10.034

Dai, S., Rajaram, M. V., Curry, H. M., Leander, R., and Schlesinger, L. S. (2013). Fine tuning inflammation at the front door: macrophage complement receptor 3-mediates phagocytosis and immune suppression for *Francisella tularensis*. *PLoS Pathog.* 9:e1003114. doi: 10.1371/journal.ppat.1003114

del Peso, L., Gonzalez-Garcia, M., Page, C., Herrera, R., and Nunez, G. (1997). Interleukin-3-induced phosphorylation of BAD through the protein kinase Akt. *Science* 278, 687–689. doi: 10.1126/science.278.5338.687

Domin, J., and Waterfield, M. D. (1997). Using structure to define the function of phosphoinositide 3-kinase family members. *FEBS Lett.* 410, 91–95. doi: 10.1016/S0014-5793(97)00617-0

Doyle, S. E., O'Connell, R. M., Miranda, G. A., Vaidya, S. A., Chow, E. K., Liu, P. T., et al. (2004). Toll-like receptors induce a phagocytic gene program through p38. *J. Exp. Med.* 199, 81–90. doi: 10.1084/jem.20031237

Echchannaoui, H., Frei, K., Letiembre, M., Strieter, R. M., Adachi, Y., and Landmann, R. (2005). CD14 deficiency leads to increased MIP-2 production, CXCR2 expression, neutrophil transmigration, and early death in pneumococcal infection. *J. Leukoc. Biol.* 78, 705–715. doi: 10.1189/jlb.0205063

Engelman, J. A., Luo, J., and Cantley, L. C. (2006). The evolution of phosphatidylinositol 3-kinases as regulators of growth and metabolism. *Nat. Rev. Genet.* 7, 606–619. doi: 10.1038/nrg1879

Feldman, C., Cockeran, R., Jedrzejas, M. J., Mitchell, T. J., and Anderson, R. (2007). Hyaluronidase augments pneumolysin-mediated injury to human ciliated epithelium. *Int. J. Infect. Dis.* 11, 11–15. doi: 10.1016/j.ijid.2005.09.002

Fitzer-Attas, C. J., Lowry, M., Crowley, M. T., Finn, A. J., Meng, F., DeFranco, A. L., et al. (2000). Fcgamma receptor-mediated phagocytosis in macrophages lacking the Src family tyrosine kinases Hck, Fgr, and Lyn. *J. Exp. Med.* 191, 669–682. doi: 10.1084/jem.191.4.669

Freeman, S. A., and Grinstein, S. (2014). Phagocytosis: receptors, signal integration, and the cytoskeleton. *Immunol. Rev.* 262, 193–215. doi: 10.1111/imr.12212

Freshney, N. W., Rawlinson, L., Guesdon, F., Jones, E., Cowley, S., Hsuan, J., et al. (1994). Interleukin-1 activates a novel protein kinase cascade that results in the phosphorylation of Hsp27. *Cell* 78, 1039–1049. doi: 10.1016/0092-8674(94)90278-X

Gamez, G., and Hammerschmidt, S. (2012). Combat pneumococcal infections: adhesins as candidates for protein-based vaccine development. *Curr. Drug Targets* 13, 323–337. doi: 10.2174/138945012799424697

Ganesan, L. P., Wei, G., Pengal, R. A., Moldovan, L., Moldovan, N., Ostrowski, M. C., et al. (2004). The serine/threonine kinase Akt Promotes Fc gamma receptor-mediated phagocytosis in murine macrophages through the activation of p70S6 kinase. *J. Biol. Chem.* 279, 54416–54425. doi: 10.1074/jbc.M408188200

Garenne, M., Ronsmans, C., and Campbell, H. (1992). The magnitude of mortality from acute respiratory infections in children under 5 years in developing countries. *World Health Stat. Q.* 45, 180–191.

Garin, J., Diez, R., Kieffer, S., Dermine, J. F., Duclos, S., Gagnon, E., et al. (2001). The phagosome proteome: insight into phagosome functions. *J. Cell Biol.* 152, 165–180. doi: 10.1083/jcb.152.1.165

Gerisch, G., Ecke, M., Schroth-Diez, B., Gerwig, S., Engel, U., Maddera, L., et al. (2009). Self-organizing actin waves as planar phagocytic cup structures. *Cell Adh. Migr.* 3, 373–382. doi: 10.4161/cam.3.4.9708

Ghiran, I., Barbashov, S. F., Klickstein, L. B., Tas, S. W., Jensenius, J. C., and Nicholson-Weller, A. (2000). Complement receptor 1/CD35 is a receptor for mannan-binding lectin. *J. Exp. Med.* 192, 1797–1808. doi: 10.1084/jem.192.12.1797

Girish, V., and Vijayalakshmi, A. (2004). Affordable image analysis using NIH Image/ImageJ. *Indian J. Cancer* 41, 47.

Gomez, F., Ruiz, P., and Schreiber, A. D. (1994). Impaired function of macrophage Fc gamma receptors and bacterial infection in alcoholic cirrhosis. *N. Engl. J. Med.* 331, 1122–1128. doi: 10.1056/NEJM199410273311704

Greenberg, S., and Grinstein, S. (2002). Phagocytosis and innate immunity. *Curr. Opin. Immunol.* 14, 136–145. doi: 10.1016/S0952-7915(01)00309-0

Hartel, T., Klein, M., Koedel, U., Rohde, M., Petruschka, L., and Hammerschmidt, S. (2011). Impact of glutamine transporters on pneumococcal fitness under infection-related conditions. *Infect. Immun.* 79, 44–58. doi: 10.1128/IAI.00855-10

Hawkins, P. T., Eguinoa, A., Qiu, R. G., Stokoe, D., Cooke, F. T., Walters, R., et al. (1995). PDGF stimulates an increase in GTP-Rac via activation of phosphoinositide 3-kinase. *Curr. Biol.* 5, 393–403. doi: 10.1016/S0960-9822(95)00080-7

Hermans, P. W., Adrian, P. V., Albert, C., Estevao, S., Hoogenboezem, T., Luijendijk, I. H., et al. (2006). The streptococcal lipoprotein rotamase A (SlrA) is a functional peptidyl-prolyl isomerase involved in pneumococcal colonization. *J. Biol. Chem.* 281, 968–976. doi: 10.1074/jbc.M510014200

Hussain, M., Melegaro, A., Pebody, R. G., George, R., Edmunds, W. J., Talukdar, R., et al. (2005). A longitudinal household study of *Streptococcus pneumoniae* nasopharyngeal carriage in a UK setting. *Epidemiol. Infect.* 133, 891–898. doi: 10.1017/S0950268805004012

Iwasaki, A., and Medzhitov, R. (2015). Control of adaptive immunity by the innate immune system. *Nat. Immunol.* 16, 343–353. doi: 10.1038/ni.3123

James, S. R., Downes, C. P., Gigg, R., Grove, S. J., Holmes, A. B., and Alessi, D. R. (1996). Specific binding of the Akt-1 protein kinase to phosphatidylinositol 3,4,5-trisphosphate without subsequent activation. *Biochem. J.* 315(Pt 3), 709–713. doi: 10.1042/bj3150709

Janeway, C. A. Jr., and Medzhitov, R. (2002). Innate immune recognition. *Annu. Rev. Immunol.* 20, 197–216. doi: 10.1146/annurev.immunol.20.083001.084359

Jonsson, S., Musher, D. M., Chapman, A., Goree, A., and Lawrence, E. C. (1985). Phagocytosis and killing of common bacterial pathogens of the lung by human alveolar macrophages. *J. Infect. Dis.* 152, 4–13. doi: 10.1093/infdis/152.1.4

Kang, Y. S., Kim, J. Y., Bruening, S. A., Pack, M., Charalambous, A., Pritsker, A., et al. (2004). The C-type lectin SIGN-R1 mediates uptake of the capsular polysaccharide of *Streptococcus pneumoniae* in the marginal zone of mouse spleen. *Proc. Natl. Acad. Sci. U.S.A.* 101, 215–220. doi: 10.1073/pnas.0307124101

Karimi, K., and Lennartz, M. R. (1998). Mitogen-activated protein kinase is activated during IgG-mediated phagocytosis, but is not required for target ingestion. *Inflammation* 22, 67–82. doi: 10.1023/A:1022347808042

Katso, R., Okkenhaug, K., Ahmadi, K., White, S., Timms, J., and Waterfield, M. D. (2001). Cellular function of phosphoinositide 3-kinases: implications for development, homeostasis, and cancer. *Annu. Rev. Cell Dev. Biol.* 17, 615–675. doi: 10.1146/annurev.cellbio.17.1.615

Kelly, S. J., and Jedrzejas, M. J. (2000). Structure and molecular mechanism of a functional form of pneumolysin: a cholesterol-dependent cytolysin from *Streptococcus pneumoniae*. *J. Struct. Biol.* 132, 72–81. doi: 10.1006/jsbi.2000.4308

Malley, R., Trzcinski, K., Srivastava, A., Thompson, C. M., Anderson, P. W., and Lipsitch, M. (2005). CD4+ T cells mediate antibody-independent acquired immunity to pneumococcal colonization. *Proc. Natl. Acad. Sci. U.S.A.* 102, 4848–4853. doi: 10.1073/pnas.0501254102

Manning, B. D., and Cantley, L. C. (2007). AKT/PKB signaling: navigating downstream. *Cell* 129, 1261–1274. doi: 10.1016/j.cell.2007.06.009

Matsumoto, A., Naito, M., Itakura, H., Ikemoto, S., Asaoka, H., Hayakawa, I., et al. (1990). Human macrophage scavenger receptors: primary structure, expression, and localization in atherosclerotic lesions. *Proc. Natl. Acad. Sci. U.S.A.* 87, 9133–9137. doi: 10.1073/pnas.87.23.9133

Miller, M., Dreisbach, A., Otto, A., Becher, D., Bernhardt, J., Hecker, M., et al. (2011). Mapping of interactions between human macrophages and *Staphylococcus aureus* reveals an involvement of MAP kinase signaling in the host defense. *J. Proteome Res.* 10, 4018–4032. doi: 10.1021/pr200224x

Mitchell, A. M., and Mitchell, T. J. (2010). *Streptococcus pneumoniae*: virulence factors and variation. *Clin. Microbiol. Infect.* 16, 411–418. doi: 10.1111/j.1469-0691.2010.03183.x

Mold, C., Rodic-Polic, B., and Du Clos, T. W. (2002). Protection from *Streptococcus pneumoniae* infection by C-reactive protein and natural antibody requires

complement but not Fc gamma receptors. *J. Immunol.* 168, 6375–6381. doi: 10.4049/jimmunol.168.12.6375

Monick, M. M., Carter, A. B., Robeff, P. K., Flaherty, D. M., Peterson, M. W., and Hunninghake, G. W. (2001). Lipopolysaccharide activates Akt in human alveolar macrophages resulting in nuclear accumulation and transcriptional activity of beta-catenin. *J. Immunol.* 166, 4713–4720. doi: 10.4049/jimmunol.166.7.4713

Noske, N., Kammerer, U., Rohde, M., and Hammerschmidt, S. (2009). Pneumococcal interaction with human dendritic cells: phagocytosis, survival, and induced adaptive immune response are manipulated by PavA. *J. Immunol.* 183, 1952–1963. doi: 10.4049/jimmunol.0804383

Orihuela, C. J., Radin, J. N., Sublett, J. E., Gao, G., Kaushal, D., and Tuomanen, E. I. (2004). Microarray analysis of pneumococcal gene expression during invasive disease. *Infect. Immun.* 72, 5582–5596. doi: 10.1128/IAI.72.10.5582-5596.2004

Pracht, D., Elm, C., Gerber, J., Bergmann, S., Rohde, M., Seiler, M., et al. (2005). PavA of *Streptococcus pneumoniae* modulates adherence, invasion, and meningeal inflammation. *Infect. Immun.* 73, 2680–2689. doi: 10.1128/IAI.73.5.2680-2689.2005

Raman, M., Chen, W., and Cobb, M. H. (2007). Differential regulation and properties of MAPKs. *Oncogene* 26, 3100–3112. doi: 10.1038/sj.onc.1210392

Rao, K. M. (2001). MAP kinase activation in macrophages. *J. Leukoc. Biol.* 69, 3–10.

Ravetch, J. V. (1997). Fc receptors. *Curr. Opin. Immunol.* 9, 121–125. doi: 10.1016/S0952-7915(97)80168-9

Rouse, J., Cohen, P., Trigon, S., Morange, M., Alonso-Llamazares, A., Zamanillo, D., et al. (1994). A novel kinase cascade triggered by stress and heat shock that stimulates MAPKAP kinase-2 and phosphorylation of the small heat shock proteins. *Cell* 78, 1027–1037. doi: 10.1016/0092-8674(94)90277-1

Schneider, C. A., Rasband, W. S., and Eliceiri, K. W. (2012). NIH Image to ImageJ: 25 years of image analysis. *Nat. Methods* 9, 671–675. doi: 10.1038/nmeth.2089

Schulz, C., Gierok, P., Petruschka, L., Lalk, M., Mader, U., and Hammerschmidt, S. (2014). Regulation of the arginine deiminase system by ArgR2 interferes with arginine metabolism and fitness of *Streptococcus pneumoniae*. *mBio* 5, 1061–1075. doi: 10.1128/mBio.01858-14

Schulz, C., and Hammerschmidt, S. (2013). Exploitation of physiology and metabolomics to identify pneumococcal vaccine candidates. *Expert Rev. Vaccines* 12, 1061–1075. doi: 10.1586/14760584.2013.824708

Silva, M. T. (2010). Neutrophils and macrophages work in concert as inducers and effectors of adaptive immunity against extracellular and intracellular microbial pathogens. *J. Leukoc. Biol.* 87, 805–813. doi: 10.1189/jlb.1109767

Sleeman, K. L., Griffiths, D., Shackley, F., Diggle, L., Gupta, S., Maiden, M. C., et al. (2006). Capsular serotype-specific attack rates and duration of carriage of *Streptococcus pneumoniae* in a population of children. *J. Infect. Dis.* 194, 682–688. doi: 10.1086/505710

Someya, M., Kojima, T., Ogawa, M., Ninomiya, T., Nomura, K., Takasawa, A., et al. (2013). Regulation of tight junctions by sex hormones in normal human endometrial epithelial cells and uterus cancer cell line Sawano. *Cell Tissue Res.* 354, 481–494. doi: 10.1007/s00441-013-1676-9

Sperandio, B., Fischer, N., and Sansonetti, P. J. (2015). Mucosal physical and chemical innate barriers: Lessons from microbial evasion strategies. *Semin. Immunol.* 27, 111–118. doi: 10.1016/j.smim.2015.03.011

Tang, J. (2011). Microbial metabolomics. *Curr. Genomics* 12, 391–403. doi: 10.2174/138920211797248619

Trappetti, C., Kadioglu, A., Carter, M., Hayre, J., Iannelli, F., Pozzi, G., et al. (2009). Sialic acid: a preventable signal for pneumococcal biofilm formation, colonization, and invasion of the host. *J. Infect. Dis.* 199, 1497–1505. doi: 10.1086/598483

Tsuchiya, S., Yamabe, M., Yamaguchi, Y., Kobayashi, Y., Konno, T., and Tada, K. (1980). Establishment and characterization of a human acute monocytic leukemia cell line (THP-1). *Int. J. Cancer* 26, 171–176. doi: 10.1002/ijc.2910260208

Ulett, G. C., and Adderson, E. E. (2006). Regulation of apoptosis by gram-positive bacteria: mechanistic diversity and consequences for immunity. *Curr. Immunol. Rev.* 2, 119–141. doi: 10.2174/157339506776843033

van Furth, R., and Cohn, Z. A. (1968). The origin and kinetics of mononuclear phagocytes. *J. Exp. Med.* 128, 415–435. doi: 10.1084/jem.128.3.415

van Furth, R., Cohn, Z. A., Hirsch, J. G., Humphrey, J. H., Spector, W. G., and Langevoort, H. L. (1972). Mononuclear phagocytic system: new classification of macrophages, monocytes and of their cell line. *Bull. World Health Organ.* 47, 651–658.

Voss, S., Gamez, G., and Hammerschmidt, S. (2012). Impact of pneumococcal microbial surface components recognizing adhesive matrix molecules on colonization. *Mol. Oral Microbiol.* 27, 246–256. doi: 10.1111/j.2041-1014.2012.00654.x

Weber, J. R., Freyer, D., Alexander, C., Schroder, N. W., Reiss, A., Kuster, C., et al. (2003). Recognition of pneumococcal peptidoglycan: an expanded, pivotal role for LPS binding protein. *Immunity* 19, 269–279. doi: 10.1016/S1074-7613(03)00205-X

Widmann, C., Gibson, S., Jarpe, M. B., and Johnson, G. L. (1999). Mitogen-activated protein kinase: conservation of a three-kinase module from yeast to human. *Physiol. Rev.* 79, 143–180.

Wood, W. B., Smith, M. R., and Watson, B. (1946). Studies on the mechanism of recovery in pneumococcal pneumonia: IV. The mechanism of phagocytosis in the absence of antibody. *J. Exp. Med.* 84, 387–402. doi: 10.1084/jem.84.4.387

Wullschleger, S., Loewith, R., and Hall, M. N. (2006). TOR signaling in growth and metabolism. *Cell* 124, 471–484. doi: 10.1016/j.cell.2006.01.016

Yoon, S., and Seger, R. (2006). The extracellular signal-regulated kinase: multiple substrates regulate diverse cellular functions. *Growth Factors* 24, 21–44. doi: 10.1080/02699050500284218

Conflict of Interest Statement: The authors declare that the research was conducted in the absence of any commercial or financial relationships that could be construed as a potential conflict of interest.

frontiers in Cellular and Infection Microbiology

ORIGINAL RESEARCH
published: 04 May 2016
doi: 10.3389/fcimb.2016.00047

Characterization of Spbhp-37, a Hemoglobin-Binding Protein of *Streptococcus pneumoniae*

*María E. Romero-Espejel[1], Mario A. Rodríguez[1], Bibiana Chávez-Munguía[1], Emmanuel Ríos-Castro[2] and José de Jesús Olivares-Trejo[3]**

[1] Departamento de Infectómica y Patogénesis Molecular, Centro de Investigación y de Estudios Avanzados del IPN, México, México, [2] Unidad de Genómica, Proteómica y Metabolómica. LaNSE-CINVESTAV, Centro de Investigación y de Estudios Avanzados del IPN, México, México, [3] Laboratorio de Bacteriología y Nanomedicina, Posgrado en Ciencias Genómicas, Universidad Autónoma de la Ciudad de México, México, México

Streptococcus pneumoniae is a Gram-positive microorganism that is the cause of bacterial pneumonia, sinusitis and otitis media. This human pathogen also can cause invasive diseases such as meningitis, bacteremia and septicemia. Hemoglobin (Hb) and haem can support the growth and viability of *S. pneumoniae* as sole iron sources. Unfortunately, the acquisition mechanism of Hb and haem in this bacterium has been poorly studied. Previously we identified two proteins of 37 and 22 kDa as putative Hb- and haem-binding proteins (Spbhp-37 and Spbhp-22, respectively). The sequence of Spbhp-37 protein was database annotated as lipoprotein without any function or localization. Here it was immunolocalized in the surface cell by transmission electron microscopy using specific antibodies produced against the recombinant protein. The expression of Spbhp-37 was increased when bacteria were grown in media culture supplied with Hb. In addition, the affinity of Sphbp-37 for Hb was determined. Thus, in this work we are presenting new findings that attempt to explain the mechanism involved in iron acquisition of this pathogen. In the future these results could help to develop new therapy targets in order to avoid the secondary effects caused by the traditional therapies.

Keywords: *Streptococcus pneumoniae*, haem, iron, iron starvation, haem-binding protein

OPEN ACCESS

Edited by:
Jorge Eugenio Vidal, Emory University, USA

Reviewed by:
Gregory T. Robertson, Colorado State University, USA
Zehava Eichenbaum, Georgia State University, USA

****Correspondence:***
José de Jesús Olivares-Trejo
olivarestrejo@yahoo.com

Received: *26 January 2016*
Accepted: *12 April 2016*
Published: *04 May 2016*

Citation:
Romero-Espejel ME, Rodríguez MA, Chávez-Munguía B, Ríos-Castro E and Olivares-Trejo JJ (2016) Characterization of Spbhp-37, a Hemoglobin-Binding Protein of Streptococcus pneumoniae. Front. Cell. Infect. Microbiol. 6:47. doi: 10.3389/fcimb.2016.00047

INTRODUCTION

Streptococcus pneumoniae is the most important cause of bacterial pneumonia and moreover this pathogen can cause infections as septicemia, bacteremia, and meningitis (Yaro et al., 2006; Thornton et al., 2010). This bacterium causes considerable human morbidity and mortality throughout the world, especially among children, the elderly and immunocompromised individuals (Gray et al., 1979; Austrian, 1989; Musher, 1992; Butler and Schuchat, 1999). However, the mechanisms for pneumococcal disease are not fully understood. There is a necessity for the discovering of novel therapeutic strategies focused on bacterial iron acquisition systems, because many bacteria pathogens require iron as an essential nutrient to infect the human (Klebba et al., 1982; Ratledge and Dover, 2000; Simpson et al., 2000; Crosa and Walsh, 2002; Andrews et al., 2003). Due to that the iron is required in several cellular processes, most bacteria have developed strategies for iron scavenging from host proteins (Wooldridge and Williams, 1993; Raymond et al., 2003; Ge and Sun, 2012; Andrews et al., 2013). One of the best studied bacterial iron acquisition systems is

based on siderophores, which are secreted from the bacterial cell to scavenge free iron (Wooldridge and Williams, 1993; Guerinot, 1994; Wandersman and Delepelaire, 2004). Even though many pathogens secrete siderophores for iron acquisition during infection (Wandersman and Stojiljkovic, 2000; Genco and Dixon, 2001; Wandersman and Delepelaire, 2004), there are not biochemical or genetic evidences that *S. pneumoniae* produces siderophores (Tai et al., 1993; Brown et al., 2001; Romero-Espejel et al., 2013). As a result of the powerful reactivity of haem, it is generally sequestered within human cells by hemoproteins such as hemoglobin (Hb; Wandersman and Stojiljkovic, 2000; Wandersman and Delepelaire, 2004). In accordance, many bacteria have developed systems involved in iron acquisition from host hemoproteins (Tai et al., 1993; Brown et al., 2001; Genco and Dixon, 2001; Romero-Espejel et al., 2013). There are several studies on bacterial haem acquisition systems based mostly on Gram-negative bacteria (Stojiljkovic et al., 1996; Lewis et al., 1998; Wandersman and Stojiljkovic, 2000; Genco and Dixon, 2001; Olczak et al., 2001). Comparatively, less is known about how Gram-positive pathogens utilize host hemoproteins as an iron source. Recently, some surface proteins of *Streptococcus pyogenes* have been shown that bind haem (Shr and Shp, and haem-specific ATP-binding cassette transporter HtsABC). Shp has been shown to rapidly transfer its haem to the HtsA lipoprotein of HtsABC (Lei et al., 2002, 2003; Bates et al., 2003). In addition, it has been proposed that Shr is a source of haem for Shp and that the Shr-to-Shp haem transfer is a step of the haem acquisition process in *S. pyogenes* (Zhu et al., 2008).

Staphylococcus aureus acquires iron from haem by the Isd (iron-regulated surface determinant) system, which is formed by cell wall-anchored surface proteins (IsdA, IsdB, IsdC, and IsdH), a membrane transporter (composed by IsdD, IsdE, and IsdF), a transpeptidase (SrtB), and cytoplasmic haem-degrading monooxygenases (IsdG and IsdI) (Mazmanian et al., 2000, 2002, 2003; Skaar and Schneewind, 2004; Wu et al., 2005). Unfortunately, the mechanism of Hb and haem uptake in *S. pneumoniae* has been poorly studied. This pathogenic bacterium can grow using Hb or haem as a sole iron source. Hb acquisition is vital to microbial survival (Tai et al., 1993; Brown et al., 2001; Romero-Espejel et al., 2013). Previously, we detected two potential *S. pneumoniae* Hb- and haem-binding proteins (Spbhp) of 22 and 37 kDa, termed by us as Spbhp-22 and Spbhp-37. The Spbhp-37 protein had homology with a lipoprotein (Bierne et al., 2002; Romero-Espejel et al., 2013). Interestingly, several proteins required for virulence in Gram-positive bacteria are lipoproteins; for instance, FhuD which is an iron-siderophore transporter (Schneider and Hantke, 1993). Therefore, the aim of this work was to confirm the role of Spbhp-37 as Hb-binding protein and to determinate the affinity of Sphbp-37 for Hb.

MATERIALS AND METHODS

S. pneumoniae Growth Conditions

S. pneumoniae strain R6 was grown under microaerophilic conditions in 5% CO_2 for 24 h at 37°C on agar plates supplemented with 5% sheep blood. The cellular cultures were then inoculated in plates containing Todd-Hewitt Broth (THB), supplemented with 0.5% yeast extract (THB-Y) and incubated for 16 h at 37°C with 5% CO_2. For testing alternative iron sources the bacteria were cultivated in well culture plates containing medium THB, supplemented with 0.5% yeast extract (THB-Y) and 700 μm of 2,2′dipyridyl (a chelating agent) was added to eliminate free iron from the culture medium. Then, incubation was followed for 16 h at 37°C with 5% CO_2. The cellular growth was adjusted to 0.1 (OD_{600}) by spectrophotometry. After 3 h under iron starvation, the culture medium was supplemented with 2 μM human Hb.

Cloning and Expression of Spbhp-37 Recombinant Protein

The coding region of the *Spbhp-37* gene, excluding the signal peptide, was amplified by PCR from *S. pneumoniae* genomic DNA. For its directional cloning we used as sense primer an oligonucleotide containing the BamHI recognition site (5′-GGGGGGGATCCATGAACAAGAAACAATGGCTAGGTC-3′), and as anti-sense primer an oligonucleotide that included the SalI recognition site (5′-GGGGGGTCGACTTATTTT TCAGGAACTTTTACGCTTCCATC-3′). Then, amplicon was cloned in frame with the glutathione-S-transferase (GST), tag of the pGEX-6P-1 construction vector (GE Healthcare) using the BamHI and SalI restriction sites. The nucleotide sequence was corroborated by automated DNA sequencer.

For expression, *Escherichia coli* (strain BL21) competent cells were transformed with the pGEX-6P-1 empty vector, used as a negative control, or with the construction containing the *Spbhp-37* gene (pGEX-spbhp-37). Induction of recombinant proteins (GST and Spbhp-37-GST) was induced with 1 mM isopropyl-β-D-thiogalactopyranoside (IPTG) for 3 h at 37°C.

Purification of the Spbhp-37 Recombinant Protein

Inclusion bodies (IB), where the recombinant protein was accumulated, were purified as described (Vallejo et al., 2002). Briefly, after protein induction, cultures were centrifuged at 1500 g for 40 min and bottom was suspended in 50 ml of buffer A (100 mM Tris-HCl pH 8.0, 10 mM EDTA, 100 mM NaCl) in the presence of 1 mM PMSF. Cells were sonicated for 30 s (100 W) and 50 s off time for a total sonication time (including the off time) of 10 min. Then, an equal volume of buffer A having 8 M urea and 1 mM PMSF was added, stirred for 1 h at 4°C and centrifuged at 10000 g for 30 min. Pellet was resuspended in 500 ml of buffer B (100 mM Tris-HCl pH 8.0, 1 mM EDTA, 1 M NaCl) and centrifuged at 10000 g for 30 min. Pellet was resuspended in 500 ml of water, centrifuged again, and frozen at −70°C. After that, pellet was resuspended in buffer C (2 M urea, 20 mM Tris-HCl pH 8.0, 0.5 M NaCl, and 2% Triton X-100), centrifuged for 15 min at 10000 g, washed with the same volume of buffer B and centrifuged again. Then, the wet pellet of IB (2.1 g) was dissolved in 20 ml of solubilization buffer (8 M urea, Tris-HCl pH 8.0, 0.5 M NaCl and 1 mM 2-mercaptoethanol) and stirred for 2 h at room temperature. Sample was centrifuged at 12000 g for 30 min at 4°C and supernatant was extensively dialyzed against a

freshly prepared solution containing 20 mM Tris-HCl pH 8.0 and 4 mM urea. Finally, dialyzed samples were filter through a 0.45 μm membrane and stored in aliquots at −70°C. Recombinant protein was then purified by affinity chromatography using Glutathione–agarose beads (GE Healthcare) following the manufacturer's recommendations. Induction of the recombinant protein and its purification were examined by SDS-PAGE and western blotting assays using antibodies against GST. Cleavage of the GST tag was achieved using Pre-Scission protease following the manufacturer's recommendations.

Production of Specific Antibodies

Recombinant protein was used as antigen to produce specific antibodies against Spbhp-37. Thus, recombinant protein was mixed with a volume of TiterMax Gold Adjuvant (Sigma 145380-33-2). Then, a New Zealand white rabbit was injected with 150 μg of protein in 1 ml of suspension. For immunization, protein suspension was divided in four doses of 250 μl each, which were injected into two subcutaneous and two intramuscular sites. Immunization was performed three times for periods of 15 days. The study was conducted in accordance with Good Laboratory Practices (GLP) and Use of Laboratory Animals (NOM-062-ZOO-1999). The study protocol was approved by the Institutional Animal Care and Use Committee (IACUC)-Cinvestav. Thereafter, antiserum was obtained and tested using total *S. pneumoniae* extracts or Spbhp-37 purified protein.

Western Immunoblotting

Protein samples from different fractions during purification of the Spbhp-37 recombinant protein or total extracts of *S. pneumoniae*, isolated as described (Romero-Espejel et al., 2013), were loaded onto 12% SDS-PAGE and transferred to nitrocellulose membranes. Membranes were soaked for 1 h with 5% non-fat milk in PBS in order to saturate all remaining active binding sites, and then they were incubated with anti-GST (glutathione transferase; 1:10000) or anti-Spbhp-37 (1:10000) antibodies. After that, membranes were incubated with anti-rabbit IgGs secondary antibodies conjugated to horseradish peroxidase (Invitrogen 65–6120; 1:10000) and the antibodies recognition was revealed by chemiluminescence (Millipore).

Immunoelectron Microscopy

Bacteria grown in THB-Y or in the presence of Hb as only iron source were fixed in 4% paraformaldehyde and 0.5% glutaraldehyde in PBS for 1 h at room temperature. Samples were embedded in the acrylic resin (LR White) and polymerized under UV at 4°C overnight. Thin sections (i.e., 60 nm) were obtained and mounted on Formvar-covered nickel grids. Later, sections were incubated in PBS with 10% fetal bovine serum before incubation with the anti-Spbhp-37 antibodies diluted (1:100) in 5% fetal bovine serum. Then, samples were incubated with anti-rabbit IgGs secondary antibodies conjugated to 20 nm colloidal gold spheres (Ted Pella Inc; 1:100). Finally, sections were contrasted with aqueous solutions of uranyl acetate and lead citrate before being examined in a Jeol JEM-1011 transmission electron microscope.

S. pneumoniae Growth in the Presence of Hb and Anti Spbhp-37-GST Antibodies

Cells of *S. pneumoniae* previously cultivated and inoculated in THB (supplemented with 0.5% of yeast extract). When it was necessary to test an iron supply alternative, a chelating agent 700 μm 2,2′-dipyridyl (Sigma D216305-25G) was used in order to eliminate iron from the medium of culture. Thereafter, the bacteria were incubated for 16 h at 37°C with an atmosphere regulated at 5% CO_2. In order to synchronize the cellular growth (OD_{600}) was adjusted to 0.1. Thus, the cellular growth was monitored each hour. After 3 h under iron starvation the medium of culture was supplemented with: (a) only 2.5 μM of Hb (Cat. H7379, Sigma®), (b) pre-immune serum (500 mg/ml) plus Hb or (c) anti-Spbhp-37 antibodies (500 mg/ml) plus Hb. After that, cellular growth was monitored each hour for 4 h, comparing under iron limiting condition vs. the condition when Hb was supplied as the sole iron source or when the anti-Spbhp-37 antibodies were added.

Overlay Assays

Total extracts of *S. pneumoniae* were separated by 12% SDS-PAGE and transferred to nitrocellulose membranes (Bio-Rad). Membranes were incubated for 1 h at 37°C with 0.5% non-fat milk in PBS and 0.05% Tween 20, pH 7.4 (PBST) to block unspecific sites and then overnight at 4°C with human Hb (2.5 μM). After that, membranes were incubated for 1 h at 37°C with anti-hemoglobin antibodies (Santa Cruz Biotechnology SC-21005) (1:10000), and lastly 1 h at 37°C with the horseradish peroxidase-conjugated secondary antibodies (Invitrogen 65-6120; 1:10000). Antibodies recognition was developed by chemiluminescence (Millipore). As a control, a membrane was incubated only with PBST before the incubation with anti-globin antibodies.

Surface Plasmon Resonance (SPR)

All SPR experiments were performed using Biacore T200 optical biosensor (GE Healthcare Life Sciences, Little Chalfont, Buckinghamshire, UK). SPR measurements were carried out in HBS-EP running buffer 10X (10 mM HEPES, 3 mM EDTA, 150 mM NaCl, 0.05% v/v of Tween 20 and pH 7.4) at 25°C in a CM5 chip (coated with carboxylated dextran). For the immobilization scouting Hb was dissolved (30 μg/ml) in acetate buffer (pH 3.5, 4, 4.5, 5, and 5.5) and injected at the Biacore system at flow rate of 10 μl/min, with a contact time of 120 s and using NaOH 50 mM as a wash solution to regenerate the chip surface. Once pH was selected (pH 4), Hb was dissolved in a corresponding acetate buffer (30 μg/ml) and immobilized to the chip using amine coupling at an immobilization level of $RL = 435\ RU$ to reach a theorical $RU\text{max} = 249.53$. During the coupling, the chip surface was activated using 1:1 mixture of 100 mM Nethyl-N-(dimethylaminopropyl)-carbodiimide (EDC) and 100 mM N-hydroxysuccinimide (NHS; both dissolved in water), and after Hb injection, the residual activated carboxy methyl groups on the chip surface were blocked by 1 M ethanolamine, pH 8.5. For this study, flow cell 1 was blank immobilized (without protein) for using as a reference. To analyze interactions of Spbhp-37 with immobilized Hb, Spbhp-37

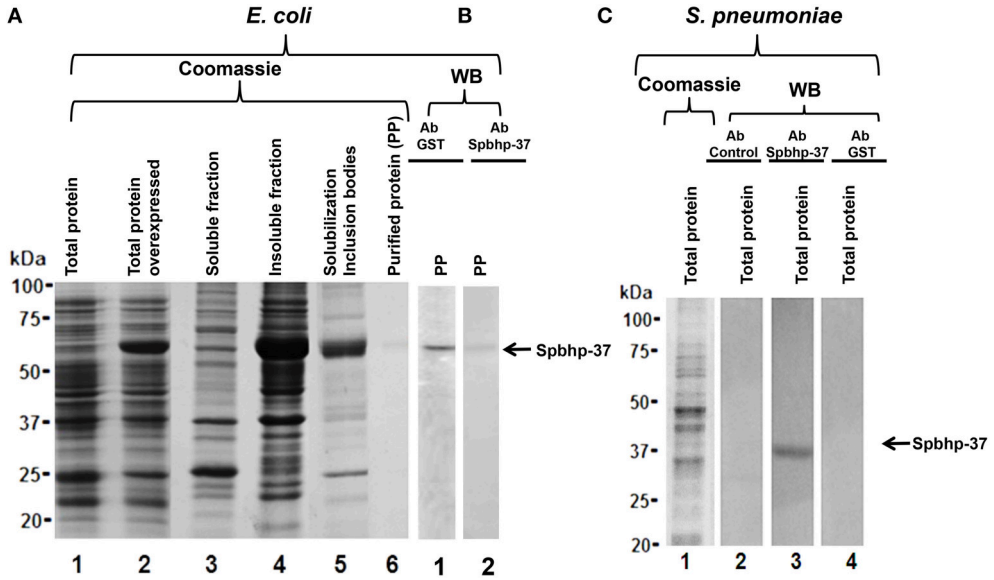

FIGURE 1 | Production of a Spbhp-37 recombinant protein and antibodies against it. The Spbhp-37 encoding gene was cloned in the pGEX-6P-1 vector, the recombinant protein was expressed in *E. coli* bacteria (BL21 strain) and purified. Then, this protein was used as antigen to obtain specific antibodies against it. Finally, antibodies were utilized in western blotting assays on the recombinant protein and total extracts of *S. pneumoniae*. **(A)** Production and purification of the Spbhp-37 recombinant protein. Proteins were analyzed by 12% SDS-PAGE stained with coomassie blue. Lane 1, total proteins of non-induced bacteria; lane 2, total proteins of IPTG-induced bacteria; lane 3, soluble fraction of IPTG-induced bacteria; lane 4, insoluble fraction of IPTG-induced bacteria; lane 5, solubilization of inclusion bodies; lane 6, purified protein. **(B)** Western blotting on purified recombinant protein. Lane 1, western blotting using an antibody directed against the GST tag; lane 2, western blotting using an antibody directed against the recombinant protein (anti-Spbhp-37). **(C)** Proteins were analyzed by 12% SDS-PAGE stained with coomassie blue and western blotting on total proteins of *S. pneumoniae*. Lane 1, total extracts of *S. pneumoniae* were analyzed by 12% SDS-PAGE stained with coomassie blue; lane 2, western blotting using the pre-immune serum; lane 3, western blotting using anti-Spbhp-37 antibodies; lane 4, western blotting using anti-GST. Molecular weight markers are indicated on the left. Arrows indicate the antibodies recognition of recombinant protein Spbhp-37.

was dissolved in buffer HBS-EP and injected. The same buffer was used as the running buffer. The flow rate was maintained constant throughout the kinetics experiment (30 μl/min), contact time was settled for 120 s and dissociation time was kept at 300 s. Regeneration was carried out with NaCl 1 M for 30 s. Experiments were performed with various concentrations of Sphbp-37 from 100 to 1000 nM, monitoring the refractive index changes as a function of time under constant flow conditions. The relative amount of Spbhp-37 bound to the Hb was determined by measuring the net increase of refractive index over time compared with that of running buffer alone. This change was reported in response units (*RU*). The data analysis was done with Biacore T200 evaluation software version 1.0 and data was fit to 1:1 binding.

RESULTS

Cloning and Expression of Spbhp-37

To investigate the participation of Spbhp-37 protein on iron acquisition, its encoding gene was cloned in the plasmid pGEX-6-P-1. The construction was termed pGEX-spbhp-37 and was used to transform BL21 strain; the expression of Spbhp-37 was induced with IPTG. The overexpression of Spbhp-37 protein was confirmed by SDS-PAGE stained with Coomassie blue, we observed a band of 63 kDa when bacteria were incubated with IPTG with respect to non-induced bacteria (**Figure 1**, lane 2). This molecular weight corresponds to the expected for the recombinant protein (26 kDa from GST and 37 kDa from Spbhp-37). Unfortunately, when soluble and insoluble fractions were separated, the Spbhp-37 recombinant protein was detected in the insoluble fraction (**Figure 1**, lane 4). Therefore, a protocol to solubilize the inclusion bodies (IB) was performed (see Materials and Methods Section) (**Figure 1**, lane 5) previous to purification of the protein by affinity chromatography (**Figure 1**, lane 6). To confirm the identity of the purified protein, we carried out western blot assays using anti-GST antibodies. Results showed that antibodies recognized the purified recombinant protein (**Figure 1B**, lane 1).

Obtaining of Anti Spbhp-37 Antibodies

In order to produce anti Spbhp-37 antibodies, the recombinant protein was used as antigen to inoculate a New Zealand rabbit. As expected, the obtained antibodies recognized the recombinant protein in western blot assays (**Figure 1B**, lane 2). After that, antibodies were characterized by western blotting on total proteins of *S. pneumoniae*. In these assays, antibodies recognized a single band of 37 kDa, which corresponds to the molecular weight of Spbhp-37 (**Figure 1C**, lane 3). This band was not revealed when western blotting was performed with pre-immune serum or with anti-GST antibodies (**Figure 1C**, lanes 2, 4, respectively). These results allowed us to demonstrate the specificity of the antibodies raised against Spbhp-37.

Spbhp-37 Protein is Increased Two Fold on the Surface of *S. pneumoniae* When it is Grown in the Presence of Hb As Only Iron Source

To investigate the location of Spbhp-37 in *S. pneumoniae* bacteria we performed immunoelectronic microscopy assays using antibodies against the recombinant protein. Our results showed the presence of Spbhp-37 protein on bacteria surface (**Figure 2B**). Signal was specific for Spbhp-37 because not signal was detected in a control incubated only with the gold-labeled secondary antibodies (**Figure 2A**). Then, to analyze the effect of Hb on the expression of Spbhp-37, we cultivated *S. pneumoniae* in THB in the presence of Hb as the sole iron source. In this condition we observed that the occurrence of Spbhp-37 on bacteria surface was more abundant than when cells were grown in normal medium (**Figure 2C**). To obtain a quantitative value, the positive signals were counted in each condition. Results revealed an increase of about two fold of Spbhp-37 in bacteria grown with Hb (**Figure 2D**). This result was corroborated by western blotting (data no showed). These results suggest that the presence of Hb increases two fold the abundance of Spbhp-37.

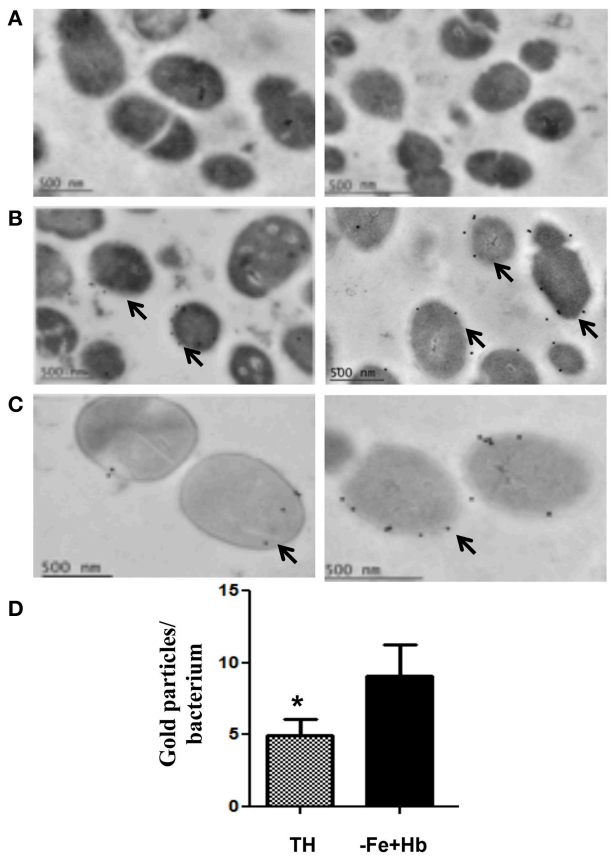

FIGURE 2 | Immunoelectron microscopy of Spbhp-37 protein. *S. pneumoniae* cellular cultures were incubated in normal Todd-Hewitt Broth or in medium with Hb as only iron source. Then, localization of Spbhp-37 was analyzed by immunoelectron microscopy. **(A)** Negative control. Bacteria incubated only with the gold-labeled secondary antibodies. **(B)** Spbhp-37 in normal medium. **(C)** Spbhp-37 in medium with Hb as only iron source. Arrowheads indicate the location of Spbhp-37 protein in *S. pneumoniae*. In right is shown the magnification of cell bacteria to compare expression in both growth conditions. **(D)** Quantitative analysis of Spbhp-37 expression. Gold particles on bacteria growth under normal conditions (TH) and in medium with Hb as only iron source (-Fe+Hb) were counted $n = 25$. Data represent mean ± *SD* of three independent experiments. Asterisk indicates a significant difference ($p < 0.05$).

Anti Spbhp-37-GST Antibodies Limited the Cellular Growth When Hb Was Supplied As the Sole Iron Source

To explore whether Spbhp-37 protein is related to utilization of Hb in the cellular growth of *S. pneumoniae*, we designed an experiment in which the anti-Spbhp-37 antibodies were supplied to block the bacteria growth under free iron limiting conditions, but using Hb as sole iron source. When *S. pneumoniae* was cultivated in THB under iron starvation, the cellular growth was limited, but when this media was supplemented with Hb as the sole iron source, the cellular growth was restored (**Figure 3**). Interestingly, the cellular growth was blocked when anti-Spbhp-37 antibodies were added to cellular cultures with Hb as the sole iron source (**Figure 3**). In addition, pre-immune serum had a minimal effect on the cellular growth in media supplemented with Hb (**Figure 3**). Results clearly showed the cellular growth under iron limiting conditions was impaired.

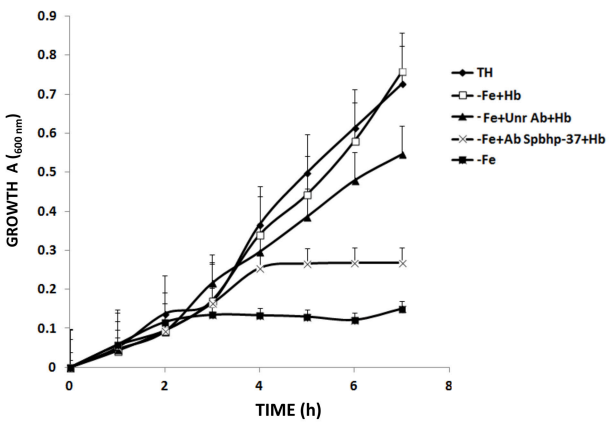

FIGURE 3 | Anti Spbhp-37-GST antibodies block the cellular growth of *S. pneumoniae*. *S. pneumoniae* strain R6 was cultivated in Todd-Hewitt Broth under conditions of: iron sufficiency (—◆—); without iron (—■—); without iron and supplemented with Hb (—□—); without iron and supplemented with Hb in the presence of anti-Spbhp-37 antibodies (—×—); and without iron and supplemented with Hb in the presence of pre-immune serum (used as unrelated antibodies) (—▲—). The cellular growth was monitored each hour for a period of 7 h by spectrophotometry (600 nm). Data represent mean ± *SD* of three independent experiments by triplicate. The cellular growth from bacteria cultivated in the medium without iron and supplemented with Hb in the presence of anti-Spbhp-37 antibodies was significantly higher compared to the cellular growth from bacteria cultivated in the medium without iron and supplemented with Hb in the presence of pre-immune serum (used as unrelated antibodies; $p < 0.05$, one-way ANOVA).

Anti-Spbhp-37 Antibodies Block the Interaction between Spbhp-37 Protein and Hb

Inhibition of cellular growth with anti-Spbhp-37 notwithstanding the presence of Hb supports the hypothesis that Spbhp-37 is a receptor for Hb and that antibodies block the interaction between both proteins. To corroborate these assumptions, the interaction between Spbhp-37 protein and Hb as well the blockage of this interaction by anti Spbhp-37 antibodies were investigated by overlay assays. Thus, total proteins of *S. pneumoniae* (**Figure 4D**) were separated in SDS-PAGE and transferred to nitrocellulose membranes. Then, membranes were incubated with Hb and interaction was revealed with anti-Hb antibodies. At least five proteins, including a 37 kDa band Spbhp-37 protein (located in the top of gel), were recognized by Hb and anti-Hb antibodies when total proteins were used (**Figure 4A**). Interestingly, the detection of the protein was not observed when anti-Spbhp-37 antibodies were added in the overlay assays (**Figure 4B**). In addition, not bands were detected when incubation of Hb was omitted in the overlay experiments (used as a negative control) (**Figure 4C**). Results confirmed that Spbhp-37 binds to Hb and that antibodies block the interaction between both proteins.

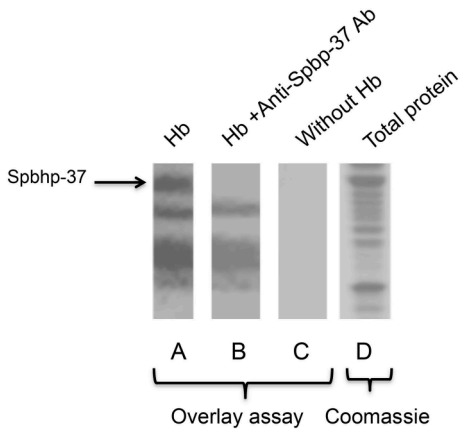

FIGURE 4 | Hb binds to Spbhp-37 protein in overlay experiments. Total proteins of *S. pneumoniae* were loaded onto 12% SDS-PAGE, transferred to nitrocellulose membrane and overlay assays were performed. **(A)** Overlay. Nitrocellulose membranes were incubated with Hb, with anti-hemoglobin antibodies, and peroxidase-conjugated secondary antibodies. **(B)** As in A, but the overlay assay was incubated first with anti-Spbhp-37 antibodies. **(C)** Negative control. Nitrocellulose membranes were incubated only with primary and secondary antibodies (omitting the incubation with Hb). **(D)** Coomassie blue staining. Total proteins of *S. pneumoniae* were loaded onto 12% SDS-PAGE. Arrow indicates the Spbhp-37 protein.

Spbhp-37 Showed High Affinity by Hb

To determine the affinity of Spbhp-37 for Hb, the GST tag of the Spbhp-37 recombinant protein was eliminated by digestion with the Pre-Scission protease and its affinity to Hb was analyzed by surface plasmon resonance (SPR). First, to confirm the cleavage of the GST tag, protein samples were analyzed by SDS-PAGE and western blotting. After SDS-PAGE and coomassie blue staining we observed the purified Spbhp-37-GST protein (**Figure 5A**, lane 1), the Spbhp-37 protein without GST (**Figure 5A**, lane 2), and the releasing of the GST tag (**Figure 5A**, lane 3). Identity of Spbhp-37 protein was corroborated by western blotting assays using the anti Spbhp-37 antibodies. These antibodies recognized the Spbhp-37-GST protein (**Figure 5B**, lane 1) and the Spbhp-37 protein without the GST tag (**Figure 5B**, lane 2), but GST was not revealed (**Figure 5B**, lane 3). As a control, western blotting was

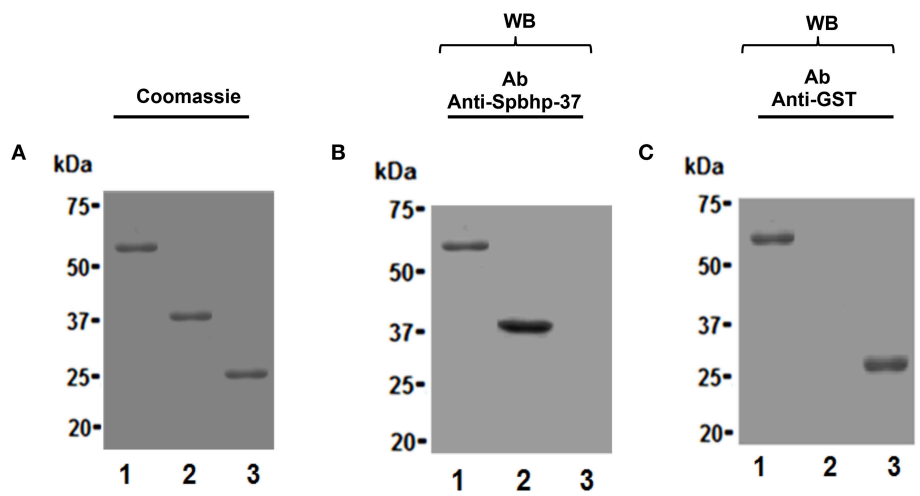

FIGURE 5 | Purification of the Spbhp-37 recombinant protein without the GST tag. Spbhp-37-GST recombinant protein was purified by chromatography affinity and the cleavage of GTS tag was performed by the PreScission protease. Then, protein samples were analyzed by 12% SDS-PAGE and western blotting using anti-Spbhp-37 antibodies was tested. **(A)** Coomassie blue staining. **(B)** Western blotting with anti-Spbhp-37. **(C)** Western blotting with anti-GST. Lane 1, Spbhp-37-GST; lane 2, Spbhp-37 without GST; lane 3, GST. Molecular weight markers are indicated at the left side.

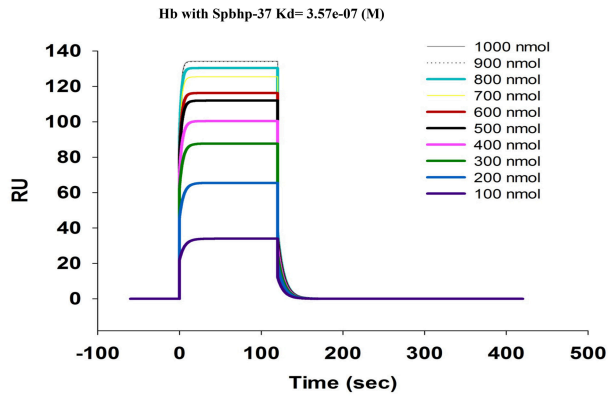

FIGURE 6 | Quantitative analysis of hemoglobin-Sphbp-37 interaction using Biacore assay (Surface Plasmon Resonance). Human hemoglobin was immobilized on sensor chips CM5 (Biacore) and binding curves for Spbhp-37 were expressed in resonance units (*RU*) as a function of time. The kinetic parameters and concentrations of the analysis are indicated.

performed using an anti-GST antibody, where only Spbhp-37-GST protein (**Figure 5C**, lane 1), and GST (**Figure 5C**, lane 3) were revealed.

To obtain kinetic binding data by SPR, Hb was immobilized on the sensor chip and the binding of Spbhp-37 (without GST tag) at concentrations ranged from 100 to 1000 nm was tested. In these experiments we observed a dose-dependent binding of Spbhp-37 to Hb (**Figure 6**). Curve fitting of the sensograms enabled us to determine that Kd was of 3.57 e-7 M, showing a high affinity of Spbhp-37 protein for Hb.

DISCUSSION

S. pneumoniae is a human pathogen that uses Hb to cover its iron necessities. However, the iron acquisition mechanism has been poorly studied. Previously, we identified a lipoprotein of 37 kDa (Spbhp-37) as a *S. pneumoniae* membrane protein, which was purified by haem affinity chromatography and that could be involved in the Hb and haem acquisition. In the present work, by use of an antibody raised against Spbhp-37 recombinant protein we showed that the expression of native protein was increased on the surface of *S. pneumoniae* when Hb was supplemented as the sole iron source. These results clearly showed the character of receptor protein, because it was detected on the surface of the bacterium (Lei et al., 2002, 2003; Bates et al., 2003; Mazmanian et al., 2003). In addition, when these antibodies were used to analyze the bacterial growth in the presence of Hb, we noticed that they diminished about 50% the cell growth with respect to that obtained in media with Hb in the absence of this antibody or in the presence of pre-immune serum, indicating the importance of Spbhp-37 on uptake of Hb when was supplied as only iron source. This hypothesis was confirmed by overlay assays, because we found that Hb bound to Spbhp-37 protein and anti Spbhp-37 antibodies were capable to inhibit the interaction between Hb and Spbhp-37 protein. In fact, antibodies only blocked the Hb binding to one (Spbhp-37) of the all bands previously identified in *S. pneumoniae* total proteins (Romero-Espejel et al., 2013), which correspond to 37 kDa size, this observation clearly showed the specificity of the antibodies produced. On the other hand, the low Kd determined by SPR for the binding of Hb and Spbhp-37 protein (3.57 e^{-7} M) is similar to that reported for the TonB-dependent haem receptor (HasR) of *Serratia marcescens*, the outer membrane haem receptor (HmuR) of *Porphyromonas gingivalis*, and haem receptor (HasA) of *S. marcescens* (Ghigo et al., 1997; Olczak et al., 2001; Deniau et al., 2003), indicating that Spbhp-37 protein binds Hb with high affinity and suggesting that this protein is necessary in the mechanisms of iron acquisition to scavenge iron. Possibly other proteins are involved in this mechanism, for example those reported previously by our group, which include a stress general protein of 22 kDa, a maltose-binding protein of 45 kDa, and a glutamine synthetase type I 50 kDa (Romero-Espejel et al., 2013). These proteins could help to introduce and store the iron source to cytoplasm as it has been described for other Gram-positive bacteria (Mazmanian et al., 2002, 2003; Skaar et al., 2004; Skaar and Schneewind, 2004; Wu et al., 2005).

Our overall results attempt to explain the iron acquisition mechanism by *S. pneumoniae* when Hb is available. We showed that Spbhp-37 is a surface protein involved in Hb uptake, an essential mechanism of this pathogen to establish an infection process in human, because this bacterium uses Hb and haem as iron sources.

AUTHOR CONTRIBUTIONS

ME conceived and carried out most of the experiments, analyzed data, and drafted the manuscript; BC was responsible for transmission electronic microscopy experiments; ER performed the surface plasmon resonance assays; MR and JO designed the study, analyzed data, and drafted the manuscript. All authors read and approved the final manuscript.

FUNDING

This work was supported by Consejo Nacional de Ciencia y Tecnología (CONACyT) [grant numbers: SALUD-2012-01-181641 and 222180].

ACKNOWLEDGMENTS

We would like to thank Carlos Vázquez-Calzada and Mario Rodríguez-Nieves (Departamento de Infectómica y Patogénesis Molecular, Centro de Investigación y de Estudios Avanzados del IPN, México City, México) for their help in the generation of specific antibodies and reagents preparation used in this work. We also thank Lorena Ramírez-Reyes (Unidad de Genómica, Proteómica y Metabolómica. LaNSE-CINVESTAV, Centro de Investigación y de Estudios Avanzados del IPN, México City, México) for her help in experiments of surface plasmon resonance.

REFERENCES

Andrews, S., Norton, I., Salunkhe, A. S., Goodluck, H., Aly, W. S., Mourad-Agha, H., et al. (2013). Control of iron metabolism in bacteria. *Met. Ions Life Sci.* 12, 203–239. doi: 10.1007/978-94-007-5561-1_7

Andrews, S., Robinsón, A. K., and Rodríguez-Quiñonez, F. (2003). Bacterial iron homeostasis. *FEMS Microbiol. Rev.* 27, 215–237. doi: 10.1016/S0168-6445(03)00055-X

Austrian, R. (1989). Pneumococcal polysaccharide vaccines. *Rev. Infect. Dis.* 11, 598–602. doi: 10.1093/clinids/11.Supplement_3.S598

Bates, C. S., Montanez, G. E., Woods, C. R., Vincent, R. M., and Eichenbaum, Z. (2003). Identification and characterization of a *Streptococcus pyogenes* operon involved in binding of hemoproteins and acquisition of iron. *Infect. Immun.* 71, 1042–1055. doi: 10.1128/IAI.71.3.1042-1055.2003

Bierne, H., Mazmanian, S. K., Trost, M., Pucciarelli, M. G., Liu, G., Dehoux, P., et al. (2002). Inactivation of the srtA gene in *Listeria monocytogenes* inhibits anchoring of surface proteins and affects virulence. *Mol. Microbiol.* 43, 869–881 doi: 10.1046/j.1365-2958.2002.02798.x

Brown, J. S., Gilliland, S. M., and Holden, D. W. (2001). A *Streptococcus pneumoniae* pathogenicity island encoding an ABC transporter involved in iron uptake and virulence. *Mol. Microbiol.* 40, 572–585. doi: 10.1046/j.1365-2958.2001.02414.x

Butler, J. C., and Schuchat, A. (1999). Epidemiology of pneumococcal infections in the elderly. *Drugs Aging* 15, 11–19. doi: 10.2165/00002512-199915001-00002

Crosa, J., and Walsh, C. (2002). Genetics and assembly line enzymology of siderophore biosynthesis in bacteria. *Microbiol. Mol. Biol. R.* 66, 223–249. doi: 10.1128/MMBR.66.2.223-249.2002

Deniau, C., Gilli, R., Izadi-Pruneyre, N., Letoffe, S., Delepierre, M., Wandersman, C., et al. (2003). Thermodynamics of heme binding to the HasA(SM) hemophore: effect of mutations at three key residues for heme uptake. *Biochemistry* 42, 10627–10633. doi: 10.1021/bi030015k

Ge, R., and Sun, X. (2012). Iron trafficking system in *Helicobacter pylori*. *BioMetals* 25, 247–258. doi: 10.1007/s10534-011-9512-8

Genco, C. A., and Dixon, D. W. (2001). Emerging strategies in microbial haem capture. *Mol. Microbiol.* 39, 1–11. doi: 10.1046/j.1365-2958.2001.02231.x

Ghigo, J. M., Letoffe, S., and Wandersman, C. (1997). A new type of hemophore-dependent heme acquisition system of *Serratia marcescens* reconstituted in *Escherichia coli*. *J. Bacteriol.* 179, 3572–3579.

Gray, B. M., Converse, J., and Dillon, H. (1979). Serotypes of *Streptococcus pneumoniae* causing disease. *J. Infect. Dis.* 140, 979–983. doi: 10.1093/infdis/140.6.979

Guerinot, M. L. (1994). Microbial iron transport. *Annu. Rev. Microbiol.* 48, 743–772. doi: 10.1146/annurev.mi.48.100194.003523

Klebba, P. E., McIntosh, M. A., and Neilands, J. B. (1982). Kinetics of biosynthesis of iron-regulated membrane proteins in *Escherichia coli*. *J. Bacteriol.* 149, 880–888.

Lei, B., Liu, M., Voyich, J. M., Prater, C. I., Kala, S. V., DeLeo, F. R., et al. (2003). Identification and characterization of HtsA, a second heme-binding protein made by *Streptococcus pyogenes*. *Infect. Immun.* 71, 5962–5969. doi: 10.1128/iai.71.10.5962-5969.2003

Lei, B., Smoot, L. M., Menning, H. M., Voyich, J. M., Kala, S. V., Deleo, F. R., et al. (2002). Identification and characterization of a novel heme-associated cell surface protein made by *Streptococcus pyogenes*. *Infect. Immun.* 70, 4494–4500. doi: 10.1128/IAI.70.8.4494-4500.2002

Lewis, L. A., Sung, M. H., Gipson, M., Hartman, K., and Dyer, D. W. (1998). Transport of intact porphyrin by HpuAB, the hemoglobin-haptoglobin utilization system of *Neisseria meningitidis*. *J. Bacteriol.* 180, 6043–6047.

Mazmanian, S. K., Liu, G., Jensen, E. R., Lenoy, E., and Schneewind, O. (2000). *Staphylococcus aureus* sortase mutants defective in the display of surface proteins and in the pathogenesis of animal infections. *Proc. Natl. Acad. Sci. U.S.A.* 97, 5510–5515. doi: 10.1073/pnas.080520697

Mazmanian, S. K., Skaar, E. P., Gaspar, A. H., Humayun, M., Gornicki, P., Jelenska, J., et al. (2003). Passage of heme-iron across the envelope of *Staphylococcus aureus*. *Science* 299, 906–909. doi: 10.1126/science.1081147

Mazmanian, S. K., Ton-That, H., Su, K., and Schneewind, O. (2002). An iron-regulated sortase anchors a class of surface protein during *Staphylococcus aureus* pathogenesis. *Proc. Natl. Acad. Sci. U.S.A.* 99, 2293–2298. doi: 10.1073/pnas.032523999

Musher, D. M. (1992). Infections caused by *Streptococcus pneumoniae*: clinical spectrum, pathogenesis, immunity, and treatment. *Clin. Infect. Dis.* 14, 801–807. doi: 10.1093/clinids/14.4.801

Olczak, T., Dixon, D. W., and Genco, C. A. (2001). Binding specificity of the *Porphyromonas gingivalis* heme and hemoglobin receptor HmuR, gingipain K, and gingipain R1 for heme, porphyrins, and metalloporphyrins. *J. Bacteriol.* 183, 5599–5608. doi: 10.1128/JB.183.19.5599-5608.2001

Ratledge, C., and Dover, L. (2000). Iron metabolism in pathogenic bacteria. *Annu. Rev. Microbiol.* 54, 881–941. doi: 10.1146/annurev.micro.54.1.881

Raymond, K. N., Dertz, E. A., and Kim, S. S. (2003). Enterobactin: an archetype for microbial iron transport. *Proc. Natl. Acad. Sci. U.S.A.* 100, 3584–3588. doi: 10.1073/pnas.0630018100

Romero-Espejel, M. E., González-López, M. A., and Olivares-Trejo, J. J. (2013). *Streptococcus pneumoniae* requires iron for its viability and expresses two membrane proteins that bind haemoglobin and haem. *Metallomics* 5, 384–389. doi: 10.1039/c3mt20244e

Schneider, R., and Hantke, K. (1993). Iron-hydroxamate uptake systems in *Bacillus subtilis*: identification of a lipoprotein as part of a binding protein dependent transport system. *Mol. Microbiol.* 8, 111–121. doi: 10.1111/j.1365-2958.1993.tb01208.x

Simpson, W., Olczak, T., and Genco, C. A. (2000). Characterization and expression of HmuR, a TonB-dependent hemoglobin receptor of *Porphyromonas gingivalis*. *J. Bacteriol.* 182, 5737–5748. doi: 10.1128/JB.182.20.5737-5748.2000

Skaar, E. P., Gaspar, A. H., and Schneewind, O. (2004). IsdG and IsdI, heme-degrading enzymes in the cytoplasm of *Staphylococcus aureus*. *J. Biol. Chem.* 279, 436–443. doi: 10.1074/jbc.m307952200

Skaar, E. P., and Schneewind, O. (2004). Iron-regulated surface determinants (Isd) of *Staphylococcus aureus*: stealing iron from heme. *Microbes Infect.* 6, 390–397. doi: 10.1016/j.micinf.2003.12.008

Stojiljkovic, I., Larson, J., Hwa, V., Anic, S., and So, M. (1996). HmbR outer membrane receptors of pathogenic Neisseria spp.: iron-regulated, hemoglobin-binding proteins with a high level of primary structure conservation. *J. Bacteriol.* 178, 4670–4678.

Tai, S. S., Lee, C. J., and Winter, R. E. (1993). Hemin utilization is related to virulence of *Streptococcus pneumoniae*. *Infect. Immun.* 61, 5401–5405.

Thornton, J., Durick-Eder, K., and Tuomanen, E. (2010). Pneumococcal pathogenesis: "innate invasion" yet organ-specific damage. *J. Mol. Med.* 88, 103–107. doi: 10.1007/s00109-009-0578-5

Vallejo, L., Brokelman, M., Marten, S., Trappe, S., Cabrera, J., Hoffmann, A., et al. (2002). Renaturation and purification of bone morphogenetic protein-2 produced as inclusion bodies in high-cell-density cultures of recombinant *Escherichia coli*. *J. Bacteriol.* 94, 185–194. doi: 10.1016/s0168-1656(01)00425-4

Wandersman, C., and Delepelaire, P. (2004). Bacterial iron sources: from siderophores to haemophores. *Annu. Rev. Microbiol.* 58, 611–647. doi: 10.1146/annurev.micro.58.030603.123811

Wandersman, C., and Stojiljkovic, I. (2000). Bacterial heme sources: the role of heme, hemoprotein receptors and haemophores. *Curr. Opin. Microbiol.* 3, 215–220. doi: 10.1016/S1369-5274(00)00078-3

Wooldridge, K. G., and Williams, P. H. (1993). Iron uptake mechanisms of pathogenic bacteria. *FEMS Microbiol. Rev.* 12, 325–348 doi: 10.1111/j.1574-6976.1993.tb00026.x

Wu, R., Skaar, E. P., Zhang, R., Joachimiak, G., Gornicki, P., Schneewind, O., et al. (2005). Staphylococcus aureus IsdG and IsdI, heme-degrading enzymes with structural similarity to monooxygenases. *J. Biol. Chem.* 280, 2840–2846. doi: 10.1074/jbc.M409526200

Yaro, S., Lourd, M., Traoré, Y., Njanpop-Lafourcade, B. M., Sawadogo, A., Sangare, L., et al. (2006). Epidemiological and molecular characteristics of a highly lethal pneumococcal meningitis epidemic in Burkina Faso. *Clin. Infect. Dis.* 43, 693–700. doi: 10.1086/506940

Zhu, H., Liu, M., and Lei, B. (2008). The surface protein Shr of *Streptococcus pyogenes* binds heme and transfers it to the streptococcal heme-binding protein Shp. *BMC Microbiol.* 8:15. doi: 10.1186/1471-2180-8-15

Conflict of Interest Statement: The authors declare that the research was conducted in the absence of any commercial or financial relationships that could be construed as a potential conflict of interest.

frontiers in Cellular and Infection Microbiology

ORIGINAL RESEARCH
published: 18 May 2016
doi: 10.3389/fcimb.2016.00055

Surface Proteins and Pneumolysin of Encapsulated and Nonencapsulated *Streptococcus pneumoniae* Mediate Virulence in a Chinchilla Model of Otitis Media

*Lance E. Keller †, Jessica L. Bradshaw, Haley Pipkins and Larry S. McDaniel **

Department of Microbiology and Immunology, University of Mississippi Medical Center, Jackson, MS, USA

Streptococcus pneumoniae infections result in a range of human diseases and are responsible for almost one million deaths annually. Pneumococcal disease is mediated in part through surface structures and an anti-phagocytic capsule. Recent studies have shown that nonencapsulated *S. pneumoniae* (NESp) make up a significant portion of the pneumococcal population and are able to cause disease. NESp lack some common surface proteins expressed by encapsulated pneumococci, but express surface proteins unique to NESp. A chinchilla model of otitis media (OM) was used to determine the effect various pneumococcal mutations have on pathogenesis in both NESp and encapsulated pneumococci. Epithelial cell adhesion and invasion assays were used to examine the effects in relation to deletion of intrinsic genes or expression of novel genes. A mouse model of colonization was also utilized for comparison of various pneumococcal mutants. It was determined that pneumococcal surface protein K (PspK) and pneumolysin (Ply) affect NESp middle ear pathogenesis, but only PspK affected epithelial cell adhesion. Experiments in an OM model were done with encapsulated strains testing the importance of native virulence factors and treatment of OM. First, a triple deletion of the common virulence factors PspA, PspC, and Ply, (ΔPAC), from an encapsulated background abolished virulence in an OM model while a PspC mutant had detectable, but reduced amounts of recoverable bacteria compared to wildtype. Next, treatment of OM was effective when starting antibiotic treatment within 24 h with resolution by 48 h post-treatment. Expression of NESp-specific virulence factor PspK in an encapsulated strain has not been previously studied, and we showed significantly increased adhesion and invasion of human epithelial cells by pneumococci. Murine colonization was not significantly increased when an encapsulated strain expressed PspK, but colonization was increased when a capsule mutant expressed PspK. The ability of PspK expression to increase colonization in a capsule mutant despite no increase in adhesion can be attributed to other functions of PspK, such as sIgA binding or immune modulation. OM is a substantial economic burden, thus a better understanding of both encapsulated pneumococcal pathogenesis and the emerging pathogen NESp is necessary for effective prevention and treatment.

Keywords: ***Streptococcus pneumoniae,*** **pneumococcal surface proteins, PspK, nonencapsulated *Streptococcus pneumoniae*, NESp, pneumococcus, chinchilla, otitis media**

OPEN ACCESS

Edited by:
Jorge Eugenio Vidal, Emory University, USA

Reviewed by:
Kevin Mason, The Ohio State University, USA
W. Edward Swords, Wake Forest University Health Sciences, USA

****Correspondence:***
Larry S. McDaniel
lmcdaniel@umc.edu

†Present Address:
Lance E. Keller, Department of Molecular Genetics, University of Groningen, Groningen, Netherlands

Received: *25 January 2016*
Accepted: *02 May 2016*
Published: *18 May 2016*

Citation:
Keller LE, Bradshaw JL, Pipkins H and McDaniel LS (2016) Surface Proteins and Pneumolysin of Encapsulated and Nonencapsulated Streptococcus pneumoniae Mediate Virulence in a Chinchilla Model of Otitis Media. Front. Cell. Infect. Microbiol. 6:55. doi: 10.3389/fcimb.2016.00055

INTRODUCTION

The pathogenesis of *Streptococcus pneumoniae* (the pneumococcus) is varied and complex due in part to surface structures (Gillespie and Balakrishnan, 2000; Hammerschmidt, 2006; Thornton et al., 2010). Pneumococcal diseases account for ∼1 million childhood deaths annually worldwide (O'Brien et al., 2009). However, introduction of the pneumococcal conjugate vaccine (PCV) has led to a dramatic decline in invasive pneumococcal disease (IPD) (Fitzwater et al., 2012). The currently available pneumococcal vaccines target specific pneumococcal polysaccharide serotypes, 23 in Pneumovax (Pneumovax® 23; PPSV23; Merck, Whitehouse Station, NJ, USA), and 13 in Prevnar [Prevnar 13®; PCV13; Pfizer (formerly Wyeth Pharmaceuticals), New York, NY, USA]. Despite extensive use of the PCV in certain parts of the world, noninvasive pneumococcal infections are still prevalent (Weinberger et al., 2011). Noninvasive pneumococcal infections include nonbacteremic pneumonia, conjunctivitis, otitis media (OM), and sinusitis. The pneumococcus is a common etiological agent of OM. In the United States, OM is responsible for most pediatrician visits (McCaig and Hughes, 1995; Gonzales et al., 2001; Lieberthal et al., 2013).

The major pneumococcal virulence factor and target of the PCV is the pneumococcal polysaccharide capsule. There are at least 97 antigenically distinct capsule types (serotypes), as well as pneumococci that do not express any capsule (Geno et al., 2015). Encapsulated strains are dependent on the presence of capsule for all stages of the life cycle, from colonization to virulence, while nonencapsulated *S. pneumoniae* (NESp) do not require a capsule (Kadioglu et al., 2008). Pneumococcal surface proteins are required for colonization and mediate virulence independent of the capsular status. Pneumococcal surface proteins are classified by means of surface attachment and include choline binding proteins (CBPs), LPxTG binding, lipoproteins, and nonclassical surface proteins (Bergmann and Hammerschmidt, 2006).

The surface of NESp and encapsulated pneumococci vary greatly, not only because of the presence or absence of capsule, but also based on the various surface proteins expressed. Regardless of what surface proteins are expressed in either NESp or encapsulated pneumococci, they are essential for colonization and pathogenesis (Valentino et al., 2014). The surface composition between different encapsulated strains also varies, usually as a result in variations of what genes are encoded and expressed, along with different protein isoforms. For instance, the encapsulated pneumococcal CBPs PspA and PspC have multiple variants and have been shown to be important for virulence in both invasive and noninvasive infections (Ogunniyi et al., 2007a). It is important to understand the alterations in virulence profiles as a consequence of differential surface protein expression in order to better understand which strains may be more pathogenic. Furthermore, genetic exchange between pneumococci occurs rapidly and can alter the virulence potential of a strain. Past studies examining alterations in surface proteins have shown that during OM, deletion of PspC reduced virulence while loss of PspA completely eliminated disease in a serotype 2 background (Schachern et al., 2014). NESp lack PspA and PspC but some express the LPxTG binding protein PspK, which has been shown to increase NESp colonization and virulence during OM (Park et al., 2012; Keller et al., 2013, 2014, 2015). We have previously demonstrated adherence to epithelial cells is an important function of NESp surface proteins, and increased adhesion of NESp correlated to increased bacterial burden during OM (Keller et al., 2013, 2014). Another important virulence factor that all known encapsulated and nonencapsulated pneumococci possess is pneumolysin (Ply). It has been shown that Ply has a significant function during infection (Mitchell and Mitchell, 2010). The role of Ply in NESp virulence during OM has not been previously established.

Pneumococci are known to exchange genetic material that has resulted in a high frequency of recombination within the *cps* locus, potentially as a consequence of selective pressure from the use of the PCV (Croucher et al., 2011). Genetic exchange at the *cps* locus between encapsulated pneumococci and NESp may allow encapsulated strains to persist transiently as a nonencapsulated variant despite vaccination. High rates of chromosomal recombination are also focused around regions harboring genes for antibiotic resistance (Croucher et al., 2011). Antibiotic resistance is commonly observed in pneumococcal strains, and NESp often harbor multiple drug resistances (Sulikowska et al., 2004; Chewapreecha et al., 2014; Keller et al., 2016). Due to rapid transfer of resistance genes between pneumococcal strains, prompt, and targeted treatment is necessary for pneumococcal infections. Timely treatment allows for faster resolution and may limit dissemination into other sites.

The current study demonstrates that the absence of Ply reduces the ability of NESp to cause OM. Also, epithelial cell adherence is an important function of OM virulence, but does not directly lead to pathogenesis of encapsulated strains. Additionally, we demonstrate that expression of PspK in capsule mutants partially compensates for the loss of capsule during colonization, thus affording pneumococci a way to circumvent increased use of capsule targeting vaccines.

METHODS

Bacterial Strains

Table 1 contains bacterial strains, relevant mutations, and selective markers used in the current study. All pneumococcal strains were grown at 37°C in 5% CO_2 in Todd-Hewitt medium with 0.5% yeast extract (THY), or on sheep blood agar (BA) with appropriate antibiotic selection as indicated in **Table 1**. Genomic and plasmid DNA was obtained using manufacturers protocols with a DNeasy blood and tissue kit (Qiagen) or a plasmid minikit (Qiagen), respectively. Plasmids were maintained in *Escherichia coli* strain DH5α and grown in Luria Bertani broth (LB) with appropriate antibiotic selection.

Genetic Manipulations

Gene deletions were made through allelic replacement. Pneumococcal transformations were performed in competence media (THY, 0.2% fresh bovine serum albumin, 0.01% $CaCl_2$, and 0.1% glucose). Bacteria were grown in competence media to approximately OD_{600} 0.2, diluted 1:20 in competence media, and

TABLE 1 | Bacterial strains used in this study.

Strain	Parent strain	Serotype	Mutation	Marker[a]	References
D39		2			Avery et al., 1944
ΔPAC	D39	2	Ply/PspA/PspC Deletion	Tmp-Tet-Erm (10 μg/ml-5 μg/ml-0.3 μg/ml)	Quin et al., 2007
R36A	D39	2	Capsule Mutation		Taylor, 1949
LEK20	D39	2	PspK Addition	Kan (500 μg/ml)	This study
AM1000	D39	2	Capsule Mutation		Magee and Yother, 2001
LEK16	D39	2	Capsule Deletion/PspK Addition	Kan (500 μg/ml)	This study
MNZ67		NESp			Park et al., 2012
LEK05	MNZ67	NESp	PspK Deletion	Spec (300 μg/ml)	This study
LEK07	MNZ67	NESp	Ply Deletion	Tmp (10 μg/ml)	This study
LEK11	MNZ67	NESp	PspK/Ply Deletion	Spec-Tmp (300 μg/ml-10 μg/ml)	This study
EF3030		19F			Andersson et al., 1983
LEK10	EF3030	19F	PspC Deletion	Erm (0.3 μg/ml)	This study
LEK12	EF3030	19F	Capsule Deletion	Spec (300 μg/ml)	This study
LEK14	EF3030	19F	PspK Addition	Kan (500 μg/ml)	This study
LEK15	EF3030	19F	Capsule Deletion/PspK Addition	Spec-Kan (300 μg/ml-500 μg/ml)	This study

[a] *Tmp-trimethoprim; Tet, Tetracycline; Erm, Erythromycin; Kan, Kanamycin; Spec, Spectinomycin.*

stimulated with 2 μg/ml of competence-stimulating peptide 1 (CSP-1) for 12 min before the addition of ∼1 μg of DNA (Yother et al., 1986). Pneumococci were incubated for 4 h at 37°C before plating on BA containing appropriate antibiotic selection.

DNA for *pspK* deletion in MNZ67 and *cps* deletion in EF3030 was obtained through polymerase chain reaction (PCR) of genomic DNA isolated from MNZ1131 (Park et al., 2012) with primers DexBF (5′-GACTATCTAGCCAAGCTAGG-3′) and AliAR (5′- CCCTGTACGAGATGTAGTTG -3′). DNA for *ply* deletion was isolated from ΔPly2 (Thornton and McDaniel, 2005) using primers UpstreamPlyF (5′-CTAGCCTTGACAACT AGCCAATC-3′) and DownstreamPlyR (5′-TGCAAATAGAAA GTTTCAGCC-3′). Expression of PspK was achieved through ectopic expression using plasmid pABG5. The *pspK* gene was isolated from genomic MNZ67 DNA using primers pABG5 PspKF (5′-GCG**GAATTC**ATGAATAATAAGAATATCATC CCGATGAG-3′) and pABG5 PspKR (5′-GCG**CTGCAG**CTA ATTTTTATGTTTAACAAATGGAAGA-3′). Primers contain restriction sites EcoRI and PstI, respectively, indicated by bolded and underlined section of primer. Plasmid pABG5 and *pspK* amplicon was digested with EcoRI (NEB) and PstI (NEB), ligated with T4 DNA ligase (Thermo Scientific) and transformed into DH5α making pABG5::*pspK*. Plasmid verified by sequencing and PspK levels in wildtype MNZ67 and PspK expression mutants were equivalent as determined by flow cytometry and Western blot analysis.

Adhesion and Invasion Assays

Adhesion and invasion assays were performed as previously described (Keller et al., 2013). In brief, 24 well-plates were seeded to ∼90% confluency with human pharyngeal cell line Detroit 562 or lung cell line A549. Epithelial cells were incubated with 1×10^7 CFU/ml of bacteria suspended in EMEM for 30 min then washed two times with 1X PBS to remove unbound pneumococci. Epithelial cells were trypsinized (100 μl 0.25% Trypsin-EDTA) and plated on BA for enumeration. Invasion assays were performed as above, but epithelial cells were incubated with bacteria for 2 h before being washed two times with 1X PBS. Washed cells were further incubated for 1 hr with EMEM containing 10 μg/ml penicillin and 200 μg/ml streptomycin to kill extracellular bacteria. Epithelial cells were washed and trypsinized as above before enumeration on BA.

Experimental OM

Experimental OM was performed as previously described (Keller et al., 2014). In brief, young adult chinchillas (*Chinchilla lanigera*, body weight 400–500 g) from Ryerson Chinchilla Ranch were allowed to acclimate for at least 7 days. Otoscopic examination was used to examine the tympanic membrane of all animals before infection. Chinchillas with no visible pathology received 100 μl transbullar injections containing 1×10^7 NESp or 1×10^2 encapsulated pneumococci in 1X PBS containing 0.04% gelatin. Differences in inoculum amounts between NESp and encapsulated pneumococci were calculated in accordance to previous studies that displayed encapsulated pneumococci to be highly invasive causing sepsis and death very rapidly at high inoculums in this model (Forbes et al., 2008). Chinchillas were injected with 1×10^4 of the D39 mutant ΔPAC due to a known reduction of virulence in other animal models (Ogunniyi et al., 2007b). Infections with encapsulated pneumococci were only performed out to 3 days due to significant pathology of these strains. Animals were monitored daily for clinical symptoms (listing, loss of appetite, and response to stimulus or noise) and tympanic membrane was visualized for inflammation immediately following euthanasia with a Karl Storz Vetcam XL 692800 20 with an otoscopic attachment. Samples were collected and visible tympanic inflammation and biofilm formation were scored. Tympanic inflammation was scored through otoscopic

examination as follows: 0 = none, 1 = inflammation, 2 = effusion, and 3 = tympanic rupture. The tympanic membrane of an uninfected chinchilla is an opalescence off-white color with inflammation defined as visible rubor or yellowing of the membrane. Effusion of the middle ear is indicated by physical presence of fluid upon sample processing or yellowing of the tympanic membrane with visible pockets of air behind the membrane. Tympanic rupture is indicated by a breach of the tympanic membrane with possible drainage. Biofilm formation was visibly scored as follows: 0 = none, 1 = surface formation, 2 = traverses bulla, and 3 = traverses bulla with thickening. For treatment experiments, ampicillin (100 mg/kg) was administered intramuscularly every 12 h starting at the indicated time points. Individual data points in OM studies represent each bulla per animal (2 total), with at least two biological replicates examining 1–2 chinchillas per replicate. All animal studies were performed in accordance with protocols approved by the University of Mississippi Medical Center Institutional Animal Care and Use Committee.

Murine Colonization

Mouse studies were performed as previously described (Keller et al., 2013). In brief, 6–8 week old C57/BL6 mice were lightly anesthetized with isoflurance and intranasally (IN) challenged with 10 μl 1X PBS containing $\sim 1 \times 10^7$ bacteria. Five days post-challenge, mice were euthanized, nasopharyngeal lavage, and tissue samples as well as bullae were collected, and bacteria were enumerated on BA containing 5 μg/ml gentamicin. Samples were collected through retrograde lavage of 200 μl sterile saline solution starting from exposed trachea and samples collected from the nares. Mice were decapitated and physically denuded of fur followed by transverse sectioning of skull posterior of orbital sockets. Anterior section of the skull was bisected down sagittal plane and nasopharyngeal tissue collected with forceps and homogenized in 200 μl 1X PBS before enumeration. Colonizing bacteria are a combination of bacterial counts from lavage and nasopharyngeal tissue from the same mouse. Pneumococcal ascension to the middle ear was assessed by bacterial enumeration of bullae collected from the IN challenged mice. The posterior section of the skull was bisected down the sagittal plane and brain removed from both sections. Bullae were located slightly posterior and caudally of external ear canal, removed with forceps, and homogenized in 200 μl 1X PBS before enumeration on BA containing 5 μg/ml gentamicin.

Statistical Analysis

Results from adhesion assays were determined by Student's *t*-test with the InStat program (GraphPad Software). For OM and colonization, the numbers of CFU in the different experimental groups were compared using the Mann-Whitney test with the InStat program. Significant results are indicated by *P* values of <0.05.

RESULTS

We have previously demonstrated that deletion of PspK from NESp MNZ11, a sequence type (ST) 6151, reduced pathogenesis in an OM model and significantly reduced epithelial cell adhesion (Keller et al., 2014). Deletion of PspK from NESp MNZ67 (ST1464) also significantly reduced bacterial burden during OM in a chinchilla model, $p < 0.0001$ (**Figure 1A**). Inflammation and biofilm formation were significantly reduced when comparing PspK deletion mutant (LEK05) to wildtype (MNZ67), $p = 0.028$ and $p = 0.0027$, respectively (**Table 2**). Next, the significance of Ply in NESp OM pathogenesis was determined because pneumolysin has been associated with increased inflammation (Hirst et al., 2004). We observed a significant reduction in recovered bacteria from the middle ear (**Figure 1A**). Also, a significant reduction in biofilm formation was observed when *ply* was deleted (**Table 2**). Next a double mutant lacking both PspK and Ply was tested for virulence during OM. Surprisingly, there was no significant difference in the number of bacteria recovered from the chinchilla middle ear in comparison to wildtype MNZ67, $p > 0.05$. (**Figure 1A**).

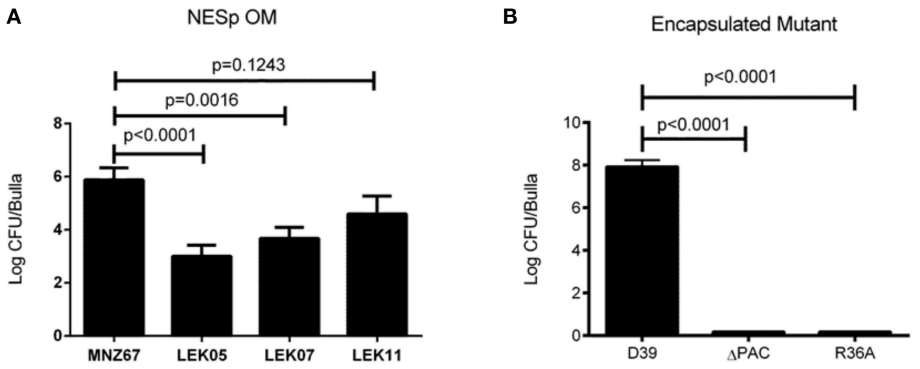

FIGURE 1 | Deletion of pneumococcal virulence factors significantly reduces bacterial burden during experimental OM. (A) Single gene deletion of *pspK* (LEK05; $p < 0.0001$) or *ply* (LEK07; $p = 0.0016$) and double gene deletions of *pspK* and *ply* (LEK11; $p = 0.1243$) had significant reductions in recovered bacteria compared to wildtype NESp MNZ67. **(B)** Serotype 2 pneumococcal strain D39 had high levels of bacteria recovered from the middle ear of chinchillas, but no bacteria were recovered when chinchillas were challenged with a D39 triple gene deletion mutant ΔPAC or acapsulalar mutant R36A ($p < 0.0001$). Data represents at least two independent experiments of four bullae per experiment.

Previous studies have shown the importance of PspA and PspC for encapsulated pneumococci (serotype 2) during OM (Schachern et al., 2014). We have shown the importance of Ply for NESp OM virulence in contrast to past work in encapsulated pneumococci (serotype 3) (Sato et al., 1996). A combination of PspA, PspC, and Ply deletion have not been tested in encapsulated strains. We found that deleting all three proteins from serotype 2 strain D39 (ΔPAC) and deletion of capsule (R36A) completely attenuated virulence in comparison to wildtype, $p < 0.0001$ (**Figure 1B**). A corresponding reduction in inflammation and biofilm formation was observed when comparing triple mutant ΔPAC and capsule mutant R36A to wildtype D39 $p < 0.0001$ (**Table 2**).

As previously reported, increased adhesion of NESp to epithelial cells correlated with increased bacterial recovery from the middle ear of chinchillas (Keller et al., 2014). Due to reduced bacterial recovery of Ply deletion mutants, we wanted to determine if Ply impacted epithelial adhesion. Although we observed a reduction in pneumococci recovered during OM, **Figure 2A** shows deletion of *ply* did not reduce epithelial cell adhesion to pharyngeal cell line Detroit 562 ($p > 0.05$). This indicated that another virulence mechanism, such as biofilm formation, may be responsible for the decrease in recovered bacteria. As expected deletion of PspK from wildtype strain MNZ67 did reduce epithelial adhesion ($p < 0.0001$). Deletion of capsule has been shown to increase epithelial cell adhesion of encapsulated strains, which we verified here (**Figure 2B**). Increased epithelial cell adherence of NESp has led to increased bacterial recovery during experimental OM, but we did not observe that correlation when capsule genes were deleted from encapsulated strains despite increased epithelial cell adherence.

We have shown that D39 (serotype 2) can infect chinchillas and specific virulence factors play a role in pathogenesis. Unfortunately D39 resulted in high virulence in the chinchilla OM model with as few as 10 CFU causing death in some chinchillas limiting its usefulness due to ethical reasons (data not shown). We wanted to determine if other serotypes were as virulent as D39 during an OM infection, so we investigated encapsulated strain EF3030 (19F, known causative serotype of OM) for our infection model (Joloba et al., 2001). High bacterial loads of EF3030 were recovered from the middle ear of chinchillas during experimental OM (**Figure 3**) with a portion of infected chinchillas becoming septic. However, chinchillas infected with EF3030 had better clinical outcomes than D39 infected animals (data not shown). No difference between inflammation or biofilm formation was observed between D39 and EF3030, $p > 0.05$ (**Table 2**). In an effort to reduce invasiveness of encapsulated EF3030, PspC was deleted. Deletion of PspC from EF3030 (LEK10) reduced bacterial burden, $p = 0.0026$, but did not prevent invasive infections in chinchillas (**Figure 3**).

We next wanted to determine if treatment of an OM infection prone to systemic invasion was treatable with commonly prescribed antibiotics, and if the time of treatment aided in outcome. Amoxicillin is a commonly prescribed antibiotic for the treatment of OM (Lieberthal et al., 2013). The use of ampicillin

TABLE 2 | Inflammation and biofilm scores of infected chinchillas.

Strain	Inflammation score	Biofilm formation	Inflammation *P*-value	Biofilm *P*-value
MNZ67	1.00 ± 0.41	2.00 ± 0.41		
LEK05	0.00 ± 0.00	0.25 ± 0.25	**0.0286**	**0.0002**
LEK07	0.50 ± 0.29	0.50 ± 0.29	0.33	**0.0015**
LEK11	1.375 ± 0.26	1.00 ± 0.27	0.45	0.061
D39	1.50 ± 0.29	2.00 ± 0.00		
ΔPAC	0.00 ± 0.00	0.00 ± 0.00	**0.0021**	**0.0001**
R36A	0.50 ± 0.25	0.60 ± 0.37	**0.04**	**0.0091**
EF3030	2.00 ± 0.00	1.75 ± 0.25		
LEK10	1.50 ± 0.29	2.00 ± 0.00	0.1354	0.4816

Scores are average with standard error of the mean with significant p-values indicated in bold. P-value is for mutant vs. parent strain.

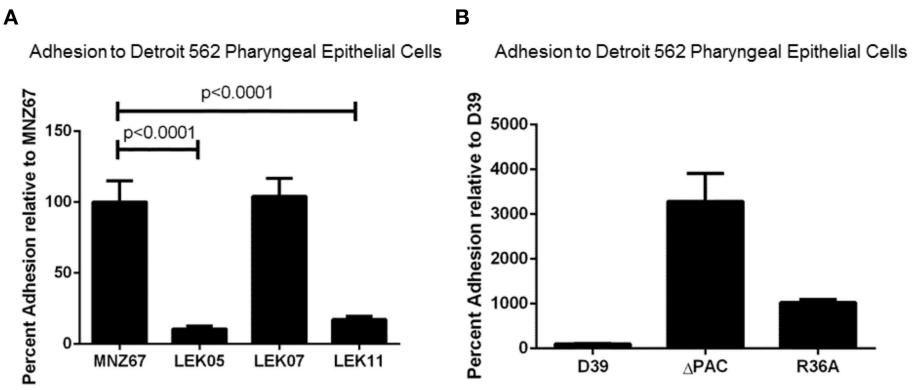

FIGURE 2 | Adhesion of pneumococci to human pharyngeal epithelial cell line Detroit 562 is affected by specific gene deletions. (A) Deletion of *pspK* from wildtype NESp MNZ67 significantly reduced bacterial adhesion to epithelial cells, but no effect was seen with a *ply* gene deletion. Deletion of *pspK* and *ply* from MNZ67 (LEK11) significantly reduced epithelial cell adhesion compared to wildtype MNZ67 ($p < 0.0001$). **(B)** Pneumococcal epithelial cell adhesion was significantly increased in both D39 mutants, ΔPAC and R36A ($p < 0.0001$). Data represents three independent experiments in triplicate.

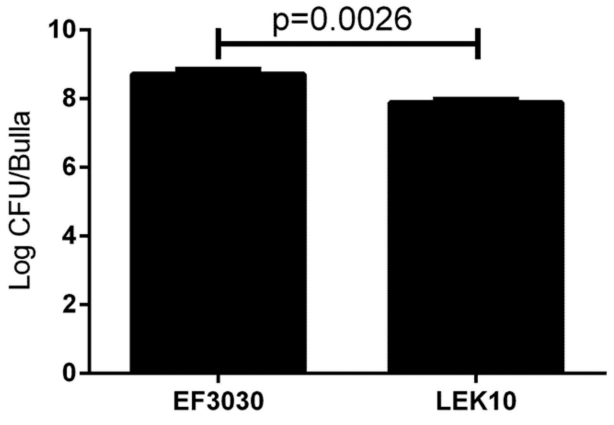

FIGURE 3 | Encapsulated strain EF3030 (serotype 19F) middle ear pathogenesis in chinchillas are not mediated by PspC. There is a significant decrease in the amount of bacteria recovered from the middle ear of chinchillas when comparing wildtype EF3030 to *pspC* gene deletion (LEK10). Data represents samples from four bullae.

for our study avoids excess stress upon the animals by reducing the handling necessary to gavage treatment into an infected chinchilla. We found that treatment starting within 24 h post-infection was able to completely clear EF3030 infection, $p < 0.0001$ (**Figure 4A**). Treatment starting 48 h after infection was also able to reduce bacterial burden, but only by two logs compared to no treatment, $p < 0.005$ (**Figure 4A**). EF3030 with no treatment had increased inflammation (**Figure 4C**) compared to treatment starting at 24 h post-infection (**Figure 4B**) or 48 h post-infection (**Figure 4D**).

We have shown that pneumolysin and surface proteins impact pneumococcal virulence and rapid treatment is necessary to efficiently clear infections and limit systemic dissemination. Genetic exchange between pneumococci occurs regardless of capsule status, but the effect of a NESp-specific surface protein expressed in an encapsulated strain has never been determined. Past studies have utilized D39 acapsular derivative R36A for PspK expression in an encapsulated background (Keller et al., 2013, 2014), but R36A has been lab adapted for decades and may not represent a capsule exchange that occurs naturally. Here, we use a PspK expressing plasmid to determine the effects of PspK expression on encapsulated pneumococcal adherence and colonization with and without the presence of capsule. As shown in **Figures 5A,B**, expression of PspK in encapsulated strains EF3030 and D39 increased their ability to adhere to lung epithelial cell line A549, $p < 0.0001$ and $p = 0.032$ respectively. While this is independent of the two serotypes tested, EF3030 (serotype 19F) had a significantly greater increase in lung epithelial cell adhesion than D39 (serotype 2). The deletion of capsule increased epithelial cell adhesion with or without the presence of PspK. Surprisingly, expression of PspK in acapsular mutants did not significantly increase epithelial cell adhesion when the capsule was absent. This is in contrast to past work using the D39 capsule mutant R36A (Keller et al., 2013). There was a concurrent increase in epithelial cell invasion in all samples in which epithelial cell adhesion was increased (**Figures 5C,D**).

We next wanted to determine if these effects *in vitro* were also observed in a mouse model. Since increased adherence may correlate to enhanced virulence of encapsulated strains, the chinchilla OM virulence model was avoided due to ethical consideration of the animals. EF3030 was chosen for this model because it is a known colonizer of the mouse nasopharynx and, unlike D39, does not disseminate into the blood in mice. As shown in **Figure 6A**, there was no difference in the ability of EF3030 to colonize when PspK was present or absent. In contrast, when the capsule is removed from EF3030 and PspK is expressed, there were significantly more bacteria recovered from the mouse nasopharynx ($p = 0.0082$), but not equivalent to wildtype EF3030 levels. The amount of bacteria that ascended through the mouse Eustachian tube into the middle ear was also quantified (**Figure 6B**). Expression of PspK in EF3030 or in EF3030 capsule mutant LEK12 did not significantly increase the number of bacteria collected from the middle ear.

DISCUSSION

PspK plays an important role in NESp pathogenesis along with pneumolysin (Ply) (**Figure 1**). While PspK mediated virulence is through increased epithelial cell adhesion, Ply virulence is not (**Figure 2A**). The expression of PspK in encapsulated strains increases adhesion *in vitro* to human epithelial cells (**Figures 5A,B**), but does not correlate to increased ability to colonize the mouse nasopharynx. Colonization by a capsule mutant of an encapsulated strain is partially rescued by the expression of PspK, but not to the level of a wildtype encapsulated strain (**Figure 6A**). We were also able to show the importance of surface proteins for OM in encapsulated strains, as well as an increased efficacy of treatment when the treatment is started early during infection.

We first described PspK as a virulence protein in the chinchilla using MNZ11, a ST6151 strain that is genetically related to other NESp based on sequence type (Keller et al., 2014). The current study uses a NESp MNZ67, a ST1464 that has been previously associated with pneumococci of the 19F serotype. We determined that PspK performs a similar function in NESp regardless of the genetic background in which it is being expressed, both in terms of *in vitro* epithelial cell adhesion and *in vivo* pathogenesis. The role of Ply, a known virulence factor found in all encapsulated and nonencapsulated pneumococci, was also examined in NESp virulence. We were able to demonstrate a significant decrease in virulence during OM when Ply was not expressed (**Figure 1**), and this is independent of epithelial cell adhesion. Decreased virulence was most notable in the amount of biofilm in the middle ear, with the Ply mutant producing significantly less biofilm than wildtype MNZ67 (**Table 2**). This is unsurprising due to previous reports on the importance of Ply for biofilm formation and helps explain the decrease in recovered bacteria (Shak et al., 2013). Recent reports of NESp have also identified a second Ply-like

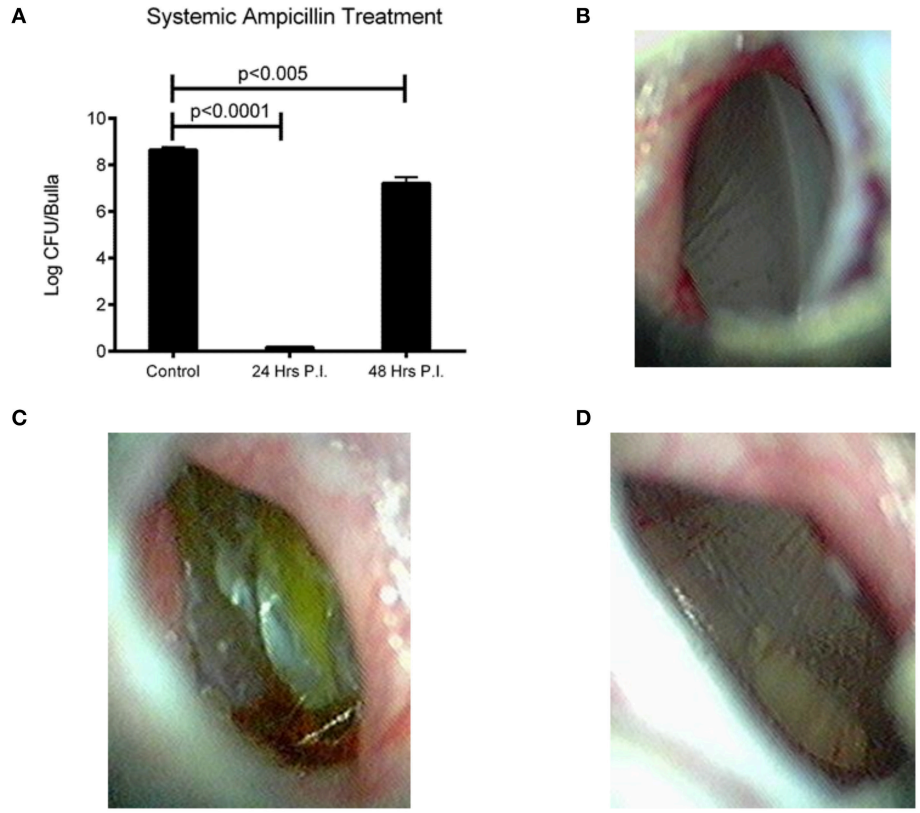

FIGURE 4 | Effect of bacterial burden and clinical symptoms of systemic ampicillin treatment of EF3030 OM model. (A) Untreated animals had high levels of recovered bacteria and ampicillin treatment significantly reduced bacterial burden. Treatment starting 24 h post-infection cleared all detectable bacteria from the middle ear and treatment starting 48 h post-infection had a smaller, but significant reduction in recovered bacteria. **(B)** Tympanic membrane of animal 72 h post-infection and 48 h after start of treatment. **(C)** Tympanic membrane of mock treated animal 72 h post-infection. **(D)** Tympanic membrane of animal 72 h post-infection and 24 h after start of treatment. Data represents samples from four bullae and representative pictures.

gene (*plyB*) that is more closely related to cytolysins of other streptococcal species (Morales et al., 2015). The presence of this second cytolysin may compensate for the deletion of the canonical Ply, but this has yet to be tested. This led to the question of the importance of pneumolysin in encapsulated strains during experimental OM.

In contrast to this study with a pneumolysin mutant in NESp, a previous study in encapsulated pneumococci showed no effect on OM virulence (Sato et al., 1996). It has been previously reported that the choline binding proteins PspA and PspC both play a role in pneumococcal pathogenesis, including middle ear infections (Schachern et al., 2014). We examined the encapsulated strain D39 and a triple deletion mutant (ΔPAC) that lacks PspA, PspC, and Ply because previous studies showed variable effects of individual mutants, but none containing all deletions (Schachern et al., 2014). The ΔPAC mutant has been found to be avirulent in other infection models (Ogunniyi et al., 2007b; Quin et al., 2007), but has not been previously tested in chinchillas. NESp lack both PspA and PspC yet are able to cause OM. Additionally, we have shown here that although virulence is reduced, a NESp Ply mutant is still able to cause an infection (**Figure 1**). The surface of the D39 mutant ΔPAC is similar to NESp by lacking these proteins, but still retains the important capsule virulence factor. Unlike NESp, ΔPAC was unable to cause OM and had no visible signs of pathology. While ΔPAC was inoculated at a lower CFU/ml than NESp, we have been able to previously recover NESp from chinchillas infected with as little as 1×10^4 inoculum but with a reduction in total number of infected animals (unpublished data). While capsule is important for encapsulated pneumococcal pathogenesis, it in itself is not sufficient to cause disease. Surprisingly, ΔPAC had increased adherence in comparison to wildtype D39. While increased adherence of NESp has been associated with higher rates of virulence in an OM model, this does not seem to hold for capsule mutants (Keller et al., 2014). Park et al. (2012) showed significantly less colonization by AM1000 in a mouse model compared to D39 despite higher rates of epithelial cell adhesion. We also examined the encapsulated strain EF3030 (serotype 19F) in a chinchilla model because it is less virulent in a mouse model and the serotype 2 D39 caused fatal pathology in several chinchillas within the time course of the study. We also tested a PspC mutant in the EF3030 background (LEK10) to reduce the invasive nature of EF3030. Both the wildtype and

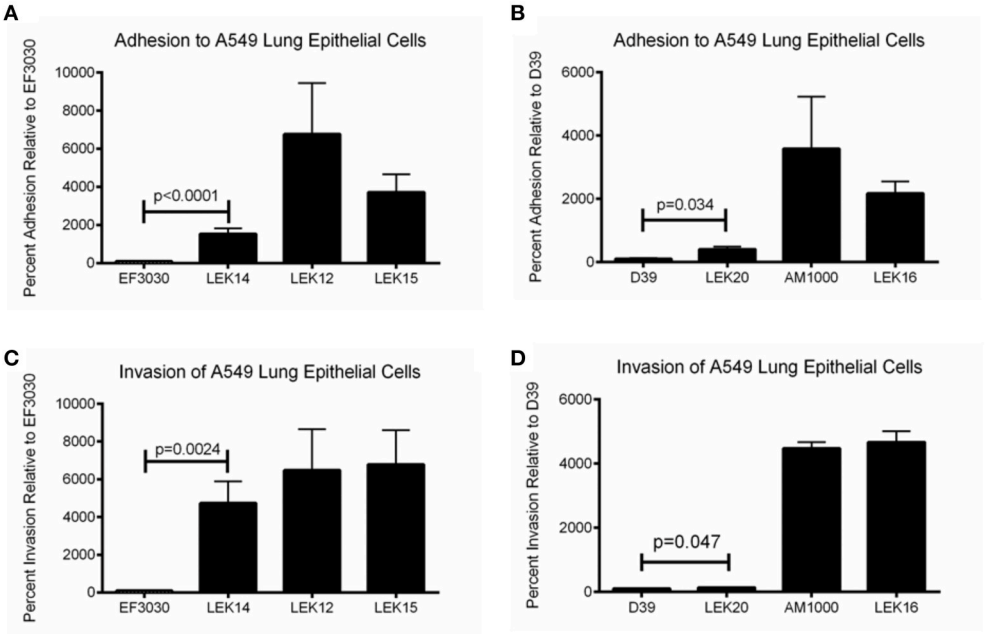

FIGURE 5 | Encapsulated strain EF3030 (serotype 19F) and mutants adherence and invasion to lung epithelial cell line A549. (A) Expression of PspK in serotype 19F EF3030 (LEK14) significantly increased epithelial cell adhesion when capsule was present ($p < 0.0001$). Deletion of capsule significantly increased epithelial cell adhesion (LEK12; $p < 0.0001$) compared to wildtype EF3030. Expression of PspK in LEK12 (EF3030Δ*cps*) did not increase adhesion of LEK15 (EF3030Δ*cps*::PspK$^+$) compared to acapsular EF3030 (LEK12). **(B)** Expression of PspK in serotype 2 D39 (LEK20) significantly increased epithelial cell adhesion when capsule was present ($p = 0.034$). Deletion of capsule significantly increased epithelial cell adhesion (AM1000; $p < 0.0001$), but expression of PspK in AM1000 (D39Δ*cps*) did not increase adhesion of LEK16 (D39Δ*cps*::PspK$^+$). **(C)** Expression of PspK in serotype 19F EF3030 (LEK14) significantly increased epithelial cell invasion when capsule was present ($p = 0.0024$). Deletion of capsule significantly increased epithelial cell invasion (LEK12; $p = 0.0149$) compared to wildtype EF3030. Expression of PspK in LEK12 (EF3030Δ*cps*) did not increase invasion of LEK15 (EF3030Δ*cps*::PspK$^+$) compared to acapsular EF3030 (LEK12). **(D)** Expression of PspK in serotype 2 D39 (LEK20) significantly increased epithelial cell invasion when capsule was present ($p = 0.047$). Deletion of capsule significantly increased epithelial cell adhesion (AM1000; $p < 0.0001$), but expression of PspK in AM1000 (D39Δ*cps*) did not increase adhesion of LEK16 (D39Δ*cps*::PspK$^+$). Data represents three independent experiments in triplicate.

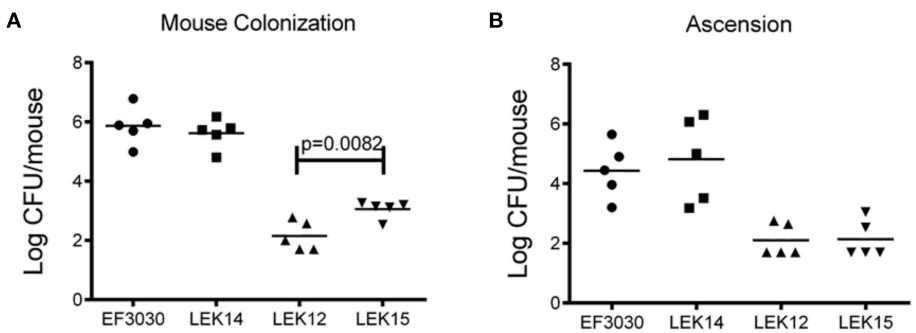

FIGURE 6 | Encapsulated strain EF3030 (serotype 19F) and mutants in a mouse model of colonization. (A) At 5 days post-infection, enumerated bacteria recovered from the mouse nasopharynx did not significantly increase when encapsulated EF3030 expressed PspK. EF3030 capsule mutant, LEK12, showed significantly more colonization when PspK was expressed (LEK15; $p = 0.0082$). **(B)** Collected bullae from colonized mice showed no significant difference in middle ear ascension when PspK was expressed independent of capsule status. Mean CFU/mouse indicated by horizontal bar on figure.

the PspC mutant were able to cause OM, but there was no significant difference between clinical symptoms. However, there was significantly fewer pneumococci recovered from the middle ear of chinchillas infected with the PspC mutant (**Figure 3**). In both EF3030 and LEK10, we were able to recover bacteria from the blood of infected chinchillas, and this led to the question of treatment.

Amoxicillin is a commonly prescribed antibiotic for middle ear infections, and EF3030 is susceptible to ampicillin and its derivations. Amoxicillin is an oral antibiotic that is absorbed

through the stomach and must be ingested for effective treatment. This entails restraining and gavaging chinchillas for treatment, inducing high amounts of stress given that treatment is administered every 12 h. Therefore, an injectable form of ampicillin was used as a substitute. We found that treatment administered 24 h after infection was able to completely clear OM within 48 h of start of treatment. This corresponded to reduced tympanic inflammation and a better clinical outcome. We also show that treatment administered 48 h after infection is still sufficient to reduce the bacterial burden during OM, even though only 24 h had elapsed since start of treatment (**Figure 4**). It was not surprising that ampicillin treatment cleared the pneumococcal infection, but it was somewhat surprising as how fast this occurred. This information is important to know as studies on treatment of NESp in middle ear infections have not been done, even though these bacteria tend to be highly drug resistant. Additionally, OM co-infections of pneumococcus and nontypeable *Haemophilus influenzae* (NTHi) are common (Casey and Pichichero, 2004; Dagan et al., 2013). It has been shown that secreted beta-lactamases from NTHi significantly improve survival of pneumococci in the middle ear (Weimer et al., 2011). Elucidating treatment and time to resolution of infection is necessary to determine the effectiveness of various antibiotics and to overcome the consequences of co-infections.

An interesting observation during this study was deletion of PspA, PspC, and Ply abolished D39 virulence even when capsule was present. Surface proteins are important for virulence, but NESp that lack common encapsulated surface proteins cause disease. We wanted to determine the effect of PspK expression on encapsulated strains and whether the expression of PspK in a capsule mutant is able to restore virulence. Despite *pspK* being located at the *cps* locus, it may be possible for an encapsulated variant to express PspK due to pneumococcal natural transformation and high levels of genetic variability. It has been observed that *aliD*, a NESp *cps* locus protein, is found in the *cps* locus of some encapsulated strains (Bentley et al., 2006; Keller et al., 2016). Ectopic expression of PspK in an encapsulated background was able to significantly increase the ability of an encapsulated strain to adhere to both lung and pharyngeal epithelial cell lines. This seems independent of capsule as the same effect was observed in a serotype 2 background (D39) and a serotype 19F background (EF3030). While an increase in adherence was observed in both serotypes, there was a significantly greater increase in adhesion when comparing EF3030 to D39 (**Figures 5A,B**). It is speculated that the capsule structure may affect the ability of PspK to increase adherence. This is because the type 2 capsule is composed of 6 repeating sugar subunits in comparison to the type 19F capsule which contains 3 repeating sugar subunits, which may alter capsule size and accessibility of PspK to epithelial cells (Bentley et al., 2006).

We were able to confirm that the deletion of the *cps* locus from encapsulated strains significantly increased epithelial cell adhesion of these mutants (**Figures 5A,B**). Surprisingly, the expression of PspK had no significant effect on epithelial cell adhesion when capsule was not present. This could be explained by a saturation of the epithelial cells, reducing the ability of PspK to interact with the epithelial cells. These findings are in contrast to our past work when expression of PspK in R36A did show a significant increase in epithelial cell adhesion. The capsule mutants made for this study were minimally passed, while the D39 derivative R36A has been passed multiple times and for several decades. This may have altered the surface of R36A compared to a recently made capsule mutant. When a mouse was colonized with these PspK expression strains with or without capsule, an opposite trend of what would be expected based on the adhesion data was observed (**Figure 6A**). The highly adherent EF3030 expressing PspK (LEK14) had no significant difference in colonization. Yet when PspK was expressed in a EF3030 capsule mutant (LEK15), there was significantly more bacteria recovered from the mouse nasopharynx. This effect must be independent of epithelial cell adhesion, as a capsule mutant was adherent with or without PspK expression. We have previously shown that PspK does bind sIgA and this may aid in colonization. Also, we have shown that PspK may be responsible for modulating the host immune response (Keller et al., 2015). If PspK down regulated innate immune responses, it would allow the more vulnerable capsule mutant to readily persist, which was our observation. The effects of PspK on cytokine expression were mild and may explain why only a small increase in colonizing bacteria was observed (Keller et al., 2015).

Taken together this work shows surface structures and Ply are important for pneumococcal OM in both encapsulated and nonencapsulated pneumococci. Also, deletion of multiple virulence factors seems to have a greater impact on virulence than single gene deletions. While this is not surprising, it emphasizes the importance for protein-based vaccines to contain multiple proteins for both broader and more complete protection. Targeting single proteins may not be sufficient to abolish virulence or clear an infection. NESp lack several of the proteins being developed for a protein vaccine, but PspK has been shown to be a protective immunogen (Keller et al., 2015). As replacement of capsule can be partially compensated for by acquisition of PspK, inclusion of PspK in future vaccine development may be necessary to provide the broadest protection possible.

AUTHOR CONTRIBUTIONS

LK and LM designed experiments. LK, JB, and HP made strains and performed experiments. LK and LM wrote the paper.

FUNDING

Funding was provided in part by institutional funds and a grant from Alcon Research to LSM.

ACKNOWLEDGMENTS

We would like to thank Jessica Friley for help with sample collection and processing of the *in vivo* models.

REFERENCES

Andersson, B., Dahmén, J., Frejd, T., Leffler, H., Magnusson, G., Noori, G., et al. (1983). Identification of an active disaccharide unit of a glycoconjugate receptor for pneumococci attaching to human pharyngeal epithelial cells. *J. Exp. Med.* 158, 559–570. doi: 10.1084/jem.158.2.559

Avery, O. T., MacLeod, C. M., and McCarty, M. (1944). Studies on the chemical nature of the substance inducing transformation of pneumococcal types: induction of transformation by a desoxyribonucleic acid fraction isolated from pneumococcus Type III. *J. Exp. Med.* 79, 137–158. doi: 10.1084/jem.79.2.137

Bentley, S. D., Aanensen, D. M., Mavroidi, A., Saunders, D., Rabbinowitsch, E., Collins, M., et al. (2006). Genetic analysis of the capsular biosynthetic locus from All 90 pneumococcal serotypes. *PLoS Genet.* 2:e31. doi: 10.1371/journal.pgen.0020031

Bergmann, S., and Hammerschmidt, S. (2006). Versatility of pneumococcal surface proteins. *Microbiology* 152, 295–303. doi: 10.1099/mic.0.28610-0

Casey, J. R., and Pichichero, M. E. (2004). Changes in frequency and pathogens causing acute otitis media in 1995–2003. *Pediatr. Infect. Dis. J.* 23, 824–828. doi: 10.1097/01.inf.0000136871.51792.19

Chewapreecha, C., Harris, S. R., Croucher, N. J., Turner, C., Marttinen, P., Cheng, L., et al. (2014). Dense genomic sampling identifies highways of pneumococcal recombination. *Nat. Genet.* 46, 305–309. doi: 10.1038/ng.2895

Croucher, N. J., Harris, S. R., Fraser, C., Quail, M. A., Burton, J., van der Linden, M., et al. (2011). Rapid pneumococcal evolution in response to clinical interventions. *Science* 331, 430–434. doi: 10.1126/science.1198545

Dagan, R., Leibovitz, E., Greenberg, D., Bakaletz, L., and Givon-Lavi, N. (2013). Mixed Pneumococcal–nontypeable *haemophilus influenzae* otitis media is a distinct clinical entity with unique epidemiologic characteristics and pneumococcal serotype distribution. *J. Infect. Dis.* 208, 1152–1160. doi: 10.1093/infdis/jit289

Fitzwater, S. P., Chandran, A., Santosham, M., and Johnson, H. L. (2012). The worldwide impact of the seven-valent pneumococcal conjugate vaccine. *Pediatr. Infect. Dis. J.* 31, 501–508. doi: 10.1097/INF.0b013e31824de9f6

Forbes, M. L., Horsey, E., Hiller, N. L., Buchinsky, F. J., Hayes, J. D., Compliment, J. M., et al. (2008). Strain-specific virulence phenotypes of *Streptococcus pneumoniae* assessed using the *Chinchilla laniger* model of otitis media. *PLoS One* 3:e1969. doi: 10.1371/journal.pone.0001969

Geno, K. A., Gilbert, G. L., Song, J. Y., Skovsted, I. C., Klugman, K. P., Jones, C., et al. (2015). Pneumococcal capsules and their types: past, present, and future. *Clin. Microbiol. Rev.* 28, 871–899. doi: 10.1128/CMR.00024-15

Gillespie, S. H., and Balakrishnan, I. (2000). Pathogenesis of pneumococcal infection. *J. Med. Microbiol.* 49, 1057–1067. doi: 10.1099/0022-1317-49-12-1057

Gonzales, R., Malone, D. C., Maselli, J. H., and Sande, M. A. (2001). Excessive antibiotic use for acute respiratory infections in the United States. *Clin. Infect. Dis.* 33, 757–762. doi: 10.1086/322627

Hammerschmidt, S. (2006). Adherence molecules of pathogenic pneumococci. *Curr. Opin. Microbiol.* 9, 12–20. doi: 10.1016/j.mib.2005.11.001

Hirst, R. A., Kadioglu, A., O'Callaghan, C., and Andrew, P. W. (2004). The role of pneumolysin in pneumococcal pneumonia and meningitis. *Clin. Exp. Immunol.* 138, 195–201. doi: 10.1111/j.1365-2249.2004.02611.x

Joloba, M. L., Windau, A., Bajaksouzian, S., Appelbaum, P. C., Hausdorff, W. P., and Jacobs, M. R. (2001). Pneumococcal conjugate vaccine serotypes of *Streptococcus pneumoniae* isolates and the antimicrobial susceptibility of such isolates in children with otitis media. *Clin. Infect. Dis.* 33, 1489–1494. doi: 10.1086/323027

Kadioglu, A., Weiser, J. N., Paton, J. C., and Andrew, P. W. (2008). The role of *Streptococcus pneumoniae* virulence factors in host respiratory colonization and disease. *Nat. Rev. Microbiol.* 6, 288–301. doi: 10.1038/nrmicro1871

Keller, L. E., Friley, J., Dixit, C., Nahm, M. H., and McDaniel, L. S. (2014). Nonencapsulated *Streptococcus pneumoniae* cause acute otitis media in the chinchilla that is enhanced by pneumococcal surface protein K. *Open Forum Infect. Dis.* 1:ofu037. doi: 10.1093/ofid/ofu037

Keller, L. E., Jones, C. V., Thornton, J. A., Sanders, M. E., Swiatlo, E., Nahm, M. H., et al. (2013). PspK of *Streptococcus pneumoniae* increases adherence to epithelial cells and enhances nasopharyngeal colonization. *Infect. Immun.* 81, 173–181. doi: 10.1128/iai.00755-12

Keller, L. E., Luo, X., Thornton, J. A., Seo, K.-S., Moon, B. Y., Robinson, D. A., et al. (2015). Immunization with pneumococcal surface protein K of nonencapsulated *Streptococcus pneumoniae* provides protection in a mouse model of colonization. *Clin. Vaccine Immunol.* 22, 1146–1153. doi: 10.1128/CVI.00456-15

Keller, L. E., Robinson, D. A., and McDaniel, L. S. (2016). Nonencapsulated *Streptococcus pneumoniae*: emergence and pathogenesis. *mBio* 7:e01792-15. doi: 10.1128/mBio.01792-15

Lieberthal, A. S., Carroll, A. E., Chonmaitree, T., Ganiats, T. G., Hoberman, A., Jackson, M. A., et al. (2013). The diagnosis and management of acute otitis media. *Pediatrics* 131, e964–e999. doi: 10.1542/peds.2012-3488

Magee, A. D., and Yother, J. (2001). Requirement for capsule in colonization by *Streptococcus pneumoniae*. *Infect. Immun.* 69, 3755–3761. doi: 10.1128/iai.69.6.3755-3761.2001

McCaig, L. F., and Hughes, J. M. (1995). TRends in antimicrobial drug prescribing among office-based physicians in the united states. *JAMA* 273, 214–219. doi: 10.1001/jama.1995.03520270048030

Mitchell, A. M., and Mitchell, T. J. (2010). *Streptococcus pneumoniae*: virulence factors and variation. *Clin. Microbiol. Infect.* 16, 411–418. doi: 10.1111/j.1469-0691.2010.03183.x

Morales, M., Martín-Galiano, A. J., Domenech, M., and García, E. (2015). Insights into the evolutionary relationships of LytA autolysin and Ply pneumolysin-like genes in *Streptococcus pneumoniae* and related Streptococci. *Genome Biol. Evol.* 7, 2747–2761. doi: 10.1093/gbe/evv178

O'Brien, K. L., Wolfson, L. J., Watt, J. P., Henkle, E., Deloria-Knoll, M., McCall, N., et al. (2009). Burden of disease caused by *Streptococcus pneumoniae* in children younger than 5 years: global estimates. *Lancet* 374, 893–902. doi: 10.1016/S0140-6736(09)61204-6

Ogunniyi, A. D., Grabowicz, M., Briles, D. E., Cook, J., and Paton, J. C. (2007a). Development of a vaccine against invasive Pneumococcal disease based on combinations of virulence proteins of *Streptococcus pneumoniae*. *Infect. Immun.* 75, 350–357. doi: 10.1128/iai.01103-06

Ogunniyi, A. D., LeMessurier, K. S., Graham, R. M. A., Watt, J. M., Briles, D. E., Stroeher, U. H., et al. (2007b). Contributions of Pneumolysin, Pneumococcal surface protein A (PspA), and PspC to Pathogenicity of *Streptococcus pneumoniae* D39 in a mouse model. *Infect. Immun.* 75, 1843–1851. doi: 10.1128/IAI.01384-06

Park, I. H., Kim, K. H., Andrade, A. L., Briles, D. E., McDaniel, L. S., and Nahm, M. H. (2012). Nontypeable pneumococci can be divided into multiple cps types, including one type expressing the novel gene pspK. *mBio* 3, e00035–e00012. doi: 10.1128/mBio.00035-12

Quin, L. R., Moore, Q. C., and McDaniel, L. S. (2007). Pneumolysin, PspA, and PspC contribute to pneumococcal evasion of early innate immune responses during bacteremia in mice. *Infect. Immun.* 75, 2067–2070. doi: 10.1128/iai.01727-06

Sato, K., Quartey, M. K., Liebeler, C. L., Le, C. T., and Giebink, G. S. (1996). Roles of autolysin and pneumolysin in middle ear inflammation caused by a type 3 *Streptococcus pneumoniae* strain in the chinchilla otitis media model. *Infect. Immun.* 64, 1140–1145.

Schachern, P. A., Tsuprun, V., Ferrieri, P., Briles, D. E., Goetz, S., Cureoglu, S., et al. (2014). Pneumococcal PspA and PspC proteins: potential vaccine candidates for experimental otitis media. *Int. J. Pediatr. Otorhinolaryngol.* 78, 1517–1521. doi: 10.1016/j.ijporl.2014.06.024

Shak, J. R., Ludewick, H. P., Howery, K. E., Sakai, F., Yi, H., Harvey, R. M., et al. (2013). Novel role for the *Streptococcus pneumoniae* toxin pneumolysin in the assembly of biofilms. *mBio* 4:e00655-13. doi: 10.1128/mBio.00655-13

Sulikowska, A., Grzesiowski, P., Sadowy, E., Fiett, J., and Hryniewicz, W. (2004). Characteristics of *Streptococcus pneumoniae*, *Haemophilus influenzae*, and *Moraxella catarrhalis* isolated from the nasopharynges of asymptomatic children and molecular analysis of *S. pneumoniae and H. influenzae* strain replacement in the nasopharynx. *J. Clin. Microbiol.* 42, 3942–3949. doi: 10.1128/jcm.42.9.3942-3949.2004

Taylor, H. E. (1949). Additive effects of certain transforming agents from some variants of pneumococcus. *J. Exp. Med.* 89, 399–424. doi: 10.1084/jem.89.4.399

Thornton, J. A., Durick-Eder, K., and Tuomanen, E. I. (2010). Pneumococcal pathogenesis: "innate invasion" yet organ-specific damage. *J. Mol. Med.* 88, 103–107. doi: 10.1007/s00109-009-0578-5

Thornton, J., and McDaniel, L. S. (2005). THP-1 monocytes up-regulate intercellular adhesion molecule 1 in response to pneumolysin

from *Streptococcus pneumoniae*. *Infect. Immun.* 73, 6493–6498. doi: 10.1128/IAI.73.10.6493-6498.2005

Valentino, M. D., McGuire, A. M., Rosch, J. W., Bispo, P. J. M., Burnham, C., Sanfilippo, C. M., et al. (2014). Unencapsulated *Streptococcus pneumoniae* from conjunctivitis encode variant traits and belong to a distinct phylogenetic cluster. *Nat. Commun.* 5, 5411. doi: 10.1038/ncomms6411

Weimer, K. E. D., Juneau, R. A., Murrah, K. A., Pang, B., Armbruster, C. E., Richardson, S. H., et al. (2011). Divergent mechanisms for passive pneumococcal resistance to β-lactam antibiotics in the presence of *Haemophilus influenzae*. *J. Infect. Dis.* 203, 549–555. doi: 10.1093/infdis/jiq087

Weinberger, D. M., Malley, R., and Lipsitch, M. (2011). Serotype replacement in disease after pneumococcal vaccination. *Lancet* 378, 1962–1973. doi: 10.1016/S0140-6736(10)62225-8

Yother, J., McDaniel, L. S., and Briles, D. E. (1986). Transformation of encapsulated *Streptococcus pneumoniae*. *J. Bacteriol.* 168, 1463–1465.

Conflict of Interest Statement: The authors declare that the research was conducted in the absence of any commercial or financial relationships that could be construed as a potential conflict of interest.

frontiers in Cellular and Infection Microbiology

ORIGINAL RESEARCH
published: 14 June 2016
doi: 10.3389/fcimb.2016.00060

Oseltamivir PK/PD Modeling and Simulation to Evaluate Treatment Strategies against Influenza-Pneumococcus Coinfection

Alessandro Boianelli[1], *Niharika Sharma-Chawla*[2,3], *Dunja Bruder*[2,3] *and Esteban A. Hernandez-Vargas*[1]*

[1] *Systems Medicine of Infectious Diseases, Department of Systems Immunology and Braunschweig Integrated Centre for Infection Research, Helmholtz Centre for Infection Research, Braunschweig, Germany,* [2] *Immune Regulation, Helmholtz Centre for Infection Research, Braunschweig, Germany,* [3] *Infection Immunology, Institute of Medical Microbiology, Infection Control and Prevention, Otto-von-Guericke-University, Magdeburg, Germany*

Influenza pandemics and seasonal outbreaks have shown the potential of Influenza A virus (IAV) to enhance susceptibility to a secondary infection with the bacterial pathogen *Streptococcus pneumoniae* (Sp). The high morbidity and mortality rate revealed the poor efficacy of antiviral drugs and vaccines to fight IAV infections. Currently, the most effective treatment for IAV is by antiviral neuraminidase inhibitors. Among them, the most frequently stockpiled is Oseltamivir which reduces viral release and transmission. However, effectiveness of Oseltamivir is compromised by the emergence of resistant IAV strains and secondary bacterial infections. To date, little attention has been given to evaluate how Oseltamivir treatment strategies alter Influenza viral infection in presence of Sp coinfection and a resistant IAV strain emergence. In this paper we investigate the efficacy of current approved Oseltamivir treatment regimens using a computational approach. Our numerical results suggest that the curative regimen (75 mg) may yield 47% of antiviral efficacy and 9% of antibacterial efficacy. An increment in dose to 150 mg (pandemic regimen) may increase the antiviral efficacy to 49% and the antibacterial efficacy to 16%. The choice to decrease the intake frequency to once per day is not recommended due to a significant reduction in both antiviral and antibacterial efficacy. We also observe that the treatment duration of 10 days may not provide a clear improvement on the antiviral and antibacterial efficacy compared to 5 days. All together, our *in silico* study reveals the success and pitfalls of Oseltamivir treatment strategies within IAV-Sp coinfection and calls for testing the validity in clinical trials.

Keywords: viral infection, *S. pneumoniae* coinfection, Oseltamivir treatment, PK/PD model, microbial resistance, population modeling, viral dynamic model

OPEN ACCESS

Edited by:
Jorge Eugenio Vidal, Emory University, USA

Reviewed by:
Francesco Santoro, University of Siena, Italy
Michael Mina, Princeton University, USA

***Correspondence:**
Esteban A. Hernandez-Vargas
esteban.vargas@helmholtz-hzi.de

Received: *25 January 2016*
Accepted: *23 May 2016*
Published: *14 June 2016*

Citation:
Boianelli A, Sharma-Chawla N, Bruder D and Hernandez-Vargas EA (2016) Oseltamivir PK/PD Modeling and Simulation to Evaluate Treatment Strategies against Influenza-Pneumococcus Coinfection. Front. Cell. Infect. Microbiol. 6:60. doi: 10.3389/fcimb.2016.00060

1. INTRODUCTION

Influenza A virus (IAV) and *Streptococcus pneumoniae* (Sp) are common causative agents of morbidity and mortality, respectively (Kilbourne, 2006; Morens et al., 2008; World Health Organization, 2009a). Over the last century four major influenza pandemics in 1918, 1957, 1968, and 2009 have had a significant impact worldwide. The Great Pandemic also known as the Spanish flu of 1918/1919 is considered as the deadliest pandemic with an estimated mortality of about 100 million around the globe (Johnson and Mueller, 2002). Interestingly, during the 1918 pandemic over 71% of the blood and sputum samples from fatal victims tested positive for Sp (Louria et al., 1959; McCullers and Rehg, 2002; McCullers, 2006, 2014), indicating a clear predisposition to lethal secondary bacterial infection in IAV preinfected patients.

Even though the mortality rate due to coinfections has decreased during the succeeding pandemics mostly because of antibiotic implementation, it still remains to be the most likely cause of death in 10–55% of the 2009 H1N1 victims. Thus, bacterial coinfection is a critical clinical outcome of viral infection and great attempts have been made to understand the pathogenesis and treatment course. The underlying mechanism for copathogenesis has been widely studied in animal models, providing evidence for a multifaceted disease affecting both lung physiology and immune responses (Shahangian et al., 2009; Small et al., 2010; Kash et al., 2011; Li et al., 2012). IAV-mediated immune aberrations such as immune cell dysfunction and apoptosis, dysregulated cytokine milieu and immunopathology in the lungs (Murray et al., 2014) have been implicated to have both immediate and long-term effects on anti-pneumococcal defense. The impact of coinfection is not limited to the bacterial outgrowth but also impairs antiviral immunity. Therefore, it is important for clinical treatment of coinfections to have a combinatorial approach to focus on all aspects of disease pathogenesis: the virus, bacteria, and host immune responses.

For prevention and treatment of acute IAV infection, antiviral drugs are an important adjunct to influenza vaccines (Goldstein and Lipsitch, 2009). The most commonly used Food and Drug Administration approved (FDA) antiviral drugs are neuraminidase inhibitors, e.g., Zanamivir, Peramivir, and Oseltamivir. The viral neuraminidase is an enzyme found on IAV surface enabling IAV virions to be released from the infected host cell. The neuraminidase inhibitors block this activity, thus interfering with viral spread and infectivity in the lungs (Moscona, 2005). *In vivo* administration of Oseltamivir is effective in controlling viral loads and immunopathology during lethal infection (McNicholl and McNicholl, 2001). In humans, the drug reduces clinical symptoms by 0.7–1.5 days when treatment is started 2 days after laboratory confirmed influenza, representing great potential if used appropriately to prevent the development of resistance (McNicholl and McNicholl, 2001). In the case of coinfections, the murine study in McCullers (2004) showed that treatment with Oseltamivir improved the survival by 75% in the coinfected group which further improved after combinatorial therapy with ampicillin. The first line of therapy following pneumococcal pneumonia is penicillin or other beta lactams, however the higher inflammatory status of the lung following coinfection with highly pathogenic virus strains may call for the use of non-lytic bacteriostatic agents such as clindamycin and azithromycin (Karlström et al., 2009). Furthermore, the anti-inflammatory and immunomodulatory action of corticosteroids used to treat many immune diseases could have a potent additive effect. In fact, the *in vivo* murine study by Trappetti et al. (2009) suggested a positive role of neuraminidase in Sp biofilm formation, thus Oseltamivir would be beneficial in preventing colonization. Following this study, the inhibiting effect of the approved anti-IAV drugs (Oseltamivir and Zanamivir) on Sp neuraminidase was confirmed by an *in vitro* kinetic study (Gut et al., 2011). Despite the existing combinatorial therapies against coinfections, the cumulative effect of neuraminidase inhibitor (Oseltamivir), the correct antibiotic and corticosteroids (Dexamethasone) is yet to be studied. With the increase in Oseltamivir use, drug resistant IAV strains may emerge bearing mutations such as H275Y in neuraminidase (Sheu et al., 2008). So far, the potentially detrimental effect of such mutant virus strains on secondary bacterial infections remains elusive.

The effectiveness of the Oseltamivir treatment depends on the dose regimen, intake frequency, time delay between infection and treatment, and treatment duration. The antiviral efficacy of neuraminidase inhibitors such as Oseltamivir, Amantadine and Peramivir has been investigated experimentally (Tanaka et al., 2015) and theoretically (Handel et al., 2007; Canini et al., 2014; Kamal et al., 2015). Recently, pharmaceutical companies have taken a strategic initiative to promote the use of modeling approaches within drug projects. The value of a model-based approach for improved efficiency and decision making during the preclinical stage of drug development has been largely advocated (Visser et al., 2013). Drug administration considers mainly two phenomena, i.e., the pharmacokinetic (PK) and pharmacodynamic (PD). The PK regards the temporal distribution of drug concentration in different organs of host body, while the PD describes the effect of a drug on the organism (Lahoz-Beneytez et al., 2015).

To the best of our knowledge, Oseltamivir treatment strategies for IAV infection in presence of Sp coinfection and a resistant IAV strain has not been investigated. In this paper, we tested the approved Oseltamivir treatment efficacy, combining a mathematical model of IAV-Sp coinfection with the PK/PD model of Oseltamivir. A possible emergence of an IAV Oseltamivir-resistant strain is also considered. Our computational results showed that Oseltamivir treatment with a dose of 150 mg, twice per day for 5 days is the minimum requirement recommended to achieve an antiviral efficacy of 49% and an antibacterial efficacy of 16%. Moreover, we found that in case of 75 mg dose administration, the intake frequency should not be lower than twice per day. A prolongation of the treatment up to 10 days with an intake frequency of twice per day, did not produce a clear benefit in terms of efficacy. This theoretical framework revealed the success and pitfalls of Oseltamivir strategies within IAV-Sp coinfection, paving the way for further refinement of therapeutic applications and clinical trials.

2. MATERIALS AND METHODS

2.1. PK/PD Model of Oseltamivir

The PK model of Oseltamivir consists of a two compartment model (Rayner et al., 2008; Wattanagoon et al., 2009; Canini et al., 2014), one for Oseltamivir phosphate (*OP*) and one for its active metabolic compound form Oseltamivir Carboxylate (*OC*). The system of ordinary differential equations describing the concentrations of *OP* and *OC* is as follows:

$$\dot{G} = -k_a G, \tag{1}$$

$$\dot{OP} = k_a G - k_f OP, \tag{2}$$

$$\dot{OC} = k_f OP - k_e OC, \tag{3}$$

where G is the depot compartment representing the *OP* dose administered, before it is adsorbed inside the blood with the adsorption rate k_a. The parameter k_f is the conversion rate from *OP* to *OC* and k_e is the *OC* elimination rate. The initial conditions of this system are $G(0) = Dose$, $OP(0) = 0$, $OC(0) = 0$. As the explicit effect of *OC* is to inhibit the viral release of IAV from infected cells, we modeled in similar vein to Canini et al. (2014) the *OC* action by modifying the viral replication rate to $p = (1 - \epsilon_S(t))p$, where $\epsilon_S(t)$ is the time varying drug efficacy defined as a function of *OC* concentration:

$$\epsilon_S(t) = \frac{OC}{EC_{50}^S + OC}. \tag{4}$$

EC_{50}^S is the *OC* concentration providing the 50% of drug efficacy. Cell culture assays found the values of EC_{50}^S in the range [0.0008−35] μM (Tamiflu (R), 2009). Simulation environments will be based on values of EC_{50}^S equal to 0.5, 10, and 35 μM.

2.2. IAV-Pneumococcus Coinfection Model

The scheme of the mathematical model of IAV-Sp coinfection and Oseltamivir interaction is illustrated in **Figure 1**. The dynamic of the IAV Oseltamivir-sensitive strain V is described by the target cell model with the eclipse phase (Nowak and May, 2000; Baccam et al., 2006; Beauchemin and Handel, 2011; Boianelli et al., 2015). Then, this is incorporated with the mathematical model of IAV-Sp coinfection proposed by Smith et al. (2013). We denote with U the uninfected cells, I_1 the non

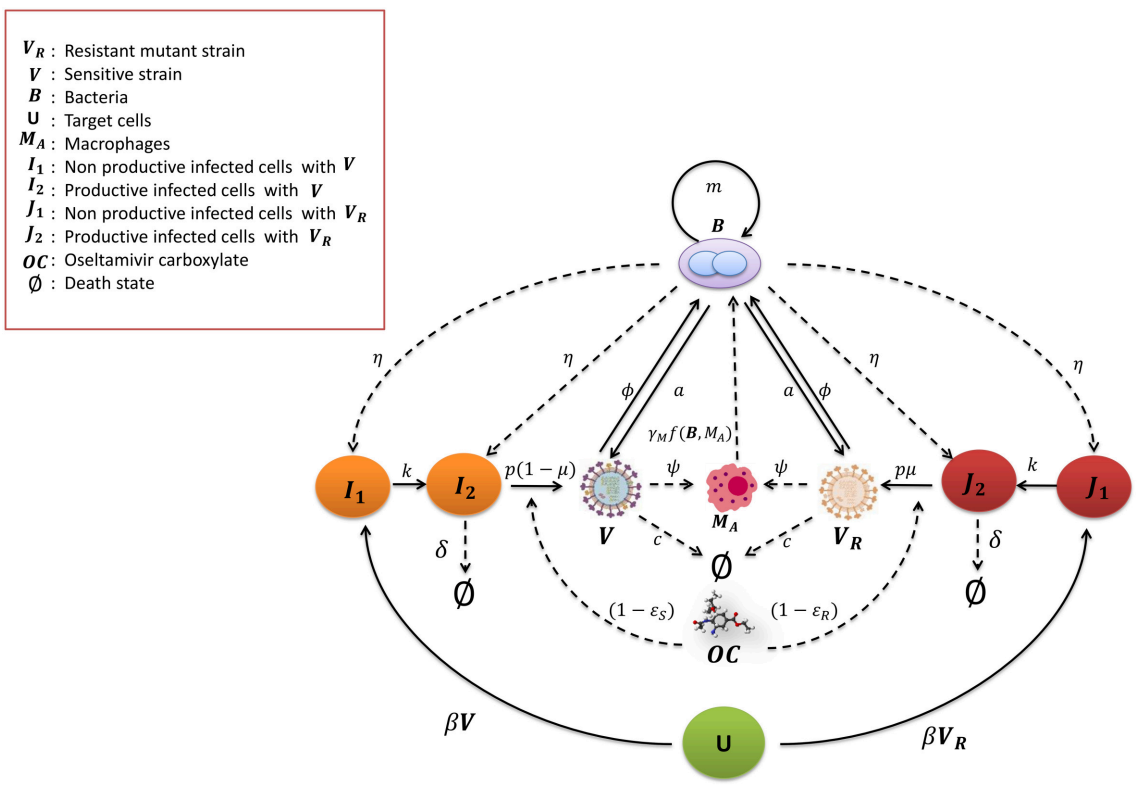

FIGURE 1 | Mathematical model for IAV-Sp coinfection with the antiviral Oseltamivir carboxylate *OC*. The IAV sensitive strain V and resistant mutant strain V_R (H275Y) are cleared at rate c. The uninfected cells become non productively infected cells I_1 and J_1 at the rate β by V and V_R respectively. I_1 and J_1 become productively infected cells at the rate k, that is I_2 and J_2 respectively. V and V_R replicate at the rate $p(1-\mu)$ and μp respectively. I_2 and J_2 are cleared at rate δ. The bacteria B proliferate at the rate m and increase the viral replication rate a. In turn V and V_R increase the bacterial carrying capacity with the parameter ϕ. Macrophages M_A phagocytose the bacteria with the rate $\gamma_M f(B, M_A)$. The phagocytosis rate is decreased by V and V_R with the parameter ψ. Bacteria increase the toxicity rate of non productively and productively infected cells of V and V_R with the rate parameter η. The Oseltamivir carboxylate *OC* decreases the V and V_R viral replication rate p to $p(1-\epsilon_S(t))$ and $p(1-\epsilon_R(t))$ respectively.

productively infected cells, I_2 the productively infected cells. U is infected by V with infection rate β. $1/k$ is the average time in which I_1 cells become productively infected cells. δ is the clearance rate of productively infected cells I_2 while p is the viral replication rate of V by I_2. c is the viral clearance rate of V. We fix the initial number of uninfected cells $U(0)$ at 10^7. The initial conditions for the sensitive strain V and Sp B are in **Table 2**, while for the others model variables are set to zero. The IAV and Sp initial conditions for performing simulations are in the concentration units of $\mathrm{TCID}_{50}\mathrm{mL}^{-1}$ and CFUmL^{-1}. The volume (mL) in the initial condition refers to the volume used (50 μL) in Smith et al. (2013) for the IAV and Sp (D39 strain) inoculum. According to the effect of *OC* on productively infected cells, the viral replication rate p is modified in $p(1-\epsilon_S(t))$. We assume that an IAV Oseltamivir-resistant mutant strain (H275Y) V_R could emerge from the sensitive type as a consequence of Oseltamivir treatment (Sheu et al., 2008; World Health Organization, 2010; Chen et al., 2011; Dobrovolny et al., 2011; Renaud et al., 2011). The kinetic parameters of V_R are assumed equal to those of V. The emergence of V_R is considered to be with the probability μ. V_R and V can compete for the same target cells U (Govorkova et al., 2010). Then, we denote with J_1 and J_2 the non productively and productively infected cells respectively of V_R, where $\epsilon_R(t)$ is the Oseltamivir efficacy against V_R having the same form in (4). It has been shown that for V_R, EC_{50}^R is 400 times higher than those for V (Gubareva et al., 2001). We also explore the case where it is 200 times higher.

To investigate the synergy between IAV and Sp, Smith et al. (2013) modeled the bacteria dynamics and interaction with alveolar macrophages M_A. The macrophages phagocytosis rate $\gamma_M f(B, M_A)$ of free bacteria is expressed by the mathematical function $\gamma_M n^2 M_A/(n^2 M_A + B^2)$, where n is the maximum number of bacteria phagocytosed per M_A, γ_M is the maximum phagocytosis rate. M_A cells number is considered in quasi steady state, denoted as M_A^*. Thus, the phagocytosis rate $f(B, M_A)$ is a decreasing function of B. The pneumococcus growth is assumed to be logistic with rate m and carrying capacity K_B. The IAV is assumed to increase the pneumococcal adherence to epithelial cells. This is translated by increasing the bacterial carrying capacity $K_B(1+\phi V)$ where ϕ is a proportionality constant. Moreover, another contribution of the IAV is the decreased rate of phagocytosis by M_A. This effect is included with the saturation function $\psi V/(K_{PV}+V)$, where ψ is the maximal reduction of the phagocytosis rate and K_{PV} is the half saturation constant. On the other hand, the pneumococcus effects on the IAV that may cause viral rebound are unknown. One plausible hypothesis assumes that the bacterial neuraminidase supports the viral neuraminidase to enhance the viral particle release from infected cells (McCullers, 2014). This is taken into account by considering an additional term in the viral replication rate $p(1+aB^z)$, where z is the nonlinearity order coefficient and a is the positive term of bacterial effect. The model also included the toxicity effect of B on I_1, J_1, and I_2, J_2 with the toxicity rate η. This model is extended including the dynamics of the resistant virus, assuming that V_R influences B in the same way of V and *vice versa*. The modified model is as follows:

$$\dot{U} = -\beta U(V+V_R), \tag{5}$$
$$\dot{I_1} = \beta UV - kI_1 - \eta BI_1, \tag{6}$$
$$\dot{I_2} = kI_1 - \delta I_2 - \eta BI_2 \tag{7}$$
$$\dot{J_1} = \beta UV_R - kJ_1 - \eta BJ_1, \tag{8}$$
$$\dot{J_2} = kJ_1 - \delta J_2 - \eta BJ_2, \tag{9}$$
$$\dot{V} = (1-\mu)p(1+aB^z)(1-\epsilon_S(t))I_2 - cV, \tag{10}$$
$$\dot{V_R} = \mu p(1+aB^z)((1-\epsilon_S(t))I_2 + (1-\epsilon_R(t))J_2) - cV_R, \tag{11}$$
$$\dot{B} = mB\left(1 - \frac{B}{K_B(1+\phi(V+V_R))}\right) - \gamma_M \frac{n^2 M_A^*}{n^2 M_A^* + B^2} B\left(1 - \frac{\psi(V+V_R)}{V+V_R+K_{PV}}\right). \tag{12}$$

The parameters value used for our population approach are in **Table 1**. These values represent the median value estimated in Canini et al. (2014), Wattanagoon et al. (2009) and Smith et al. (2013). More specifically, IAV-Sp model parameters were estimated from adult mice in Smith et al. (2013). It should be noted that kinetics and time scales of viral titer as well as immune parameters estimated from murine data can offer a reasonable approximation of IAV-Sp dynamics in humans (Small et al., 2010; Beauchemin and Handel, 2011). The parameter μ was estimated from human studies in Hayden (2001), as well as the Oseltamivir PK/PD model was inferred for human adults (Wattanagoon et al., 2009).

2.2.1. Drug Regimen Evaluation

The approved regimens stated by the guidelines for Oseltamivir administration in human adults (World Health Organization, 2009b; Canini et al., 2014) are: 75 mg twice per day for 5 days (curative regimen), 150 mg twice per day for 5 days (recommended regimen for pandemic influenza). These regimens are shown in **Table 2** as a benchmark for the treatment evaluation. Oseltamivir regimens were evaluated with the antiviral efficacy index defined in Canini et al. (2014) as:

$$VEFF = 1 - \frac{AUCV_T + AUCR_T}{AUCV + AUCR}, \tag{13}$$

where AUCV_T and AUCR_T are the area under the curve of V and V_R in presence of treatment, while AUCV and AUCR are the area under the curve without treatment. We also computed the antibacterial efficacy of the Oseltamivir treatment:

$$BEFF = 1 - \frac{AUCB_T}{AUCB}, \tag{14}$$

where AUCB_T and AUCB are the area under the curve of the bacterial time course with and without treatment.

2.2.2. Population Approach

In order to take into account the individual heterogeinity observed *in vivo* (Canini and Carrat, 2011), we performed 10,000 simulations by sampling from a uniform distribution centered in the estimated values of **Table 1** with a variation of ±30%.

TABLE 1 | IAV-Sp and PK/PD Oseltamivir model parameters with ranges used for the population approach.

Parameter	Definition	Median (Range)[a]	Unit	References
IAV-Sp MODEL PARAMETERS				
β	Virus infectivity	2.8 (1.96 3.64) $\times 10^{-6}$	$TCID_{50}mL^{-1}$	Smith et al., 2013
k	Eclipse phase	4.0 (2.8 5.2)	day^{-1}	Smith et al., 2013
δ	Productive cell clearance rate	0.89 (0.62 1.16)	day^{-1}	Smith et al., 2013
p	Viral replication rate	25.1 (17.7 32.89)	$TCID_{50}mL^{-1}day^{-1}$	Smith et al., 2013
c	Viral clearance rate	28.4 (19.88 36.92)	day^{-1}	Smith et al., 2013
η	Toxicity of infected cell rate	5.2 (3.64 6.76) $\times 10^{-10}$	CFU mL^{-1}	Smith et al., 2013
μ	Resistant virus appearance rate	2 (1.4 2.6) $\times 10^{-6}$	adim	Hayden, 2001
ϕ	Increase in carrying capacity	1.2 (0.84 1.56) $\times 10^{-8}$	$TCID_{50}mL^{-1}$	Smith et al., 2013
ψ	Decrease in phagocytosis rate	0.87 (0.61 1.13)	adim	Smith et al., 2013
a	Positive feedback rate	1.2 (0.84 1.56) $\times 10^{-3}$	CFU mL^{-z}	Smith et al., 2013
m	Bacterial growth rate	27 (19 35)	day^{-1}	Smith et al., 2013
K_B	Pneumococcus carrying capacity	2.3 (1.61 2.99) $\times 10^{8}$	$CFUmL^{-1}$	Smith et al., 2013
K_{PV}	Half saturation constant	1.8 (1.26 2.34) $\times 10^{3}$	$TCID_{50}mL^{-1}$	Smith et al., 2013
γ_M	Macrophages phagocytosis rate	1.35 (0.95 1.75) $\times 10^{-4}$	$cell^{-1}day^{-1}$	Smith et al., 2013
n	Maximum bacteria number for M_A	5.0 (3.5 6.5)	$CFUmL^{-1}$ $cell^{-1}$	Smith et al., 2013
z	Non linear coefficient	0.5 (0.35 0.65)	adim	Smith et al., 2013
OSELTAMIVIR PK/PD PARAMETERS				
k_a	OP adsorption rate	1.01 (0.7 1.31)	h^{-1}	Wattanagoon et al., 2009
k_f	OP conversion rate in OC	0.684 (0.48 0.88)	h^{-1}	Wattanagoon et al., 2009
k_e	OC clearance rate	0.136 (0.09 0.177)	h^{-1}	Wattanagoon et al., 2009

[a] *Parameter ranges used for the population approach. The values are computed with ± 30% of variation from the median values.*
The volume (mL) in model parameters was related to the total volume used (50 μL) in Smith et al. (2013) for the IAV and Sp (D39 strain) inoculum.

Model parameter ranges are showed in **Table 1**. We computed the antiviral and antibacterial efficacy defined in Equations (13)–(14) of the curative regimen with 75, 150, 300, and 450 mg, twice per day for 5 days. Moreover, a different intake frequency of once per day for 5 days with dosage of 75 mg was explored. A different treatment duration of 10 days with 75 mg and intake frequency of twice per day was also investigated. In order to mimic a realistic scenario, we assumed a random sampling for the starting time of drug treatment, time of coinfection and initial values of viral and bacterial titers. In fact, the amount of viral and bacterial burden is unknown when an individual is infected by IAV and Sp. Moreover, it is also unknown after how many days post the infection time the antiviral treatment is started. This is because the time of infection is not known. In the same way, the time of coinfection is typically unknown in naturally acquired Sp coinfection. The ranges of experimental values are presented in **Table 2**. For the correct viral dynamics simulation, we imposed the viral titer V to be constant when it crosses lower values than the threshold of 2.8×10^{-7} $TCID_{50}mL^{-1}$. The minimum therapy initiation time was considered starting at 2 days post infection, because at this time symptoms are clearly visible (Aoki et al., 2003; Louie et al., 2012; Muthuri et al., 2012).

TABLE 2 | Simulation settings and approved Oseltamivir treatment regimens.

Variable	Range	Units
Therapy initiation time	[2 3 4]	days
Time of pneumococcus coinfection after influenza infection	[4 5 6 7]	days
Intial viral load/titer	[2 100]	$TCID_{50}mL^{-1}$
Initial pneumococcal (D39 strain) load	[20 600]	CFU mL^{-1}
APPROVED REGIMENS (World Health Organization, 2009b)		
Dose	**Intake frequency**	**Treatment duration**
75 mg (curative)	Twice per day	5 days
150 mg (pandemic)	Twice per day	5 days

The volume (mL) was related to that used (50 μL) in Smith et al. (2013) for the IAV and Sp (D39 strain) inoculum.

2.2.3. Statistical Analysis

We performed the one way ANOVA statistical significance test and then Bonferroni test on the 10,000 stochastic simulations. The statistical significance difference for antiviral and antibacterial distributions between the 75 mg dose (curative regimen) and 150 (pandemic regimen), 300, and 450 mg were computed. We compared also the curative regimen intake frequency of twice per day with intake frequency of once per day. Moreover, we investigated the statistical significance between treatment duration of 5 and 10 days. The comparison is done for EC_{50}^{S} values of 0.5, 10, and 35 μM.

2.2.4. Sensitivity Analysis

To analyse to which extent each parameter affected the model outputs, we simulated the viral and bacterial dynamics by changing the parameters in **Table 1** once per time of 10, 30 and

50% and keeping the others fixed (see Supplementary Figures S4, S5).

3. RESULTS

3.1. Influence of Oseltamivir Dose

In this section we evaluated the antiviral and antibacterial efficacy for Oseltamivir dose of 75, 150, 300, 450 mg, twice per day for a treatment duration of 5 days. **Figure 2** displays histograms obtained for different doses and EC_{50}^{S}. The histograms represent the distribution of antiviral and antibacterial efficacy values computed from 10,000 samples. **Tables 3** and **4** show the median values of antiviral and antibacterial efficacy for different doses and EC_{50}^{S} values. Interestingly, the antibacterial efficacy histograms in **Figure 2** presented a bimodal distribution for both different doses and EC_{50}^{S} values. The antibacterial *dichotomy* may be a result of two factors. The first could be attributed to the bacterial growth rate (m) and macropaghes phagocytosis rate (γ_M), greatly affecting Sp dynamics. The second refers to IAV parameters responsible for macrophages phagocytosis decrease (K_{pv}) and bacterial carrying capacity increase (ϕ) that influence the pneumococcal time course as well (Supplementary Figure S5). Then, combinations of these viral and bacterial parameters can promote alternatively bacterial colonization or bacterial clearance. This implies that in favorable conditions, Oseltamivir treatment strategies may be able to inhibit viral dynamics (high antiviral efficacy) and in turn modulate bacterial growth (high antibacterial efficacy). Otherwise, in worst scenarios, Oseltamivir treatment strategies may fail to control bacterial dynamics.

For the best scenario where Oseltamivir treatment is effective ($EC_{50}^{S} = 0.5\ \mu M$), the first set of 10,000 simulations revealed that the distribution of antiviral and antibacterial efficacy were significantly different by changing the dose from 75 to 150 mg. In fact, for the curative regimen of 75 mg, the antiviral efficacy median value was 47%, remaining quite stable for higher values of dose (49%). The same pattern was conserved for higher values of EC_{50}^{S}, where for the highest dosage tested (450 mg), the median antiviral efficacy values were 45 and 28.9%, while for the curative regimen were 22 and 8.7% respectively. Concurrently, in **Table 4**, the antibacterial efficacy for the curative regimen with $EC_{50}^{S} = 0.5\ \mu M$ presented a value of 9% that further decreased to 0.3% for

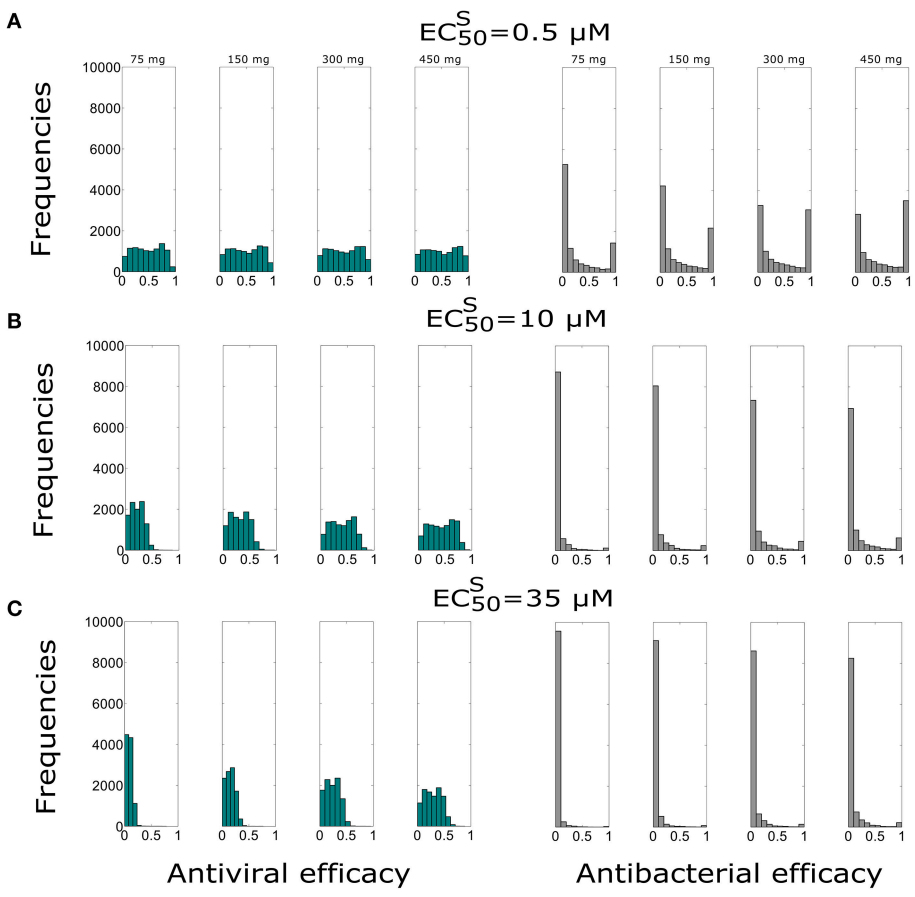

FIGURE 2 | Histograms of the antiviral (green) and antibacterial efficacy (grey) for different Oseltamivir dose of 75, 150, 300, and 450 mg, with intake frequency of twice per day and a duration of 5 days for (A) $EC_{50}^{S} = 0.5\ \mu M$, (B) $EC_{50}^{S} = 10\ \mu M$, and (C) $EC_{50}^{S} = 35\ \mu M$. The x-axis represents the Oseltamivir antiviral/antibacterial efficacy against IAV ranging from 0 (0%) to 1 (100%).

TABLE 3 | Antiviral efficacy median values for different EC_{50}^S and different dose regimens with intake frequency of twice per day and treatment duration of 5 days.

Dose (mg)	EC_{50}^S (μM)		
	0.5	10	35
75	0.47*	0.22*	0.087*
150	0.49*	0.31*	0.153*
300	0.49	0.40*	0.237*
450	0.49	0.45*	0.289*

*Statistically significant.
For $EC_{50}^S = 0.5\ \mu M$, statistically significant difference was observed between the antiviral efficacy distributions for the dose of 75 and 150 mg ($P < 0.05$), while significant differences were found ($P < 0.05$) between all the dose for $EC_{50}^S = 10, 35\ \mu M$.

TABLE 4 | Antibacterial efficacy median values for different EC_{50}^S and different dose regimens with intake frequency of twice per day for a duration of 5 days.

Dose (mg)	$EC^S{}_{50}$ (μM)		
	0.5	10	35
75	0.09*	0.010*	0.003*
150	0.16*	0.017*	0.006*
300	0.31*	0.030*	0.010*
450	0.41*	0.036*	0.015*

*Statistically significant.
For $EC_{50}^S = 0.5, 10, 35\ \mu M$, the differences between the antibacterial efficacy for all doses of 75, 150, 300, and 450 mg were statistically significant ($P < 0.05$).

$EC_{50}^S = 35\ \mu M$. Similarly, for 450 mg, the antibacterial efficacy dropped from 41 to 1.5%.

We also investigated the sensitivity of the Oseltamivir antiviral and antibacterial efficacy with respect to the EC_{50}^R values. The previous results were with $EC_{50}^R = 400 \times EC_{50}^S$. Thus, we tested the same treatment regimens of 75, 150, 300, and 450 mg with intake frequency of twice per day, for 5 days where $EC_{50}^R = 200 \times EC_{50}^S$. We computed the antiviral and antibacterial efficacy for the previous existing three different values of EC_{50}^S (see Supplementary Figure S1). Histograms of antiviral and antibacterial efficacy presented the same properties observed when $EC_{50}^R = 400 \times EC_{50}^S$. More specifically, in agreement with the previous case with $EC_{50}^R = 400 \times EC_{50}^S$, a statistically significant difference was observed between 75 and 150 mg for the lowest value of EC_{50}^S. We noted similar median values of the antiviral efficacy for different doses and EC_{50}^S with respect to the case where $EC_{50}^R = 400 \times EC_{50}^S$. In the same way, the antibacterial efficacy for 200 and 400 times the value of EC_{50}^S also presented consistent values (see Supplementary Tables S1, S2).

3.2. Role of Oseltamivir Intake Frequency

In order to investigate the effect of the intake frequency treatment on the coinfection course dynamics, we simulated in another set of 10,000 simulations, the administration of 75 mg dose with intake frequency of once per day, for 5 days. These treatment regimens are explored for the same values of EC_{50}^S considered previously and with the value of $EC_{50}^R = 400 \times EC_{50}^S$. The antiviral and antibacterial efficacy values are reported in **Table 5**. Histograms obtained from 10,000 simulations are shown in **Figure 3**.

TABLE 5 | Comparison of antiviral and antibacterial efficacy median values for different $EC^S{}_{50}$ values with intake frequency of once and twice per day and treatment duration of 5 days.

Intake frequency	$EC^S{}_{50}$ (μM)		
	0.5	10	35
ANTIVIRAL EFFICACY			
Twice per day	0.47*	0.22*	0.09*
Once per day	0.43*	0.135*	0.04*
ANTIBACTERIAL EFFICACY			
Twice per day	0.09*	0.010*	0.005*
One per day	0.04*	0.005*	0.002*

*Statistically significant.
Statistical significance difference of antiviral/antibacterial efficacy distributions ($P < 0.05$) was obtained between different intake frequency of once and twice per day.

Both antiviral and antibacterial histogram values significantly decreased when the intake frequency was once per day or for higher EC_{50}^S. The bimodal distribution was conserved for the antibacterial histograms due to reasons stated previously. The distributions of antiviral and antibacterial efficacy presented statistically significant difference ($P < 0.05$) for both different values of intake frequency and EC_{50}^S. Notably, the values in **Table 5** with intake frequency of once per day were lower compared to the median values of the antiviral efficacy of the curative regimens for different values of EC_{50}^S. Therefore, the antibacterial efficacy medians with intake frequency of once per day showed approximately half values with respect to those with intake frequency of twice per day. These results stressed the importance of intake frequency to determine the clearance of the IAV-Sp coinfection. Furthermore, the case where $EC_{50}^R = 200 \times EC_{50}^S$ (Supplementary Figure S2) was also investigated, noting that in this regimen both the antiviral and antibacterial efficacy medians possessed similar ranges compared with those obtained when $EC_{50}^R = 400 \times EC_{50}^S$ (see Supplementary Table S3).

3.3. Effect of Treatment Duration

In order to test the influence of the treatment duration on the Oseltamivir efficacy against coinfection dynamics, we assumed the possibility of treatment duration of 10 days with dose of 75 mg and intake frequency of twice per day. The median values of antiviral and antibacterial efficacy are in **Table 6**. The histograms showing the antiviral and antibacterial efficacy distributions obtained from 10,000 simulations for different EC_{50}^S values are presented in **Figure 4**.

Antiviral efficacy distributions for treatment duration of 5 and 10 days show similar median values for all of EC_{50}^S (no statistical significance differences are noted, $P > 0.05$). Moreover, the antibacterial efficacy with treatment durations of 5 and 10 days confirmed the same pattern, in particular for $EC_{50}^S = 10\ \mu M$. We also investigated the same treatment regimens using the value of

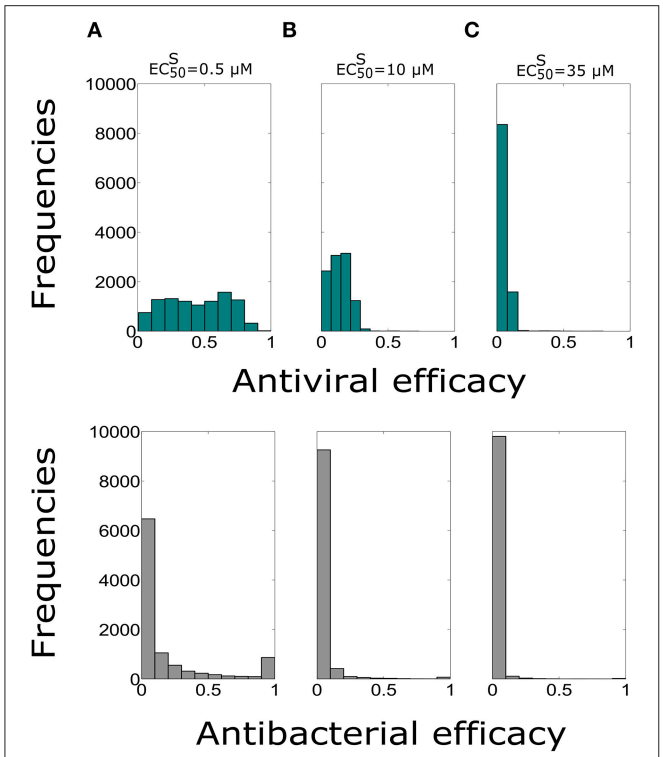

FIGURE 3 | Histograms of the antiviral (green) and antibacterial (grey) efficacy for the dose of 75 mg and intake frequency of once per day, with the duration of 5 days for (A) $EC_{50}^S = 0.5\ \mu M$, (B) $EC_{50}^S = 10\ \mu M$, (C) $EC_{50}^S = 35\ \mu M$. The x-axis represents the Oseltamivir antiviral/antibacterial efficacy against IAV/Sp ranging from 0 (0%) to 1 (100%).

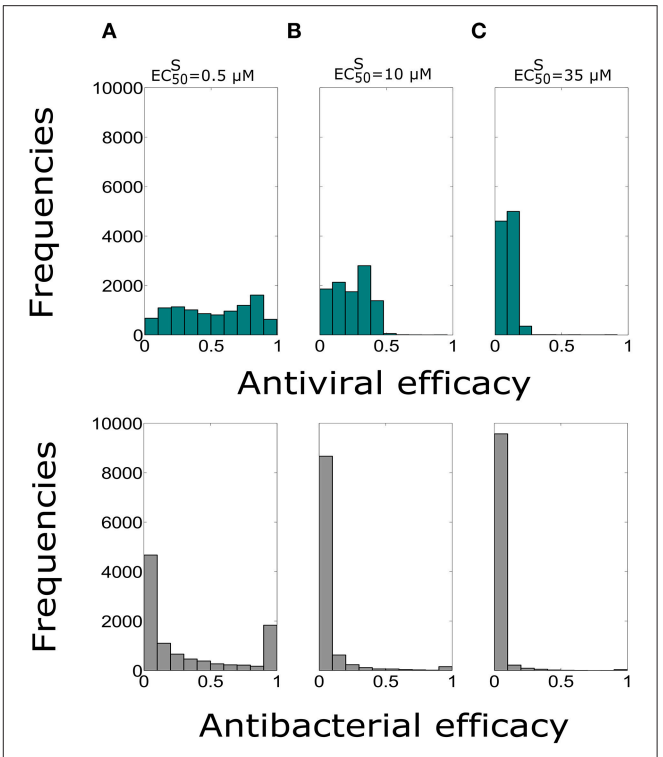

FIGURE 4 | Histograms of the antiviral (green) and antibacterial (grey) efficacy for the dose of 75 mg and intake frequency of twice per day with the duration of 10 days for (A) $EC_{50}^S = 0.5$, (B) $EC_{50}^S = 10\ \mu M$, (C) $EC_{50}^S = 35\ \mu M$. The x-axis represents the Oseltamivir antiviral/antibacterial efficacy against IAV/Sp ranging from 0 (0%) to 1 (100%).

TABLE 6 | Comparison of antiviral and antibacterial efficacy medians for different EC_{50}^S values and intake frequency of twice per day with the treatment duration of 5 and 10 days.

Treatment duration	EC_{50}^S (μM)		
	0.5	10	35
ANTIVIRAL EFFICACY			
5 days	0.47	0.22	0.09
10 days	0.52	0.24	0.10
ANTIBACTERIAL EFFICACY			
5 days	0.08	0.01	0.005
10 days	0.12	0.01	0.003

For the antiviral/antibacterial efficacy, statistical significance difference was not found ($P > 0.05$) for both treatment durations and different EC_{50}^S values.

$EC_{50}^R = 200 \times EC_{50}^S$ (see Supplementary Figure S3). In this setting also the antiviral efficacy distributions with treatment durations for 5 and 10 days were not statistically significant. We noted similar median values for the antiviral and antibacterial efficacy when $EC_{50}^R = 200 \times EC_{50}^S$ (see Supplementary Table S4), for all the values of EC_{50}^S considered. Overall analysis suggested that the resistant mutant strain behavior may not really altered the efficacy of the Oseltamivir against IAV-Sp coinfection.

4. DISCUSSION

In the last decades many mathematical models have been developed describing the IAV infection dynamics in different hosts (Baccam et al., 2006; Tridane and Kuang, 2010; Hernandez-Vargas and Meyer-Hermann, 2012; Smith et al., 2013; Canini and Perelson, 2014; Boianelli et al., 2015), and in presence of treatment (Beauchemin and Handel, 2011; Canini and Perelson, 2014; Canini et al., 2014; Boianelli et al., 2015). However, the history of IAV pandemics have highlighted the role of the secondary bacterial infection in the increased morbidity and mortality. To date, the only mathematical model describing the IAV-pneumococcus coinfection was developed by Smith et al. (2013).

In this paper, we extend the coinfection model from Smith et al. (2013), by adding the pharmacokinetic and pharmacodynamic effects of Oseltamivir and taking into account a possible emergence of resistant mutant strain (H275Y) induced by Oseltamivir treatment. In our model, we simulate the intra-subject variability of influenza infection and also a time dependent Oseltamivir drug efficacy. We test the capability of the current approved Oseltamivir treatment regimens to achieve antiviral and antibacterial efficacy in a stochastic environment. Here, we simulate a more realistic scenario for coinfection and Oseltamivir treatment strategies.

For example, we assume a random time of treatment as we do not know the delay between viral infection and treatment initiation. Secondly, we consider the time of coinfection randomly, because the time of secondary Sp infection is unknown. Moreover, in real life infection the exact amount of the viral and bacterial burden is usually unknown as well. The possibility of different intake frequencies and treatment duration according to the approved treatment regimens is explored.

Our results show that the curative regimen (75 mg for 5 days, twice per day) may offer the 47% of antiviral efficacy and 9% of antibacterial efficacy only in the case where the Oseltamivir is effective ($EC_{50}^{S} = 0.5\ \mu M$) against IAV. Increasing the dose from 75 to 150 mg with the same value of EC_{50}^{S} results in a statistically significant gain in terms of antiviral (49%) and antibacterial efficacy (16%). Then, for the case of IAV-Sp coinfection, the pandemic regimen could be recommended. Moreover, increasing the dose may not represent a reasonable gain of antiviral and antibacterial efficacy. However, in the case of the lowest efficiency of Oseltamivir ($EC_{50}^{S} = 35\ \mu M$), a significant increase in antiviral and antibacterial efficacy is obtained with a dose of 450 mg. With this dose, twice per day, for 5 days, antiviral and antibacterial efficacy display 28.9 and 1.5% median values, respectively. In the same range of treatment strategies for the value of $EC_{50}^{R} = 200 \times EC_{50}^{S}$ the antiviral and antibacterial efficacy presented no significant differences compared to the case where $EC_{50}^{R} = 400 \times EC_{50}$. Moreover, reducing the intake frequency from twice to once per day with a dose of 75 mg could determine a significant reduction in the antiviral and antibacterial efficacy for the ranges of EC_{50}^{S} explored. In particular, from the best scenario ($EC_{50}^{S} = 0.5\ \mu M$), the antiviral efficacy reduces from 47 to 43% and the antibacterial efficacy from 9 to 4%. This reduction is more pronounced in the worst case ($EC_{50}^{S} = 35\ \mu M$), where both antiviral and antibacterial efficacy reduce approximately to the half of those values presented for a dosage of twice per day.

Against intuition, when the treatment duration is prolonged to 10 days with dose of 75 mg, this does not significantly increase the antiviral and antibacterial efficacy for all the values of EC_{50}^{S}. Concerning the antiviral efficacy, this result can be mainly attributed to the positive feedback of the bacterial secondary infection on IAV dynamics and in turn on the viral area under the curve. On the other hand, the antibacterial efficacy is also influenced, since the viral dynamics can modulate the bacterial growth via macrophages deactivation and can increase bacterial carrying capacity. The latter statement is also one of the factors that could lead to the bimodal distribution of the antibacterial efficacy histograms observed in all the treatment strategies. Importantly, from our computational study, the pharmacokinetic parameter EC_{50}^{S} directly influences the outcome of the Oseltamivir drug on IAV-Sp coinfection for all the tested treatment regimens. On the contrary, it turns out that the sensitivity of the antiviral and antibacterial efficacy to the EC_{50}^{R} parameter is low. This implies to presume that the resistant mutant strain does not really affect the antiviral and antibacterial efficacy. This is in agreement with *in silico* results obtained in Canini et al. (2014) where the authors evaluated the impact of Oseltamivir treatment strategies in the presence of the emerging resistant strain. In fact, for the treatment strategies considered in our work, the authors observed similar values of the antiviral efficacy (Treanor et al., 2000) when treatment is initiated at day 2 post infection. Therefore, our results of antibacterial efficacy (9%) obtained with curative regimen are lower than the experimental work of McCullers (2004), reporting an antibacterial efficacy value of 25% for murine data.

However, there are limitations in our simulation studies. Concerning the applied model (1)–(12), we did not consider the role of the immune response to clear the influenza virus. In fact, our investigations cannot be applied with hosts shedding preexisting immunity. Future studies should consider different models for the viral infection including the dynamics of the immune response such as CD8+T cells (Hancioglu et al., 2007; Lee et al., 2009; Miao et al., 2010; Tridane and Kuang, 2010; Dobrovolny et al., 2013), Interferon type I (Canini and Carrat, 2011; Pawelek et al., 2012; Hernandez-Vargas et al., 2014) and Natural killer cells (Canini and Carrat, 2011). In addition, the PK/PD dynamics have been estimated only for adults (Wattanagoon et al., 2009). This implies that for other groups such as children and seniors, our computational study should be tested with appropriate PK/PD parameter estimates. In fact for elderly, PK/PD parameters, e.g., apparent volume of distribution (prolongation of elimination half-life) can have important changes due to age modification in organ physiology (Mangoni and Jackson, 2004).

In summary, we find that the actual recommended regimens for Oseltamivir, i.e., curative and pandemic regimens may not completely able to control the colonization of a secondary bacterial coinfection. Higher doses, such as 150 and 300 mg, are recommended. Nevertheless, even this treatment regimen may not control coinfection in case of low Oseltamivir effectiveness. Moreover, our computational study suggests clear disadvantages of reducing the intake frequency below twice per day for a treatment duration of 5 and 10 days. Future clinical studies are needed to verify our results towards improved therapeutic treatments to fight coinfections (Dunning et al., 2014).

AUTHOR CONTRIBUTIONS

AB and EH designed the computational study and revised the manuscript. AB performed the simulations. AB, EH, NS, and DB discussed and wrote the manuscript.

ACKNOWLEDGMENTS

This work was supported by iMed — the Helmholtz Initiative on Personalized Medicine and DAAD Germany through the program PROALMEX funding the project "OPTREAT." In addition, we thank for support provided by the Department of Systems immunology (HZI), the Measures for the Establishment of Systems Medicine (e:Med) projects in Systems Immunology and Image Mining in Translational Bio-marker Research (SYSIMIT), contract number 01ZX1308B and in identification

of predictive response and resistance factors to targeted therapy in gastric cancer using a systems medicine approach (SYS-Stomach), contract number 01ZX1310C by the Federal Ministry of Education and Research (BMBF), Germany. We thank for support by the Human Frontier Science Program (HFSP), RGP0033/2015. We also thank the support of the German Research Foundation (DFG), contract number SFB854. We thank the support by the International Research Training Group 1273 (IRTG1273) funded by the German Research Foundation (DFG).

SUPPLEMENTARY MATERIAL

The Supplementary Material for this article can be found online at: http://journal.frontiersin.org/article/10.3389/fcimb.2016.00060

REFERENCES

Aoki, F. Y., Macleod, M. D., Paggiaro, P., Carewicz, O., El Sawy, A., Wat, C., et al. (2003). Early administration of oral oseltamivir increases the benefits of influenza treatment. *J. Antimicrob. Chemother.* 51, 123–129. doi: 10.1093/jac/dkg007

Baccam, P., Beauchemin, C., Macken, C. A., Hayden, F. G., and Perelson, A. S. (2006). Kinetics of influenza A virus infection in humans. *J. Virol.* 80, 7590–7599. doi: 10.1128/JVI.01623-05

Beauchemin, C. A., and Handel, A. (2011). A review of mathematical models of influenza A infections within a host or cell culture: lessons learned and challenges ahead. *BMC Public Health* 11:S7. doi: 10.1186/1471-2458-11-S1-S7

Boianelli, A., Nguyen, V. K., Ebensen, T., Schulze, K., Wilk, E., Sharma, N., et al. (2015). Modeling influenza virus infection: a roadmap for influenza research. *Viruses* 7, 5274–5304. doi: 10.3390/v7102875

Canini, L., and Carrat, F. (2011). Population modeling of influenza A/H1N1 virus kinetics and symptom dynamics. *J. Virol.* 85, 2764–2770. doi: 10.1128/JVI.01318-10

Canini, L., Conway, J. M., Perelson, A. S., and Carrat, F. (2014). Impact of different oseltamivir regimens on treating influenza A virus infection and resistance emergence: insights from a modelling study. *PLoS Comput. Biol.* 10:e1003568. doi: 10.1371/journal.pcbi.1003568

Canini, L., and Perelson, A. S. (2014). Viral kinetic modeling: state of the art. *J. Pharmacokinet. Pharmacodyn.* 41, 431–443. doi: 10.1007/s10928-014-9363-3

Chen, L. F., Dailey, N. J., Rao, A. K., Fleischauer, A. T., Greenwald, I., Deyde, V. M., et al. (2011). Cluster of oseltamivir-resistant 2009 pandemic influenza A (H1N1) virus infections on a hospital ward among immunocompromised patientsnorth carolina, 2009. *J. Infect. Diseases* 203, 838–846. doi: 10.1093/infdis/jiq124

Dobrovolny, H. M., Gieschke, R., Davies, B. E., Jumbe, N. L., and Beauchemin, C. A. (2011). Neuraminidase inhibitors for treatment of human and avian strain influenza: a comparative modeling study. *J. Theoret. Biol.* 269, 234–244. doi: 10.1016/j.jtbi.2010.10.017

Dobrovolny, H. M., Reddy, M. B., Kamal, M. A., Rayner, C. R., and Beauchemin, C. A. (2013). Assessing mathematical models of influenza infections using features of the immune response. *PLoS ONE* 8:e57088. doi: 10.1371/journal.pone.0057088

Dunning, J., Baillie, J. K., Cao, B., Hayden, F. G., and International Severe Acute Respiratory and Emerging Infection Consortium (ISARIC) (2014). Antiviral combinations for severe influenza. *Lancet Infect. Diseases* 14, 1259–1270. doi: 10.1016/S1473-3099(14)70821-7

Goldstein, E., and Lipsitch, M. (2009). Antiviral usage for H1N1 treatment: pros, cons and an argument for broader prescribing guidelines in the united states. *PLoS Curr.* 1:RRN1122. doi: 10.1371/currents.RRN1122

Govorkova, E. A., Ilyushina, N. A., Marathe, B. M., McClaren, J. L., and Webster, R. G. (2010). Competitive fitness of oseltamivir-sensitive and-resistant highly pathogenic H5N1 influenza viruses in a ferret model. *J. Virol.* 84, 8042–8050. doi: 10.1128/JVI.00689-10

Gubareva, L. V., Webster, R. G., and Hayden, F. G. (2001). Comparison of the activities of zanamivir, oseltamivir, and RWJ-270201 against clinical isolates of influenza virus and neuraminidase inhibitor-resistant variants. *Antimicrob. Agents Chemother.* 45, 3403–3408. doi: 10.1128/AAC.45.12.3403-3408.2001

Gut, H., Xu, G., Taylor, G. L., and Walsh, M. A. (2011). Structural basis for *Streptococcus pneumoniae* nana inhibition by influenza antivirals zanamivir and oseltamivir carboxylate. *J. Molecul. Biol.* 409, 496–503. doi: 10.1016/j.jmb.2011.04.016

Hancioglu, B., Swigon, D., and Clermont, G. (2007). A dynamical model of human immune response to influenza A virus infection. *J. Theoret. Biol.* 246, 70–86. doi: 10.1016/j.jtbi.2006.12.015

Handel, A., Longini, I. M. Jr., and Antia, R. (2007). Neuraminidase inhibitor resistance in influenza: assessing the danger of its generation and spread. *PLoS Comput. Biol.* 3:e240. doi: 10.1371/journal.pcbi.0030240

Hayden, F. G. (2001). Perspectives on antiviral use during pandemic influenza. *Philos. Trans. R Soc. Lond. B Biol. Sci.* 356, 1877–1884. doi: 10.1098/rstb.2001.1007

Hernandez-Vargas, E. A., and Meyer-Hermann, M. (2012). "Innate immune system dynamics to influenza virus," in *Proceedings of the 8th IFAC Symposium on Biological and Medical Systems* (Budapest), 29–31.

Hernandez-Vargas, E. A., Wilk, E., Canini, L., Toapanta, F. R., Binder, S. C., Uvarovskii, A., et al. (2014). Effects of aging on influenza virus infection dynamics. *J. Virol.* 88, 4123–4131. doi: 10.1128/JVI.03644-13

Johnson, N. P., and Mueller, J. (2002). Updating the accounts: global mortality of the 1918-1920 "spanish" influenza pandemic. *Bull. Hist. Med.* 76, 105–115. doi: 10.1353/bhm.2002.0022

Kamal, M. A., Gieschke, R., Lemenuel-Diot, A., Beauchemin, C. A., Smith, P. F., and Rayner, C. R. (2015). A drug-disease model describing the effect of oseltamivir neuraminidase inhibition on influenza virus progression. *Antimicrob. Agents Chemother.* 59, 5388–5395. doi: 10.1128/AAC.00069-15

Karlström, Å., Boyd, K., English, B. K., and McCullers, J. A. (2009). Treatment with protein synthesis inhibitors improves outcomes of secondary bacterial pneumonia after influenza. *J. Infect. Diseases* 199, 311–319. doi: 10.1086/596051

Kash, J. C., Walters, K.-A., Davis, A. S., Sandouk, A., Schwartzman, L. M., Jagger, B. W., et al. (2011). Lethal synergism of 2009 pandemic H1N1 influenza virus and *Streptococcus pneumoniae* coinfection is associated with loss of murine lung repair responses. *MBio* 2, e00172–11. doi: 10.1128/mBio.00172-11

Kilbourne, E. D. (2006). Influenza pandemics of the 20th century. *Emerging Infect. Diseases* 12:9. doi: 10.3201/eid1201.051254

Lahoz-Beneytez, J., Schnizler, K., and Eissing, T. (2015). A pharma perspective on the systems medicine and pharmacology of inflammation. *Mathemat. Biosci.* 260, 2–5. doi: 10.1016/j.mbs.2014.07.006

Lee, H. Y., Topham, D. J., Park, S. Y., Hollenbaugh, J., Treanor, J., Mosmann, T. R., et al. (2009). Simulation and prediction of the adaptive immune response to influenza a virus infection. *J. Virol.* 83, 7151–7165. doi: 10.1128/JVI.00098-09

Li, W., Moltedo, B., and Moran, T. M. (2012). Type I interferon induction during influenza virus infection increases susceptibility to secondary *Streptococcus pneumoniae* infection by negative regulation of $\gamma\delta$ T cells. *J. Virol.* 86, 12304–12312. doi: 10.1128/JVI.01269-12

Louie, J. K., Yang, S., Acosta, M., Yen, C., Samuel, M. C., Schechter, R., et al. (2012). Treatment with neuraminidase inhibitors for critically ill patients with influenza A (H1N1) pdm09. *Clin. Infect. Diseases* 55, 1198–1204. doi: 10.1093/cid/cis636

Louria, D. B., Blumenfeld, H. L., Ellis, J. T., Kilbourne, E. D., and Rogers, D. E. (1959). Studies on influenza in the pandemic of 1957-1958. II. pulmonary complications of influenza. *J. Clin. Invest.* 38(1 Pt 1-2), 213.

Mangoni, A. A., and Jackson, S. H. (2004). Age-related changes in pharmacokinetics and pharmacodynamics: basic principles and practical applications. *Br. J. Clin. Pharmacol.* 57, 6–14. doi: 10.1046/j.1365-2125.2003.02007.x

McCullers, J. A. (2004). Effect of antiviral treatment on the outcome of secondary bacterial pneumonia after influenza. *J. Infect. Diseases* 190, 519–526. doi: 10.1086/421525

McCullers, J. A. (2006). Insights into the interaction between influenza virus and pneumococcus. *Clin. Microbiol. Rev.* 19, 571–582. doi: 10.1128/CMR.00058-05

McCullers, J. A. (2014). The co-pathogenesis of influenza viruses with bacteria in the lung. *Nat. Rev. Microbiol.* 12, 252–262. doi: 10.1038/nrmicro3231

McCullers, J. A., and Rehg, J. E. (2002). Lethal synergism between influenza virus and *Streptococcus pneumoniae*: characterization of a mouse model and the role of platelet-activating factor receptor. *J. Infect. Diseases* 186, 341–350. doi: 10.1086/341462

McNicholl, I. R., and McNicholl, J. J. (2001). Neuraminidase inhibitors: zanamivir and oseltamivir. *Ann. Pharmacother.* 35, 57–70. doi: 10.1345/aph.10118

Miao, H., Hollenbaugh, J. A., Zand, M. S., Holden-Wiltse, J., Mosmann, T. R., Perelson, A. S., et al. (2010). Quantifying the early immune response and adaptive immune response kinetics in mice infected with influenza A virus. *J. Virol.* 84, 6687–6698. doi: 10.1128/JVI.00266-10

Morens, D. M., Taubenberger, J. K., and Fauci, A. S. (2008). Predominant role of bacterial pneumonia as a cause of death in pandemic influenza: implications for pandemic influenza preparedness. *J. Infect. Diseases* 198, 962–970. doi: 10.1086/591708

Moscona, A. (2005). Neuraminidase inhibitors for influenza. *New England J. Med.* 353, 1363–1373. doi: 10.1056/NEJMra050740

Murray, P. J., Allen, J. E., Biswas, S. K., Fisher, E. A., Gilroy, D. W., Goerdt, S., et al. (2014). Macrophage activation and polarization: nomenclature and experimental guidelines. *Immunity* 41, 14–20. doi: 10.1016/j.immuni.2014.06.008

Muthuri, S. G., Myles, P. R., Venkatesan, S., Leonardi-Bee, J., and Nguyen-Van-Tam, J. S. (2012). Impact of neuraminidase inhibitor treatment on outcomes of public health importance during the 2009-10 influenza A (H1N1) pandemic: a systematic review and meta-analysis in hospitalized patients. *J. Infect. Diseases.* 207:jis726. doi: 10.1093/infdis/jis726

Nowak, M., and May, R. M. (2000). *Virus Dynamics: Mathematical Principles of Immunology and Virology: Mathematical Principles of Immunology and Virology*. Oxford, UK: Oxford University Press.

Pawelek, K. A., Huynh, G. T., Quinlivan, M., Cullinane, A., Rong, L., and Perelson, A. S. (2012). Modeling within-host dynamics of influenza virus infection including immune responses. *PLoS Comput. Biol.* 8:e1002588. doi: 10.1371/journal.pcbi.1002588

Rayner, C. R., Chanu, P., Gieschke, R., Boak, L. M., and Jonsson, E. N. (2008). Population pharmacokinetics of oseltamivir when coadministered with probenecid. *J. Clin. Pharmacol.* 48, 935–947. doi: 10.1177/0091270008320317

Renaud, C., Boudreault, A. A., Kuypers, J., Lofy, K. H., Corey, L., Boeckh, M. J., et al. (2011). H275Y mutant pandemic (H1N1) 2009 virus in immunocompromised patients. *Emerg. Infect. Dis.* 17, 653–660. doi: 10.3201/eid1704.101429

Shahangian, A., Chow, E. K., Tian, X., Kang, J. R., Ghaffari, A., Liu, S. Y., et al. (2009). Type I IFNs mediate development of postinfluenza bacterial pneumonia in mice. *J. Clin. Invest.* 119, 1910. doi: 10.1172/JCI35412

Sheu, T. G., Deyde, V. M., Okomo-Adhiambo, M., Garten, R. J., Xu, X., Bright, R. A., et al. (2008). Surveillance for neuraminidase inhibitor resistance among human influenza A and B viruses circulating worldwide from 2004 to 2008. *Antimicrob. Agents Chemother.* 52, 3284–3292. doi: 10.1128/AAC.00555-08

Small, C.-L., Shaler, C. R., McCormick, S., Jeyanathan, M., Damjanovic, D., Brown, E. G., et al. (2010). Influenza infection leads to increased susceptibility to subsequent bacterial superinfection by impairing NK cell responses in the lung. *J. Immunol.* 184, 2048–2056. doi: 10.4049/jimmunol.0902772

Smith, A. M., Adler, F. R., Ribeiro, R. M., Gutenkunst, R. N., McAuley, J. L., McCullers, J. A., et al. (2013). Kinetics of coinfection with influenza a virus and *Streptococcus pneumoniae*. *PLoS Pathog.* 9:e1003238. doi: 10.1371/journal.ppat.1003238

Tamiflu (R). (2009). *Tamiflu (R) (oseltamivir phosphate) Capsules and for Oral Suspension*. Package insert. Foster city, California: Roche laboratories Inc., Gilead Sciences Inc. Available online at: http://www.fda.gov/downloads/Drugs/DrugSafety/DrugShortages/UCM183850.pdf

Tanaka, A., Nakamura, S., Seki, M., Iwanaga, N., Kajihara, T., Kitano, M., et al. (2015). The effect of intravenous peramivir, compared with oral oseltamivir, on the outcome of post-influenza pneumococcal pneumonia in mice. *Antiv. Ther.* 20, 11–19. doi: 10.3851/IMP2744

Trappetti, C., Kadioglu, A., Carter, M., Hayre, J., Iannelli, F., Pozzi, G., et al. (2009). Sialic acid: a preventable signal for pneumococcal biofilm formation, colonization, and invasion of the host. *J. Infect. Diseases* 199, 1497–1505. doi: 10.1086/598483

Treanor, J. J., Hayden, F. G., Vrooman, P. S., Barbarash, R., Bettis, R., Riff, D., et al. (2000). Efficacy and safety of the oral neuraminidase inhibitor oseltamivir in treating acute influenza: a randomized controlled trial. *Jama* 283, 1016–1024. doi: 10.1001/jama.283.8.1016

Tridane, A., and Kuang, Y. (2010). Modeling the interaction of cytotoxic T lymphocytes and influenza virus infected epithelial cells. *Mathemat. Biosci. Eng.* 7, 171–185. doi: 10.3934/mbe.2010.7.171

Visser, S. A., Aurell, M., Jones, R. D., Schuck, V. J., Egnell, A.-C., Peters, S. A., et al. (2013). Model-based drug discovery: implementation and impact. *Drug Discov. Today* 18, 764–775. doi: 10.1016/j.drudis.2013.05.012

Wattanagoon, Y., Stepniewska, K., Lindegårdh, N., Pukrittayakamee, S., Silachamroon, U., Piyaphanee, W., et al. (2009). Pharmacokinetics of high-dose oseltamivir in healthy volunteers. *Antimicrob. Agents Chemother.* 53, 945–952. doi: 10.1128/AAC.00588-08

World Health Organization. (2009a). Influenza (seasonal). Fact sheet no. 211. *World Health Organization, Geneva, Switzerland*. Available online at: http://www.who.int/mediacentre/factsheets/fs211/en/index.html

World Health Organization. (2009b). *WHO Guidelines for Pharmacological Management of Pandemic (H1N1) 2009: Influenza and Other Influenza Viruses*. Geneva: World Health Organization.

World Health Organization. (2010). Update on oseltamivir-resistant influenza A (H1N1) 2009 influenza virus: January 2010. *Wkly Epidemiol Rec.* 85, 37–40.

Conflict of Interest Statement: The authors declare that the research was conducted in the absence of any commercial or financial relationships that could be construed as a potential conflict of interest.

frontiers in Cellular and Infection Microbiology

ORIGINAL RESEARCH
published: 20 June 2016
doi: 10.3389/fcimb.2016.00063

Physiological Roles of the Dual Phosphate Transporter Systems in Low and High Phosphate Conditions and in Capsule Maintenance of *Streptococcus pneumoniae* D39

*Jiaqi J. Zheng, Dhriti Sinha, Kyle J. Wayne and Malcolm E. Winkler**

Department of Biology, Indiana University Bloomington, Bloomington, IN, USA

Unlike most bacteria, *Streptococcus pneumoniae* (pneumococcus) has two evolutionarily distinct ABC transporters (Pst1 and Pst2) for inorganic phosphate (P_i) uptake. The genes encoding a two-component regulator (PnpRS) are located immediately upstream of the *pst1* operon. Both the *pst1* and *pst2* operons encode putative PhoU-family regulators (PhoU1 and PhoU2) at their ends. This study addresses why *S. pneumoniae* contains dual P_i uptake systems and the regulation and contribution of the Pst1 and Pst2 systems in conditions of high (mM) P_i amount and low (μM) P_i amount. We show that in unencapsulated mutants, both *pst1* and *pst2* can be deleted, and P_i is taken up by a third Na^+/P_i co-transporter, designated as NptA. In contrast, either *pst1* or *pst2* is unexpectedly required for the growth of capsule producing strains. We used a combination of mutational analysis, transcript level determinations by qRT-PCR and RNA-Seq, assays for cellular PnpR∼P amounts by SDS-PAGE, and pulse-P_i uptake experiments to study the regulation of P_i uptake. In high P_i medium, PhoU2 serves as the master negative regulator of Pst2 transporter function and PnpR∼P levels (post-transcriptionally). Δ*phoU2* mutants have high PnpR∼P levels and induction of the *pst1* operon, poor growth, and sensitivity to antibiotics, possibly due to high P_i accumulation. In low P_i medium, Pst2 is still active, but PnpR∼P amount and *pst1* operon levels increase. Together, these results support a model in which pneumococcus maintains high P_i transport in high and low P_i conditions that is required for optimal capsule biosynthesis.

Keywords: PhoU, PnpRS two-component system (TCS), PnpR∼P phosphorylation, Pst1 and Pst2 P_i ABC transporters, NptA Na^+/P_i co-transporter

OPEN ACCESS

Edited by:
Guangchun Bai,
Albany Medical College, USA

Reviewed by:
Jan-Willem Veening,
University of Groningen, Netherlands
William R. McCleary,
Brigham Young University, USA

****Correspondence:***
Malcolm E. Winkler
winklerm@indiana.edu

Received: *22 April 2016*
Accepted: *27 May 2016*
Published: *20 June 2016*

Citation:
Zheng JJ, Sinha D, Wayne KJ and Winkler ME (2016) Physiological Roles of the Dual Phosphate Transporter Systems in Low and High Phosphate Conditions and in Capsule Maintenance of Streptococcus pneumoniae D39. Front. Cell. Infect. Microbiol. 6:63. doi: 10.3389/fcimb.2016.00063

INTRODUCTION

Phosphorus is an essential element in all cells because of its structural and metabolic roles in nearly all biological processes, including the composition of nucleic acids, phospholipids, and energy intermediates. A preferred source of phosphorous for bacterial cells is environmental inorganic orthophosphate (PO_4^-; P_i). The mechanism of extracellular P_i uptake has been studied intensively

in *Escherichia coli* and *Bacillus subtilis* as model organisms (Hulett, 1993; Takemaru et al., 1996; Wanner, 1996; Qi et al., 1997; Lamarche et al., 2008; Hsieh and Wanner, 2010; Botella et al., 2011, 2014), and recently in other bacterial species (Braibant et al., 1996; Gonin et al., 2000; Zaborina et al., 2008; Rifat et al., 2009; Shi and Zhang, 2010; Burut-Archanai et al., 2011; Cheng et al., 2012; Wang et al., 2013; de Almeida et al., 2015; Lubin et al., 2016). Generally, bacterial high-affinity P_i uptake systems consist of an ATP-binding cassette (ABC) transporter, designated as Pst (for phosphate-specific transporter), which contains at least four component subunits: an extracellular P_i binding protein (PstS), two transmembrane channel proteins (PstCA), and a cytoplasmic ATPase (PstB) (see **Figure 1**; Hsieh and Wanner, 2010). The expression of most bacterial Pst transporters is regulated at the transcriptional level by a two-component regulatory system (TCS), which has different designations in different bacteria (Hulett, 1993; Novak et al., 1999; Throup et al., 2000; Howell et al., 2006; Glover et al., 2007). Many bacteria also regulate P_i uptake by an ancillary negative regulatory protein, designated PhoU (Steed and Wanner, 1993; Botella et al., 2011, 2014; de Almeida et al., 2015; Lubin et al., 2016).

In *E. coli* and related enterobacteria, the histidine kinase (HK) and response regulator (RR) that mediate P_i transport are designated as PhoR and PhoB, respectively, and the regulation of P_i uptake involves a PhoU regulator (Hsieh and Wanner, 2010; Gardner et al., 2014, 2015). Briefly, when $[P_i] > 4.0\,\mu M$, the expression of the *phoB-phoR* regulator and *pst* transporter operons is inhibited by PhoU by a mechanism described below (Hsieh and Wanner, 2010). When the $[P_i]$ is depleted to $<4.0\,\mu M$, PhoU releases inhibition of the PhoR HK and the PstB subunit of the transporter, allowing autophosphorylation of the PhoR HK, phosphoryl transfer to the PhoB RR, and activation of transcription by PhoB∼P of operons in the phosphate (pho) regulon, including the *pst* transporter, the *phoB-phoR* regulator, and other operons involved in the uptake and assimilation of phosphorous-containing compounds (Wanner, 1996; Hsieh and Wanner, 2010). PhoB∼P activates transcription by binding to the Pho box sequence upstream from the promoters of the regulon operons, including *phoB-phoR*, which provides autoregulation of the TCS proteins (Wanner, 1996; Martin, 2004; Lubin et al., 2016). Usually, the sequence of the consensus Pho box is different between Gram-negative (e.g., *E. coli*) and Gram-positive (e.g., *B. subtilis*) bacteria (Martin, 2004). Since the Pst transporter is not activated in *E. coli* at high P_i concentrations, this system is considered as a high-affinity transporter that works predominantly at low P_i concentrations (Wanner, 1996). PhoB/R, the Pst transporter, and members of the Pho regulon are important for virulence in many pathogenic Gram-negative bacteria, including *E. coli*, *Vibrio cholerae*, *Proteus mirabilis*, and *Pseudomonas aeruginosa* (Jacobsen et al., 2008; Lamarche et al., 2008; Zaborina et al., 2008; Pratt et al., 2010; Chekabab et al., 2014a,b). In *P. aeruginosa,* the PstS P_i binding protein also plays roles in adhesion and a P_i-independent role in biofilm formation (Zaborina et al., 2008; Neznansky et al., 2014; Shah et al., 2014).

PhoU is a negative regulator of Pho regulon expression in *E. coli* and many other bacteria (Muda et al., 1992; Wanner, 1996; Hsieh and Wanner, 2010; Gardner et al., 2014; de Almeida et al., 2015). Although, PhoU is an important regulator in many bacteria, it is notably absent from certain Gram-positive bacteria, including *B. subtilis* (Qi et al., 1997; Moreno-Letelier et al., 2011). *phoU* deletion in *E. coli*, *P. aeruginosa*, and *Mycobacterium marinum* leads to growth defects (Steed and Wanner, 1993; Wanner, 1996; Rice et al., 2009; Wang et al., 2013; de Almeida et al., 2015). In *E. coli*, this growth defect is reversed by deletion of the *pst* transporter operon or the *phoBR* TCS operon (Steed and Wanner, 1993; Wanner, 1996). These observations suggest that the growth defect of *phoU* mutants is caused by unregulated function of the Pst transport system, leading to excess P_i accumulation (Wanner, 1996; Rice et al., 2009). Δ*phoU* mutants also accumulate increased amounts of poly-orthophosphate (poly-P_i) in *E. coli*, *M. marinum*, *P. aeruginosa*, and *Caulobacter crescentus* (Morohoshi et al., 2002; Hirota et al., 2013; Wang et al., 2013; de Almeida et al., 2015; Lubin et al., 2016). Poly-P_i also accumulates in *E. coli* K-12 cells in stationary phase in high P_i medium, and this accumulation is correlated with inhibition of biofilm formation mediated by PhoB∼P RR phosphorylation with acetyl-phosphate acting as donor (Grillo-Puertas et al., 2016). The rate of P_i uptake was reported to increase in an *E. coli* Δ*phoU* in one study (Rice et al., 2009), but not in another (Steed and Wanner, 1993). Besides defective growth, Δ*phoU* mutants exhibit higher sensitivity to a diverse range of antibiotics in *E. coli*, *Mycobacterium tuberculosis*, *M. marinum,* and *P. aeruginosa* (Li and Zhang, 2007; Shi and Zhang, 2010; Wang et al., 2013; de Almeida et al., 2015) and a defect in mutagenic DNA break repair in *E. coli* (Gibson et al., 2015).

Recent papers demonstrate that *E. coli* PhoU interacts with the PAS domain of the PhoR HK and with the PstB ATPase protein, in support of the dual inhibition of Pho regulon transcription and Pst mediated transport in *E. coli* (Gardner et al., 2014, 2015). Three crystal structures of PhoU-like proteins have been reported from *Aquifex aeolicus*, *Thermotoga maritima*, and *P. aeruginosa* (Liu et al., 2005; Oganesyan et al., 2005; Lee et al., 2014), showing that PhoU consists of two symmetric, three-alpha-helix bundles. However, these PhoU proteins showed several quaternary structures in crystals, including monomer, dimer, or hexamer packing (Liu et al., 2005; Oganesyan et al., 2005; Lee et al., 2014). Gel filtration shows that purified *E. coli* PhoU forms a dimer in solution (Gardner et al., 2014). In addition, divalent cation binding of magnesium and manganese is required for *E. coli* PhoU binding to the cytoplasmic side of the inner membrane and may play a role in formation of a ternary regulatory complex containing PhoU, PhoR, and PstB (Gardner et al., 2014). On the other hand, a recent study suggests that a different paradigm operates in *C. crescentus*, where PhoU does not modulate PhoR HK activity directly (Lubin et al., 2016). Instead, PhoU may negatively regulate the activity of the Pst transporter in response to P_i availability in *C. crescentus* (Lubin et al., 2016).

Besides Pst ABC transporters, P_i is taken up by symporter secondary transport systems. In *E. coli*, two additional P_i transporters, PitA and PitB, have been identified that are symporters of divalent cations, such as Mg^{2+} and Ca^{2+} (van Veen

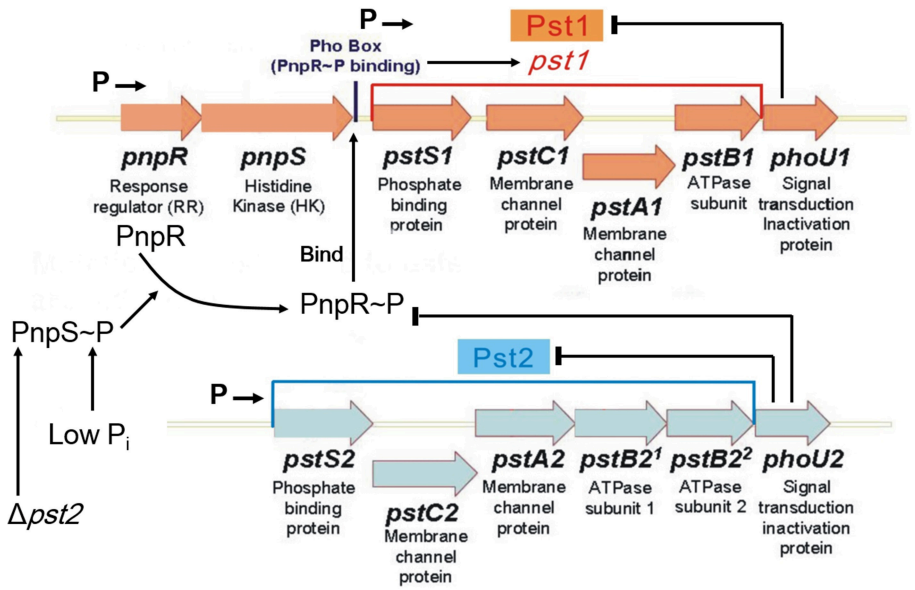

FIGURE 1 | Model for regulation of the dual Pst1 and Pst2 ABC P_i transporters in *Streptococcus pneumoniae* D39. Genomic sequencing and transcriptome analyses show that *pnpRS, pst1-phoU1,* and *pst2-phoU2* are organized into three distinct operons that are transcribed from separate promoters, indicated by Ps followed by arrows (see text). The Pst2 ABC P_i transporter is constitutively expressed in both high and low P_i conditions. PhoU2 inhibits phosphorylation of the PnpR response regulator (RR) and negatively regulates the transport activity of Pst2. In the absence of PhoU2, PnpR is phosphorylated by the PnpS histidine kinase (HK). PnpR~P binds to the Pho box upstream of the *pst1-phoU1* operon and activates transcription and expression of the genes encoding the Pst1 transporter and PhoU1 regulator; however, PnpR~P does not autoregulate its own (*pnpRS*) transcription. In contrast to PhoU2, PhoU1 negatively regulates the transport activity of Pst1, but does not regulate phosphorylation of PnpR. In the absence of the Pst2 transporter or in low P_i conditions, the PnpRS two component system (TCS) activates the expression of the genes encoding the Pst1 transporter and PhoU1 regulator. Either the Pst1 or Pst2 P_i transporter is required in encapsulated cells. Therefore, the regulated Pst1 and constitutive Pst2 P_i transport systems may act as a redundant failsafe to ensure that capsule biosynthesis is maintained during variations in P_i conditions. See the text for additional details.

et al., 1994; Wanner, 1996; Harris et al., 2001; Jackson et al., 2008). PitA and PitB have been considered as low-affinity P_i transporters that predominantly function in high P_i environments (Wanner, 1996; Hsieh and Wanner, 2010). Moreover, expression of *pitA* is induced by Zn^{2+} addition (Jackson et al., 2008), suggesting that PitA may act primarily as a metal ion transporter instead of a P_i transporter (Beard et al., 2000).

Unlike *E. coli*, *B. subtilis*, or *C. crescentus*, which contain only one Pst transporter, *Streptococcus pneumoniae* (pneumococcus) encodes two evolutionarily distinct P_i ABC pump transporters, Pst1 and Pst2 (**Figure 1**; Lanie et al., 2007; Moreno-Letelier et al., 2011). The multigene *pst1* and *pst2* operons are located at different locations in the pneumococcus chromosome (Lanie et al., 2007). Only one *phoBR*-like TCS, *pnpRS,* encoding the PnpR RR and the PnpS HK, is encoded upstream of the *pst1* operon, and both the *pst1* and *pst2* transporter operons encode separate PhoU-family regulators, designated PhoU1 and PhoU2 (**Figure 1**). The PnpRS TCS, Pst1 transporter, and PhoU1 were initially studied in unencapsulated *S. pneumoniae* laboratory strain R6x (Novak et al., 1999), before the discovery of the second Pst2 transporter and PhoU2 regulator. This work indicated that *pnpRS* operon expression was not regulated by P_i amount, and that mutants deficient in the PstB1 ATPase subunit seemed to show decreased P_i uptake in certain growth media (Novak et al., 1999). Subsequent work suggests that upregulation of *pst1* operon expression is correlated with increased β-lactam antibiotic resistance in low-affinity *pbp2x* mutants and some clinical isolates of *S. pneumoniae* (Soualhine et al., 2005; Engel et al., 2014).

S. pneumoniae is a common commensal bacterium that primarily colonizes the human nasopharynx (Donkor, 2013; Chao et al., 2014; Hakansson et al., 2015; Short and Diavatopoulos, 2015), but can become an opportunistic pathogen, causing several serious respiratory and invasive diseases (Henriques-Normark and Tuomanen, 2013; Vernatter and Pirofski, 2013; Ferreira and Gordon, 2015; Gratz et al., 2015; Oliver and Swords, 2015). Therefore, the Pst1 and Pst2 transporters must mediate P_i acquisition from several niches with vastly different P_i concentrations in human hosts (Orihuela et al., 2001; Wilson, 2005, 2008). Signature-tagged mutagenesis (STM) screens and a study of the role of the PnpR RR (also called RR04) indicated that the *pnpRS*, *pst1,* and *pst2* operons are all required for full pneumococcal virulence (Polissi et al., 1998; Throup et al., 2000; Hava and Camilli, 2002; McCluskey et al., 2004; Paterson et al., 2006; Trihn et al., 2013). Consistent with these earlier studies, a recent Tn-Seq study showed that PhoU1 is important for nasopharynx colonization, whereas PhoU2 is important for lung infection (van Opijnen and Camilli, 2012).

In this report, we studied the transcriptional and functional regulation of the pneumococcal Pst1 and Pst2 P_i transporters

under growth conditions containing high (≈18 mM) or low (≈100 μM) concentrations of P_i. Our results show that *pst2* operon transcription is constitutive, but Pst2 transporter activity is negatively regulated by PhoU2. In addition, PhoU2 negatively regulates PnpR RR phosphorylation and transcription of the *pst1* operon at high concentrations of P_i. Therefore, PhoU2 resembles *E. coli* PhoU in that it functions in regulating the level of RR phosphorylation, besides modulating Pst2 transporter activity. In contrast, PhoU1 resembles *C. crescentus* PhoU in that it only regulates Pst1 transporter activity and does not modulate PnpRS TCS function. Our results also indicate that encapsulated *S. pneumoniae* requires the function of Pst1 or Pst2 for growth, whereas a symporter, named NptA, can provide sufficient P_i to allow the growth of unencapsulated mutants in high P_i conditions.

MATERIALS AND METHODS

Bacterial Strains and Growth Conditions

Strains used in this study are listed in Table S1. Encapsulated strains were derived from parent strain IU1781 (D39 *cps*$^+$ *rpsL1*), and unencapsulated strains were derived from parent strains IU1945 (D39 Δ*cps*), IU1824 (D39 Δ*cps rpsL1*), and IU3309 (D39 Δ*cps2E rpsL1*), which are derivatives of serotype 2 *S. pneumoniae* strain D39 IU1690 (Lanie et al., 2007). Strains containing antibiotic markers were constructed by transformation of competent pneumococcal cells with linear DNA amplicons synthesized by overlapping fusion PCR (Ramos-Montanez et al., 2008; Tsui et al., 2010). Strains containing markerless alleles in native chromosomal loci were constructed using allele replacement via the Pc-[*kan-rpsL*$^+$] (Janus cassette; Sung et al., 2001). Primers used to synthesize different amplicons are listed in Table S2. All constructs were confirmed by DNA sequencing of chromosomal regions corresponding to the amplicon region used for transformation. Bacteria were grown on plates containing trypticase soy agar II (modified; Becton-Dickinson) and 5% (vol/vol) defibrinated sheep blood (TSAII-BA). Plates were incubated at 37°C in an atmosphere of 5% CO_2. For selections of transformants, TSAII-BA plates contained 250 μg/mL kanamycin, 0.3 μg/mL erythromycin, or 250 μg/mL streptomycin. Strains were cultured statically in Becton-Dickinson brain heart infusion (BHI) broth at 37°C in an atmosphere of 5% CO_2, and growth was monitored by OD_{620} as described before (Tsui et al., 2016). Transformants were single-colony-isolated on TSAII-BA plates containing antibiotics twice before growth in antibiotic-containing BHI broth for storage (Tsui et al., 2016). All mutant constructs were confirmed by DNA sequencing of chromosomal regions corresponding to the amplicon region used for transformation.

Static growth in BHI broth, which contains ≈18 mM P_i, was used as a high P_i condition. For growth curves, strains were inoculated into 3 mL of BHI broth, serially diluted, and grown overnight. The next day, cultures with OD_{620} = 0.1–0.3 were diluted into 5 mL of fresh BHI broth to OD_{620}≈0.002, and growth was monitored hourly. C+Y medium (Lacks and Hotchkiss, 1960) was used for studies of moderately low P_i condition. We determined that C+Y broth (no added P_i) already contains ≈1.5 mM P_i (see Results). A modified chemically defined medium (mCDM) (Carvalho et al., 2013) was used for moderate and low P_i conditions. To optimize growth, the concentrations of choline-HCl and all amino acids amounts were increased by 1000-fold and tyrosine was added to 100 mg/L compared to the CDM recipe in Carvalho et al. (2013). In addition, 40 mM MOPS buffer was added to mCDM, which was adjusted to a final pH = 7.4 with 10 M NaOH. mCDM contains 36.4 mM P_i(Carvalho et al., 2013). mCDM with no P_i was made by omitting KH_2PO_4 and K_2HPO_4 and adding KCl to 50.8 mM. mCDM media with 2 mM or 1 mM P_i was made by mixing mCDM and mCDM lacking P_i in a ratio of 2–34.4 or 1–35.4, respectively. mCDM with 1 mM P_i was diluted 10 or 100-fold with mCDM lacking P_i make mCDM with 100 μM and 10 μM P_i, respectively. For growth in mCDM, 3 mL overnight cultures were grown as described above, and the next day, cultures with OD_{620} = 0.1–0.3 were centrifuged (5125 × g, 5 min, 25°C), washed with 3 mL mCDM lacking P_i twice, and resuspended in 3 mL mCDM lacking P_i. Cells were then diluted in 5 mL of mCDM with 2, 1 mM, 100, 10 μM, or no P_i to OD≈0.005 and growth of static cultures in an atmosphere of 5% CO_2 was monitored hourly at OD_{620}.

Antibiotic Disk Diffusion Assays

Overnight cultures were diluted and grown in 5 mL of BHI to OD_{620}≈0.1. 100 μL of cultures were mixed with 3 mL of nutrient-broth soft agar [0.8% (w/v) nutrient broth and 0.7% (w/v) Bacto Agar (Difco)] and poured onto TSAII-BA plates. After 15 min, antibiotics disks were placed at the middle of plates, which were incubated at 37°C in an atmosphere of 5% CO_2 overnight for 16 h. Diameters of zones of growth inhibition were measured with a ruler, and *P*-values were calculated by unpaired *t*-test in GraphPad Prism. Antibiotic disks were from Becton, Dickinson Co.: cefotaxime (30 μg); cefazolin (30 μg); cefamandole (30 μg); ceftazidime (30 μg); amdinocillin (10 μg); vancomycin (30 μg); gentamicin (120 μg); and tetracycline (30 μg).

RNA Preparation, qRT-PCR, and RNA-Seq Analyses

To study high P_i conditions, overnight cultures were diluted and grown in 5 mL of BHI to OD ≈0.15. Cells were collected by centrifuging at 16,000 × g for 5 min at 4°C. 1 mL of RNApro solution (MP Biomedicals) was added to resuspend cell pellets. The suspension was transferred to a Lysing Matrix B tube (MP Biomedicals), which was shaken 3X in FastPrep homogenizer (6.0 M/s for 40 s each). Cell debris and lysing matrix were removed by centrifugation at 16,000 × *g* for 5 min at 4°C. 700 μL of supernates was transferred to a new microcentrifuge tube and incubated at room temperature for 5 min. 300 μL of chloroform was then added followed by incubation at room temperature for 5 min. Mixtures were centrifuged at 16,000 × *g* for 5 min at 4°C. 280 μL of the upper, aqueous phase was collected and mixed with 140 μL of 100% Ethanol in a new microcentrifuge tube for RNA precipitation. RNA purification was done using miRNeasy minikit (Qiagen), including on-column treatment

with DNase I (Qiagen), following the manufacturer's instructions. 5 μg of purified RNA was treated by DNase from a DNA-free DNA removal kit (Ambion). 125 ng of treated RNA was used to synthesize cDNA by a qScript Felex cDNA synthesis kit (Quanta Biosciences). Synthesized cDNA was diluted 1:6 in water and then serially diluted 1:5 in water three more times. qRT-PCR reactions contained 10 μL of 2 × Brilliant III Ultra-Fast SYBR Green QPCR Master Mix (Agilent), 2 μL of each 2 μM primers (Table S3), 0.3 μL of a 1:500 dilution of ROX reference dye, and 6 μL of diluted cDNA. Samples were run in an MX3000P thermocycler (Stratagene) with Program MxPro v. 3.0. Transcript amounts were normalized to *gyrA* mRNA amount and compared with transcript amounts of the wild-type parent strain by unpaired *t*-test in GraphPad Prism (Kazmierczak et al., 2009).

To study low P_i conditions, bacteria from overnight BHI broth cultures were washed, diluted, and grown in 5 mL of mCDM medium containing 36.4 mM P_i to $OD_{620}\approx0.15$. Cells were collected by centrifugation, washed twice with 5 mL mCDM lacking P_i, and resuspended in mCDM containing 36.4 mM P_i or 10 μM P_i. Cultures were incubated at 37°C in an atmosphere of 5% CO_2 for 30 min. Lysis, RNA extraction, purification, and qRT-PCR reactions were performed as described above, except that 16S rRNA was used to normalize transcript amounts, because *gyrA* was down-regulated under low P_i condition. All transcript amounts were compared with the wild-type parent strain grown in mCDM containing 36.4 mM.

RNA samples for RNA-Seq analyses were prepared from 30 mL cultures as described previously (Hoover et al., 2015) cDNA library construction, single-end, 100 bp-sequencing on a HiSeq 2000 sequencer (Illumina), and bioinformatic analyses were performed as described in Hoover et al. (2015). False-discovery rates (FDR) were calculated using Benjamini and Hochberg's algorithm (Benjamini and Hochberg, 1995) and a gene or region was defined as differentially expressed if it had an up- or down-fold change of 1.8 with a FDR < 0.05. RNA-Seq data were deposited in the NCBI GEO database under accession number GSE80637.

Phos-Tag SDS-PAGE and Western Blot

Phos-tag SDS-PAGE and standard Western blotting were carried out as described previously (Wayne et al., 2010, 2012; Tsui et al., 2014). To study high P_i conditions, overnight BHI broth cultures were diluted and grown up to $OD_{620}\approx0.2$ in 30 mL of BHI. Cells expressing PnpR-L-FLAG^3 were lysed using a FastPrep homogenizer, and cell lysates were resolved by Phos-tag SDS-PAGE at 4°C (Wayne et al., 2012). Cells expressing PstS2-HA were lysed by the same method, but resolved by standard SDS-PAGE (Tsui et al., 2014). PnpR-L-FLAG^3 and PstS2-HA were detected by Western blotting as described previously (Tsui et al., 2014) using anti-FLAG or anti-HA antibody as primary antibody. Chemiluminescent signal in protein bands was quantitated by using an IVIS imaging system as described in Wayne et al. (2010).

To study low P_i conditions, strains were grown in 30 mL of mCDM to $OD_{620}\approx0.2$ as described above. Cells were collected by centrifugation and washed twice with 30 mL of mCDM lacking P_i. Cell pellets were resuspended in 30 mL of mCDM containing 36.4 mM P_i or lacking P_i and incubated statically at 37°C in an atmosphere of 5% CO_2 for 40 min. Proteins samples were extracted and Phos-tag SDS-PAGE was performed as described above.

Qualitative Quellung Assay for Capsule

Overnight cultures were diluted and grown in 5 mL of BHI to $OD\approx0.15$. 1 μL of culture was mixed with 1 μL of Type 2 pneumococcal antiserum (Statens Serum Institut) on a glass slide. A cover slip was placed on top of the mixture, which was viewed immediately with a 100X objective by a phase-contrast microscope. Cells surrounded by capsule appear enlarged or swollen.

P_i Concentration Determination

The P_i amount in C+Y broth was determined by the colorimetric method described in Katewa and Katyare (2003). Briefly, standards were prepared by dilution of a KH_2PO_4 stock to give final P_i concentrations of 2.5, 5.0, 10.0, 20.0, and 40.0 μM P_i in 2.4 mL of water in glass tubes. 0.8 mL of 3N H_2SO_4 was added to each standard tube. 0.4 mL of 2.5% (w/v) ammonium molybdate (prepared in 3N H_2SO_4) was added in each tube. Last, 0.4 mL of reducing agents (20 mg of hydrazine sulfate and 20 mg of ascorbic acid dissolved in 1 mL of 0.1N H_2SO_4) was added to each tube. After 2 h at room temperature, A_{820} was determined and plotted to generate a standard curve. C+Y broth (no added P_i) was diluted 100X with water, P_i content was assayed as described above, and P_i concentration was determined from the standard curve.

P_i Uptake Assays

To study high P_i conditions, strains were grown in 5 mL of BHI broth to $OD_{600}\approx0.2$. Cells were centrifuged at 5125 × *g* for 5 min at room temperature, washed twice with 5 mL of mCDM lacking P_i, and resuspended at room temperature in 5 mL of mCDM lacking P_i. $K_2H^{32}PO_4$ (10^7–10^8 dpm; 8500–9120 Ci/mmole; Perkin Elmer) was added to a final concentration of 1 mM at t=0, and 100 μL of cells was collected by vacuum filtration (0.22 μm GSWP; 13 mm diameter; Millipore) at 1, 2, 4, 6, 10 min after addition of ^{32}P. Filters were washed 3X with 3 mL of room-temperature 1 × PBS (Ambion). Washed filters were transferred individually into 20-mL glass scintillation vials to which 5 mL of a biodegradable counting cocktail was added. Dpm of each sample was determined using a TRI-CARB 2100TR Liquid Scintillation Counter (Perkin Elmer), P_i amount incorporated at each time point was calculated.

To study low P_i condition, strains were grown to $OD_{600}\approx0.2$ in mCDM containing 36.4 mM Pi as described above. Cells were centrifuged at 5125 × g for 5 min at room temperature, and washed twice with 5 mL of mCDM lacking P_i. Cell pellets were resuspended in 5 mL of mCDM lacking P_i and incubated 1 h at 37°C in an atmosphere of 5% CO_2. 200 μM of $K_2H^{32}PO_4$ (10^7–10^8 dpm) was added at $t = 0$, and samples were withdrawn, filtered, and counted as described above.

RESULTS

Δ*phoU2* Mutants Show a Growth Defect and Increased Sensitivity to a Range of Antibiotics That is Reversed by Inactivation of Pst2 Transport

The Pst transporter is not needed for growth of *E. coli* at high P_i concentrations >4 μM, and Δ*phoU* mutations lead to a severe growth defect that is reversed by inactivation of the Pst transporter (Steed and Wanner, 1993; Rice et al., 2009). To determine the roles of the Pst1 and Pst2 transporters and their regulation, we constructed a series of markerless deletion mutants [Δ*phoU2* (IU6375); Δ*phoU1* (IU6377); Δ*pnpRS* (IU6381); Δ*pst2* (IU6610); Δ*pst1* (IU6638)] in *S. pneumoniae* serotype 2 strain D39, which is encapsulated and virulent (Lanie et al., 2007; **Figure 1**, Table S1). Mutants were first grown in BHI broth, which contains a high P_i concentration (≈18 mM). Only the Δ*phoU2* mutant showed a significant decrease in growth yield compared to the parent and other mutants (**Figure 2A**, Figure S1A, Table S4). Growth yield was restored when the Δ*phoU2* mutation was complemented by an ectopic copy of the *phoU2*$^+$ gene expressed from the P_{ftsA} promoter at the *bgaA* site (IU6397) (**Figure 2A**, Table S4). Similar results were obtained in mutants in unencapsulated D39 derivative strain K579 and E579 (data not shown).

Inactivation of *phoU* in *E. coli* generates higher sensitivity to various kinds of antibiotics than the parent strain (Li and Zhang, 2007). Since the pneumococcal Δ*phoU2* mutant shows a similar growth defect as the Δ*phoU* mutant in *E. coli* (**Figure 2A**, Figure S1A), we tested antibiotic sensitivity to several antibiotics. Of the Pho regulon mutants tested in the encapsulated strain, only the Δ*phoU2* mutant showed increased sensitivity to β-lactams and other classes of antibiotics, including glycopeptides and protein synthesis inhibitors, on plates that contain relatively high P_i content (**Figure 2B**, Figure S1B, and Table S5).

Previous work in *E. coli* (Steed and Wanner, 1993; Wanner, 1996; Rice et al., 2009; Hsieh and Wanner, 2010) and *C. crescentus,* in which PhoU is essential for growth (Lubin et al., 2016), indicated that the reduced growth of *phoU* deletion or depletion mutants could be reversed by inactivation of the Pst pump. This reversal was interpreted to mean that PhoU negatively regulates the Pst transporter itself, and in its absence, deleterious phosphate compounds accumulate that disrupt growth and metabolism. In the pneumococcal encapsulated D39 genetic background, a Δ*pst2-phoU2* deletion mutant lacking the Pst2 transporter and PhoU2 regulator grew similar to the parent strain and did not show increased sensitivity to antibiotics caused by the absence of PhoU2 alone (**Figures 2C,D**, Table S4). Likewise, single deletions of genes encoding each component of the Pst2 transporter restored growth yield of a Δ*phoU2*

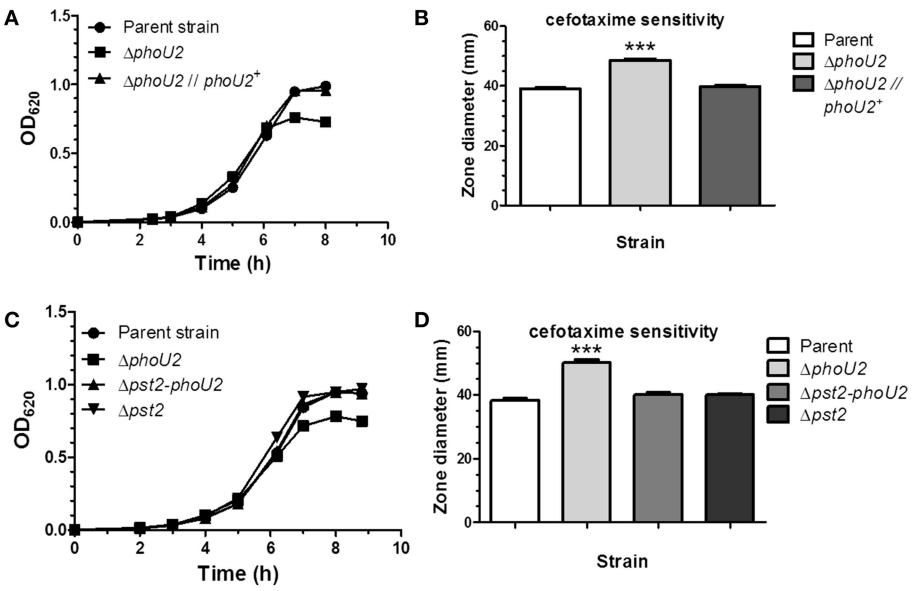

FIGURE 2 | Deletion of *phoU2* leads to a lower growth yield and increased β-lactam antibiotic sensitivity that are reversed by a Δ*pst2* mutation. (A) Representative growth curves in BHI broth (≈18 mM P_i) of encapsulated parent strain (IU1781), a Δ*phoU2* mutant (IU6375), and a Δ*phoU2* mutant complemented by ectopic expression of PhoU2$^+$ (IU6397). Strains were grown as described in Materials and Methods. A linear scale for OD_{620} is used to emphasize differences in growth yields. Growth yields and rates are quantitated for multiple determinations in Table S4. **(B)** Cefotaxime sensitivity assays of encapsulated parent strain (IU1781), a Δ*phoU2* mutant (IU6375), and a PhoU2$^+$-complemented Δ*phoU2* mutant (IU6397). Cefotaxime disk sensitivity assays of bacteria grown in BHI broth were performed as described in Material and Methods. *P*-values were calculated by unpaired *t*-tests relative to the parent strain using GraphPad Prism; ($n \geq 3$); ***$P < 0.001$. Increased sensitivity to other β-lactam antibiotics, vancomycin, gentamicin, and tetracycline of a Δ*phoU2* mutant compared to its isogenic parent strain is shown in Table S5. **(C)** Representative growth curves of encapsulated parent strain (IU1781) and Δ*phoU2* (IU6375), Δ*pst2-phoU2* (IU6550), and Δ*pst2* (IU6610) mutants in BHI broth. **(D)** Cefotaxime sensitivity assays for encapsulated parent strain (IU1781), and Δ*phoU2* (IU6375), Δ*pst2-phoU2* (IU6550), and Δ*pst2* (IU6610) mutants. ($n \geq 3$); ***$P < 0.001$.

mutant back to wild-type (data not shown). Western blot analysis showed that the Δ*phoU2* mutation did not change the cellular amount of the PstS2 transporter subunit fused to the HA epitope tag (Figure S3), and by inference the amount of the Pst2 transporter. We conclude that the decreased growth yield and antibiotic sensitivity of encapsulated pneumococcus Δ*phoU2* mutants in high P_i conditions are dependent on function of the Pst2 transporter, consistent with negative regulation of the Pst2 transporter by PhoU2.

PhoU2 Negatively Regulates Transcription Activation of the *pst1* Operon by the PnpRS TCS in High P_i Conditions

As noted in the Introduction, PhoU negatively regulates the PhoBR TCS in *E. coli*, but not in *C. crescentus* (Hsieh and Wanner, 2010; Lubin et al., 2016). Consequently, we tested whether Δ*phoU1* or Δ*phoU2* deletions affected transcript levels of the *pst1* or *pst2* operons under high P_i conditions (see **Figure 1**). We first performed RNA-Seq analyses of Δ*phoU2*::*kanrpsL*$^+$ and Δ*phoU2*::*kanrpsL*$^+$ Δ*phoU1*::P_c-*erm* mutants growing in early-middle exponential phase in BHI broth, which contains a high (18 mM) concentration of P_i (Table S6). In both strains, only transcript amounts of the *pst1* transporter operon, including *phoU1* in the single mutant, were strongly induced (≈22X). The transcript amounts of the *pnpRS* regulator and *pst2* transporter operons were not induced, and the number of other genes in the Pho regulon appears to be limited in *S. pneumoniae* D39 (Table S6). Notably, pneumococcus encodes neither an alkaline phosphatase (*phoA*) nor a pathway for synthesis of teichuronic acids lacking phosphate (Wanner, 1996; Botella et al., 2011, 2014). Besides the strong induction of *pst1* operon transcription, there were small (2-4X) changes in the relative amounts of only a handful of other transcripts, including some corresponding to metabolic and stress-responsive genes, possibly reflecting the defective growth of these *phoU2* mutants. In both mutants, one of the stronger responses was a decrease in the relative transcript amounts of the genes encoding the glycerol facilitator (GlpF) and glycerol kinase (GlpK). A putative, somewhat degenerate Pho box is located -125 bp upstream of the *glpK* reading frame. Together, these results suggested that PhoU2 negatively regulates *pst1* operon expression under high P_i conditions, whereas the *pnpRS* and *pst2* operons are constitutively expressed.

These conclusions were confirmed by qRT-PCR analysis of combinations of markerless deletion mutations in the *pst* and *pnpRS* genes (**Table 1**). RNA-Seq transcriptome analysis indicates that the *pnpRS*, *pst1-phoU1*, and *pst2-phoU2* operons are separately transcribed (Table S6, **Figure 1**, Figures S2A,B). Hence, we quantitated the relative amounts of the *pnpR, pstS1*, and *pstS2* transcripts normalized to *gyrA* transcript amount by qRT-PCR to represent *pnpRS*, *pst1-phoU1*, and *pst2-phoU2* operon expression (see Materials and Methods; Wayne et al., 2012). Consistent with the RNA-Seq results, the Δ*phoU2* mutations caused ≈16X increase in *pst1-phoU1* operon transcript amount, but no change in expression of *pst2* or *pnpRS* operon (**Table 1**, line 2). In contrast, a Δ*phoU1* mutation did not cause a significant change in the relative amounts of transcript from any of the three operons (**Table 1**, line 3). No increase in *pst1-phoU1* transcript

TABLE 1 | Relative transcript amounts of the *pst1*, *pst2*, and *pnpRS* operons in regulatory mutants[a].

Strains[b]	Relative transcript amount of *pstS1*[c]	Relative transcript amount of *pstS2*[d]	Relative transcript amount of *pnpR*[e]
1. Parent strain (IU1781)	≡1	≡1	≡1
2. Δ*phoU2* (IU6375)	+16.0 ± 1.8 (*n* = 4) (***)[f]	+1.2 ± 0.6 (*n* = 2) (ns)	−1.2 (*n* = 1)
3.Δ*phoU1* (IU6377)	+1.6 ± 0.4 (*n* = 4) (ns)	+1.3 ± 0.4 (*n* = 2) (ns)	+1.1 (*n* = 1)
4. Δ*phoU2//phoU2*$^+$ (IU6397)	+1.3 ± 0.3 (*n* = 3) (ns)	ND[g]	ND
4. Δ*pnpR* (IU6379)	−4.8 ± 0.2 (*n* = 2) (**)	−1.1 ± 0.1 (*n* = 2) (ns)	ND
6. Δ*pnpS* (IU6496)	−2.4 ± 0.4 (*n* = 2) (**)	−1.4 ± 0.1 (*n* = 2) (ns)	ND
7. Δ*pnpRS* (IU6381)	−2.0 ± 0.6 (*n* = 2) (*)	−1.1 ± 0.2 (*n* = 2) (ns)	ND
8. Δ*phoU2* Δ*pnpR* (IU6573)	−4.4 ± 1.1 (*n* = 4) (***)	ND	ND
9. Δ*phoU2* Δ*pnpS* (IU6595)	−2.1 ± 0.3 (*n* = 4) (**)	ND	ND
10. Δ*phoU2* Δ*pnpRS* (IU6575)	−2.5 ± 0.6 (*n* = 5) (**)	ND	ND
11. Δ*phoU2* Δ*phoU1* (IU6499)	+19.6 ± 1.6 (*n* = 5) (***)	−1.4 ± 0.1(*n* = 2) (ns)	+1.0 (*n* = 1)
12. Δ*pst2-phoU2* (IU6550)	+43.8 ± 4.2 (*n* = 4) (***)	–	+1.1 ± 0.0 (*n* = 3) (ns)
13. Δ*pst2* (IU6610)	+44.8 ± 1.5 (*n* = 4) (***)	–	ND
14. Δ*pst2-phoU2* Δ*phoU1* (IU6612)	+44.8 ± 5.5 (*n* = 3) (**)	–	ND
15. Δ*pst1* (IU6638)	–	+1.0 (*n* = 1)	ND

[a] *RNA preparation and qRT-PCR were performed as described in Materials and Methods.*
[b] *Strains were markerless deletion mutants derived from encapsulated parent strain IU1781.*
[c] *Relative pstS1 gene transcript amount was used to represent pst1 operon expression.*
[d] *Relative pstS2 gene transcript amount was used to represent pst2 operon expression.*
[e] *Relative pnpR gene transcript amount was used to represent pnpRS operon expression.*
[f] ****P < 0.001; **P < 0.01; *P < 0.05; ns, not significant. P-values were calculated by an unpaired t-test in GraphPad Prism. P-value is not available when n = 1.*
[g] *ND, not determined.*

amount in the Δ*phoU2* mutant was detected in complementation experiments in which a wild-type copy of *phoU2*$^+$ was expressed from an ectopic site (**Table 1**, line 4).

We next determined that the increased transcription of the *pst1-phoU1* operon in the Δ*phoU2* mutant is mediated by the PnpRS TCS through increased phosphorylation of the PnpR∼P RR. Δ*pnpR,* Δ*pnpS*, or Δ*pnpRS* mutants showed slightly reduced *pst1-phoU1* operon transcript amounts compared to the parent strain, with no change in *pst2-phoU2* operon expression (**Table 1**, lines 5–7). Likewise, Δ*pnpR* Δ*phoU2*, Δ*pnpS* Δ*phoU2,* and Δ*pnpRS* Δ*phoU2* double mutants showed reduced *pst1-phoU1* operon relative transcript amounts (**Table 1**, lines 8–10), instead of the sizable increase observed for the Δ*phoU2* single mutant containing an active PnpRS TCS (**Table 1**, line 2). To confirm directly that PhoU2 acts as a negative regulator of PnpRS function under high P_i conditions, we performed Phos-tag SDS PAGE analysis to determine PnpR∼P RR phosphorylation levels (see Materials and Methods; **Figure 3**). In these experiments, we fused three tandem copies of the FLAG epitope tag to the C-terminus of the PnpR RR regulator expressed from its normal chromosomal locus (**Figure 3**, Table S1). The PnpR-L-FLAG^3 RR induced *pst1-phoU1* transcription to a similar extent as wild-type (untagged) PnpR$^+$ in a Δ*phoU2* mutant (data not shown). In the *phoU2*$^+$ strain, essentially no PnpR∼P (<1%) was detected in cells growing exponentially in high-P_i BHI broth (**Figure 3**). In contrast, the Δ*phoU2* mutant contained ≈45% PnpR∼P, which accounts for the high (≈16X) increase in *pst1-phoU1* transcript detected (**Table 1**, line 2). We conclude that PhoU2 negatively regulates PnpR∼P amounts and transcription of the *pst1-phoU1* operon, but does not regulate transcription of the *pnpRS* or *pst2-phoU2* operon, which are constitutively expressed.

Consistent with this interpretation, a putative PnpR∼P binding site (Pho-box) sequence (TTTACACAATCTTTACA; Martin, 2004) is located 92 bp upstream of *pstS1* reading frame gene (**Figure 1**), but no recognizable Pho-box sequences can be found upstream of the *pnpRS* or *pst2-phoU2* operon. Finally, we tested whether induction of *pst1-phoU1* operon expression contributes to the growth defect and antibiotic sensitivity of a Δ*phoU2* mutant (**Figure 2**). A Δ*phoU2* Δ*pst1* or Δ*phoU2* Δ*pst1-phoU1* double mutant showed the same decrease in growth yield (**Figure 4A**, Table S4) and antibiotic sensitivity (**Figure 4B**) as the Δ*phoU2* single mutant, indicating that these defects were caused primarily by misregulation of the Pst2 transporter in high P_i conditions, instead of induced expression of the Pst1 transporter.

Transcription of the *pst1* Operon is Further Induced by the Absence of the Pst2 Transporter Under High P_i Conditions

We next tested whether absence of the Pst2 transporter affects *pst1* operon expression in bacteria growing in high P_i-BHI broth. Surprisingly, relative transcript amounts from the *pst1* operon increased by ≈44 fold in the Δ*pst2 phoU2*$^+$, Δ*pst2-phoU2*, and Δ*pst2-phoU2* Δ*phoU1* mutant compared to the parent strain (**Table 1**, lines 12, 13, and 14). By contrast, *pst2* operon transcription is unchanged in a Δ*pst1 phoU1*$^+$ mutant compared to the parent (**Table 1**, line 15). The similar induction in the Δ*pst2 phoU2*$^+$ and Δ*pst2-phoU2* mutants (**Table 1**, lines 12 and 13) implies that negative regulation of the PnpRS TCS by PhoU2 depends on a functional Pst2 transporter system. Moreover, the similarity of *pst1* induction in the Δ*pst2-phoU2* Δ*phoU1* and other mutants implies that PhoU1 does not directly regulate *pst1* transcription. This conclusion was supported by the similar induction of *pst1* operon transcription

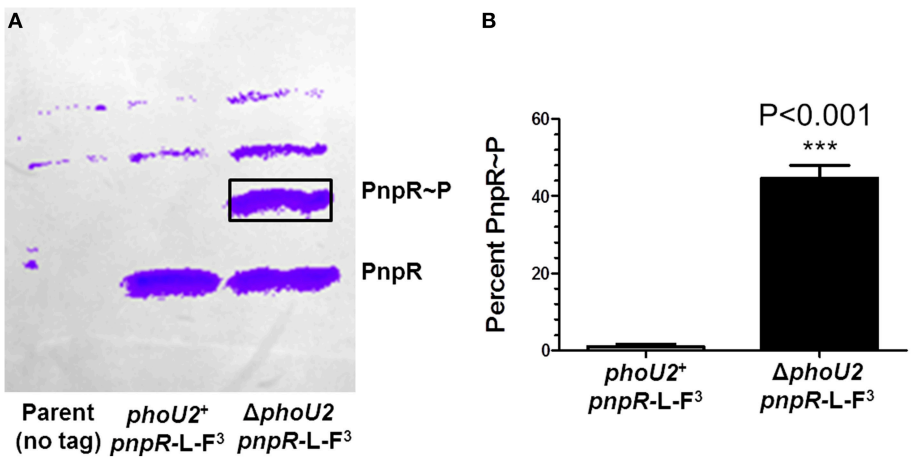

FIGURE 3 | Approximately 45% of PnpR is phosphorylated (PnpR∼P) in a Δ*phoU2* mutant. (A) Representative Phos-tag SDS-PAGE of the encapsulated parent strain not expressing a FLAG-tagged protein (IU1781, lane 1) and of the *pnpR*-L-FLAG^3 (IU6689, lane 2), and Δ*phoU2 pnpR*-L-FLAG^3 (IU6687, lane 3) mutants growing exponentially in BHI broth. The gel was Western blotted with anti-FLAG antibody as described in Materials and Methods. The top two bands in all lanes are nonspecific. The upper anti-FLAG-specific band corresponds to phosphorylated PnpR∼P, and the lower band corresponds to unphosphorylated PnpR. Control experiments show that the upper band is heat-sensitive, as expected for PnpR∼P (Figure S4). **(B)** Quantification of 3 independent Phos-tag SDS-PAGE experiments. Less than 1% of PnpR was phosphorylated in the *phoU2*$^+$ strain, whereas ≈45% of PnpR is phosphorylated (PnpR∼P) in the Δ*phoU2* mutant. *P*-value was determined by an unpaired *t*-test in GraphPad Prism; ***P < 0.001.

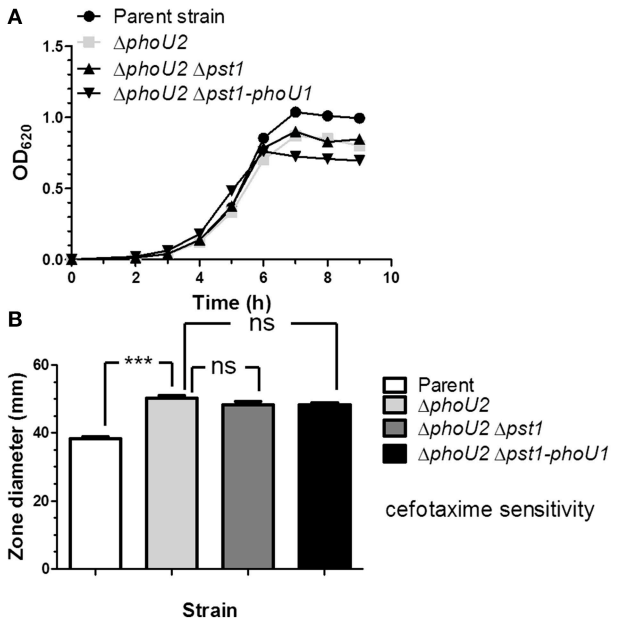

FIGURE 4 | Deletion of *pst1* or *pst1-phoU1* in a Δ*phoU2* mutant does not recover growth yield or antibiotic sensitivity. (A) Representative growth curves of encapsulated parent strain (IU1781), and Δ*phoU2* (IU6375), Δ*phoU2* Δ*pst1* (IU6664), and Δ*phoU2* Δ*pst1-phoU1* (IU6854) mutants in BHI broth. Growth yields and rates are quantitated in Table S4. **(B)** Cefotaxime sensitivity assays for encapsulated parent strain (IU1781), and Δ*phoU2* (IU6375), Δ*phoU2* Δ*pst1* (IU6664), and Δ*phoU2* Δ*pst1-phoU1* (IU6854) mutants. ($n \geq 3$); ***P < 0.001. See Materials and Methods, the legend to **Figure 2**, and the text for additional details.

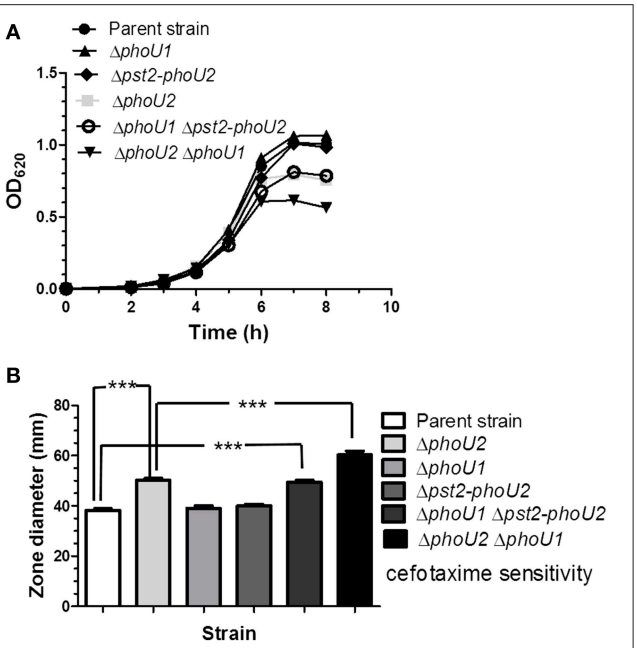

FIGURE 5 | A Δ*phoU1* Δ*pst2-phoU2* double mutant phenocopies a Δ*phoU2* single mutant for decreased growth yield and increased cefotaxime sensitivity, which are even greater in a Δ*phoU1* Δ*phoU2* double mutant. (A) Representative growth curves of encapsulated parent strain (IU1781) and Δ*phoU2* (IU6375), Δ*phoU1* (IU6377), Δ*pst2-phoU2* (IU6550), Δ*phoU1* Δ*pst2-phoU2* (IU6612), and Δ*phoU2* Δ*phoU1* (IU6499) mutants in BHI broth. ($n \geq 3$) Growth yields and rates are quantitated in Table S4. **(B)** Cefotaxime sensitivity assays for encapsulated parent strain (IU1781) and Δ*phoU2* (IU6375), Δ*phoU1* (IU6377), Δ*pst2-phoU2* (IU6550), Δ*phoU1* Δ*pst2-phoU2* (IU6612), and Δ*phoU2* Δ*phoU1* (IU6499) mutants. ($n \geq 3$); ***$P < 0.001$. See Materials and Methods, the legend to **Figure 2**, and the text for additional details.

in the Δ*phoU2 phoU1*$^+$ and Δ*phoU2* Δ*phoU1* mutants (**Table 1**, lines 2 and 11). Instead, the growth characteristics of these mutants imply that PhoU1 negatively regulates the activity of the Pst1 transporter, in parallel to the negative regulation of the activity of Pst2 by PhoU2 (**Figure 5A**, Table S4). In BHI broth, the parent, Δ*phoU1*, and Δ*pst2-phoU2* mutant show similar growth and antibiotic sensitivity (**Figure 5**; Table S4). In contrast, the Δ*phoU2* and Δ*phoU1* Δ*pst2-phoU2* mutants showed reduced growth yield and increased antibiotic sensitivity (**Figure 5**, Table S4), consistent with increased P_i accumulation caused by misregulation of the Pst2 and Pst1 transporters, respectively. This interpretation was further supported by the reduced growth rate and yield and increased antibiotic sensitivity of the Δ*phoU2* Δ*phoU1* mutant compared to the Δ*phoU2* and Δ*pst2-phoU2* Δ*phoU1* mutants (**Figure 5**; Table S4).

Either the Pst1 or Pst2 Transporter is Required in the Encapsulated, But Not in the Unencapsulated, D39 Strain

E. coli encodes an alternate low-affinity P_i uptake (Pit) system that functions in the absence of the high-affinity Pst transporter in high P_i conditions (Wanner, 1996; Harris et al., 2001; Hsieh and Wanner, 2010). However, we were unable to construct Δ*pst2* Δ*pst1* mutants in the encapsulated strain of D39 (**Table 2**, top two sections), where the Δ*nptA* amplicon was used as a positive control in the transformations. Likewise, we were unable to construct a Δ*pst2* Δ*pnpRS* double mutant, where induction of the Pst1 transporter was negated by the absence of the PnpRS TCS (**Table 1**, top section; **Figure 1**). As expected, the *cps*$^+$ Δ*pnpRS-pst1* mutant could be constructed (IU6133), where the Pst2 transporter is functional.

In all Δ*pst2* Δ*pst1* *cps*$^+$ transformations, several colonies (<10) appeared upon prolonged incubation (**Table 2**, top two sections). These suppressor colonies had a rougher appearance than the smooth colonies of D39 *cps*$^+$ strains (data not shown), suggesting that capsule production was lost or reduced in these Δ*pst2* Δ*pst1* transformants. The Quellung test for serotype 2 capsule (see Materials and Methods) confirmed that a suppressor strain (IU6413) had lost its capsule (data not shown). This result suggested that unlike in *cps*$^+$ strains, we would be able to construct Δ*cps* Δ*pst1* Δ*pst2* mutants in the D39 genetic background. This hypothesis was confirmed by transformation experiments (**Table 2**, bottom two sections), and growth experiments showing that Δ*cps* Δ*pst1* Δ*pst2* triple mutants grew comparably to the Δ*cps* single mutant in BHI broth (Figure S5). Thus, we conclude that either the Pst1 or Pst2 P_i transporter must be functional in encapsulated D39 strains and that the Δ*pst1* Δ*pst2* *cps*$^+$ double mutant is not viable.

TABLE 2 | The Δ*pst1* Δ*pst2* double mutant cannot be constructed in encapsulated strain D39[a].

Recipient strain[b]	Amplicon[c]	Number of colonies on transformation plates after ≈20 h[d]
Δ*pst2 cps*$^+$ (encapsulated)	Δ*nptA* (control)	100–150 ($n = 3$)
	Δ*pnpRS*	0–10 ($n = 3$)
	Δ*pst1*	0–4 ($n = 3$)
	Δ*pst1-phoU1*	0 ($n = 3$)
	No DNA (control)	0 ($n = 3$)
Δ*pst1 cps*$^+$ (encapsulated)	Δ*nptA* (control)	100–150 ($n = 3$)
	Δ*pst2*	0 ($n = 3$)
	Δ*pst2-phoU2*	0 ($n = 3$)
	No DNA (control)	0 ($n = 3$)
Δ*pst2 cps* mutants (unencapsulated)	Δ*nptA* (control)	100–150 ($n = 3$)
	Δ*pnpRS*	250–300 ($n = 3$)
	Δ*pst1*	100–150 ($n = 3$)
	Δ*pst1-phoU1*	250–300 ($n = 3$)
	No DNA (control)	0 ($n = 3$)
Δ*pst1 cps* mutants (unencapsulated)	Δ*nptA* (control)	100–150 ($n = 3$)
	Δ*pst2*	100–150 ($n = 3$)
	Δ*pst2-phoU2*	150–200 ($n = 3$)
	No DNA (control)	0 ($n = 3$)

[a] *Transformations were performed as described in Materials and Methods.*
[b] *Transformations were performed into multiple cps$^+$ strains [IU1690 (D39); IU1781 (D39 rpsL1)] and cps mutants [IU1824 (D39 Δcps rpsL1); IU1945 (D39 Δcps); IU3309 (D39 Δcps2E rpsL1)] with similar results. D39 Δcps2E rpsL1 Δpst1 Δpst2 mutants could not be repaired back to cps$^+$ (data not shown).*
[c] *Amplicons were synthesized as described in Materials and Methods (see Table S2). Amplicons used for transformations contained the P_c-kanrpsL$^+$ or P_c-erm antibiotic cassette for selection. Transformations with the ΔnptA amplicon or without DNA were the positive or negative control, respectively.*
[d] *≤10 colonies on plates indicates accumulation of unencapsulated suppressor mutants (see text).*

NptA is the Third P_i Uptake System That Functions in Δ*cps* Δ*pst1* Δ*pst2* Mutants

Normal growth of the Δ*cps* Δ*pst1* Δ*pst2* mutant in high P_i medium (**Figure 5**) implies that sufficient P_i is being taken up by a third uptake system. BLAST searches did not reveal a close pneumococcal homolog of the Pit symporters of *E. coli* and *B. subtilis*. During these searches, we found another candidate gene, *spd_0443*, which encodes a putative Na^+/P_i-cotransporter II-like protein. Spd_0443 homologs have been shown to act as P_i transporters in mammalian intestines and kidneys (Katai et al., 1999) and in certain bacterial species, such as *V. cholerae* and *Vibrio vulnificus* (Lebens et al., 2002; Staley and Harwood, 2014). Consistent with a role in P_i uptake, we could not delete *spd_0443* in a Δ*cps* Δ*pst1* Δ*pst2* mutant in high P_i medium (**Table 3**), but we could delete *spd_0443* in the Δ*pst1* or Δ*pst2* single mutant (**Table 2**). Thus, the Spd_0443 Na^+/P_i-cotransporter likely acts as a third Pi uptake system in *S. pneumoniae*. Because the iron transporter in *S. pneumoniae* is already named "Pit," we renamed Spd_0443 as NptA (Na^+-dependent phosphate transporter A), similar to *Vibrio* species (Lebens et al., 2002).

TABLE 3 | NptA (Na^+/Pi co-transporter) is a third P_i uptake system.

Recipient strain[a]	Amplicon[b]	Number of colonies on transformation plates after ≈20 h
Δ*pst1 cps*	Δ*pnpR* (control)	150–200 ($n = 3$)
	Δ*nptA*	100–150 ($n = 3$)
	No DNA (control)	0 ($n = 3$)
Δ*pst2 cps*	Δ*pnpR* (control)	150–200 ($n = 3$)
	Δ*nptA*	100–150 ($n = 3$)
	No DNA (control)	0 ($n = 3$)
Δ*pst1* Δ*pst2 cps*	Δ*pnpR* (control)	150–200 ($n = 3$)
	Δ*nptA*	0 ($n = 3$)
	No DNA (control)	0 ($n = 3$)

[a] *Transformations were performed as described in Materials and Methods. Transformations were performed into two cps mutants [IU1824 (D39 Δcps rpsL1); IU3309 (D39 Δcps2E rpsL1)] with similar results.*
[b] *Amplicons were synthesized as described in Materials and Methods (see Table S2). Amplicons used for transformations contained the P_c-kanrpsL$^+$ or P_c-erm antibiotic cassette for selection. Transformations with the ΔpnpR amplicon or without DNA were the positive and negative control, respectively.*

Δ*pst1-phoU1* or Δ*pst2-phoU2* Deletion Has No Effect on Growth Under Low P_i Conditions

We next examined the roles of the Pst1 and Pst2 transporters and their regulators (**Figure 1**) under low P_i culture conditions. A previous study used the semi-defined C+Y medium as a low P_i condition (Novak et al., 1999). However, encapsulated strains grew in C+Y broth without P_i addition (Figure S6), and direct chemical assay (see Materials and Methods; Katewa and Katyare, 2003) showed that C+Y broth (with no added P_i) contains ≈1.5 mM P_i (Figure S7). Therefore, a modified chemically defined medium (mCDM) was used to study low P_i culture conditions (see Materials and Methods; Carvalho et al., 2013). The growth yield of the wild-type encapsulated strain was dependent on P_i concentration below 1 mM P_i, with growth detectable down to ≈10 μM and no growth without P_i addition (**Figure 6A**). Growth rates and yields of the Δ*pst2-phoU2* and Δ*pst1-phoU1* mutants were similar to those of the parent strain (**Figures 6B,C**), implying that a functional Pst1 or Pst2 transporter is sufficient for optimal growth under low P_i conditions.

We used unencapsulated (Δ*cps*) mutants to determine the effects of P_i concentration when both the Pst1 and Pst2 transporters were absent. Similar to the encapsulated strains (**Figure 6**), growth yield of the parent, Δ*pst1-phoU1*, and Δ*pst2-*Δ*phoU2* single mutants decreased below 1 mM P_i and was still detectable at 10 μM P_i (**Figures 7A–C**). By contrast, the growth of the Δ*pst2-phoU2* Δ*pst1-phoU1* double mutant was not fully supported even by 2 mM P_i, and growth yield showed apparent autolysis in 1 mM P_i and no growth with ≥100 μM P_i (**Figure 7D**). We conclude that in low P_i conditions, the NptA transporter alone is not sufficient for growth of D39-derived *S. pneumoniae*, consistent with NptA acting as a low-affinity P_i transporter compared to Pst1 or Pst2.

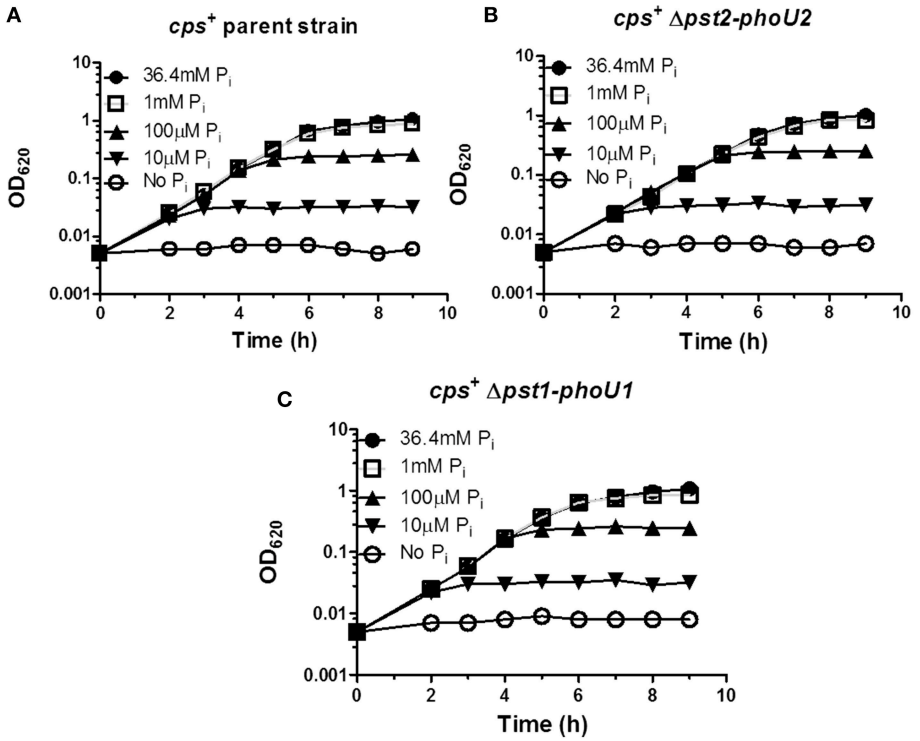

FIGURE 6 | Deletion of the *pst1-phoU1* or *pst2-phoU2* operon does not affect growth under low P_i conditions in mCDM media. (A) Representative growth curves of encapsulated parent strain (IU1781) in mCDM with 36.4, 1 mM, 100, 10 μM, and no P_i. **(B)** Representative growth curves of a Δ*pst2-phoU2* mutant (IU6550) in mCDM with 36.4, 1 mM, 100, 10 μM, and no P_i. **(C)** Representative growth curves of a Δ*pst1-phoU1* mutant (IU6830) in mCDM with 36.4, 1 mM, 100, 10 μM, and no P_i. mCDM with different concentrations of P_i was prepared as described in Materials and Methods. Growth curves were determined at least 3X independently.

Low P_i Induces *pst1* Operon Transcript Amount >100X via Phosphorylation of the PnpR∼P RR

We determined the effect of low P_i concentration on *pst1* operon expression in the encapsulated D39 strain. Strains were grown in high-P_i (36.4 mM) mCDM, washed, and resuspended in mCDM containing high (36.4 mM) or low (10 μM) P_i (see Materials and Methods). After 30 min, samples were taken for qRT-PCR using 16S rRNA as the normalization standard (see Materials and Methods). In all strains tested, P_i limitation to 10 μM induced relative *pst1* transcript amount by >100X compared to the wild-type parent strain in high (36.4 mM) P_i (**Table 4**). Similar to strains grown in BHI (**Table 1**), Δ*phoU2* and Δ*phoU2* Δ*phoU1* mutants showed ≈25X induction of *pst1* operon transcript amount when grown in mCDM containing high P_i (**Table 4**), whereas a Δ*phoU1* mutant showed no increase (**Table 4**). In these mutants, reduction of P_i concentration to 10 μM induced *pst1* transcript amounts by an additional ≈5–100X (**Table 4**). P_i limitation of a Δ*pnpRS* TCS mutant showed no increase in relative *pst1* operon transcript amounts (data not shown), indicating a dependence on the PnpRS TCS for induction of *pst1* operon transcription in low P_i media. This conclusion was confirmed by Phos-tag SDS PAGE, which showed that phosphorylation of the PnpR RR (PnpR∼P) went from <1% in mCDM containing 36.4 mM P_i to ≈80% following a shift to mCDM lacking P_i for 40 min (Figure S8A). We conclude that transcription of pneumococcal *pst1* transporter operon is strongly induced by the PnpR∼P RR in low P_i conditions.

Deletion of *pst1-phoU1* and *pst2-phoU2* Reduces the Rate of P_i Uptake by ≈50% in an Unencapsulated Strain

Previously, the relative rate of P_i uptake was reported to be reduced by ≈30% in a Δ*pstB1* mutant of laboratory strain R6x grown in C+Y medium (no added P_i) (Novak et al., 1999), which turns out to contain a relatively high (1.5 mM) P_i content (above; Figure S7). To the contrary, $^{32}P_i$ uptake experiments in encapsulated and unencapsulated D39 mutants lacking the Pst1 (Δ*pst1-phoU1*) or Pst2 (Δ*pst2-phoU2*) transporter showed linear rates of $^{32}P_i$ uptake for at least 10 min that were similar to those of the wild-type parent strains in mCDM containing 1 mM total P_i (**Figures 8A,B**, Table S7). R6x is a derivative of R6 (Tiraby and Fox, 1973), which is an unencapsulated derivative of D39 (Lanie et al., 2007). The difference between this and the previous result (Novak et al., 1999) may partly reflect the large number of mutations in the R6 laboratory strain compared to the D39 strain progenitor genetic background (Lanie et al., 2007). In contrast to the single mutants, the unencapsulated Δ*pst1-phoU1* Δ*pst2-phoU2* double mutant showed a significant drop (≈50%) in the rate of P_i uptake compared to the wild-type parent strain or

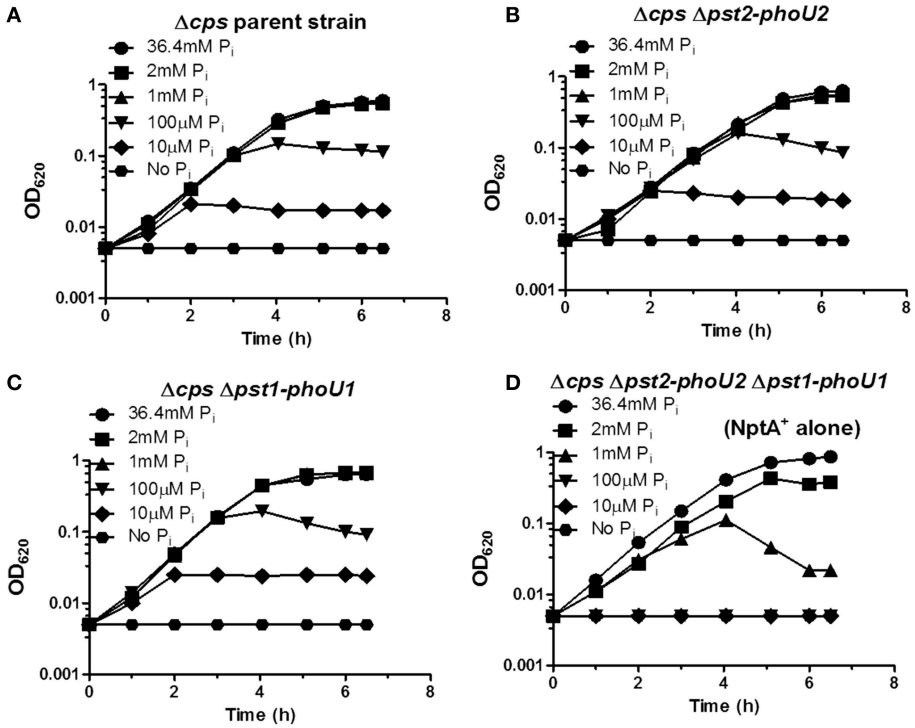

FIGURE 7 | The NptA Na^+/P_i co-transporter alone cannot provide sufficient P_i for long-term growth in mCDM containing moderately high (1 mM) and lower P_i concentrations. (A) Representative growth curves of unencapsulated parent strain Δ*cps* (IU1945) in mCDM with 36.4, 2, 1 mM, 100, 10 μM, and no P_i. **(B)** Representative growth curves of unencapsulated Δ*cps* Δ*pst2-phoU2* mutant (K583) in mCDM with 36.4, 2, 1 mM, 100, 10 μM, and no P_i. **(C)** Representative growth curves of unencapsulated Δ*cps* Δ*pst1-phoU1* mutant (E595) in mCDM with 36.4, 2, 1 mM, 100, 10 μM, and no P_i. **(D)** Representative growth curves of unencapsulated Δ*cps* Δ*pst2-phoU2* Δ*pst1-phoU1* mutant (IU5774), which only contains the NptA Na^+/P_i transporter, in mCDM with 36.4, 2, 1 mM, 100, 10 μM, and no P_i. Growth curves were determined at least 3X independently.

the single mutants in mCDM containing 1 mM P_i (**Figure 8B**, Table S7) or in C+Y broth (data not shown). This result implicates both the Pst1 and Pst2 transporters in P_i uptake in *S. pneumoniae* D39.

P_i Uptake is Reduced in a Δ*pst1-phoU1* Mutant Limited for Total P_i

To determine P_i uptake under low P_i conditions, we incubated encapsulated parent, Δ*pst1-phoU1*, or Δ*pst2-phoU2* mutants in mCDM lacking P_i for 1 h, and then added $^{32}P_i$ (total $[P_i]$ = 200 μM), and sampled P_i uptake with time (**Figure 8C**). Unlike the constant rate of ^{32}P uptake observed at 1 mM total P_i (**Figures 8A,B**), P_i uptake leveled off after about 5 min in 200 μM P_i (**Figure 8C**). The initial rate of P_i uptake by the encapsulated parent strain was markedly greater (≈8X) in 200 μM P_i than in 1 mM P_i (**Figures 8A,C**, Tables S7, S8). The initial rate of P_i uptake was comparable for the parent strain and the Δ*pst2-phoU2* mutant (**Figure 8C**, Table S8). In contrast, the initial rate of P_i uptake was reduced by ≈2X in the Δ*pst1-phoU1* mutant compared to the parent or Δ*pst2-phoU2* mutant (**Figure 8C**, Table S8). These results support a primary role for the Pst1 transporter in low-P_i conditions.

DISCUSSION

In this paper we demonstrate for the first time that regulation of the two evolutionarily distinct Pst P_i transport systems is linked in several ways in the human commensal and pathogen, *S. pneumoniae*. Niches encountered by pneumococcus in human hosts contain different P_i concentrations, including nasal fluid (≈5 mM), saliva (≈1 mM), and serum (≈1 mM) (Bansal, 1990; Wilson, 2005, 2008). Several aspects of this regulatory network are unusual, compared to the usual negative regulation of P_i uptake even at moderate P_i concentrations in other bacterial species (**Figure 1**; Hulett, 1993; Hsieh and Wanner, 2010; Botella et al., 2011). The *pst1-phoU1* and *pst2-phoU2* operons are completely separated in the pneumococcal chromosome, and although upstream of the *pst1-phoU1* operon, the *pnpRS* operon, which encodes the PnpRS TCS, is independently expressed and not autoregulated (**Table 1**, **Figure 1**). Deletion of gene *spd_1614*, which encodes a third putative PhoU-like protein, did not lead to growth phenotypes and was not studied further (data not shown).

Expression of the Pst2 transporter is constitutive under the conditions tested here, including media containing high P_i concentrations (**Table 1**, Table S6, and Figure S3). However, Pst2 uptake of P_i is likely negatively regulated by the PhoU2 protein, whose absence causes a drop in growth yield and

TABLE 4 | Relative transcript amounts of the *pst1* operon in different mutants in mCDM containing high and low P_i concentrations[a].

Strains[b]	P_i concentration in mCDM	Relative transcript amount of *pstS1* operon[c]
Parent strain (IU1781)	36.4 mM	≡1
	10 μM	209.7 ± 37.9 ($n = 6$) (***)[d]
Δ*phoU2* (IU6375)	36.4 mM	24.1 ± 3.9 ($n = 3$) (***)
	10 μM	201.6 ± 47.6 ($n = 3$) (***)
Δ*phoU1* (IU6377)	36.4 mM	1.4 ± 0.1 ($n = 3$) (ns)
	10 μM	145.4 ± 25.3 ($n = 4$) (***)
Δ*phoU2* Δ*phoU1* (IU6499)	36.4 mM	28.3 ± 0.5 ($n = 3$) (***)
	10 μM	136.3 ± 12.6 ($n = 3$) (***)

[a] *RNA preparation and qRT-PCR from strains in mCDM containing high and low P_i concentrations were performed as described in Materials and Methods.*
[b] *Strains were markerless deletion mutants derived from encapsulated parent strain IU1781 (see Table S1).*
[c] *Relative pstS1 gene transcript amount was used to represent pst1 operon expression.*
[d] *$^{***}P < 0.001$; ns, not significant. P-values were calculated by an unpaired t-test in GraphPad Prism.*

increased antibiotic sensitivity in mutants growing in high P_i medium (Tables S4, S5, **Figures 1**, **2**, and Figure S3). In addition, PhoU2 negatively regulates the transcription activation of the *pst1-phoU1* operon by the phosphorylated PnpR∼P RR, such that a Δ*phoU2* deletion mutation leads to a substantial increase in *pst1-phoU1* transcript amounts (**Table 1**, **Figures 1**, **3**, and Figure S4). The PhoU1 protein, which shares only 34% amino acid identities with PhoU2, does not play a reciprocal role in negatively regulating *pst1-phoU1* transcription (**Table 1**, lines 3, 11, and 14), but PhoU1 likely negatively regulates P_i uptake by the Pst1, but not the Pst2, P_i transporter (**Figures 1**, **4**, **5**). Thus, the PhoU2 protein can regulate both PnpR phosphorylation level and Pst2 transporter function, similar to the PhoU homolog in *E. coli* (Hsieh and Wanner, 2010; Gardner et al., 2014, 2015). In contrast, PhoU1 function is restricted to regulating transporter but not TCS function, similar to the PhoU in *C. crescentus* (Lubin et al., 2016). *E. coli* PhoU interacts with the PAS domain of the PhoR HK (Gardner et al., 2014, 2015). However, the pneumococcal PnpS HK lacks a recognizable PAS domain, and it remains to be determined whether PhoU2 regulation of PnpR∼P levels is through direct interactions with the PnpS HK. Likewise, it is unknown whether PhoU2 interacts with the PstB1 subunit of the Pst1 transporter to exert control over *pst1-phoU1* operon transcription, by analogy to control in *E. coli* (Gardner et al., 2014, 2015). Interactions of PhoU1 or PhoU2 with subunits of the Pst1 or Pst2 transporters also remain to be determined.

The requirement of a functional Pst1 or Pst2 for growth of the encapsulated serotype 2 strain provides a biological rationale for the constitutive expression and function of the Pst2 transporter at high P_i concentrations (**Table 2**) and why *S. pneumoniae* maintains dual P_i uptake systems. Capsule is one of the most important factors required for pneumococcal colonization, carriage, and virulence in its human host (Briles et al., 1992; Morona et al., 2004, 2006; Bentley et al., 2006; Hyams et al., 2010). Expression of the Pst1 transporter is strongly induced by low P_i conditions (**Table 4**), and lack of PhoU1 does not change *pst1-phoU1* operon expression in high P_i media (**Tables 2, 4**). These results, and a reduced rate of P_i uptake by mutants lacking Pst1 (**Figure 8C**, Table S8) indicate that Pst1 functions mainly at low P_i concentrations. However, encapsulated *S. pneumoniae* strains require high-affinity P_i transport even in high-P_i media (**Table 2**), and this P_i uptake cannot be provided by the low-affinity NptA Na^+/P_i cotransporter that replaces Pst1 and Pst2 in unencapsulated strains (**Figure 8B**, Table S7). The reason underlying this link between Pst-mediated P_i transport and the maintenance of capsule is not currently clear. A recent report suggests that low P_i conditions induce capsule biosynthesis in *M. tuberculosis* (van de Weerd et al., 2016). Overexpression of capsule could alter the metabolism of *S. pneumoniae* thereby inhibiting the growth of *cps*$^+$ Δ*pst1* Δ*pst2* mutants and leading to the appearance of spontaneous *cps* mutants (**Table 2**). However, starvation of the wild-type D39 *cps*$^+$ strain for P_i for 1 h did not reveal a qualitative change in capsule amount in the Quellung reaction (data not shown). Moreover, pneumococcal capsule biosynthesis is positively regulated by phosphorylation of regulatory protein CpsD (Yother, 2011), and this protein phosphorylation would likely be reduced during P_i limitation.

The regulatory pathways that mediate capsule induction in *M. tuberculosis* involve sigma factors and poly-P_i kinases (van de Weerd et al., 2016) that are absent from *S. pneumoniae.* As mentioned in the Introduction, Δ*phoU* mutants of other bacteria accumulate poly-P_i (Morohoshi et al., 2002; Hirota et al., 2013; Wang et al., 2013; de Almeida et al., 2015; Lubin et al., 2016), possibly because high intracellular Pi concentration disrupt metabolic homeostasis leading to defects in growth accompanied by general antibiotic sensitivity. RNA-Seq results reported here indicate that the pneumococcal Pho regulon contains a limited number of recognizable genes involved in P_i accumulation (Table S6). Notably, *S. pneumoniae* serotype 2 strain D39 as well as some other serotype strains, such as TIGR4, lack recognizable homologs of poly-P_i kinases Ppk1 and Ppk2 (Zhang et al., 2002) and Mg^{2+}-dependent poly-P_i exopolyphosphatase Ppx (Akiyama et al., 1993), but do encode a degradative Mn^{2+}-dependent, inorganic pyrophosphatase (PpaC) (Lanie et al., 2007); therefore, it is unclear whether these *S. pneumoniae* strains produces poly-P_i. DAPI staining experiments that revealed poly-P_i accumulation in *C. crescentus* Δ*phoU* mutants (Lubin et al., 2016) were inconclusive and did not indicate any differences in staining of the *phoU2*$^+$ parent and Δ*phoU2* mutant in high-P_i BHI broth (data not shown). Similarly, DAPI-based assays of extracts did not show any difference between the parent and Δ*phoU2* mutant indicative of different poly-Pi amounts (data not shown).

Taken together, our results suggest that *S. pneumoniae* may maintain the regulated Pst1 and constitutive Pst2 P_i transport systems as a failsafe to ensure capsule biosynthesis is maintained during variations in P_i conditions. Coordination between the two Pst P_i transport systems is coordinated by the PhoU2 protein that modulates transcription of the *pst1-phoU1* operon by the PnpRS TCS and separately regulates the function of

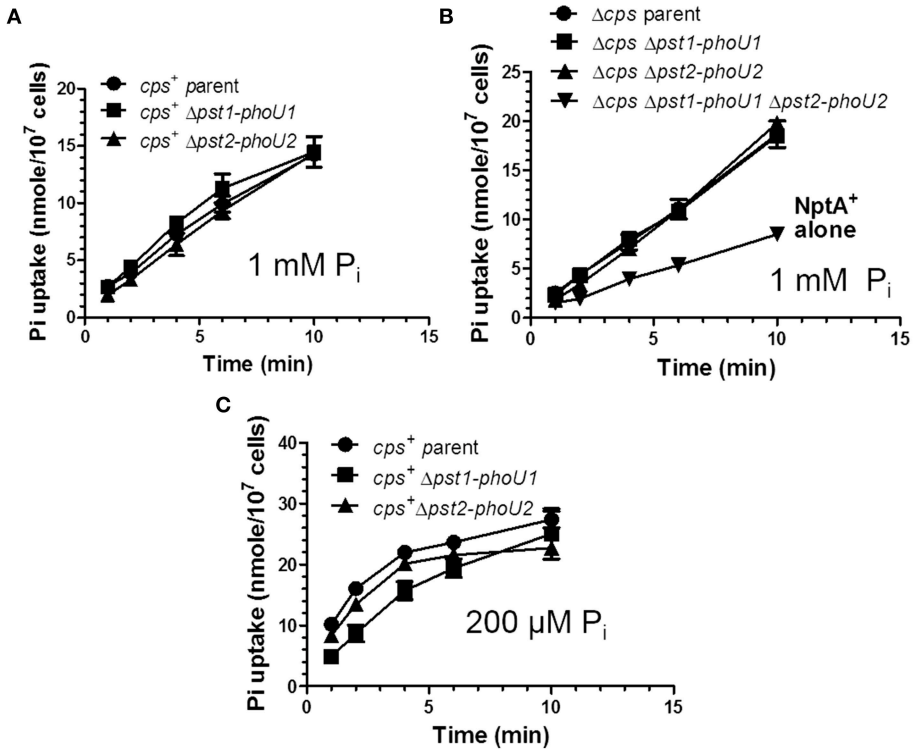

FIGURE 8 | The Pst1 or Pst2 transporter is sufficient for P_i uptake under moderately high P_i conditions (1 mM), but the Pst1 transporter is required for optimal P_i uptake under low P_i conditions (200 μM) following P_i limitation. (A) P_i uptake assays of encapsulated parent strain (IU1781) and Δ*pst2-phoU2* (IU6550) and Δ*pst1-phoU1* (IU6830) mutants in 1 mM total $^{32}P_i$ in mCDM ($n = 3$). P_i uptake was determined as the initial rate of $^{32}P_i$ incorporation into cells in mCDM in pulse-labeling experiments described in Materials and Methods. See Tables S7 for initial rates of P_i uptake ($n = 3$). **(B)** P_i uptake assays of unencapsulated parent strain Δ*cps* (IU1945) and Δ*cps* Δ*pst2-phoU2* (K583), Δ*cps* Δ*pst1-phoU1* (E595), and Δ*cps* Δ*pst1-phoU1* Δ*pst2-phoU2* (IU5774) mutants in 1 mM P_i mCDM. See Tables S7 for initial rates of P_i uptake ($n = 3$). **(C)** P_i uptake assay of encapsulated parent strain (IU1781) and Δ*pst2-phoU2* (IU6550) and Δ*pst1-phoU1* (IU6830) mutants in 200 μM total P_i mCDM following P_i starvation for 1 h as described in Materials and Methods ($n = 3$). Initial rates of Pi uptake were determined with the first min of labeling and are listed in Table S8 ($n = 3$).

the Pst2 transporter. Most bacteria encode a single Pst-type P_i transporter as part of a Pho regulon that encode numerous phosphate accumulation and sparing proteins (Hulett, 1993; Wanner, 1996; Hsieh and Wanner, 2010). The limited Pho regulon of *S. pneumoniae* may reflect restriction to the human host, where P_i is the primary source of phosphorus (Wilson, 2008). Even among the *Streptococcus*, dual Pst systems are limited to only a few species, including *S. pneumoniae, S. pseudopneumoniae*, *S. dysgalactiae, S. equi* (Group C), *S. porcinus, S. agalactiae* (Group B), and *S. equinus*, and are absent from the major Viridans and A Groups. Outside of the *Streptococcus*, multiple Pst P_i transporters have only been reported in a very limited number of bacteria, including *Synechocystis sp.* PCC 6803 and *M. tuberculosis* (Braibant et al., 1996; Suzuki et al., 2004; Burut-Archanai et al., 2011; Tischler et al., 2013). In *Synechocystis*, low P_i conditions activate expression of both of the Pst P_i transporters that are present (Suzuki et al., 2004), whereas in *M. tuberculosis one* Pst transporter is activated by low P_i and at least one other Pst transporter seems to be constitutively expressed, like Pst2 in *S. pneumoniae* (Tischler et al., 2013).

AUTHOR CONTRIBUTIONS

JZ, DS, KW, MW contributed to the conception and design of the work; JZ, DS carried out acquisition and analysis of data; JZ, DS, KW, MW interpreted data for the work; JZ, MW drafted and wrote the final version of the paper; JZ, DS, KW, MW approved the final version to be published.

ACKNOWLEDGMENTS

We thank Kevin Bruce, Tiffany Tsui, and other laboratory members for methods and critical discussions of this work, and James Ford, Kurt Zimmer, and Doug Rusch for assistance with Illumina DNA sequencing and RNA-Seq analyses. This work was supported by grants R21AI095814 and R01GM114315 (to MW).

SUPPLEMENTARY MATERIAL

The Supplementary Material for this article can be found online at: http://journal.frontiersin.org/article/10.3389/fcimb.2016.00063

REFERENCES

Akiyama, M., Crooke, E., and Kornberg, A. (1993). An exopolyphosphatase of *Escherichia coli*. *J. Biol. Chem.* 268:633–639.

Bansal, V. K. (1990). "Serum Inorganic Phosphorus," in *Clinical Methods: The History, Physical, and Laboratory Examinations*, eds H. K. Walker, W. D. Hall, and J. W. Hurst (Boston, MA: Butterworths Butterworth Publishers, a division of Reed Publishing), 895–899.

Beard, S. J., Hashim, R., Wu, G., Binet, M. R., Hughes, M. N., and Poole, R. K. (2000). Evidence for the transport of zinc(II) ions via the Pit inorganic phosphate transport system in *Escherichia coli*. *FEMS Microbiol. Lett.* 184, 231–235. doi: 10.1111/j.1574-6968.2000.tb09019.x

Benjamini, Y., and Hochberg, Y. (1995). Controlling the false discovery rate - a practical and powerful approach to multiple testing. *J. Roy. Stat. Soc. B. Met.* 57, 289–300.

Bentley, S. D., Aanensen, D. M., Mavroidi, A., Saunders, D., Rabbinowitsch, E., Collins, M., et al. (2006). Genetic analysis of the capsular biosynthetic locus from all 90 pneumococcal serotypes. *PLoS Genet.* 2:e31. doi: 10.1371/journal.pgen.0020031

Botella, E., Devine, S. K., Hubner, S., Salzberg, L. I., Gale, R. T., Brown, E. D., et al. (2014). PhoR autokinase activity is controlled by an intermediate in wall teichoic acid metabolism that is sensed by the intracellular PAS domain during the PhoPR-mediated phosphate limitation response of *Bacillus subtilis*. *Mol. Microbiol.* 94, 1242–1259. doi: 10.1111/mmi.12833

Botella, E., Hübner, S., Hokamp, K., Hansen, A., Bisicchia, P., Noone, D., et al. (2011). Cell envelope gene expression in phosphate-limited *Bacillus subtilis* cells. *Microbiology* 157, 2470–2484. doi: 10.1099/mic.0.049205-0

Braibant, M., Lefèvre, P., de Wit, L., Ooms, J., Peirs, P., Huygen, K., et al. (1996). Identification of a second *Mycobacterium tuberculosis* gene cluster encoding proteins of an ABC phosphate transporter. *FEBS Lett.* 394, 206–212. doi: 10.1016/0014-5793(96)00953-2

Briles, D. E., Crain, M. J., Gray, B. M., Forman, C., and Yother, J. (1992). Strong association between capsular type and virulence for mice among human isolates of *Streptococcus pneumoniae*. *Infect. Immun.* 60, 111–116.

Burut-Archanai, S., Eaton-Rye, J. J., and Incharoensakdi, A. (2011). Na^+-stimulated phosphate uptake system in *Synechocystis* sp. PCC 6803 with Pst1 as a main transporter. *BMC Microbiol.* 11:225. doi: 10.1186/1471-2180-11-225

Carvalho, S. M., Kuipers, O. P., and Neves, A. R. (2013). Environmental and nutritional factors that affect growth and metabolism of the pneumococcal serotype 2 strain D39 and its nonencapsulated derivative strain R6. *PLoS ONE* 8:e58492. doi: 10.1371/journal.pone.0058492

Chao, Y., Marks, L. R., Pettigrew, M. M., and Hakansson, A. P. (2014). *Streptococcus pneumoniae* biofilm formation and dispersion during colonization and disease. *Front. Cell. Infect. Microbiol.* 4:194. doi: 10.3389/fcimb.2014.00194

Chekabab, S. M., Harel, J., and Dozois, C. M. (2014a). Interplay between genetic regulation of phosphate homeostasis and bacterial virulence. *Virulence* 5, 786–793. doi: 10.4161/viru.29307

Chekabab, S. M., Jubelin, G., Dozois, C. M., and Harel, J. (2014b). PhoB activates *Escherichia coli* O157:H7 virulence factors in response to inorganic phosphate limitation. *PLoS ONE* 9:e94285. doi: 10.1371/journal.pone.0094285

Cheng, C., Wakefield, M. J., Yang, J., Tauschek, M., and Robins-Browne, R. M. (2012). Genome-wide analysis of the Pho regulon in a *pstCA* mutant of *Citrobacter rodentium*. *PLoS ONE* 7:e50682. doi: 10.1371/journal.pone.0050682

de Almeida, L. G., Ortiz, J. H., Schneider, R. P., and Spira, B. (2015). *phoU* inactivation in *Pseudomonas aeruginosa* enhances accumulation of ppGpp and polyphosphate. *Appl. Environ. Microbiol.* 81, 3006–3015. doi: 10.1128/AEM.04168-14

Donkor, E. S. (2013). Understanding the pneumococcus: transmission and evolution. *Front. Cell. Infect. Microbiol.* 3:7. doi: 10.3389/fcimb.2013.00007

Engel, H., Mika, M., Denapaite, D., Hakenbeck, R., Mühlemann, K., Heller, M., et al. (2014). A low-affinity penicillin-binding protein 2x variant is required for heteroresistance in *Streptococcus pneumoniae*. *Antimicrob. Agents Chemother.* 58, 3934–3941. doi: 10.1128/AAC.02547-14

Ferreira, D. M., and Gordon, S. B. (2015). "Mechanisms Causing the Inflammatory Response to *Streptococcus pneumoniae*," in *Streptococcus pneumoniae Molecular Mechanisms of Host-Pathogen Interactions*, eds J. M. Brown, S. Hammerschmidt, and C. Orihuela (London: Academic Press), 383–400.

Gardner, S. G., Johns, K. D., Tanner, R., and McCleary, W. R. (2014). The PhoU protein from *Escherichia coli* interacts with PhoR, PstB, and metals to form a phosphate-signaling complex at the membrane. *J. Bacteriol.* 196, 1741–1752. doi: 10.1128/JB.00029-14

Gardner, S. G., Miller, J. B., Dean, T., Robinson, T., Erickson, M., Ridge, P. G., et al. (2015). Genetic analysis, structural modeling, and direct coupling analysis suggest a mechanism for phosphate signaling in *Escherichia coli*. *BMC Genet.* 16 (Suppl. 2):S2. doi: 10.1186/1471-2156-16-S2-S2

Gibson, J. L., Lombardo, M. J., Aponyi, I., Vera Cruz, D., Ray, M. P., and Rosenberg, S. M. (2015). Atypical role for PhoU in mutagenic break repair under stress in *Escherichia coli*. *PLoS ONE* 10:e0123315. doi: 10.1371/journal.pone.0123315

Glover, R. T., Kriakov, J., Garforth, S. J., Baughn, A. D., and Jacobs, W. R. Jr. (2007). The two-component regulatory system *senX3-regX3* regulates phosphate-dependent gene expression in *Mycobacterium smegmatis*. *J. Bacteriol.* 189, 5495–5503. doi: 10.1128/JB.00190-07

Gonin, M., Quardokus, E. M., O'Donnol, D., Maddock, J., and Brun, Y. V. (2000). Regulation of stalk elongation by phosphate in *Caulobacter crescentus*. *J. Bacteriol.* 182, 337–347. doi: 10.1128/JB.182.2.337-347.2000

Gratz, N., Loh, L. N., and Tuomanen, E. (2015). "Pneumococcal invasion: development of Bacteremia and Meningitis," in *Streptococcus pneumoniae Molecular Mechanisms of Host-Pathogen Interactions*, eds J. M. Brown, S. Hammerschmidt, and C. Orihuela (London: Academic Press), 433–451.

Grillo-Puertas, M., Rintoul, M. R., and Rapisarda, V. A. (2016). PhoB activation in non-limiting phosphate condition by the maintenance of high polyphosphate levels in stationary phase inhibits biofilm formation in *Escherichia coli*. *Microbiology*. doi: 10.1099/mic.0.000281. [Epub ahead of print].

Hakansson, A. P., Marks, L. R., and Roche-Hakansson, H. (2015). "Pneumococcal genetic transformation during colonization and biofilm formation," in *Streptococcus pneumoniae Molecular Mechanisms of Host-Pathogen Interactions*, eds J. M. Brown, S. Hammerschmidt, and C. Orihuela (London: Academic Press), 129–142.

Harris, R. M., Webb, D. C., Howitt, S. M., and Cox, G. B. (2001). Characterization of PitA and PitB from *Escherichia coli*. *J. Bacteriol.* 183, 5008–5014. doi: 10.1128/JB.183.17.5008-5014.2001

Hava, D. L., and Camilli, A. (2002). Large-scale identification of serotype 4 *Streptococcus pneumoniae* virulence factors. *Mol. Microbiol.* 45, 1389–1406. doi: 10.1046/j.1365-2958.2002.03106.x

Henriques-Normark, B., and Tuomanen, E. I. (2013). The pneumococcus: epidemiology, microbiology, and pathogenesis. *Cold Spring Harb. Perspect. Med.* 3:a010215. doi: 10.1101/cshperspect.a010215

Hirota, R., Motomura, K., Nakai, S., Handa, T., Ikeda, T., and Kuroda, A. (2013). Stable polyphosphate accumulation by a pseudo-revertant of an *Escherichia coli phoU* mutant. *Biotechnol. Lett.* 35, 695–701. doi: 10.1007/s10529-012-1133-y

Hoover, S. E., Perez, A. J., Tsui, H.-C. T., Sinha, D., Smiley, D. L., DiMarchi, R. D., et al. (2015). A new quorum sensing system (TprA/PhrA) for *Streptococcus pneumoniae* D39 that regulates a lantibiotic biosynthesis gene cluster. *Mol. Microbiol.* 97, 229–243. doi: 10.1111/mmi.13029

Howell, A., Dubrac, S., Noone, D., Varughese, K. I., and Devine, K. (2006). Interactions between the YycFG and PhoPR two-component systems in *Bacillus subtilis*: the PhoR kinase phosphorylates the non-cognate YycF response regulator upon phosphate limitation. *Mol. Microbiol.* 59, 1199–1215. doi: 10.1111/j.1365-2958.2005.05017.x

Hsieh, Y. J., and Wanner, B. L. (2010). Global regulation by the seven-component P_i signaling system. *Curr. Opin. Microbiol.* 13, 198–203. doi: 10.1016/j.mib.2010.01.014

Hulett, F. M. (1993). "Regulation of phosphorus metabolism," in *Bacillus Subtilis and Other Gram-Positive Bacteria Biochemistry, Physiology, and Molecular Genetics*, eds A. L. Sonenshein, J. A. Hoch, and R. Losick (Washington, DC: ASM Press), 229–235.

Hyams, C., Camberlein, E., Cohen, J. M., Bax, K., and Brown, J. S. (2010). The *Streptococcus pneumoniae* capsule inhibits complement activity and neutrophil phagocytosis by multiple mechanisms. *Infect. Immun.* 78, 704–715. doi: 10.1128/IAI.00881-09

Jackson, R. J., Binet, M. R., Lee, L. J., Ma, R., Graham, A. I., McLeod, C. W., et al. (2008). Expression of the PitA phosphate/metal transporter of *Escherichia coli*

is responsive to zinc and inorganic phosphate levels. *FEMS Microbiol. Lett.* 289, 219–224. doi: 10.1111/j.1574-6968.2008.01386.x

Jacobsen, S. M., Lane, M. C., Harro, J. M., Shirtliff, M. E., and Mobley, H. L. (2008). The high-affinity phosphate transporter Pst is a virulence factor for *Proteus mirabilis* during complicated urinary tract infection. *FEMS Immunol. Med. Microbiol.* 52, 180–193. doi: 10.1111/j.1574-695X.2007.00358.x

Katai, K., Miyamoto, K., Kishida, S., Segawa, H., Nii, T., Tanaka, H., et al. (1999). Regulation of intestinal Na^+-dependent phosphate co-transporters by a low-phosphate diet and 1,25-dihydroxyvitamin D3. *Biochem. J.* 343, 705–712. doi: 10.1042/bj3430705

Katewa, S. D., and Katyare, S. S. (2003). A simplified method for inorganic phosphate determination and its application for phosphate analysis in enzyme assays. *Anal. Biochem.* 323, 180–187. doi: 10.1016/j.ab.2003.08.024

Kazmierczak, K. M., Wayne, K. J., Rechtsteiner, A., and Winkler, M. E. (2009). Roles of *rel*(Spn) in stringent response, global regulation and virulence of serotype 2 *Streptococcus pneumoniae* D39. *Mol. Microbiol.* 72, 590–611. doi: 10.1111/j.1365-2958.2009.06669.x

Lacks, S., and Hotchkiss, R. D. (1960). A study of the genetic material determining an enzyme in Pneumococcus. *Biochim. Biophys. Acta* 39, 508–518. doi: 10.1016/0006-3002(60)90205-5

Lamarche, M. G., Wanner, B. L., Crépin, S., and Harel, J. (2008). The phosphate regulon and bacterial virulence: a regulatory network connecting phosphate homeostasis and pathogenesis. *FEMS Microbiol. Rev.* 32, 461–473. doi: 10.1111/j.1574-6976.2008.00101.x

Lanie, J. A., Ng, W. L., Kazmierczak, K. M., Andrzejewski, T. M., Davidsen, T. M., Wayne, K. J., et al. (2007). Genome sequence of Avery's virulent serotype 2 strain D39 of *Streptococcus pneumoniae* and comparison with that of unencapsulated laboratory strain R6. *J. Bacteriol.* 189, 38–51. doi: 10.1128/JB.01148-06

Lebens, M., Lundquist, P., Söderlund, L., Todorovic, M., and Carlin, N. I. (2002). The *nptA* gene of *Vibrio cholerae* encodes a functional sodium-dependent phosphate cotransporter homologous to the type II cotransporters of eukaryotes. *J. Bacteriol.* 184, 4466–4474. doi: 10.1128/JB.184.16.4466-4474.2002

Lee, S. J., Park, Y. S., Kim, S. J., Lee, B. J., and Suh, S. W. (2014). Crystal structure of PhoU from *Pseudomonas aeruginosa*, a negative regulator of the Pho regulon. *J. Struct. Biol.* 188, 22–29. doi: 10.1016/j.jsb.2014.08.010

Li, Y., and Zhang, Y. (2007). PhoU is a persistence switch involved in persister formation and tolerance to multiple antibiotics and stresses in *Escherichia coli*. *Antimicrob. Agents Chemother.* 51, 2092–2099. doi: 10.1128/AAC.00052-07

Liu, J., Lou, Y., Yokota, H., Adams, P. D., Kim, R., and Kim, S. H. (2005). Crystal structure of a PhoU protein homologue: a new class of metalloprotein containing multinuclear iron clusters. *J. Biol. Chem.* 280, 15960–15966. doi: 10.1074/jbc.M414117200

Lubin, E. A., Henry, J. T., Fiebig, A., Crosson, S., and Laub, M. T. (2016). Identification of the PhoB regulon and role of PhoU in the phosphate starvation response of *Caulobacter crescentus*. *J. Bacteriol.* 198, 187–200. doi: 10.1128/JB.00658-15

Martín, J. F. (2004). Phosphate control of the biosynthesis of antibiotics and other secondary metabolites is mediated by the PhoR-PhoP system: an unfinished story. *J. Bacteriol.* 186, 5197–5201. doi: 10.1128/JB.186.16.5197-5201.2004

McCluskey, J., Hinds, J., Husain, S., Witney, A., and Mitchell, T. J. (2004). A two-component system that controls the expression of pneumococcal surface antigen A (PsaA) and regulates virulence and resistance to oxidative stress in *Streptococcus pneumoniae*. *Mol. Microbiol.* 51, 1661–1675. doi: 10.1111/j.1365-2958.2003.03917.x

Moreno-Letelier, A., Olmedo, G., Eguiarte, L. E., Martinez-Castilla, L., and Souza, V. (2011). Parallel evolution and horizontal gene transfer of the *pst* operon in Firmicutes from oligotrophic environments. *Int. J. Evol. Biol.* 2011:781642. doi: 10.4061/2011/781642

Morohoshi, T., Maruo, T., Shirai, Y., Kato, J., Ikeda, T., Takiguchi, N., et al. (2002). Accumulation of inorganic polyphosphate in *phoU* mutants of *Escherichia coli* and *Synechocystis* sp. strain PCC6803. *Appl. Environ. Microbiol.* 68, 4107–4110. doi: 10.1128/AEM.68.8.4107-4110.2002

Morona, J. K., Miller, D. C., Morona, R., and Paton, J. C. (2004). The effect that mutations in the conserved capsular polysaccharide biosynthesis genes *cpsA*, *cpsB*, and *cpsD* have on virulence of *Streptococcus pneumoniae*. *J. Infect. Dis.* 189, 1905–1913. doi: 10.1086/383352

Morona, J. K., Morona, R., and Paton, J. C. (2006). Attachment of capsular polysaccharide to the cell wall of *Streptococcus pneumoniae* type 2 is required for invasive disease. *Proc. Natl. Acad. Sci. U.S.A.* 103, 8505–8510. doi: 10.1073/pnas.0602148103

Muda, M., Rao, N. N., and Torriani, A. (1992). Role of PhoU in phosphate transport and alkaline phosphatase regulation. *J. Bacteriol.* 174, 8057–8064.

Neznansky, A., Blus-Kadosh, I., Yerushalmi, G., Banin, E., and Opatowsky, Y. (2014). The *Pseudomonas aeruginosa* phosphate transport protein PstS plays a phosphate-independent role in biofilm formation. *FASEB J.* 28, 5223–5233. doi: 10.1096/fj.14-258293

Novak, R., Cauwels, A., Charpentier, E., and Tuomanen, E. (1999). Identification of a *Streptococcus pneumoniae* gene locus encoding proteins of an ABC phosphate transporter and a two-component regulatory system. *J. Bacteriol.* 181, 1126–1133.

Oganesyan, V., Oganesyan, N., Adams, P. D., Jancarik, J., Yokota, H. A., Kim, R., et al. (2005). Crystal structure of the "PhoU-like" phosphate uptake regulator from *Aquifex aeolicus*. *J. Bacteriol.* 187, 4238–4244. doi: 10.1128/JB.187.12.4238-4244.2005

Oliver, M. B., and Swords, W. E. (2015). "Pneumococcal biofilms and bacterial persistence during otitis media infections," in *Streptococcus pneumoniae Molecular Mechanisms of Host-Pathogen Interactions*, eds J. M. Brown, S. Hammerschmidt, and C. Orihuela (London: Academic Press), 293–308.

Orihuela, C. J., Mills, J., Robb, C. W., Wilson, C. J., Watson, D. A., and Niesel, D. W. (2001). *Streptococcus pneumoniae* PstS production is phosphate responsive and enhanced during growth in the murine peritoneal cavity. *Infect. Immun.* 69, 7565–7571. doi: 10.1128/IAI.69.12.7565-7571.2001

Paterson, G. K., Blue, C. E., and Mitchell, T. J. (2006). Role of two-component systems in the virulence of *Streptococcus pneumoniae*. *J. Med. Microbiol.* 55, 355–363. doi: 10.1099/jmm.0.46423-0

Polissi, A., Pontiggia, A., Feger, G., Altieri, M., Mottl, H., Ferrari, L., et al. (1998). Large-scale identification of virulence genes from *Streptococcus pneumoniae*. *Infect. Immun.* 66, 5620–5629.

Pratt, J. T., Ismail, A. M., and Camilli, A. (2010). PhoB regulates both environmental and virulence gene expression in *Vibrio cholerae*. *Mol. Microbiol.* 77, 1595–1605. doi: 10.1111/j.1365-2958.2010.07310.x

Qi, Y., Kobayashi, Y., and Hulett, F. M. (1997). The *pst* operon of *Bacillus subtilis* has a phosphate-regulated promoter and is involved in phosphate transport but not in regulation of the pho regulon. *J. Bacteriol.* 179, 2534–2539.

Ramos-Montañez, S., Tsui, H. C., Wayne, K. J., Morris, J. L., Peters, L. E., Zhang, F., et al. (2008). Polymorphism and regulation of the *spxB* (pyruvate oxidase) virulence factor gene by a CBS-HotDog domain protein (SpxR) in serotype 2 *Streptococcus pneumoniae*. *Mol. Microbiol.* 67, 729–746. doi: 10.1111/j.1365-2958.2007.06082.x

Rice, C. D., Pollard, J. E., Lewis, Z. T., and McCleary, W. R. (2009). Employment of a promoter-swapping technique shows that PhoU modulates the activity of the $PstSCAB_2$ ABC transporter in *Escherichia coli*. *Appl. Environ. Microbiol.* 75, 573–582. doi: 10.1128/AEM.01046-08

Rifat, D., Bishai, W. R., and Karakousis, P. C. (2009). Phosphate depletion: a novel trigger for *Mycobacterium tuberculosis* persistence. *J. Infect. Dis.* 200, 1126–1135. doi: 10.1086/605700

Shah, M., Zaborin, A., Alverdy, J. C., Scott, K., and Zaborina, O. (2014). Localization of DING proteins on PstS-containing outer-surface appendages of *Pseudomonas aeruginosa*. *FEMS Microbiol. Lett.* 352, 54–61. doi: 10.1111/1574-6968.12368

Shi, W., and Zhang, Y. (2010). PhoY2 but not PhoY1 is the PhoU homologue involved in persisters in *Mycobacterium tuberculosis*. *J. Antimicrob. Chemother.* 65, 1237–1242. doi: 10.1093/jac/dkq103

Short, K. R., and Diavatopoulos, D. A. (2015). "Nasopharyngeal Colonization with *Streptococcus pneumoniae*," in *Streptococcus pneumoniae Molecular Mechanisms of Host-Pathogen Interactions,* eds. J. M. Brown, S. Hammerschmidt, and C. Orihuela (London: Academic Press), 279–291.

Soualhine, H., Brochu, V., Ménard, F., Papadopoulou, B., Weiss, K., Bergeron, M. G., et al. (2005). A proteomic analysis of penicillin resistance in *Streptococcus pneumoniae* reveals a novel role for PstS, a subunit of the phosphate ABC transporter. *Mol. Microbiol.* 58, 1430–1440. doi: 10.1111/j.1365-2958.2005.04914.x

Staley, C., and Harwood, V. J. (2014). Differential expression of a sodium-phosphate cotransporter among *Vibrio vulnificus* strains. *Microb. Ecol.* 67, 24–33. doi: 10.1007/s00248-013-0300-6

Steed, P. M., and Wanner, B. L. (1993). Use of the rep technique for allele replacement to construct mutants with deletions of the *pstSCAB-phoU* operon: evidence of a new role for the PhoU protein in the phosphate regulon. *J. Bacteriol.* 175, 6797–6809.

Sung, C. K., Li, H., Claverys, J. P., and Morrison, D. A. (2001). An *rpsL* cassette, janus, for gene replacement through negative selection in *Streptococcus pneumoniae*. *Appl. Environ. Microbiol.* 67, 5190–5196. doi: 10.1128/AEM.67.11.5190-5196.2001

Suzuki, S., Ferjani, A., Suzuki, I., and Murata, N. (2004). The SphS-SphR two component system is the exclusive sensor for the induction of gene expression in response to phosphate limitation in *synechocystis*. *J. Biol. Chem.* 279, 13234–13240. doi: 10.1074/jbc.M313358200

Takemaru, K., Mizuno, M., and Kobayashi, Y. (1996). A *Bacillus subtilis* gene cluster similar to the *Escherichia coli* phosphate-specific transport (*pst*) operon: evidence for a tandemly arranged *pstB* gene. *Microbiology* 142, 2017–2020. doi: 10.1099/13500872-142-8-2017

Throup, J. P., Koretke, K. K., Bryant, A. P., Ingraham, K. A., Chalker, A. F., Ge, Y., et al. (2000). A genomic analysis of two-component signal transduction in *Streptococcus pneumoniae*. *Mol. Microbiol.* 35, 566–576. doi: 10.1046/j.1365-2958.2000.01725.x

Tiraby, J. G., and Fox, M. S. (1973). Marker discrimination in transformation and mutation of pneumococcus. *Proc. Natl. Acad. Sci. U.S.A.* 70, 3541–3545. doi: 10.1073/pnas.70.12.3541

Tischler, A. D., Leistikow, R. L., Kirksey, M. A., Voskuil, M. I., and McKinney, J. D. (2013). *Mycobacterium tuberculosis* requires phosphate-responsive gene regulation to resist host immunity. *Infect. Immun.* 81, 317–328. doi: 10.1128/IAI.01136-12

Trihn, M., Ge, X., Dobson, A., Kitten, T., Munro, C. L., and Xu, P. (2013). Two-component system response regulators involved in virulence of *Streptococcus pneumoniae* TIGR4 in infective endocarditis. *PLoS ONE* 8:e54320. doi: 10.1371/journal.pone.0054320

Tsui, H. C., Boersma, M. J., Vella, S. A., Kocaoglu, O., Kuru, E., Peceny, J. K., et al. (2014). Pbp2x localizes separately from Pbp2b and other peptidoglycan synthesis proteins during later stages of cell division of *Streptococcus pneumoniae* D39. *Mol. Microbiol.* 94, 21–40. doi: 10.1111/mmi.12745

Tsui, H. C., Mukherjee, D., Ray, V. A., Sham, L. T., Feig, A. L., and Winkler, M. E. (2010). Identification and characterization of noncoding small RNAs in *Streptococcus pneumoniae* serotype 2 strain D39. *J. Bacteriol.* 192, 264–279. doi: 10.1128/JB.01204-09

Tsui, H. T., Zheng, J. J., Magallon, A. N., Ryan, J. D., Yunck, R., Rued, B. E., et al. (2016). Suppression of a deletion mutation in the gene encoding essential PBP2b reveals a new lytic transglycosylase involved in peripheral peptidoglycan synthesis in *Streptococcus pneumoniae* D39. *Mol. Microbiol.* 100, 1039–1065. doi: 10.1111/mmi.13366

van de Weerd, R., Boot, M., Maaskant, J., Sparrius, M., Verboom, T., van Leeuwen, L. M., et al. (2016). Inorganic phosphate limitation modulates capsular polysaccharide composition in Mycobacteria. *J. Biol. Chem.* 291, 11787–11799. doi: 10.1074/jbc.M116.722454

van Opijnen, T., and Camilli, A. (2012). A fine scale phenotype-genotype virulence map of a bacterial pathogen. *Genome Res.* 22, 2541–2551. doi: 10.1101/gr.137430.112

van Veen, H. W., Abee, T., Kortstee, G. J., Konings, W. N., and Zehnder, A. J. (1994). Translocation of metal phosphate via the phosphate inorganic transport system of *Escherichia coli*. *Biochemistry* 33, 1766–1770. doi: 10.1021/bi00173a020

Vernatter, J., and Pirofski, L. A. (2013). Current concepts in host-microbe interaction leading to pneumococcal pneumonia. *Curr. Opin. Infect. Dis.* 26, 277–283. doi: 10.1097/QCO.0b013e3283608419

Wang, C., Mao, Y., Yu, J., Zhu, L., Li, M., Wang, D., et al. (2013). PhoY2 of Mycobacteria is required for metabolic homeostasis and stress response. *J. Bacteriol.* 195, 243–252. doi: 10.1128/JB.01556-12

Wanner, B. L. (1996). "Phosphorus assimilation and control of the phosphate regulon," in *Escherichia coli and Salmonella typhimurium cellular and molecular biology, Vol. 2,* eds F. C. Neidhardt, R. III. Curtis, J. L. Ingraham, E. C. C. Lin, K. B. Low, B. Magasanik, W. S. Reznikoff, M. Riley, M. Schaechter, and H. E. Umbarger (Washington, DC: ASM Press), 1357–1381.

Wayne, K. J., Li, S., Kazmierczak, K. M., Tsui, H. C., and Winkler, M. E. (2012). Involvement of WalK (VicK) phosphatase activity in setting WalR (VicR) response regulator phosphorylation level and limiting cross-talk in *Streptococcus pneumoniae* D39 cells. *Mol. Microbiol.* 86, 645–660. doi: 10.1111/mmi.12006

Wayne, K. J., Sham, L. T., Tsui, H. C., Gutu, A. D., Barendt, S. M., Keen, S. K., et al. (2010). Localization and cellular amounts of the WalRKJ (VicRKX) two-component regulatory system proteins in serotype 2 *Streptococcus pneumoniae*. *J. Bacteriol.* 192, 4388–4394. doi: 10.1128/JB.00578-10

Wilson, M. (2005). *Microbial Inhabitants of Humans: Their Ecology and Role in Health and Disease.* Cambridge: Cambridge University Press.

Wilson, M. (2008). *Bacteriology of Humans an Ecological Perspective.* Malen, MA: Blackwell Publishing.

Yother, J. (2011). Capsules of *Streptococcus pneumoniae* and other bacteria: paradigms for polysaccharide biosynthesis and regulation. *Annu. Rev. Microbiol.* 65, 563–581. doi: 10.1146/annurev.micro.62.081307.162944

Zaborina, O., Holbrook, C., Chen, Y., Long, J., Zaborin, A., Morozova, I., et al. (2008). Structure-function aspects of PstS in multi-drug-resistant *Pseudomonas aeruginosa*. *PLoS Pathog.* 4:e43. doi: 10.1371/journal.ppat.0040043

Zhang, H., Ishige, K., and Kornberg, A. (2002). A polyphosphate kinase (PPK2) widely conserved in bacteria. *Proc. Natl. Acad. Sci. U.S.A.* 99, 16678–16683. doi: 10.1073/pnas.262655199

Conflict of Interest Statement: The authors declare that the research was conducted in the absence of any commercial or financial relationships that could be construed as a potential conflict of interest.

frontiers in Cellular and Infection Microbiology

MINI REVIEW
published: 21 September 2016
doi: 10.3389/fcimb.2016.00098

Macrolide Resistance in *Streptococcus pneumoniae*

Max R. Schroeder[1] *and David S. Stephens*[1, 2, 3]*

[1] Departments of Medicine, Emory University, Atlanta, GA, USA, [2] Departments of Microbiology and Immunology, Emory University, Atlanta, GA, USA, [3] Departments of Epidemiology, Emory University, Atlanta, GA, USA

Streptococcus pneumoniae is a common commensal and an opportunistic pathogen. Suspected pneumococcal upper respiratory infections and pneumonia are often treated with macrolide antibiotics. Macrolides are bacteriostatic antibiotics and inhibit protein synthesis by binding to the 50S ribosomal subunit. The widespread use of macrolides is associated with increased macrolide resistance in *S. pneumoniae*, and the treatment of pneumococcal infections with macrolides may be associated with clinical failures. In *S. pneumoniae*, macrolide resistance is due to ribosomal dimethylation by an enzyme encoded by *erm*(B), efflux by a two-component efflux pump encoded by *mef*(E)/*mel*(*msr*(D)) and, less commonly, mutations of the ribosomal target site of macrolides. A wide array of genetic elements have emerged that facilitate macrolide resistance in *S. pneumoniae*; for example *erm*(B) is found on Tn*917*, while the *mef*(E)/*mel* operon is carried on the 5.4- or 5.5-kb Mega element. The macrolide resistance determinants, *erm*(B) and *mef*(E)/*mel*, are also found on large composite Tn*916*-like elements most notably Tn*6002*, Tn*2009*, and Tn*2010*. Introductions of 7-valent and 13-valent pneumococcal conjugate vaccines (PCV-7 and PCV-13) have decreased the incidence of macrolide-resistant invasive pneumococcal disease, but serotype replacement and emergence of macrolide resistance remain an important concern.

Keywords: *Streptococcus pneumoniae*, antibiotic resistance, macrolide resistance, *erm*(B), *mef*(A/E)/*mel*(*msr*(D)), Mega, pneumococci

OPEN ACCESS

Edited by:
Guangchun Bai,
Albany Medical College, USA

Reviewed by:
Lesley McGee,
Centers for Disease Control and Prevention, USA
Werner Albrich,
Kantonsspital St. Gallen, Switzerland
Lucia Martins Teixeira,
Federal University of Rio de Janeiro, Brazil

***Correspondence:**
David S. Stephens
dstep01@emory.edu

Received: *12 May 2016*
Accepted: *26 August 2016*
Published: *21 September 2016*

Citation:
Schroeder MR and Stephens DS (2016) Macrolide Resistance in Streptococcus pneumoniae. Front. Cell. Infect. Microbiol. 6:98. doi: 10.3389/fcimb.2016.00098

INTRODUCTION

Streptococcus pneumoniae, the pneumococcus, is a commensal of the human nasopharynx and an opportunistic pathogen that is a leading worldwide cause of death for children under the age of 5 years (Walker et al., 2013). In addition to localized infections such as otitis media and pneumonia, the pneumococcus may cause severe invasive disease (IPD) including bacteremia and meningitis. Development of penicillin resistance in the pneumococcus in the 1980s–1990s shifted antibiotic treatment of suspected pneumococcal upper respiratory infections and pneumonia to macrolides. Widespread macrolide use, however, is associated with increased macrolide resistance in *S. pneumoniae* (Bergman et al., 2006; Malhotra-Kumar et al., 2007). Clinical failures of macrolide treatment of pneumococcal infections have been reported for lower respiratory tract infections (Klugman, 2002) and bacteremia (Lonks et al., 2002; Schentag et al., 2007). Widespread macrolide use is a strong selective pressure contributing to the expansion of macrolide-resistant *S. pneumoniae* (Bergman et al., 2006; Keenan et al., 2015). Globally, macrolide resistance among *S. pneumoniae* is geographically variable but ranges from <10% to >90% of isolates (Farrell et al., 2008; Pan et al., 2015; Xiao et al., 2015).

MACROLIDE ANTIBIOTICS

Macrolides are defined by a complex macrocyclic structure with a 14-, 15-, or 16-membered lactone ring substituted with neutral or amino sugar groups. Macrolides inhibit bacterial protein synthesis by binding to the large 50S ribosomal subunit and disrupting protein elongation by causing the dissociation of the peptidyl-tRNA.

Erythromycin, discovered in 1952, is a 14-membered macrolide produced by *Saccharopolyspora erythraeus* (formerly *Streptomyces erythraeus*; McGuire et al., 1952). After the discovery of erythromycin and other naturally-produced macrolides, research focused on the creation of synthetic and semisynthetic macrolides (Kirst, 2010; Seiple et al., 2016). Azithromycin and clarithromycin are semisynthetic macrolides approved for use in the United States, and azithromycin is one of the most prescribed antibiotics in the US (Hicks et al., 2015). Additional macrolides such as roxithromycin and josamycin are approved in other countries worldwide. Macrolides bind reversibly to the 23S rRNA at a site near the peptidyl transferase center of the 50S ribosomal subunit (Kannan and Mankin, 2011). Macrolide binding occurs in pre-structured ribosomal assemblies (Pokkunuri and Champney, 2007). The smaller macrolides (14- and 15-membered) partially block the nascent peptide channel to inhibit the elongating peptide chain while larger macrolides (16-membered) fully block the nascent peptide channel and cause ribosomal disassociation that reversibly inhibits protein synthesis (Weisblum, 1995b). Though distinct in chemical structure, the lincosamide and streptogramin class antibiotics have overlapping binding sites with macrolides and have similar mechanisms of action (Kirst, 2010).

MECHANISMS OF MACROLIDE RESISTANCE

Ribosomal Modification

Erythromycin ribosomal methylase (*erm*) family genes encode adenine-specific N-methyltransferases that methylate the 23S rRNA to prevent antibiotic binding (Weisblum, 1995a). The ribosomal methylase found in *S. pneumoniae* is primarily encoded by *erm*(B) whose gene product dimethylates the target site of the 23S rRNA (A2058 in *Escherichia coli*; Skinner et al., 1983; Johnston et al., 1998). The *erm*(B) gene is the most common macrolide resistance determinant in *S. pneumoniae* (**Table 1**). Erm(A) subclasses *erm*(A) (Syrogiannopoulos et al., 2001) and *erm*(TR) (Camilli et al., 2008) are rarely found in *S. pneumoniae*. Ribosomal methylation by Erm(B) confers resistance to macrolides, lincosamides, and streptogramin B, which is characterized as the MLS_B phenotype (Weisblum, 1995a). In addition to the expanded spectrum of resistance, *erm*(B) provides high-level resistance to macrolides (erythromycin MICs usually $\geq$256 μg/ml).

The induction of *erm*(B) allows high-level translation of Erm(B) in the presence of inducers such as erythromycin (Chancey et al., 2011). In the pneumococcus, *erm*(B) expression may be inducible or constitutively expressed to high levels. As expression of *erm* genes is repressed in the absence of inducing drugs through a mechanism of translational attenuation; *erm*(B) expression has been proposed to have a bacterial fitness cost (Min et al., 2008; Chancey et al., 2012; Gupta et al., 2013). A recent study found that a *Staphylococcus aureus* strain expressing *erm*(C) was outcompeted by *S. aureus* expressing catalytically-inactive *erm*(C) (Gupta et al., 2013), supporting the need for tight regulation of expression. Interestingly, deletion of the leader sequence of *erm*(B) in *S. pneumoniae* was found to confer resistance to telithromycin, the first-generation ketolide, a semi-synthetic macrolide antibiotic, by allowing constitutive expression (Wolter et al., 2008).

Macrolide Efflux

Macrolide efflux in *S. pneumoniae* has been the most common cause of macrolide resistance in North America, the United Kingdom, and others (**Table 1**). Pneumococcal macrolide efflux is encoded by the *mef*(E)/*mel* operon and occurs through an as yet incompletely understood mechanism of macrolide binding and membrane targeting for efflux (Chancey et al., 2012). Macrolide resistance in *S. pneumoniae* requires both *mef*(E) and *mel*. These genes are carried on the macrolide efflux genetic assembly (Mega) element and are expressed from a single promoter inducible by 14- and 15-membered macrolides (e.g., erythromycin, clarithromycin, and azithromycin; Gay and Stephens, 2001; Ambrose et al., 2005; Chancey et al., 2015b). Expression of *mef*(E) and *mel* is tightly controlled through transcriptional attenuation (Chancey et al., 2015b).

The first gene, *mef*(E) shares 90% sequence identity with *mef*(A) from *Streptococcus pyogenes* (Tait-Kamradt et al., 1997; Roberts et al., 1999). While *mef*(E) is most common, *mef*(A) is more common in Germany, Denmark, and Australia (**Table 1**). Another homolog, *mef*(I), also shares 91% identity with *mef*(A), has been found in *S. pneumoniae* (Cochetti et al., 2005; Wierzbowski et al., 2005b) but is rarely found (**Table 1**). Most studies do not distinguish between *mef*(E) and *mef*(A) and thus report only *mef*(E) or *mef*(A) rather than *mef*(A/E), which is a more accurate description of the data. In *S. pneumoniae*, *mef*(E) encodes a 405 amino acid protein that belongs to the major facilitator superfamily, which utilizes proton motive force-driven efflux to expel molecules from cells (Tait-Kamradt et al., 1997). The second gene, *mel* (also known as *msr*(D)) is a homolog of the *S. aureus* gene *mrs*(*A*) (Roberts et al., 1999), which encodes an ATP-binding cassette (ABC) transporter protein but lacks typical hydrophobic, membrane-binding domains, and is predicted to interact with chromosomally encoded transmembrane complexes (Ambrose et al., 2005). Mef(E) and Mel have been shown to synergistically provide macrolide resistance and operate as a two-component efflux pump in *S. pneumoniae* (Ambrose et al., 2005; Zhang et al., 2016). A recent *E. coli* study suggests a physical interaction between Mef(E) and Mel and that Mel may bind macrolides and localize to the membrane (Nunez-Samudio and Chesneau, 2013). In *S. pyogenes* the presence of *msr*(D) alone was required for macrolide resistance (Zhang et al., 2016) and recent evidence suggests antibiotic resistance by ATP-binding cassette proteins may occur through ribosomal protection by displacing ribosome-bound macrolide molecules (Sharkey et al., 2016). Thus, the working

TABLE 1 | Distribution of macrolide resistance genotypes by country.

Continent Country	Macrolide resistance genotype distribution %						Years	References
	erm(B)	*mef*(A/E)	*mef*(E)	*mef*(A)	*erm*(B) + *mef*(E)	Negative[a]		
AFRICA								
Morocco	90.2		6.5	0	3.3	0	2007–2014	Diawara et al., 2016
South Africa	36.5	16.3			46.4	0.4	2003–2004	Farrell et al., 2008
ASIA								
China	63.4	0.6			36.0	0	2006–2008	Ma et al., 2013
	69.6	0			30.4		2010	Zhou et al., 2011
	62.9				37.1		2012–2013	Geng et al., 2014
Hong Kong	45.9	27.7			26.4	0	2008–2009	Kim et al., 2012
Iran	44	16			40		2011–2013	Azadegan et al., 2015
Japan	56.3	28.8			10.9	4.0	2011	Kawaguchiya et al., 2014
	59.5	25.2			12.6	2.7	2011–2012	Okade et al., 2014
	53.2	21.8			17.9	7.1	2012	Chiba et al., 2014
Jordan	26.4	24.5			13.2	35.8	2012–2013	Swedan et al., 2016
Lebanon	65.3	0			19.5	14.6	2005–2009	Daoud et al., 2011
	36.4	18.1			31.8	13.6	2008–2010	Taha et al., 2012
Malaysia	35.2	42.6			9.3	13.0	2008–2009	Kim et al., 2012
Saudi Arabia	37.5	62.5			0	0	2003–2004	Farrell et al., 2008
Sri Lanka	73.3	13.3			13.3	0	2008–2009	Kim et al., 2012
South Korea	43.3	13.0			43.3	0.4	2008–2009	Kim et al., 2012
Taiwan	55.1	22.5			21.4	1.0	2008–2009	Kim et al., 2012
	70.0	5.0			25.0		2010	Safari et al., 2014
Thailand	47.9	37.2			11.7	3.2	2008–2009	Kim et al., 2012
Vietnam	56.9	2.1			41.0	0	2008–2009	Kim et al., 2012
AUSTRALIA								
Australia	32.4		3.9	20.6	35.3 (6.9)[b]	0.9	2005	Xu et al., 2010
EUROPE								
Austria	45.5	54.5			0	0	2003–2004	Farrell et al., 2008
Belgium	90.2	1.6			3.3	4.9	2007–2009	Lismond et al., 2012
Bulgaria	63.2	21.0			15.8		2006–2010	Setchanova et al., 2012
Denmark	30.4		15.9	49.3 (1.4)[c]	0	2	2007	Nielsen et al., 2010
France	90.0	2.4			1.2	6.5	2003–2004	Farrell et al., 2008
Finland	30.5		40.4	15.7	0.9	12.6	2002–2006	Siira et al., 2009
Germany	27.0		11.2	57.7	4.1	0	2005–2006	Bley et al., 2011
	66.8		8.3	20.7	3.6		2012–2013	Imöhl et al., 2015
Greece	22.0		45.8	0	32.2		2009	Grivea et al., 2012
Hungary	82.4	11.8			5.9	0	2003–2004	Farrell et al., 2008
Ireland	38.9	61.1			0	0	2003–2004	Farrell et al., 2008
Italy	55.8	38.5			1.0	4.8	2003–2004	Farrell et al., 2008
Poland	80.8	7.7			3.8	7.7	2003–2004	Farrell et al., 2008
Russia	54.1	12.7			30.6	2.6	2009–2013	Mayanskiy et al., 2014
Slovak Republic	64.7	5.9			17.6	11.8	2003–2004	Farrell et al., 2008
Spain	74.3	7.7			17.9		2000–2007	De La Pedrosa et al., 2009
Switzerland	70.6	23.5			0	5.9	2003–2004	Farrell et al., 2008
Turkey	44.4	11.1			44.4		2008–2009	Sirekbasan et al., 2015
United Kingdom	20.8	70.8			4.2	4.2	2003–2004	Farrell et al., 2008
NORTH AMERICA								
Canada	27.0	50.0	95	5	19.0	3.6	1997–2002	Wierzbowski et al., 2005b
							2008	Wierzbowski et al., 2014
Mexico	17.2	72.4			10.3	0	2003–2004	Farrell et al., 2008

(Continued)

TABLE 1 | Continued

Continent Country	Macrolide resistance genotype distribution %						Years	References
	erm(B)	*mef*(A/E)	*mef*(E)	*mef*(A)	*erm*(B) + *mef*(E)	Negative[a]		
USA	19.5	51.3			28.7	0.5	2007	Hawkins et al., 2015
Alaska	15.0	58.8			20.0	6.3	2006–2010	Rudolph et al., 2013
Arizona	5		25	2.5	67.5		2007–2008	Bowers et al., 2012
SOUTH AMERICA								
Argentina	19.2	76.9			3.8		2009–2010	Reijtman et al., 2013
Brazil	36.0	44.0			20.0		2007–2012	Caierão et al., 2014
Colombia	56.9	40.2	30.7	0.9	7.1	4.4	1994–2008	Ramos et al., 2014
	53.7				0	6.1	2005–2008	Hidalgo et al., 2011
Peru	53.3	33.3			0	13.3	2003–2004	Farrell et al., 2008
Venezuela	83.3		12.5	0.0	4.2		2007	Quintero et al., 2011

[a] *PCR negative for erm(B), mef(A/E), mef(A), and mef(E). Some authors have determined these to be ribosomal mutations.*
[b] *Strains contain both erm(B) and mef(A).*
[c] *Strains contain mef(I).*

model for macrolide efflux in *S. pneumoniae* may be macrolide displacement from ribosomes by *mel*, which transfers macrolide molecules to *mef*(E) for efflux.

S. pneumoniae with *mef*(E)/*mel* have been shown to have an M phenotype, which is resistant to 14- and 15-membered macrolides but susceptible to lincosamides and streptogramin B (Tait-Kamradt et al., 1997). While *mef*(E)/*mel*-containing strains display low level resistance (MICs 1–8 μg/ml) to erythromycin, macrolide induction increases expression of *mef*(E)/*mel* and results in increased levels of macrolide resistance (Wierzbowski et al., 2005a). Induction of *mef*(E)/*mel* by macrolides increases MICs to ≥16 μg/ml (Ambrose et al., 2005; Chancey et al., 2011). The presence of the two-component efflux pump encoded by *mef*(E)/*mel* also increases resistance to the human antimicrobial peptide LL-37 (Zähner et al., 2010). LL-37 also induces expression of the efflux pump (Zähner et al., 2010). These data may suggest the efflux pump is induced during nasopharyngeal colonization and primes the *mef*(E)/*mel*-containing pneumococci to resist macrolide antibiotics.

Ribosomal Mutations

Point mutations in 23S rRNA at or near the macrolide binding residue A2058 (*E. coli* ribosome) have resulted in high-level macrolide resistance (Vester and Douthwaite, 2001; Franceschi et al., 2004). Mutations of ribosomal proteins L4 and L22 confer macrolide resistance in pathogenic and nonpathogenic bacteria including pneumococci. L4 and L22 are ribosomal proteins with domains on the surface of the ribosome as well as tentacles that extend into the exit tunnel in proximity to the macrolide-binding site (Schuwirth et al., 2005). In *E. coli*, a Lys-63-Glu change in the L4 protein (*rplD*) as well as a triple amino acid deletion of Met-82, Lys-83, and Glu-84 from L22 (*rplV*) confer resistance to macrolides (Wittmann et al., 1973; Chittum and Champney, 1994). A variety of additional L4 and L22 mutations have also been found to confer macrolide resistance (Zaman et al., 2007; Diner and Hayes, 2009). While the overall incidence is rare in *S. pneumoniae*, L4 and L22 mutations have been shown to result in macrolide resistance (Franceschi et al., 2004).

Dual Macrolide Resistance Genotype

S. pneumoniae containing both *erm*(B) and *mef*(E)/*mel* were first reported in the late-1990s (Corso et al., 1998; Nishijima et al., 1999) and are now found worldwide (Farrell et al., 2008). The dual macrolide resistance genotype occurred in 12% of global isolates collected from 2003 to 2004, which is twice the frequency reported from 1999 to 2000 (Farrell et al., 2008). In 2004, 18.4% of *S. pneumoniae* isolates from the US were found to have the dual *erm*(B) and *mef*(E)/*mel* genotype (Jenkins et al., 2008); in a recent study, up to 52% of macrolide-resistant isolates from Arizona were found to contain both macrolide resistance genes (Bowers et al., 2012). Tn*2010* has been identified as the major composite mobile element that contains *erm*(B) and *mef*(E)/*mel* (Mega) (Del Grosso et al., 2006). Following introduction of the 7-valent pneumococcal conjugate vaccine (PCV-7) the "replacement" serotype 19A (ST320) with Tn*2010* emerged (Del Grosso et al., 2007). ST320 is a multidrug resistant strain that appears to represent a "capsule switch" from serotype 19F and is responsible for a global pandemic in the wake of PCV-7 introduction (Moore et al., 2008; Li et al., 2011). The high-level and broader resistance conferred by *erm*(B) would predict that *mef*(E)/*mel* is functionally redundant in *erm*(B)-containing *S. pneumoniae*.

DISSEMINATION OF RESISTANCE DETERMINANTS

Macrolide Resistance Chromosomal Locations

The *mef*(E)/*mel*-containing genetic element Mega is found in at least six distinct chromosomal sites within the pneumococcal genome (Chancey et al., 2015a), while *mef*(A) is found on Tn*1207.1* (Xu et al., 2010). Mega insertion sites are distributed around the chromosome: (I)

a phosphomethylpyrimidine kinase (TIGR4 SP_1598), (II) a DNA-3-methyladenine glycosylase (SP_0180), (III) a capsule biosynthesis gene (SP_0103), (IV) the RNA methyltransferase *rumA* (SP_1029) (Gay and Stephens, 2001), (V) *orf6* of Tn*916*-like elements (Del Grosso et al., 2006), and (VI) a novel insertion into a *S. suis* homolog element found in *S. pneumoniae* (Chancey et al., 2015a). Due to genetic variations at insertion site IV, this class is subdivided: (IVa) Mega and IS*Smi* element insertion along with deletion of the 30.7 kb pneumococcal pathogenicity island-1 (PPI-1), and (IVb) simple insertion of Mega into *rumA* with PPI-1 intact, and (IVc) same organization as IVa with a *S. equi* subspecies *zooepidemicus*-related integrative and conjugative element (42 kb) inserted upstream of Mega (Chancey et al., 2015a).

The Mega element lacks genes required for transposition (Gay and Stephens, 2001). Analysis of the Mega insertion sites revealed a putative target sequence of 5′-TTTCCNCAA-3′ about six base pairs upstream of the insertion and Tn*916*-like coupling sequences (Chancey et al., 2015a). The genes required for Mega transposition may be present on other conjugative elements of the pneumococcal genome and in non-*S. pneumoniae* commensal organisms (Gay and Stephens, 2001; Chancey et al., 2015a). While Mega is infrequently transferred through transposition, once stabilized in the genome Mega is widely disseminated through horizontal DNA exchange and homologous recombination.

Tn*916* is the prototype conjugative transposon that contains the tetracycline resistance gene *tet*(M), and is found in many Gram-positive bacteria. Tn*916* may incorporate additional antibiotic resistance determinants which comprise larger Tn*916*-like composite elements (Roberts and Mullany, 2011). The history and molecular mechanisms of the Tn*916* family are beyond the scope of this review, but have been explored previously (Roberts and Mullany, 2009). The most common Tn*916*-like elements in *S. pneumoniae* containing erythromycin resistance cassettes include Tn*2009*, Tn*6002*, and Tn*2010* (Chancey et al., 2015a). Tn*2009* is a Tn*916*-like element with Mega inserted into *orf6* of Tn*916* to provide macrolide resistance, the M phenotype (Del Grosso et al., 2004). Tn*6002* is also a Tn*916*-like element with macrolide resistance, with a MLS_B phenotype due to the incorporation of an *erm*(B)-containing element into *orf20* of Tn*916* (Brenciani et al., 2007). The *erm*(B) gene may also be incorporated into Tn*916*. Tn*917*, an *erm*(B)-containing transposon insertion into *orf9* of Tn*916* creates Tn*3872* (Brenciani et al., 2007). *S. pneumoniae* with the dual macrolide resistance genotype most often contain Tn*2010* or rarely the newly described element Tn*2017* (Del Grosso et al., 2009). Tn*2010* is a Tn*916*-like element with Mega in *orf6* and the *erm*(B) element in *orf20* of Tn*916* (Del Grosso et al., 2007). Tn*2010* likely arose through the homologous recombination of Tn*2009* with Tn*6002* (Chancey et al., 2015a). A similar recombination event likely occurred with Tn*2009* and Tn*3872* to create Tn*2017*, which is a Tn*916*-like element with a Mega insertion in *orf6* and Tn*917* in *orf9* of Tn*916* (Del Grosso et al., 2009).

Interspecies Exchange of Macrolide Resistance

During the growth cycle, pneumococci develop a natural state of competence and can acquire DNA from the environment. A mechanism of DNA repair allows for integration of new DNA through homologous recombination (Straume et al., 2015). The human nasopharynx is the primary ecological niche for the pneumococcus during asymptomatic carriage (Simell et al., 2012), where *S. pneumoniae* has the opportunity to acquire DNA from other pneumococci and from commensal bacteria of the upper respiratory tract that may act as a reservoir for antibiotic resistance.

Other bacteria that reside in the human upper respiratory tract carry the macrolide resistance genes. Tn*6002* is the most common *erm*(B)-containing mobile genetic element of *S. pyogenes* (Brenciani et al., 2007). A recent study found Mega, Tn*2009*, Tn*6002*, and Tn*2010* in commensal viridans group streptococci isolated from the human oropharynx (Brenciani et al., 2014). In this study, *S. mitis* was the most commonly isolated streptococcal species with the macrolide resistance elements. Other Gram-positive bacteria have been shown to carry *erm*(B) and/or *mef*(E) (Luna et al., 1999; Seppälä et al., 2003; Santoro et al., 2014). The Tn*2009* element has been found in commensal, Gram-negative *Acinetobacter junii*, and there is evidence of this Mega-containing transposon in other Gram-negative species including *E. coli*, *Enterobacter cloacae*, *Klebsiella* sp., *Proteus* sp., and *Pseudomonas* sp. (Ojo et al., 2006). Interspecies dissemination of mobile genetic elements containing antibiotic resistance cassettes appears common.

Asymptomatic pneumococcal carriage occurs in children and adults with rates in children ranging from <15% to >90% in developing countries (Shak et al., 2013). Carriage varies based on factors including geography and socioeconomic class (O'Brien and Nohynek, 2003; Simell et al., 2012). During nasopharyngeal carriage, *S. pneumoniae* forms biofilms that enhance natural transformation (Chao et al., 2014) and genetic exchange during co-colonization by two pneumococcal strains is efficient with transformation efficiencies up to 10^{-2} (Marks et al., 2012). This environment may have allowed for the dissemination of macrolide resistance determinants including the assembly and selection of the dual macrolide resistance elements, e.g., Tn*2017* and the more common Tn*2010* (discussed above).

IMPACT OF PNEUMOCOCCAL CONJUGATE VACCINES ON MACROLIDE RESISTANCE

Between 1994 and 1999, macrolide-resistant invasive pneumococcal disease (MR-IPD) rapidly emerged in the US largely due infections caused by isolates containing *mef*(E)/*mel* (Gay et al., 2000; Stephens et al., 2005). Introduction of PCV-7 in 2000 significantly reduced the incidence of MR-IPD in the US as the highest rates of macrolide resistance were present in PCV-7 vaccine serotypes (Stephens et al., 2005; Rudolph et al., 2013; Hawkins et al., 2015). Similar vaccine specific reductions were observed worldwide, which was observed in Germany through

the reduction of *mef*(A)-containing serotype 14 (ST9) isolates (Bley et al., 2011; Imöhl et al., 2015). The incidence of MR-IPD from 2002 through 2009 stabilized while macrolide-resistant PCV-7 serotypes continued to decline; this decline was offset by the rapid emergence of macrolide-resistant serotypes not covered by PCV-7, specifically serotype 19A, ST320 (formerly CC271; Del Grosso et al., 2007; Bowers et al., 2012; Chancey et al., 2015a).

The incidence of MR-IPD caused by serotype 19A isolates with the dual macrolide resistance phenotype (both *erm*(B) and *mef*(E)/*mel*) rapidly increased from 2003 through 2010 in the US and worldwide (Li et al., 2011; Quintero et al., 2011; Bowers et al., 2012; Sharma et al., 2013; Pan et al., 2015; Lyu et al., 2016). Selective pressure by PCV-7 and the continued high-level use of macrolides provided an opportunity for this 19A clone to expand worldwide. The introduction of PCV-13 in the later-2010, which contains serotype 19A, was successful in reducing carriage and IPD caused by vaccine serotypes including macrolide-resistant serotype 19A isolates (Desai et al., 2015; Imöhl et al., 2015). Overall, pneumococcal conjugate vaccination has yielded sustained reductions in pneumococcal disease (Pilishvili et al., 2010). Despite challenges with serotype replacement, PCVs are an effective intervention in reducing the incidence of disease caused by macrolide-resistant pneumococcal serotypes contained in the vaccine. Continued expansion of pediatric pneumococcal vaccination into developing countries is predicted to greatly reduce the global burden of pneumococcal disease and antibiotic resistant pneumococci (Rodgers and Klugman, 2011).

CONCLUSIONS

Macrolide resistance rapidly emerged in *S. pneumoniae* in the early-1990s. The introduction and widespread use of semisynthetic macrolides including azithromycin and clarithromycin were important drivers of macrolide resistance in pneumococci. Macrolide resistance in *S. pneumoniae* is predominantly due to ribosomal methylation by the gene product encoded by *erm*(B) and macrolide efflux by a two-component efflux pump encoded by *mef*(E)/*mel* on the transformable genetic element Mega. Both of these macrolide resistance determinants are associated with larger composite elements (i.e., Tn*6002* and Tn*2009*) and can be found on the same element. PCVs are effective in reducing macrolide resistance caused by vaccine serotypes and thus have been effective in the reduction of MR-IPD caused by vaccine strains. But "serotype replacement" has been an issue (e.g., 19A) and emergence of macrolide resistance in new serotypes is a concern. Continued research is needed to better understand the mechanism of macrolide efflux by Mef(E)/Mel, the emergence of genetic elements containing both *erm*(B) and *mef*(E)/*mel*, and to continue surveillance to monitor new changes in macrolide resistance in pneumococci.

AUTHOR CONTRIBUTIONS

MS wrote the paper and MS and DS developed and edited the paper.

FUNDING

The work was supported by Emory University (Ph. D. thesis).

ACKNOWLEDGMENTS

Thanks to Yih-Ling Tzeng and Sarah Satola for discussions of macrolide resistance and Valaria Cantos and Jeffery Collins for clinical insight.

REFERENCES

Ambrose, K. D., Nisbet, R., and Stephens, D. S. (2005). Macrolide efflux in *Streptococcus pneumoniae* is mediated by a dual efflux pump (*mel* and *mef*) and is erythromycin inducible. *Antimicrob. Agents Chemother.* 49, 4203–4209. doi: 10.1128/AAC.49.10.4203-4209.2005

Azadegan, A., Ahmadi, A., Lari, A. R., and Talebi, M. (2015). Detection of the efflux-mediated erythromycin resistance transposon in *Streptococcus pneumoniae*. *Ann. Lab. Med.* 35, 57–61. doi: 10.3343/alm.2015.35.1.57

Bergman, M., Huikko, S., Huovinen, P., Paakkari, P., and Seppälä, H. (2006). Macrolide and azithromycin use are linked to increased macrolide resistance in *Streptococcus pneumoniae*. *Antimicrob. Agents Chemother.* 50, 3646–3650. doi: 10.1128/AAC.00234-06

Bley, C., Van Der Linden, M., and Reinert, R. R. (2011). *mef*(A) is the predominant macrolide resistance determinant in *Streptococcus pneumoniae* and *Streptococcus pyogenes* in Germany. *Int. J. Antimicrob. Agents* 37, 425–431. doi: 10.1016/j.ijantimicag.2011.01.019

Bowers, J. R., Driebe, E. M., Nibecker, J. L., Wojack, B. R., Sarovich, D. S., Wong, A. H., et al. (2012). Dominance of multidrug resistant CC271 clones in macrolide-resistant *Streptococcus pneumoniae* in Arizona. *BMC Microbiol.* 12:12. doi: 10.1186/1471-2180-12-12

Brenciani, A., Bacciaglia, A., Vecchi, M., Vitali, L. A., Varaldo, P. E., and Giovanetti, E. (2007). Genetic elements carrying *erm*(B) in *Streptococcus pyogenes* and association with *tet*(M) tetracycline resistance gene. *Antimicrob. Agents Chemother.* 51, 1209–1216. doi: 10.1128/AAC.01484-06

Brenciani, A., Tiberi, E., Tili, E., Mingoia, M., Palmieri, C., Varaldo, P. E., et al. (2014). Genetic determinants and elements associated with antibiotic resistance in viridans group streptococci. *J. Antimicrob. Chemother.* 69, 1197–1204. doi: 10.1093/jac/dkt495

Caierão, J., Hawkins, P., Sant'anna, F. H., Da Cunha, G. R., D'azevedo, P. A., Mcgee, L., et al. (2014). Serotypes and genotypes of invasive *Streptococcus pneumoniae* before and after PCV10 implementation in southern Brazil. *PLoS ONE* 9:e111129. doi: 10.1371/journal.pone.0111129

Camilli, R., Del Grosso, M., Iannelli, F., and Pantosti, A. (2008). New genetic element carrying the erythromycin resistance determinant *erm*(TR) in *Streptococcus pneumoniae*. *Antimicrob. Agents Chemother.* 52, 619–625. doi: 10.1128/AAC.01081-07

Chancey, S. T., Agrawal, S., Schroeder, M. R., Farley, M. M., Tettelin, H., and Stephens, D. S. (2015a). Composite mobile genetic elements disseminating macrolide resistance in *Streptococcus pneumoniae*. *Front. Microbiol.* 6:26. doi: 10.3389/fmicb.2015.00026

Chancey, S. T., Bai, X., Kumar, N., Drabek, E. F., Daugherty, S. C., Colon, T., et al. (2015b). Transcriptional attenuation controls macrolide inducible efflux and resistance in *Streptococcus pneumoniae* and in other Gram-positive bacteria containing *mef*/*mel*(*msr*(D)) elements. *PLoS ONE* 10:e0116254. doi: 10.1371/journal.pone.0116254

Chancey, S. T., Zähner, D., and Stephens, D. S. (2012). Acquired inducible antimicrobial resistance in Gram-positive bacteria. *Future Microbiol.* 7, 959–978. doi: 10.2217/fmb.12.63

Chancey, S. T., Zhou, X., Zähner, D., and Stephens, D. S. (2011). Induction of efflux-mediated macrolide resistance in *Streptococcus pneumoniae*. *Antimicrob. Agents Chemother.* 55, 3413–3422. doi: 10.1128/AAC.00060-11

Chao, Y., Marks, L. R., Pettigrew, M. M., and Hakansson, A. P. (2014). *Streptococcus pneumoniae* biofilm formation and dispersion during colonization and disease. *Front. Cell. Infect. Microbiol.* 4:194. doi: 10.3389/fcimb.2014.00194

Chiba, N., Morozumi, M., Shouji, M., Wajima, T., Iwata, S., and Ubukata, K. (2014). Changes in capsule and drug resistance of Pneumococci after introduction of PCV7, Japan, 2010-2013. *Emerging Infect. Dis.* 20, 1132–1139. doi: 10.3201/eid2007.131485

Chittum, H. S., and Champney, W. S. (1994). Ribosomal protein gene sequence changes in erythromycin-resistant mutants of *Escherichia coli*. *J. Bacteriol.* 176, 6192–6198.

Cochetti, I., Vecchi, M., Mingoia, M., Tili, E., Catania, M. R., Manzin, A., et al. (2005). Molecular characterization of pneumococci with efflux-mediated erythromycin resistance and identification of a novel mef gene subclass, *mef*(I). *Antimicrob. Agents Chemother.* 49, 4999–5006. doi: 10.1128/AAC.49.12.4999-5006.2005

Corso, A., Severina, E. P., Petruk, V. F., Mauriz, Y. R., and Tomasz, A. (1998). Molecular characterization of penicillin-resistant *Streptococcus pneumoniae* isolates causing respiratory disease in the United States. *Microb. Drug Resist.* 4, 325–337. doi: 10.1089/mdr.1998.4.325

Daoud, Z., Kourani, M., Saab, R., Nader, M. A., and Hajjar, M. (2011). Resistance of *Streptococcus pneumoniae* isolated from Lebanese patients between 2005 and 2009. *Rev. Esp. Quimioter.* 24, 84–90.

De La Pedrosa, E. G., Baquero, F., Loza, E., Nadal-Serrano, J. M., Fenoll, A., Del Campo, R., et al. (2009). High clonal diversity in erythromycin-resistant *Streptococcus pneumoniae* invasive isolates in Madrid, Spain (2000-07). *J. Antimicrob. Chemother.* 64, 1165–1169. doi: 10.1093/jac/dkp364

Del Grosso, M., Camilli, R., Iannelli, F., Pozzi, G., and Pantosti, A. (2006). The *mef*(E)-carrying genetic element (mega) of *Streptococcus pneumoniae*: insertion sites and association with other genetic elements. *Antimicrob. Agents Chemother.* 50, 3361–3366. doi: 10.1128/AAC.00277-06

Del Grosso, M., Camilli, R., Libisch, B., Füzi, M., and Pantosti, A. (2009). New composite genetic element of the Tn*916* family with dual macrolide resistance genes in a *Streptococcus pneumoniae* isolate belonging to clonal complex 271. *Antimicrob. Agents Chemother.* 53, 1293–1294. doi: 10.1128/AAC.01066-08

Del Grosso, M., Northwood, J. G., Farrell, D. J., and Pantosti, A. (2007). The macrolide resistance genes *erm*(B) and *mef*(E) are carried by Tn*2010* in dual-gene *Streptococcus pneumoniae* isolates belonging to clonal complex CC271. *Antimicrob. Agents Chemother.* 51, 4184–4186. doi: 10.1128/AAC.00598-07

Del Grosso, M., Scotto D'abusco, A., Iannelli, F., Pozzi, G., and Pantosti, A. (2004). Tn*2009*, a Tn*916*-like element containing *mef*(E) in *Streptococcus pneumoniae*. *Antimicrob. Agents Chemother.* 48, 2037–2042. doi: 10.1128/AAC.48.6.2037-2042.2004

Desai, A. P., Sharma, D., Crispell, E. K., Baughman, W., Thomas, S., Tunali, A., et al. (2015). Decline in pneumococcal nasopharyngeal carriage of vaccine serotypes after the introduction of the 13-valent pneumococcal conjugate vaccine in children in Atlanta, Georgia. *Pediatr. Infect. Dis. J.* 34, 1168–1174. doi: 10.1097/INF.0000000000000849

Diawara, I., Zerouali, K., Katfy, K., Barguigua, A., Belabbes, H., Timinouni, M., et al. (2016). Phenotypic and genotypic characterization of *Streptococcus pneumoniae* resistant to macrolide in Casablanca, Morocco. *Infect. Genet. Evol.* 40, 200–204. doi: 10.1016/j.meegid.2016.03.003

Diner, E. J., and Hayes, C. S. (2009). Recombineering reveals a diverse collection of ribosomal proteins L4 and L22 that confer resistance to macrolide antibiotics. *J. Mol. Biol.* 386, 300–315. doi: 10.1016/j.jmb.2008.12.064

Farrell, D. J., Couturier, C., and Hryniewicz, W. (2008). Distribution and antibacterial susceptibility of macrolide resistance genotypes in *Streptococcus pneumoniae*: PROTEKT Year 5 (2003-2004). *Int. J. Antimicrob. Agents* 31, 245–249. doi: 10.1016/j.ijantimicag.2007.10.022

Franceschi, F., Kanyo, Z., Sherer, E. C., and Sutcliffe, J. (2004). Macrolide resistance from the ribosome perspective. *Curr. Drug Targets Infect. Disord.* 4, 177–191. doi: 10.2174/1568005043340740

Gay, K., Baughman, W., Miller, Y., Jackson, D., Whitney, C. G., Schuchat, A., et al. (2000). The emergence of *Streptococcus pneumoniae* resistant to macrolide antimicrobial agents: a 6-year population-based assessment. *J. Infect. Dis.* 182, 1417–1424. doi: 10.1086/315853

Gay, K., and Stephens, D. S. (2001). Structure and dissemination of a chromosomal insertion element encoding macrolide efflux in *Streptococcus pneumoniae*. *J. Infect. Dis.* 184, 56–65. doi: 10.1086/321001

Geng, Q., Zhang, T., Ding, Y., Tao, Y., Lin, Y., Wang, Y., et al. (2014). Molecular characterization and antimicrobial susceptibility of *Streptococcus pneumoniae* isolated from children hospitalized with respiratory infections in Suzhou, China. *PLoS ONE* 9:e93752. doi: 10.1371/journal.pone.0093752

Grivea, I. N., Sourla, A., Ntokou, E., Chryssanthopoulou, D. C., Tsantouli, A. G., and Syrogiannopoulos, G. A. (2012). Macrolide resistance determinants among *Streptococcus pneumoniae* isolates from carriers in Central Greece. *BMC Infect. Dis.* 12:255. doi: 10.1186/1471-2334-12-255

Gupta, P., Sothiselvam, S., Vázquez-Laslop, N., and Mankin, A. S. (2013). Deregulation of translation due to post-transcriptional modification of rRNA explains why erm genes are inducible. *Nat. Commun.* 4:1984. doi: 10.1038/ncomms2984

Hawkins, P. A., Chochua, S., Jackson, D., Beall, B., and Mcgee, L. (2015). Mobile elements and chromosomal changes associated with MLS resistance phenotypes of invasive pneumococci recovered in the United States. *Microb. Drug Resist.* 21, 121–129. doi: 10.1089/mdr.2014.0086

Hicks, L. A., Bartoces, M. G., Roberts, R. M., Suda, K. J., Hunkler, R. J., Taylor, T. H. Jr., et al. (2015). US outpatient antibiotic prescribing variation according to geography, patient population, and provider specialty in 2011. *Clin. Infect. Dis.* 60, 1308–1316. doi: 10.1093/cid/civ076

Hidalgo, M., Santos, C., Duarte, C., Castañeda, E., and Agudelo, C. I. (2011). [Increase in erythromycin-resistant *Streptococcus pneumoniae* in Colombia, 1994-2008]. *Biomedica* 31, 124–131. doi: 10.7705/biomedica.v31i1.343

Imöhl, M., Reinert, R. R., and Van Der Linden, M. (2015). Antibiotic susceptibility rates of invasive pneumococci before and after the introduction of pneumococcal conjugate vaccination in Germany. *Int. J. Med. Microbiol.* 305, 776–783. doi: 10.1016/j.ijmm.2015.08.031

Jenkins, S. G., Brown, S. D., and Farrell, D. J. (2008). Trends in antibacterial resistance among *Streptococcus pneumoniae* isolated in the USA: update from PROTEKT US Years 1–4. *Ann. Clin. Microbiol. Antimicrob.* 7:1. doi: 10.1186/1476-0711-7-1

Johnston, N. J., De Azavedo, J. C., Kellner, J. D., and Low, D. E. (1998). Prevalence and characterization of the mechanisms of macrolide, lincosamide, and streptogramin resistance in isolates of *Streptococcus pneumoniae*. *Antimicrob. Agents Chemother.* 42, 2425–2426.

Kannan, K., and Mankin, A. S. (2011). Macrolide antibiotics in the ribosome exit tunnel: species-specific binding and action. *Ann. N. Y. Acad. Sci.* 1241, 33–47. doi: 10.1111/j.1749-6632.2011.06315.x

Kawaguchiya, M., Urushibara, N., Ghosh, S., Kuwahara, O., Morimoto, S., Ito, M., et al. (2014). Serotype distribution and susceptibility to penicillin and erythromycin among noninvasive or colonization isolates of *Streptococcus pneumoniae* in northern Japan: a cross-sectional study in the pre-PCV7 routine immunization period. *Microb. Drug Resist.* 20, 456–465. doi: 10.1089/mdr.2013.0196

Keenan, J. D., Klugman, K. P., Mcgee, L., Vidal, J. E., Chochua, S., Hawkins, P., et al. (2015). Evidence for clonal expansion after antibiotic selection pressure: pneumococcal multilocus sequence types before and after mass azithromycin treatments. *J. Infect. Dis.* 211, 988–994. doi: 10.1093/infdis/jiu552

Kim, S. H., Song, J. H., Chung, D. R., Thamlikitkul, V., Yang, Y., Wang, H., et al. (2012). Changing trends in antimicrobial resistance and serotypes of *Streptococcus pneumoniae* isolates in Asian countries: an Asian Network for Surveillance of Resistant Pathogens (ANSORP) study. *Antimicrob. Agents Chemother.* 56, 1418–1426. doi: 10.1128/AAC.05658-11

Kirst, H. A. (2010). New macrolide, lincosaminide and streptogramin B antibiotics. *Expert Opin. Ther. Pat.* 20, 1343–1357. doi: 10.1517/13543776.2010.505921

Klugman, K. P. (2002). Bacteriological evidence of antibiotic failure in pneumococcal lower respiratory tract infections. *Eur. Respir. J. Suppl.* 36, 3s–8s. doi: 10.1183/09031936.02.00400402

Li, Y., Tomita, H., Lv, Y., Liu, J., Xue, F., Zheng, B., et al. (2011). Molecular characterization of *erm*(B)- and *mef*(E)-mediated erythromycin-resistant

Streptococcus pneumoniae in China and complete DNA sequence of Tn*2010*. *J. Appl. Microbiol.* 110, 254–265. doi: 10.1111/j.1365-2672.2010.04875.x

Lismond, A., Carbonnelle, S., Verhaegen, J., Schatt, P., De Bel, A., Jordens, P., et al. (2012). Antimicrobial susceptibility of *Streptococcus pneumoniae* isolates from vaccinated and non-vaccinated patients with a clinically confirmed diagnosis of community-acquired pneumonia in Belgium. *Int. J. Antimicrob. Agents* 39, 208–216. doi: 10.1016/j.ijantimicag.2011.11.011

Lonks, J. R., Garau, J., Gomez, L., Xercavins, M., Ochoa De Echagüen, A., Gareen, I. F., et al. (2002). Failure of macrolide antibiotic treatment in patients with bacteremia due to erythromycin-resistant *Streptococcus pneumoniae*. *Clin. Infect. Dis.* 35, 556–564. doi: 10.1086/341978

Luna, V. A., Coates, P., Eady, E. A., Cove, J. H., Nguyen, T. T., and Roberts, M. C. (1999). A variety of gram-positive bacteria carry mobile *mef* genes. *J. Antimicrob. Chemother.* 44, 19–25. doi: 10.1093/jac/44.1.19

Lyu, S., Yao, K.-H., Dong, F., Xu, B.-P., Liu, G., Wang, Q., et al. (2016). Vaccine serotypes of *Streptococcus pneumoniae* with high-level antibiotic resistance isolated more frequently seven years after the licensure of PCV7 in Beijing. *Pediatr. Infect. Dis. J.* 35, 316–321. doi: 10.1097/INF.0000000000001000

Ma, X., Yao, K.-H., Xie, G.-L., Zheng, Y.-J., Wang, C.-Q., Shang, Y. X., et al. (2013). Characterization of erythromycin-resistant *Streptococcus pneumoniae* isolates causing invasive diseases in Chinese children. *Chin. Med. J.* 126, 1522–1527. doi: 10.3760/cma.j.issn.0366-6999.20122185

Malhotra-Kumar, S., Lammens, C., Coenen, S., Van Herck, K., and Goossens, H. (2007). Effect of azithromycin and clarithromycin therapy on pharyngeal carriage of macrolide-resistant streptococci in healthy volunteers: a randomised, double-blind, placebo-controlled study. *Lancet* 369, 482–490. doi: 10.1016/S0140-6736(07)60235-9

Marks, L. R., Reddinger, R. M., and Hakansson, A. P. (2012). High levels of genetic recombination during nasopharyngeal carriage and biofilm formation in *Streptococcus pneumoniae*. *MBio* 3:e00200-12. doi: 10.1128/mBio.00200-12

Mayanskiy, N., Alyabieva, N., Ponomarenko, O., Lazareva, A., Katosova, L., Ivanenko, A., et al. (2014). Serotypes and antibiotic resistance of non-invasive *Streptococcus pneumoniae* circulating in pediatric hospitals in Moscow, Russia. *Int. J. Infect. Dis.* 20, 58–62. doi: 10.1016/j.ijid.2013.11.005

McGuire, J. M., Bunch, R. L., Anderson, R. C., Boaz, H. E., Flynn, E. H., and Powell, H. M. (1952). 'Ilotycin,' a new antibiotic. *Antibiot. Chemother.* 2, 281–283.

Min, Y. H., Kwon, A. R., Yoon, E. J., Shim, M. J., and Choi, E. C. (2008). Translational attenuation and mRNA stabilization as mechanisms of *erm*(B) induction by erythromycin. *Antimicrob. Agents Chemother.* 52, 1782–1789. doi: 10.1128/AAC.01376-07

Moore, M. R., Gertz, R. E. Jr., Woodbury, R. L., Barkocy-Gallagher, G. A., Schaffner, W., Lexau, C., et al. (2008). Population snapshot of emergent *Streptococcus pneumoniae* serotype 19A in the United States, 2005. *J. Infect. Dis.* 197, 1016–1027. doi: 10.1086/528996

Nielsen, K. L., Hammerum, A. M., Lambertsen, L. M., Lester, C. H., Arpi, M., Knudsen, J. D., et al. (2010). Characterization and transfer studies of macrolide resistance genes in *Streptococcus pneumoniae* from Denmark. *Scand. J. Infect. Dis.* 42, 586–593. doi: 10.3109/00365541003754451

Nishijima, T., Saito, Y., Aoki, A., Toriya, M., Toyonaga, Y., and Fujii, R. (1999). Distribution of *mefE* and *ermB* genes in macrolide-resistant strains of *Streptococcus pneumoniae* and their variable susceptibility to various antibiotics. *J. Antimicrob. Chemother.* 43, 637–643. doi: 10.1093/jac/43.5.637

Nunez-Samudio, V., and Chesneau, O. (2013). Functional interplay between the ATP binding cassette Msr(D) protein and the membrane facilitator superfamily Mef(E) transporter for macrolide resistance in *Escherichia coli*. *Res. Microbiol.* 164, 226–235. doi: 10.1016/j.resmic.2012.12.003

O'Brien, K. L., and Nohynek, H. (2003). Report from a WHO Working Group: standard method for detecting upper respiratory carriage of *Streptococcus pneumoniae*. *Pediatr. Infect. Dis. J.* 22, e1–e11. doi: 10.1097/01.inf.0000049347.42983.77

Ojo, K. K., Ruehlen, N. L., Close, N. S., Luis, H., Bernardo, M., Leitao, J., et al. (2006). The presence of a conjugative Gram-positive Tn*2009* in Gram-negative commensal bacteria. *J. Antimicrob. Chemother.* 57, 1065–1069. doi: 10.1093/jac/dkl094

Okade, H., Funatsu, T., Eto, M., Furuya, Y., Mizunaga, S., Nomura, N., et al. (2014). Impact of the pneumococcal conjugate vaccine on serotype distribution and susceptibility trends of pediatric non-invasive *Streptococcus pneumoniae* isolates in Tokai, Japan over a 5-year period. *J. Infect. Chemother.* 20, 423–428. doi: 10.1016/j.jiac.2014.03.010

Pan, F., Han, L., Huang, W., Tang, J., Xiao, S., Wang, C., et al. (2015). Serotype distribution, antimicrobial susceptibility, and molecular epidemiology of *Streptococcus pneumoniae* isolated from Children in Shanghai, China. *PLoS ONE* 10:e0142892. doi: 10.1371/journal.pone.0142892

Pilishvili, T., Lexau, C., Farley, M. M., Hadler, J., Harrison, L. H., Bennett, N. M., et al. (2010). Sustained reductions in invasive pneumococcal disease in the era of conjugate vaccine. *J. Infect. Dis.* 201, 32–41. doi: 10.1086/648593

Pokkunuri, I., and Champney, W. S. (2007). Characteristics of a 50S ribosomal subunit precursor particle as a substrate for *erm*E methyltransferase activity and erythromycin binding in *Staphylococcus aureus*. *RNA Biol.* 4, 147–153. doi: 10.4161/rna.4.3.5346

Quintero, B., Araque, M., Van Der Gaast-De Jongh, C., and Hermans, P. W. (2011). Genetic diversity of Tn*916*-related transposons among drug-resistant *Streptococcus pneumoniae* isolates colonizing healthy children in Venezuela. *Antimicrob. Agents Chemother.* 55, 4930–4932. doi: 10.1128/AAC.00242-11

Ramos, V., Duarte, C., Díaz, A., and Moreno, J. (2014). [Mobile genetic elements associated with erythromycin-resistant isolates of *Streptococcus pneumoniae* in Colombia]. *Biomedica* 34(Suppl. 1), 209–216. doi: 10.1590/S0120-41572014000500023

Reijtman, V., Gagetti, P., Faccone, D., Fossati, S., Sommerfleck, P., Hernández, C., et al. (2013). Macrolide resistance in *Streptococcus pneumoniae* isolated from Argentinian pediatric patients suffering from acute otitis media. *Rev. Argent. Microbiol.* 45, 262–266. doi: 10.1016/s0325-7541(13)70034-8

Roberts, A. P., and Mullany, P. (2009). A modular master on the move: the Tn*916* family of mobile genetic elements. *Trends Microbiol.* 17, 251–258. doi: 10.1016/j.tim.2009.03.002

Roberts, A. P., and Mullany, P. (2011). Tn*916*-like genetic elements: a diverse group of modular mobile elements conferring antibiotic resistance. *FEMS Microbiol. Rev.* 35, 856–871. doi: 10.1111/j.1574-6976.2011.00283.x

Roberts, M. C., Sutcliffe, J., Courvalin, P., Jensen, L. B., Rood, J., and Seppala, H. (1999). Nomenclature for macrolide and macrolide-lincosamide-streptogramin B resistance determinants. *Antimicrob. Agents Chemother.* 43, 2823–2830.

Rodgers, G. L., and Klugman, K. P. (2011). The future of pneumococcal disease prevention. *Vaccine* 29S, C43–C48. doi: 10.1016/j.vaccine.2011.07.047

Rudolph, K., Bulkow, L., Bruce, M., Zulz, T., Reasonover, A., Harker-Jones, M., et al. (2013). Molecular resistance mechanisms of macrolide-resistant invasive *Streptococcus pneumoniae* isolates from Alaska, 1986 to 2010. *Antimicrob. Agents Chemother.* 57, 5415–5422. doi: 10.1128/AAC.00319-13

Safari, D., Kuo, L.-C., Huang, Y.-T., Liao, C.-H., Sheng, W.-H., and Hsueh, P.-R. (2014). Increase in the rate of azithromycin-resistant *Streptococcus pneumoniae* isolates carrying the *erm*(B) and *mef*(A) genes in Taiwan, 2006–2010. *BMC Infect. Dis.* 14:704. doi: 10.1186/s12879-014-0704-z

Santoro, F., Vianna, M. E., and Roberts, A. P. (2014). Variation on a theme; an overview of the Tn*916*/Tn*1545* family of mobile genetic elements in the oral and nasopharyngeal streptococci. *Front. Microbiol.* 5:535. doi: 10.3389/fmicb.2014.00535

Schentag, J. J., Klugman, K. P., Yu, V. L., Adelman, M. H., Wilton, G. J., Chiou, C. C., et al. (2007). *Streptococcus pneumoniae* bacteraemia: pharmacodynamic correlations with outcome and macrolide resistance–a controlled study. *Int. J. Antimicrob. Agents* 30, 264–269. doi: 10.1016/j.ijantimicag.2007.04.013

Schuwirth, B. S., Borovinskaya, M. A., Hau, C. W., Zhang, W., Vila-Sanjurjo, A., Holton, J. M., et al. (2005). Structures of the bacterial ribosome at 3.5 A resolution. *Science* 310, 827–834. doi: 10.1126/science.1117230

Seiple, I. B., Zhang, Z., Jakubec, P., Langlois-Mercier, A., Wright, P. M., Hog, D. T., et al. (2016). A platform for the discovery of new macrolide antibiotics. *Nature* 533, 338–345. doi: 10.1038/nature17967

Seppälä, H., Haanperä, M., Al-Juhaish, M., Järvinen, H., Jalava, J., and Huovinen, P. (2003). Antimicrobial susceptibility patterns and macrolide resistance genes of viridans group streptococci from normal flora. *J. Antimicrob. Chemother.* 52, 636–644. doi: 10.1093/jac/dkg423

Setchanova, L. P., Alexandrova, A., Mitov, I., Nashev, D., and Kantardjiev, T. (2012). Serotype distribution and antimicrobial resistance of invasive *Streptococcus pneumoniae* isolates in Bulgaria before the introduction

of pneumococcal conjugate vaccine. *J. Chemother.* 24, 12–17. doi: 10.1179/1120009X12Z.0000000004

Shak, J. R., Vidal, J. E., and Klugman, K. P. (2013). Influence of bacterial interactions on pneumococcal colonization of the nasopharynx. *Trends Microbiol.* 21, 129–135. doi: 10.1016/j.tim.2012.11.005

Sharkey, L. K., Edwards, T. A., and O'neill, A. J. (2016). ABC-F proteins mediate antibiotic resistance through ribosomal protection. *MBio* 7:e01975. doi: 10.1128/mBio.01975-15

Sharma, D., Baughman, W., Holst, A., Thomas, S., Jackson, D., Da Gloria Carvalho, M., et al. (2013). Pneumococcal carriage and invasive disease in children before introduction of the 13-valent conjugate vaccine: comparison with the era before 7-valent conjugate vaccine. *Pediatr. Infect. Dis. J.* 32, e45–e53. doi: 10.1097/inf.0b013e3182788fdd

Siira, L., Rantala, M., Jalava, J., Hakanen, A. J., Huovinen, P., Kaijalainen, T., et al. (2009). Temporal trends of antimicrobial resistance and clonality of invasive *Streptococcus pneumoniae* isolates in Finland, 2002 to 2006. *Antimicrob. Agents Chemother.* 53, 2066–2073. doi: 10.1128/AAC.01464-08

Simell, B., Auranen, K., Käyhty, H., Goldblatt, D., Dagan, R., and O'brien, K. L. (2012). The fundamental link between pneumococcal carriage and disease. *Expert Rev. Vaccines* 11, 841–855. doi: 10.1586/erv.12.53

Sirekbasan, L., Gönüllü, N., Sirekbasan, S., Kuskucu, M., and Midilli, K. (2015). Phenotypes and genotypes of macrolide-resistant *Streptococcus pneumoniae*. *Balkan Med. J.* 32, 84–88. doi: 10.5152/balkanmedj.2015.15169

Skinner, R., Cundliffe, E., and Schmidt, F. J. (1983). Site of action of a ribosomal RNA methylase responsible for resistance to erythromycin and other antibiotics. *J. Biol. Chem.* 258, 12702–12706.

Stephens, D. S., Zughaier, S. M., Whitney, C. G., Baughman, W. S., Barker, L., Gay, K., et al. (2005). Incidence of macrolide resistance in *Streptococcus pneumoniae* after introduction of the pneumococcal conjugate vaccine: population-based assessment. *Lancet* 365, 855–863. doi: 10.1016/S0140-6736(05)71043-6

Straume, D., Stamsås, G. A., and Håvarstein, L. S. (2015). Natural transformation and genome evolution in *Streptococcus pneumoniae*. *Infect. Genet. Evol.* 33, 371–380. doi: 10.1016/j.meegid.2014.10.020

Swedan, S. F., Hayajneh, W. A., and Bshara, G. N. (2016). Genotyping and serotyping of macrolide and multidrug resistant *Streptococcus pneumoniae* isolated from carrier children. *Indian J. Med. Microbiol.* 34, 159–165. doi: 10.4103/0255-0857.176840

Syrogiannopoulos, G. A., Grivea, I. N., Tait-Kamradt, A., Katopodis, G. D., Beratis, N. G., Sutcliffe, J., et al. (2001). Identification of an *erm*(A) erythromycin resistance methylase gene in *Streptococcus pneumoniae* isolated in Greece. *Antimicrob. Agents Chemother.* 45, 342–344. doi: 10.1128/AAC.45.1.342-344.2001

Taha, N., Araj, G. F., Wakim, R. H., Kanj, S. S., Kanafani, Z. A., Sabra, A., et al. (2012). Genotypes and serotype distribution of macrolide resistant invasive and non-invasive *Streptococcus pneumoniae* isolates from Lebanon. *Ann. Clin. Microbiol. Antimicrob.* 11:2. doi: 10.1186/1476-0711-11-2

Tait-Kamradt, A., Clancy, J., Cronan, M., Dib-Hajj, F., Wondrack, L., Yuan, W., et al. (1997). *mefE* is necessary for the erythromycin-resistant M phenotype in *Streptococcus pneumoniae*. *Antimicrob. Agents Chemother.* 41, 2251–2255.

Vester, B., and Douthwaite, S. (2001). Macrolide resistance conferred by base substitutions in 23S rRNA. *Antimicrob. Agents Chemother.* 45, 1–12. doi: 10.1128/AAC.45.1.1-12.2001

Walker, C. L., Rudan, I., Liu, L., Nair, H., Theodoratou, E., Bhutta, Z. A., et al. (2013). Global burden of childhood pneumonia and diarrhoea. *Lancet* 381, 1405–1416. doi: 10.1016/S0140-6736(13)60222-6

Weisblum, B. (1995a). Erythromycin resistance by ribosome modification. *Antimicrob. Agents Chemother.* 39, 577–585.

Weisblum, B. (1995b). Insights into erythromycin action from studies of its activity as inducer of resistance. *Antimicrob. Agents Chemother.* 39, 797–805.

Wierzbowski, A. K., Boyd, D., Mulvey, M., Hoban, D. J., and Zhanel, G. G. (2005a). Expression of the *mef*(E) gene encoding the macrolide efflux pump protein increases in *Streptococcus pneumoniae* with increasing resistance to macrolides. *Antimicrob. Agents Chemother.* 49, 4635–4640. doi: 10.1128/AAC.49.11.4635-4640.2005

Wierzbowski, A. K., Karlowsky, J. A., Adam, H. J., Nichol, K. A., Hoban, D. J., Zhanel, G. G., et al. (2014). Evolution and molecular characterization of macrolide-resistant *Streptococcus pneumoniae* in Canada between 1998 and 2008. *J. Antimicrob. Chemother.* 69, 59–66. doi: 10.1093/jac/dkt332

Wierzbowski, A. K., Swedlo, D., Boyd, D., Mulvey, M., Nichol, K. A., Hoban, D. J., et al. (2005b). Molecular epidemiology and prevalence of macrolide efflux genes *mef*(A) and *mef*(E) in *Streptococcus pneumoniae* obtained in Canada from 1997 to 2002. *Antimicrob. Agents Chemother.* 49, 1257–1261. doi: 10.1128/AAC.49.3.1257-1261.2005

Wittmann, H. G., Stöffler, G., Apirion, D., Rosen, L., Tanaka, K., Tamaki, M., et al. (1973). Biochemical and genetic studies on two different types of erythromycin resistant mutants of *Escherichia coli* with altered ribosomal proteins. *Mol. Gen. Genet.* 127, 175–189. doi: 10.1007/BF00333665

Wolter, N., Smith, A. M., Farrell, D. J., Northwood, J. B., Douthwaite, S., and Klugman, K. P. (2008). Telithromycin resistance in *Streptococcus pneumoniae* is conferred by a deletion in the leader sequence of *erm*(B) that increases rRNA methylation. *Antimicrob. Agents Chemother.* 52, 435–440. doi: 10.1128/AAC.01074-07

Xiao, Y., Wei, Z., Shen, P., Ji, J., Sun, Z., Yu, H., et al. (2015). Bacterial-resistance among outpatients of county hospitals in China: significant geographic distinctions and minor differences between central cities. *Microbes Infect.* 17, 417–425. doi: 10.1016/j.micinf.2015.02.001

Xu, X., Cai, L., Xiao, M., Kong, F., Oftadeh, S., Zhou, F., et al. (2010). Distribution of serotypes, genotypes, and resistance determinants among macrolide-resistant *Streptococcus pneumoniae* isolates. *Antimicrob. Agents Chemother.* 54, 1152–1159. doi: 10.1128/AAC.01268-09

Zähner, D., Zhou, X., Chancey, S. T., Pohl, J., Shafer, W. M., and Stephens, D. S. (2010). Human antimicrobial peptide LL-37 induces MefE/Mel-mediated macrolide resistance in *Streptococcus pneumoniae*. *Antimicrob. Agents Chemother.* 54, 3516–3519. doi: 10.1128/AAC.01756-09

Zaman, S., Fitzpatrick, M., Lindahl, L., and Zengel, J. (2007). Novel mutations in ribosomal proteins L4 and L22 that confer erythromycin resistance in *Escherichia coli*. *Mol. Microbiol.* 66, 1039–1050. doi: 10.1111/j.1365-2958.2007.05975.x

Zhang, Y., Tatsuno, I., Okada, R., Hata, N., Matsumoto, M., Isaka, M., et al. (2016). Predominant role of *msr*(D) over *mef*(A) in macrolide resistance in *Streptococcus pyogenes*. *Microbiology* 162, 46–52. doi: 10.1099/mic.0.000206

Zhou, L., Yu, S.-J., Gao, W., Yao, K.-H., Shen, A. D., and Yang, Y.-H. (2011). Serotype distribution and antibiotic resistance of 140 pneumococcal isolates from pediatric patients with upper respiratory infections in Beijing, 2010. *Vaccine* 29, 7704–7710. doi: 10.1016/j.vaccine.2011.07.137

Conflict of Interest Statement: The authors declare that the research was conducted in the absence of any commercial or financial relationships that could be construed as a potential conflict of interest.

frontiers in Cellular and Infection Microbiology

ORIGINAL RESEARCH
published: 27 September 2016
doi: 10.3389/fcimb.2016.00104

Streptococcus pneumoniae Eradicates Preformed *Staphylococcus aureus* Biofilms through a Mechanism Requiring Physical Contact

Faidad Khan[1,2†], Xueqing Wu[1†], Gideon L. Matzkin[1], Mohsin A. Khan[2], Fuminori Sakai[1] and Jorge E. Vidal[1]*

[1] Hubert Department of Global Health at the Rollins School of Public Health, Emory University, Atlanta, GA, USA, [2] National Centre of Excellence in Molecular Biology, University of the Punjab, Lahore, Pakistan

Staphylococcus aureus (Sau) strains are a main cause of disease, including nosocomial infections which have been linked to the production of biofilms and the propagation of antibiotic resistance strains such as methicillin-resistant *Staphylococcus aureus* (MRSA). A previous study found that *Streptococcus pneumoniae* (Spn) strains kill planktonic cultures of Sau strains. In this work, we have further evaluated in detail the eradication of Sau biofilms and investigated ultrastructural interactions of the biofilmicidal effect. Spn strain D39, which produces the competence stimulating peptide 1 (CSP1), reduced Sau biofilms within 8 h of inoculation, while TIGR4, producing CSP2, eradicated Sau biofilms and planktonic cells within 4 h. Differences were not attributed to pherotypes as other Spn strains producing different pheromones eradicated Sau within 4 h. Experiments using Transwell devices, which physically separated both species growing in the same well, demonstrated that direct contact between Spn and Sau was required to efficiently eradicate Sau biofilms and biofilm-released planktonic cells. Physical contact-mediated killing of Sau was not related to production of hydrogen peroxide as an isogenic TIGR4Δ*spx*B mutant eradicated Sau bacteria within 4 h. Confocal micrographs confirmed eradication of Sau biofilms by TIGR4 and allowed us to visualize ultrastructural point of contacts between Sau and Spn. A time-course study further demonstrated spatial colocalization of Spn chains and Sau tetrads as early as 30 min post-inoculation (Pearson's coefficient >0.72). Finally, precolonized biofilms produced by Sau strain Newman, or MRSA strain USA300, were eradicated by mid-log phase cultures of washed TIGR4 bacteria within 2 h post-inoculation. In conclusion, Spn strains rapidly eradicate pre-colonized Sau aureus biofilms, including those formed by MRSA strains, by a mechanism(s) requiring bacterium-bacterium contact, but independent from the production of hydrogen peroxide.

Keywords: ***Staphylococcus aureus*, *Streptococcus pneumoniae*, biofilms, physical contact, eradication**

OPEN ACCESS

Edited by:
Eric Ghigo,
Centre National de la Recherche Scientifique, France

Reviewed by:
Fadi Bittar,
Aix-Marseille Université, France
Jean-Marc Ghigo,
Institut Pasteur, France
Eric Chabriere,
Aix-Marseille University, France

***Correspondence:**
Jorge E. Vidal
jvidalg@emory.edu

[†] These authors have contributed equally to this work.

Received: *09 May 2016*
Accepted: *01 September 2016*
Published: *27 September 2016*

Citation:
Khan F, Wu X, Matzkin GL, Khan MA, Sakai F and Vidal JE (2016) Streptococcus pneumoniae Eradicates Preformed Staphylococcus aureus Biofilms through a Mechanism Requiring Physical Contact. Front. Cell. Infect. Microbiol. 6:104. doi: 10.3389/fcimb.2016.00104

INTRODUCTION

Two important human pathogens, *Streptococcus pneumoniae* (Spn) and *Staphylococcus aureus* (Sau) persist by forming biofilms in the nasopharynx of healthy humans (Bogaert et al., 2004; Regev-Yochay et al., 2004; Bakaletz, 2007; Chien et al., 2013; Dunne et al., 2013; Shak et al., 2013, 2014; Vidal et al., 2013; Chao et al., 2014). Spn is a common childhood commensal, but also causes otitis media, pneumonia and severe diseases including bacteremia, septicemia, and meningitis (Regev-Yochay et al., 2004; Vidal et al., 2013). Spn, which displays nasopharyngeal carriage rates of up to 90% in children, shifts to a meshed biofilm structure which promotes its persistence in the nasopharynx, increases resistance to antibiotics and acts as a source of planktonic pneumococci, which infiltrate into other parts of the respiratory system (i.e., lungs), bloodstream, and spinal fluid to cause disease (Yarwood et al., 2004; Shak et al., 2013; Vidal et al., 2013; Gritzfeld et al., 2014).

Sau strains, including methicillin-resistant Sau strains (MRSA), colonize the nasopharynx, anterior nares, and skin in 30–50% of healthy individuals, but also produce a variety of infections involving the skin and soft tissue, the bloodstream, the respiratory system, and the skeletal system (Regev-Yochay et al., 2004, 2008; Yarwood et al., 2004; Chien et al., 2013; Dunne et al., 2013; Bhattacharya et al., 2015). Given its location in healthy individuals (i.e., skin), Sau can be easily transmitted in hospital environments, causing a variety of nosocomial infections. Sau-associated nosocomial infections are recognized for their strong ability to form biofilms on abiotic surfaces such as catheters, or indwelling devices. Once a biofilm is established, Sau tolerate concentrations of antimicrobials that would otherwise eradicate planktonic growth (Kiedrowski and Horswill, 2011; Bhattacharya et al., 2015).

Epidemiological studies in children, including those from our laboratory, have demonstrated a negative association for nasopharyngeal carriage of Spn and Sau strains, i.e., children carrying Spn strains in the nasopharynx are less likely to also carry Sau (Chien et al., 2013; Dunne et al., 2013). With the recent introduction of pneumococcal vaccines, this competition for the nasopharyngeal niche has been more evident. For example, a study by Bogaert et al. (2004) that included 3198 children from the Netherlands showed that those vaccinated against Spn experienced a decrease in carriage of Spn vaccine types with a subsequent increase in nasopharyngeal carriage of Sau (Bogaert et al., 2004). Similar evidences were provided by Regev-Yochay et al. (2004) and Chien et al. (2013), in the pre-vaccine era (Regev-Yochay et al., 2004; Chien et al., 2013).

The molecular mechanism(s) behind these epidemiological observations has been investigated without conclusive findings. A study by Regev-Yochay et al. (2006), for example, showed that Spn strains (e.g., Pn20 and TIGR4) interfere with the growth of planktonic cultures of Sau strain Newman by a mechanism likely involving the release of H_2O_2 into the supernatant (Regev-Yochay et al., 2006). Killing of Sau planktonic cultures by Spn strains was observed after 6 h of incubation and it was inhibited by the addition of catalase, or by incubating Sau with Spn mutant in the *spx*B gene which encodes for the enzyme producing H_2O_2 (i.e., Pn20Δ*spx*B, or TIGR4Δ*spx*B). In contrast, studies using a neonatal rat model of colonization demonstrated that Sau colonizes the nasal passages whether co-inoculated along with TIGR4 or with a TIGR4Δ*spx*B mutant (Margolis, 2009). Moreover, Margolis et al. (2010) showed, using a similar neonatal rat model, that Spn strain TIGR4 coexisted in the nasal epithelium along with Sau, whether Spn or Sau was already colonizing the nasal passages and the other strain was introduced (Margolis et al., 2010). The inconsistencies for the *in vitro* killing vs. co-existence in animal models have not yet been resolved.

Since Sau biofilms have been linked to the persistence of chronic infections that cannot otherwise be eradicated with available antimicrobials (Kiedrowski and Horswill, 2011; Bhattacharya et al., 2015), eradication of Sau biofilms has drawn considerable interest in the last few years. In this study, we have further investigated killing of Sau biofilms using different approaches, including those aimed to eradicate preformed biofilms. We have demonstrated at the ultrastructural level that physical contact is required for efficient killing of Sau by Spn; killing by physical contact eradicated Sau strains, including MRSA strain USA300, within 2 h post-inoculation. In support of these findings, washed bacteria more efficiently killed Sau biofilms than supernatant indicating that the mechanism is more complex than we originally thought. The molecular mechanism, however, warrants further development as complete eradication of Sau biofilms was rapidly achieved.

MATERIALS AND METHODS

Bacterial Strains and Culture Media

Spn and Sau strains utilized in this study are shown in **Table 1**. Spn strains were cultured on blood agar plates (BAP), or BAP with 25 μg/ml gentamicin, whereas Sau strains were grown on salt mannitol agar (SMA) plates or Luria-Bertani agar ([LBA] 1% tryptone [Becton- Dickinson], 0.5% yeast extract, 1% NaCl, and 1.5% agar [Becton-Dickinson]). Todd Hewitt broth containing 0.5% (w/v) yeast extract (THY) was utilized in all experiments.

Preparation of Inoculum for Experiments

Inoculum was prepared essentially as previously described (Vidal et al., 2011). Briefly, an overnight BAP (for Spn), or LBA (for Sau), culture was used to prepare a cell suspension in THY broth to an OD_{600} of ∼0.08. This suspension was incubated at 37°C in a 5% CO_2 atmosphere until the culture reached an OD_{600} of ∼0.2 (early-log phase). Then glycerol was added to give a final 10% (v/v) and stored at −80°C until used. An aliquot of these stocks was further diluted and plated to obtain bacterial counts (cfu/ml).

Co-incubation Experiments

Experiments were conducted using 8-well glass slide (Lab-Tek), polystyrene 6-well plates and 24-well plates (Corning). Spn and Sau strains were inoculated at a density of $\sim 1 \times 10^6$ cfu/ml each in THY and incubated at 37°C in a 5% CO_2 atmosphere for the indicated time. Control wells were only inoculated with Spn or Sau. Where indicated, bovine liver catalase (Sigma) was added to a final concentration of 1000 U/ml. Planktonic cells were removed, diluted and platted onto BAP or BAP with

TABLE 1 | Strains utilized in this study.

Strain	Description	Reference or source
D39	Avery strain, pherotype CSP1, clinical isolate capsular serotype 2	Avery et al., 1944; Lanie et al., 2007
TIGR4	Invasive clinical isolate, pherotype CSP2, capsular serotype 4	Tettelin et al., 2001
TIGR4Δ*spx*B	TIGR4 with an insertion within the *spx*B gene, *spxB*::*kan-rpsL*$^+$	Regev-Yochay et al., 2006
SPJV01	D39 encoding pMV158GFP, Tet^R	Vidal et al., 2011
SPJV09	TIGR4 encoding pMV158GFP, Tet^R	Vidal et al., 2013
GA13499	Phenotype CSP1, capsular serotype 19F	Kindly provided by Dr. Scott Chancey
A66.1	Phenotype CSP2, capsular serotype 3	Benton et al., 1997
S. aureus Newman	NCTC 8178, ATCC 13420	Boake, 1956
S. aureus ATCC 25923	Clinical isolate, utilized as quality control strain for antimicrobial susceptibility testing	Laboratory stock
S. aureus SAJV01	Strain isolated from a post-surgery knee infection in our laboratory at Emory University.	Laboratory stock
S. aureus USA300	NRSA384, methicillin-resistant strain isolated from a wound in Mississippi	Centers for Disease Control Prevention, 2003

gentamicin to obtain cfu/ml for Spn or onto LBA or SMA to obtain cfu/ml of Sau. Biofilms were washed once with PBS, mixed with with 1 ml of sterile PBS and sonicated for 15 s in a Bransonic ultrasonic water bath (Branson, Danbury, CT), followed by extensive pipetting to remove remaining attached biofilm bacteria. Biofilms were diluted and platted as above.

Experiments with Preformed Sau Biofilms

Sau was inoculated into a 6-well microplate and incubated at 37°C with 5% CO_2 for 4 h after which planktonic cells were removed and biofilms were washed once with sterile PBS. THY was added to the washed Sau biofilms and then these were inoculated with $\sim 1 \times 10^6$ cfu/ml of the early-log phase inoculum, prepared as described above, or with supernatants, planktonic cells, biofilms or washed bacteria obtained from 4 h cultures of Spn. These inoculants were prepared as follows: $\sim 1 \times 10^6$ cfu/ml of the early-log phase inoculum was inoculated into 6-well plates and incubated for 4 h. Planktonic cells were then removed, centrifuged, and washed twice with PBS. The supernatant was separated and filter sterilized using a 0.45 μm syringe filter (Puradisc, GE Healthcare, UK). Biofilms were harvested as mentioned earlier and washed twice with sterile PBS. In another set of wells, biofilms were detached by sonication, then both biofilms and planktonic cells were collected by centrifugation, and the pellet was washed twice with PBS. The same amount ($\sim 1 \times 10^6$ cfu/ml) of washed bacteria, planktonic cells, or biofilms were inoculated into preformed Sau biofilms; an aliquot of supernatant (100 μl) was inoculated as well. Inoculated and control cultures were incubated for 2 h at 37°C with 5% CO_2 after which bacteria were counted as described.

Transwell Experiments

To physically separate Spn and Sau within the same wells, two chambers were created by installing a Transwell filter device (Corning, NY USA). The Transwell membrane (0.4 μM) creates a physical barrier impermeable to bacteria, but allows passage of small molecules between the two chambers (top and bottom). In some experiments Spn was inoculated in the top chamber and Sau in the bottom chamber, whereas in other experiments bacteria were reversed, i.e., Sau in the top and Spn in the bottom. In control wells, which did not contain the Transwell device, Spn and Sau were inoculated together. Plates were incubated for 4 h at 37°C in a 5% CO_2 atmosphere and then planktonic and biofilm bacteria were removed from both the top and bottom chamber and counted.

Confocal Microscopy Studies

Spn, Sau, or Spn with Sau were inoculated ($\sim 1 \times 10^6$ cfu/ml each) into 8-well glass slide (Lab-Tek) containing THY and incubated at 37°C in a 5% CO_2 atmosphere. Planktonic cells were then removed, and biofilms were washed with sterile PBS, after which bacteria were fixed with 2% paraformaldehyde (PFA) for 15 min at room temperature. Fixed biofilms were then blocked with 1% BSA for 30 min at 37°C and incubated first with a rabbit polyclonal anti-Sau antibody (4 μg/ml) (Santa Cruz, Biotechnology Inc.,) for 1 h at room temperature, followed by PBS washes and 1-h incubation with a secondary Alexa-555, labeled goat anti-rabbit antibody (20 μg/ml) (Molecular probes). Then the preparation was washed with sterile PBS and incubated 30 min with rabbit raised anti-Spn antibodies (Staten Serum Institute) that had been previously labeled with Alexa-488 (50 μg/ml) (Molecular Probes) following the manufacturer instructions. In some experiments, Spn strains expressed the green fluorescent protein (GFP), SPJV01 or SPJV09. Stained preparations were finally washed two times with PBS, mounted with ProLong Diamond Antifade mountant with DAPI (Molecular Probes), and analyzed with an Olympus FV1000 confocal microscope. Confocal images were analyzed with ImageJ version 1.49k (National Institutes of Health, USA) or The Imaris software (Bitplane, South Windsor CT).

Colocalization Analysis

The Imaris 8.2 software (Bitplane) was utilized for colocalization analysis. Briefly, the Costes method was utilized to set up a threshold for both the green channel and the red channel in confocal slices of z-stacks images (Costes et al., 2004). The Pearson's coefficient (PC) of colocalized volume was calculated using ranges from −1 to 1 where a PC = −1 indicates a mutually exclusive localization of two signals, PC = 0 random overlap, and PC = 1 indicates perfect colocalization (Costes et al., 2004).

Counts of colocalized bacteria and free Sau bacteria was also performed with Imaris 8.2 software.

Statistical Analysis

Statistical analysis presented in this study was conducted using the Mann Whitney *U*-test and the software SigmaPlot Version 12.0 (Systat Software, Inc.).

RESULTS

Spn Strain TIGR4, but not D39, Kills Sau Biofilm Cells

Since epidemiological reports have suggested a negative association between Sau and Spn for nasopharyngeal colonization, we assessed populations of biofilm cells when strains where co-incubated on abiotic surfaces or cultures of human pharyngeal cells. This study showed similar counts of Sau biofilms attached to abiotic surfaces, or pharyngeal cells, whether incubated alone or with Spn strain D39 for 4 h (**Figures 1A,B**). However, Sau biofilms were significantly reduced, but not eradicated (i.e., completely killed), 8 h post-inoculation ($p = 0.03$) in wells inoculated along with D39 (**Figures 1A,B**). Bacterial counts of Spn biofilms did not change whether incubated alone or with Sau at 4 or 8 h post-inoculation (**Figures 1C,D**). A non-statistically significant decrease of Spn biomass was observed, however, when incubated with Sau at 4 or 8 h post-inoculation of abiotic or human cells, respectively.

Experiments with another Spn reference strain TIGR4, and Sau strain Newman, were also conducted. Whereas, Sau planktonic cells and biofilms reached, 4 h post-inoculation, a bacterial density of $\sim 4.6 \times 10^7$ cfu/ml and $\sim 9.8 \times 10^6$ cfu/ml, respectively, Sau planktonic cells and biofilms were eradicated (<50 cfu/ml) when they were incubated with strain TIGR4 for 4 h (**Figure 2A**). TIGR4 planktonic cells, or biofilms, remained unchanged whether incubated alone or with Sau for 4 h (**Figure 2B**). MRSA strain USA300, Sau ATCC 25923, SAJV01, were also challenged with TIGR4 for 4 h and eradication of both planktonic and biofilms was similarly observed (**Figures 2C,D** and not shown).

Since strain D39 produces the competence stimulating peptide 1 (CSP1) and TIGR4 produces CSP2, to further investigate if differences in killing of Sau was due to the quorum sensing pherotype (i.e., CSP1 or CSP2) we inoculated strains GA13499 (pherotype 1) or Spn A66.1 (pherotype 2) along with Sau and the mixtures were incubated for 4 h. Eradication of both Sau planktonic and Sau biofilms by both strains was observed indicating that Sau killing does not depend on the pneumococcal pherotype (not shown).

Direct Contact between Sau and Spn Is Required for Killing of Sau

To investigate whether Spn biofilm cells or their supernatants were responsible for the observed phenotype against Sau, strains were inoculated into the same wells, but bacteria were separated using a Transwell system device, which has a membrane with a pore size of 0.4 μm. The Transwell device allows the supernatants to flow throughout the well, but separates bacteria inoculated in the top chamber from those inoculated in the bottom of the well. Neither Sau planktonic cells (**Figure 3A**), nor biofilms (**Figure 3B**) were killed when TIGR4 was inoculated in the Transwell device and Sau was inoculated in the bottom of the well (i.e., Spn/Sau). Since the Transwell membrane has a smaller diameter than the bottom of the well, in another set of experiments we inoculated TIGR4 in the bottom of the well and Sau was inoculated directly in the Transwell chamber (i.e., Sau/Spn). Once again, TIGR4 was not able to kill Sau planktonic cells or Sau biofilms within 4 h (**Figures 3A,B**). TIGR4 planktonic cells and biofilms were similar, whether (1) coincubated with Sau (positive control), (2) inoculated in the Transwell chamber and Sau in the bottom or (3) in the bottom of the well when Sau was inoculated in the Transwell chamber (**Figure 3C**). Experiments were conducted using Transwell devices with different membrane areas (4.67 and 1.12 cm^2) to account for variations in the volume of culture medium obtaining similar results. Altogether, these experiments demonstrated that physical contact is necessary for Spn to kill Sau.

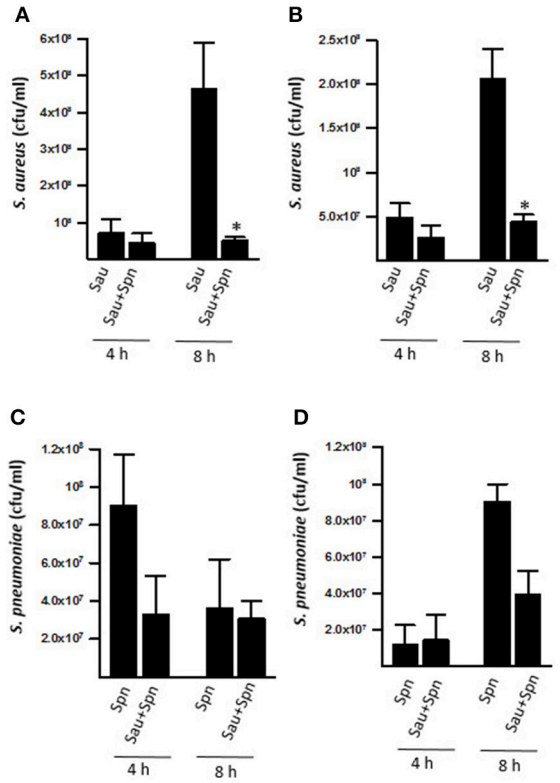

FIGURE 1 | Spn D39 reduces the population of Sau biofilms. Sau was inoculated alone (Sau) or with Spn strain D39 (Sau+Spn) in abiotic polystyrene plates **(A,C)** or human pharyngeal cells **(B,D)**. Plates were incubated for 4 or 8 h at 37°C. Planktonic cells were removed, biofilms were harvested, diluted and then plated onto salt mannitol agar plates to obtain Sau biofilm counts (cfu/ml) or blood agar plates with gentamicin to obtain Spn biofilm counts (cfu/ml). Error bars represent the standard errors of the means, calculated using data from at least three independent experiments. *statistical significance ($p < 0.05$) in comparison to wells inoculated only with Sau.

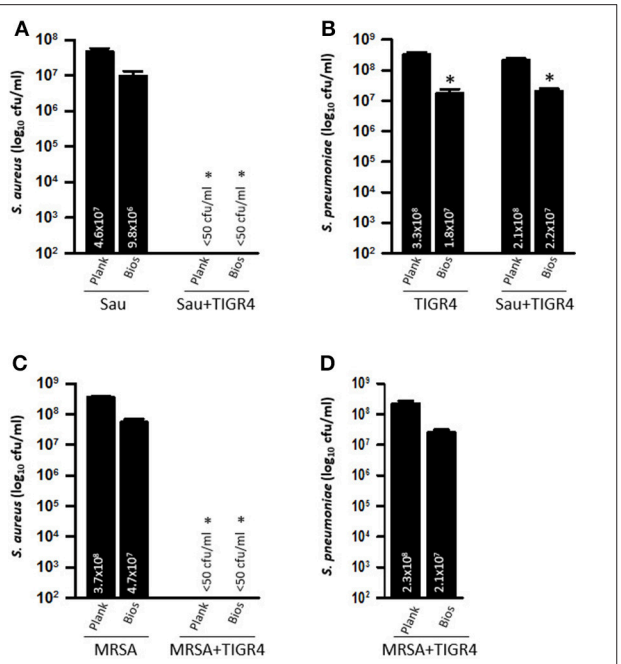

FIGURE 2 | Spn TIGR4 eradicates Sau biofilms produced by strain Newman and MRSA USA300. Sau strain Newman **(A,B)** or USA300 **(C,D)** was inoculated alone or with Spn strain TIGR4 and plates were incubated for 4 h at 37°C. Planktonic cells or biofilms were harvested, serially diluted and plated onto salt mannitol agar plates to obtain Sau counts or blood agar plates with gentamicin to obtain TIGR4 counts. Error bars represent the standard errors of the means calculated using data from at least three independent experiments. The median (cfu/ml) is shown inside the bars. *statistical significance ($p < 0.05$) in comparison to wells inoculated only with Sau.

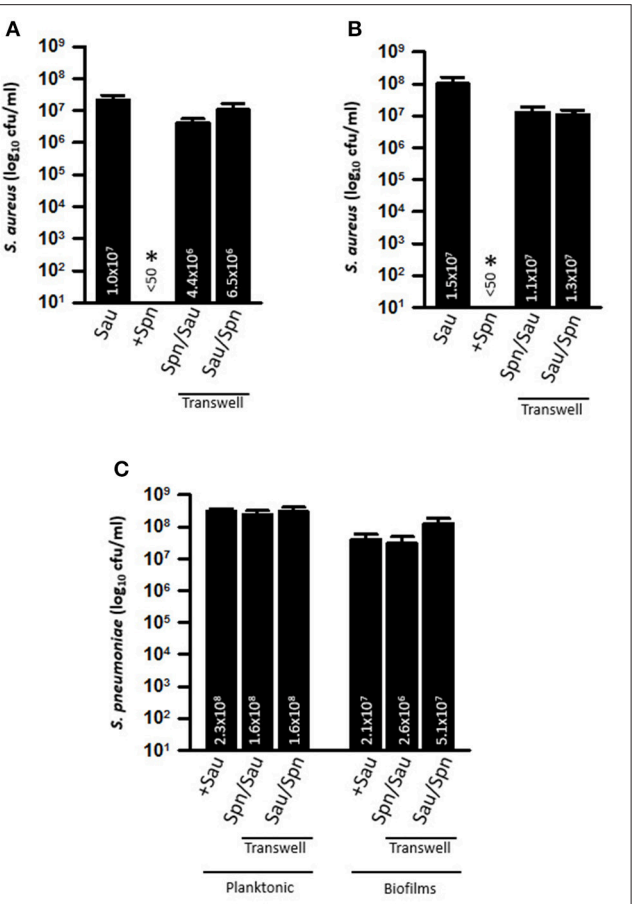

FIGURE 3 | Efficient Killing of Sau by Spn requires direct contact. Transwell chambers were installed into 6-well plates and THY was added. TIGR4 was inoculated directly in the Transwell chamber and Sau in the bottom of the well (Sp/Sau), or Sau was inoculated in the Transwell chamber and TIGR4 in the bottom (Sau/Spn). As a control Sau was inoculated alone or with TIGR4 (+Spn). Cultures were incubated for 4 h at 37°C, after which planktonic bacteria **(A)** or biofilms **(B)** were harvested from the Transwell chamber, or from the bottom of the well, serially diluted and plated onto salt mannitol agar plates. **(C)** Planktonic and biofilms were also plated onto BAP plates with gentamicin to obtain Spn counts. Error bars represent the standard errors of the means calculated using data from at least three independent experiments; the median (cfu/ml) is shown inside bars. *Statistical significance ($p < 0.05$) in comparison to wells inoculated with Sau.

Direct Killing of Sau by Spn Does not Require SpxB, but Is Inhibited by Catalase

Interference of planktonic cultures of Sau by Spn has been demonstrated to occur via hydrogen peroxide, a byproduct of the enzyme SpxB (Regev-Yochay et al., 2006). To investigate whether the observed physical contact-mediated killing requires hydrogen peroxide, we conducted experiments with an isogenic TIGR4Δ*spx*B mutant, which does not produce detectable levels of hydrogen peroxide (Regev-Yochay et al., 2006). As shown in **Figure 4A**, the hydrogen peroxide TIGR4Δ*spx*B mutant was able to eradicate Sau Newman strain within 4 h of incubation. The population of the isogenic mutant was not affected by co-incubation with Sau (**Figure 4B**).

We next incubated Sau and Spn in the presence of bovine liver catalase. In comparison to co-cultures incubated without catalase, incubation of TIGR4 wt with catalase inhibited killing of Sau (**Figure 5A**). To investigate whether the inhibitory effect of catalase was separate from its enzymatic activity against H_2O_2, the isogenic TIGR4Δ*spx*B mutant, which does not produce H_2O_2, was also incubated with catalase and this treatment was enough to render TIGR4Δ*spx*B unable to eradicate Sau bacteria (**Figure 5A**). Whereas, Spn density was similar whether incubated alone or with Sau (**Figure 5B**), we noticed that in control wells inoculated only with Sau, or Spn, and incubated in the presence of catalase, the bacterial density of both populations, planktonic and biofilms, significantly increased in comparison to wells incubated without the enzyme (**Figures 5A,B**).

Together, these experiments demonstrate that SpxB-generated hydrogen peroxide is not involved in the direct-killing of Sau. These experiments also indicate that the inhibitory effect of catalase is due to other changes induced by incubating with the enzyme, which are separate from catalase's enzymatic activity against H_2O_2.

Physical Interaction within Biofilms Formed by Sau and Spn

To gain insights on ultrastructural interactions between TIGR4, or D39, and Sau, we obtained confocal micrographs. At 4 h

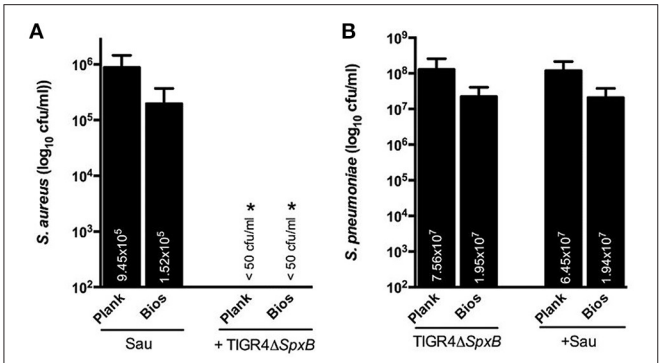

FIGURE 4 | TIGR4Δ*spx*B mutant eradicate Sau bacteria. Sau Newman strain was inoculated alone or with TIGR4Δ*spx*B and incubated for 4 h at 37°C. Planktonic cells or biofilms were harvested, serially diluted and plated onto salt mannitol agar plates to obtain Sau counts **(A)** or blood agar plates with gentamicin to obtain TIGR4Δ*spx*B counts **(B)**. Error bars represent the standard errors of the means calculated using data from at least three independent experiments. The median (cfu/ml) is shown inside bars. *statistical significance ($p < 0.05$) in comparison to wells inoculated only with Sau.

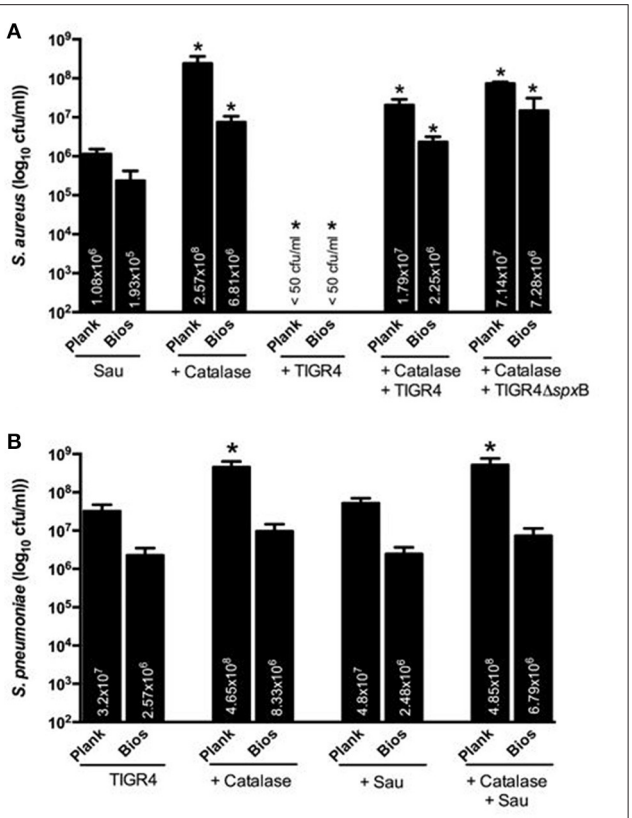

FIGURE 5 | Catalase inhibits Sau killing by Spn. Sau Newman strain was inoculated either alone, with catalase, with wt strain TIGR4, with TIGR4 and catalase or with TIGR4Δ*spx*B and catalase and incubated for 4 h at 37°C. Planktonic cells or biofilms were harvested, serially diluted and plated onto salt mannitol agar plates to obtain Sau counts **(A)** or blood agar plates with gentamicin to obtain TIGR4 **(B)**. Error bars represent the standard errors of the means calculated using data from at least three independent experiments. The median (cfu/ml) is shown inside bars. *statistical significance ($p < 0.05$) in comparison to wells inoculated only with Sau.

post-inoculation, control Sau biofilms were robust and covered ∼90% of the abiotic substrate (**Figure 6A**) whereas in wells co-incubated with TIGR4, Sau biofilms were eradicated (**Figure 6D**). The few Sau cells attached to the substratum appeared to be in close proximity to TIGR4 bacteria suggesting physical interaction between the two species (**Figure 6F**, arrows). TIGR4 biofilms remained similar whether co-incubated with Sau or incubated alone (**Figures 6B,E**). Biofilms formed by Sau, when co-incubated with D39, were reduced to ∼60% in comparison to control wells (**Figures 6G,I**). D39 biofilms were similarly observed whether incubated alone or with Sau (**Figures 6C,H**).

Given that TIGR4 killed Sau and MRSA strain USA300, a time course study was conducted to evaluate physical interactions in detail. As shown in **Figures 7A–D**, Sau rapidly formed aggregates, i.e., tetrads, at 1 h post-inoculation, which continued growing until forming a bacterial lawn 4 h later. TIGR4 formed chains that aggregated on the bottom of the well (**Figures 7E–H**) but did not produce, at this time-point, the robust bacterial lawn observed with Sau. When incubated with TIGR4, Sau biofilms were not produced. The few bacteria attached to the bottom were surrounded by TIGR4 (**Figures 7I–L**).

Spatial Ultrastructural Colocalization between Spn and Sau

Experiments showed above suggested that Sau and Spn colocalize; to further confirm physical colocalization, we stained the pneumococcal capsule and Sau capsule by fluorescence, and confocal micrographs were analyzed using the Imaris software. As shown in **Figure 8**, there was a spatial colocalization between Sau and TIGR4 bacteria as early as 1 h post-inoculation. The Pearson's coefficient (PC) of colocalized volume was 0.78, which statistically confirmed true spatial colocalization. TIGR4 surrounded Sau making contact with individual bacterium and those Sau bacteria forming tetrads (**Figures 8A–C**). Removing the channel of the Spn capsule (green), or Sau capsule (red), allowed us to better visualize specific points of contact (**Figure 8**, arrows in Sau+DNA and Spn+DNA). Colocalization between Sau and TIGR4 was also observed at 2 h post-inoculation (PC = 0.72) indicating bacteria remained joint (**Figures 8D–F**). Further analysis of more than 30 confocal micrographs demonstrated that most Sau bacteria are in contact with Spn (mean = 5.16, median = 4), in comparison to those Sau bacteria observed alone (mean = 1.2, median = 0.0; **Figure 8M**). Whereas, Spn strain D39 did not eradicate Sau biofilms, D39 bacteria were observed colocalizing with Sau at 1 h (PC = 0.73) or 2 h (PC = 0.89) post-inoculation (**Figures 8G–L**). In most cases a long chain of Spn made contact with tetrads or aggregates of Sau bacteria.

Pre-colonized Sau Is Eradicated by TIGR4, but not by Strain D39

We then tested whether pre-colonized Sau biofilms could be eradicated by Spn. To assess this, Sau was incubated for 4 h to form biofilms, after which planktonic cells were removed. Early

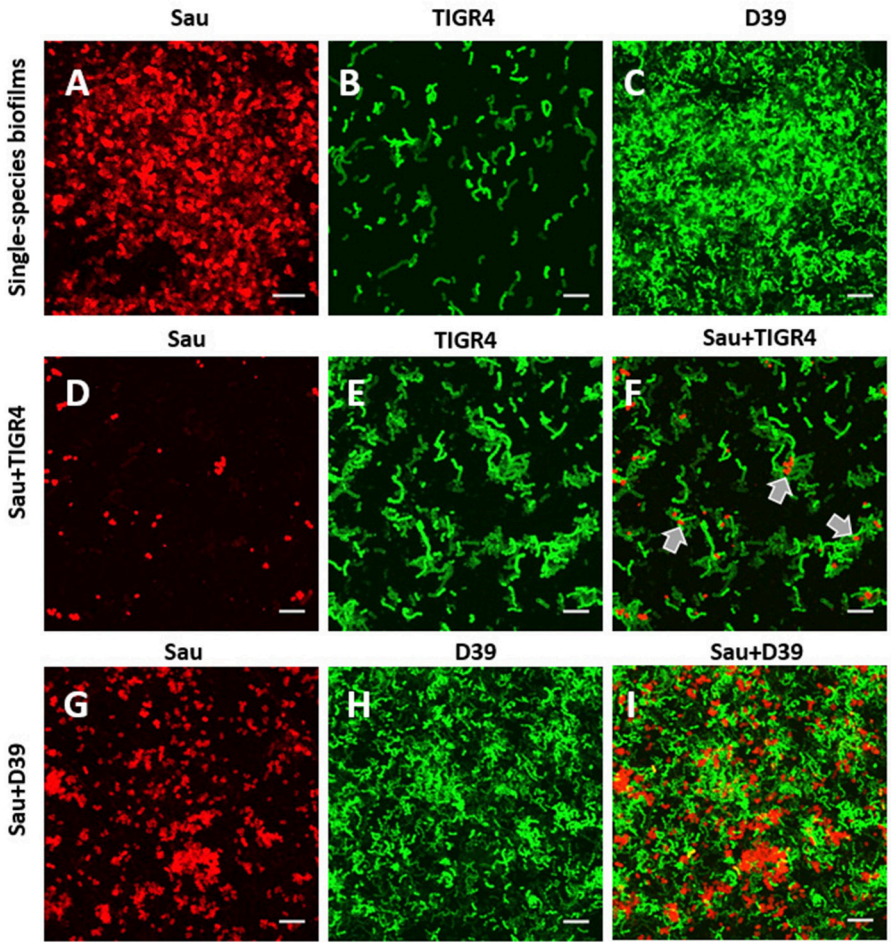

FIGURE 6 | Confocal studies of Sau coincubated with Spn strains. (A) Sau, **(B)** SPJV09 (TIGR4), or **(C)** SPJV01 (D39), or mixtures of Sau and SPJV09 **(D–F)** or Sau and SPJV01 **(G–I)** was inoculated into an eight-well slide and incubated for 4 h at 37°C. Biofilms were fixed with 2% PFA and stained with an anti-Sau antibody followed by an Alexa 555-labeled anti-rabbit secondary antibody (red). Spn strains were expressing the green fluorescent protein. Preparations were analyzed by confocal microscopy. A representative xy optical section is shown. Bar = 20 μm. Gray arrows point out areas where Sau and TIGR4 are located.

log-phase cultures of D39, or TIGR4 cells, ($\sim 1 \times 10^6$ cfu/ml) were inoculated into preformed Sau biofilms and then incubated for an additional 4 h period. As seen in **Figure 9**, pre-colonized Sau biofilms were significantly reduced by incubating with D39, or TIGR4. Furthermore, reduction of pre-formed Sau biofilms by TIGR4 ($\sim 1.5 \times 10^3$ cfu/ml) was significantly different than Sau reduction produced by incubating with D39 ($\sim 3.2 \times 10^5$ cfu/ml).

Since biofilms releases planktonic cells into the supernatant, viable planktonic bacteria were also counted. In control wells, Sau planktonic cells released by preformed biofilms reached a density of $\sim 1.7 \times 10^8$ cfu/ml (**Figure 9B**), whereas in pre-formed Sau biofilms inoculated with D39 the population of Sau planktonic cells was reduced, although the reduction was not statistically significant (**Figure 9B**). Sau planktonic cells (<50 cfu/ml) were eradicated in wells infected with Spn strain TIGR4 (**Figure 9B**).

Spn counts were obtained in order to investigate if the observed differences in D39 and TIGR4's ability to reduce pre-colonized Sau biofilms and kill planktonic cells was due to an increased population of TIGR4. Both planktonic cells and biofilms were significantly lower in wells inoculated with TIGR4 in comparison to D39 (~200-fold lower) confirming that an increased population was not a factor in the killing of Sau by TIGR4 (**Figure 9C**).

Spn Bacteria, but not Supernatants, Efficiently Kill Sau Pre-colonized Biofilms

Our next experiments fractionated TIGR4 cultures into planktonic cells, biofilms and supernatants and evaluated killing of Sau by these fractions. Since inoculating TIGR4 with Sau at the same time eradicated Sau biofilms in 4 h, cultures of TIGR4 were grown for 4 h and then planktonic cells, biofilms and culture supernatant were separated and incubated with preformed Sau biofilms. We hypothesized that Spn from 4 h cultures (i.e., activated cultures) would kill Sau biofilms faster and therefore preformed biofilms were incubated for 2 h. As expected, inoculating preformed Sau biofilms with early log-phase TIGR4 cultures reduced, but did not eradicate, preformed biofilms within 2 h (**Figure 10A**).

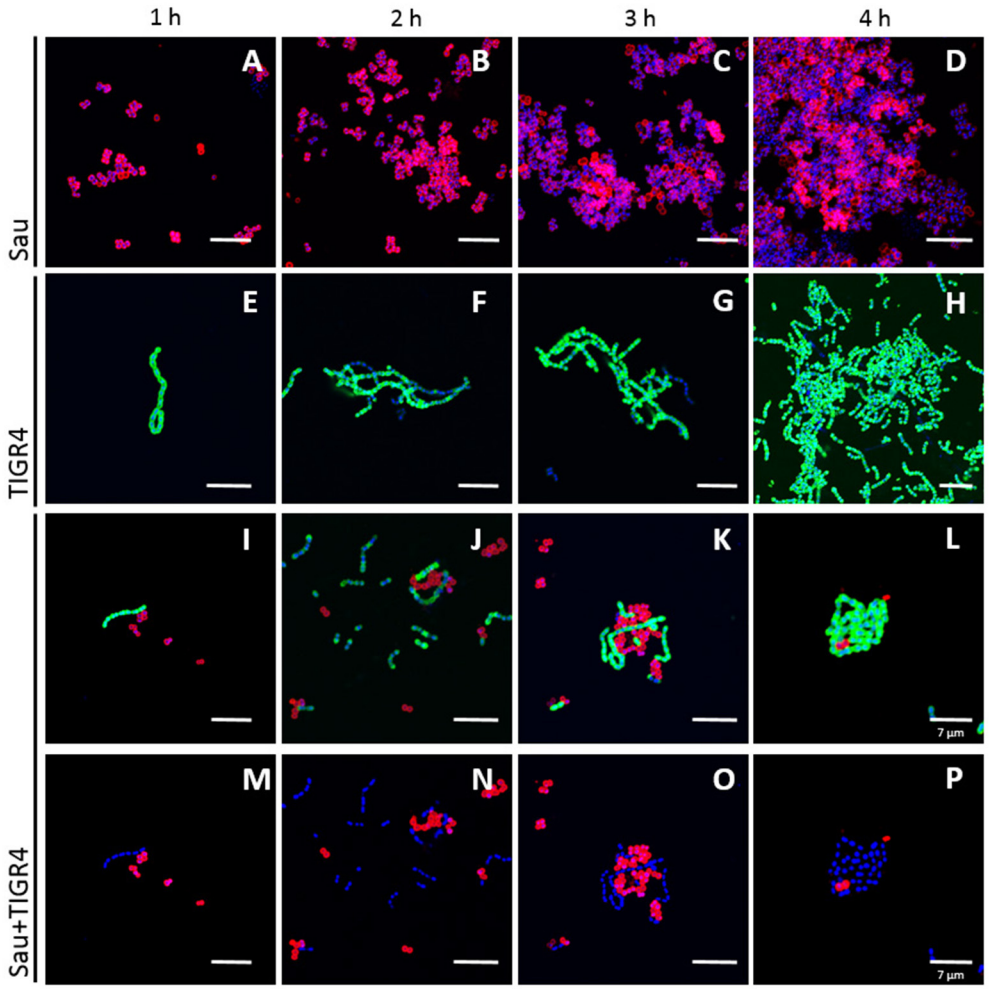

FIGURE 7 | Time course study of physical interaction between Sau and Spn strains. Sau **(A–D)**, TIGR4 **(E–H)**, or Sau and TIGR4 **(I–P)** were inoculated into an eight-well slide and incubated for 1, 2, 3, or 4 h at 37°C. Biofilms were fixed with 2% PFA and stained with an anti-Sau antibody followed by an Alexa 555-labeled anti-rabbit secondary antibody (red) and then an anti-Spn antibody labeled with Alexa 488 (green). Bacterial DNA was stained by DAPI (blue). Micrographs were taken by confocal microscopy. Panels show representative xy optical sections (~0.4 µm each). Bar at the right panel is valid for its corresponding horizontal panels. Panels **(I–L)** show the red and green channels while panels **(M–P)** the red and blue channels. Bars = 10 µm, except were indicated (7 µm).

However, washed Spn (planktonic+biofilms), planktonic, or biofilms harvested from 4 h cultures eradicated Sau biofilms (**Figure 10A**). Sterile supernatant from this 4 h culture was only able to reduce Sau biofilms (5.6×10^3 cfu/ml) in comparison with the non-inoculated control (1.1×10^6 cfu/ml).

Experiments were also conducted with supernatants from 6 to 8 h cultures with similar reduction (not shown). Accordingly, confocal micrographs showed robust preformed Sau biofilms, 4 h post-inoculation (**Figure 10B**), that were significantly reduced within 30 min and 1 h post-inoculation of washed Spn (**Figures 10B–D**) and completely eradicated within 2 h (**Figure 10E**). TIGR4 bacteria, however, were not able to recolonize the substrate once Sau biofilms were removed as TIGR4 was only observed attached to the few Sau bacteria, but not attached to the bottom (**Figure 10E**).

DISCUSSION

We have demonstrated in this study that TIGR4, and other Spn strains, rapidly eradicated preformed Sau biofilms, including biofilms produced by MRSA strain USA300. To kill Sau biofilms, the pneumococcus required physical contact which was documented by several lines of evidence including confocal microscopy, colocalization experiments, and experiments utilizing a Transwell system to separate both species. The physical contact-mediated killing was very efficient as it completely eradicated a viable lawn of Sau biofilms within 2 h (i.e., viable counts under the limit of detection of 50 cfu/ml).

This efficient mechanism however, was not mediated by production of H_2O_2, as an isogenic mutant lacking the enzyme responsible for producing hydrogen peroxide was able to eradicate Sau biofilms and planktonic bacteria. As shown in

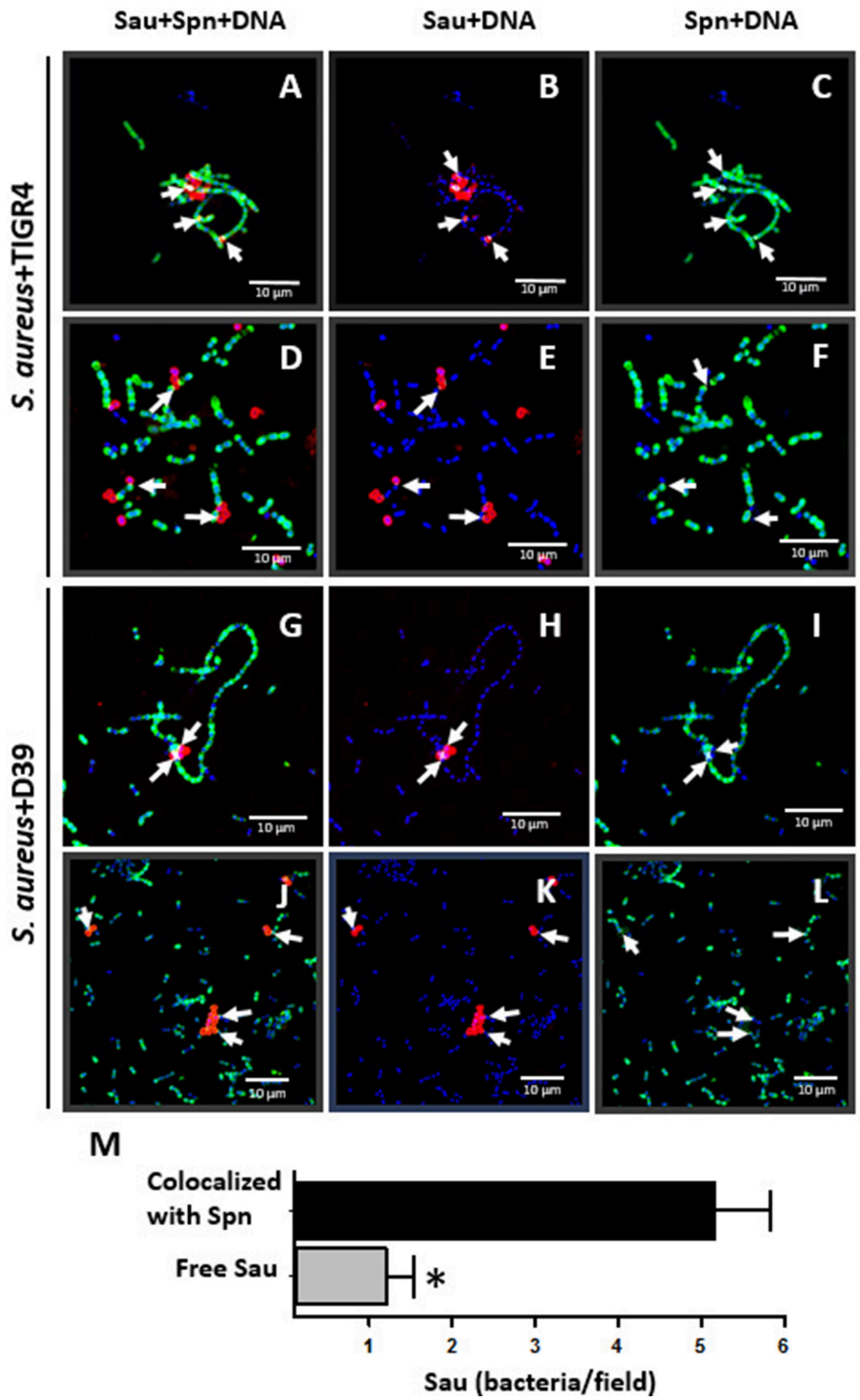

FIGURE 8 | Colocalization between Sau and Spn. Sau and TIGR4 **(A–F)** or Sau and D39 **(G–L)** were inoculated together into an eight-well slide and incubated for 1 h **(A–C, G–I)** or 2 h **(D–F, J–L)** at 37°C. Biofilms were fixed with 2% PFA and stained with an anti-Sau antibody followed by an Alexa 555-labeled anti-rabbit secondary antibody (red) and then an anti-Spn antibody labeled with Alexa 488 (green). Bacterial DNA was stained by DAPI (blue). Micrographs were taken by confocal microscopy and analyzed using Imaris software. Panels show representative xy optical sections (~0.4 µm each). Bar = 10 µm at right panels and is valid for its corresponding horizontal panels. Vertical panels show specific channels. Arrows point out areas of colocalization between Sau and Spn. **(M)** Sau colocalized with Spn after 1 h of co-incubation, or free Sau bacteria, were counted in 30 different micrographs. Means were plotted and error bars represent the standard errors. (*), statistical significance ($p < 0.001$).

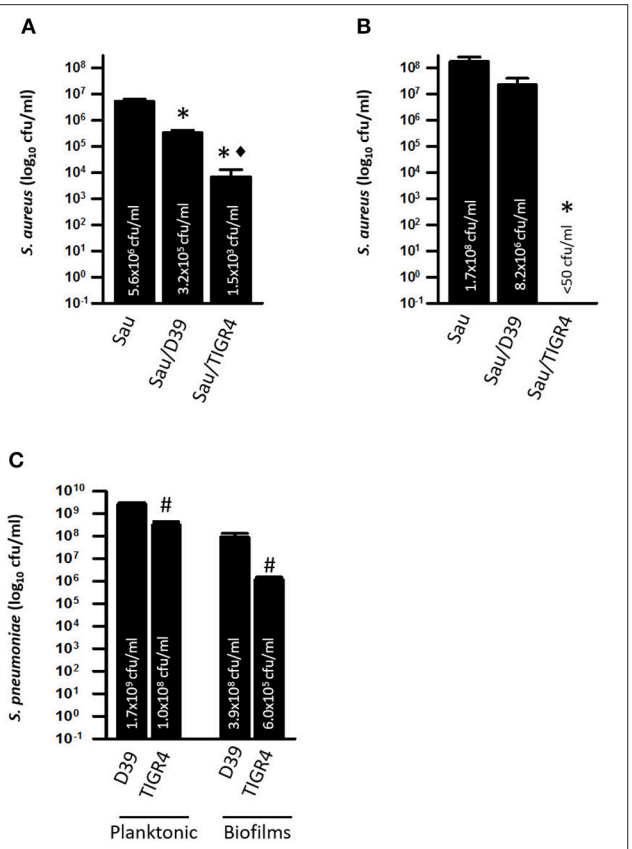

FIGURE 9 | Spn TIGR4 kills preformed Sau biofilms. Sau was inoculated in microtiter plates containing THY and incubated for 4 h, after which planktonic cells were removed and fresh THY medium was added. Sau biofilms were left uninoculated (Sau) or co-inoculated with Spn strain D39 (Sau/D39) or TIGR4 (Sau/TIGR4) and incubated for 4 h at 37°C. Biofilms **(A)** or planktonic cells **(B)** were harvested, serially diluted and plated onto salt mannitol agar plates to obtain bacterial counts. **(C)** Dilutions were also plated onto blood agar plates with gentamicin to obtain Spn planktonic and biofilm counts. Error bars represent the standard errors of the means calculated using data from at least three independent experiments; the median (cfu/ml) is shown inside bars. Statistical significance ($p < 0.05$) in comparison to wells inoculated with Sau (*), Sau/D39 (♦) or D39 (#).

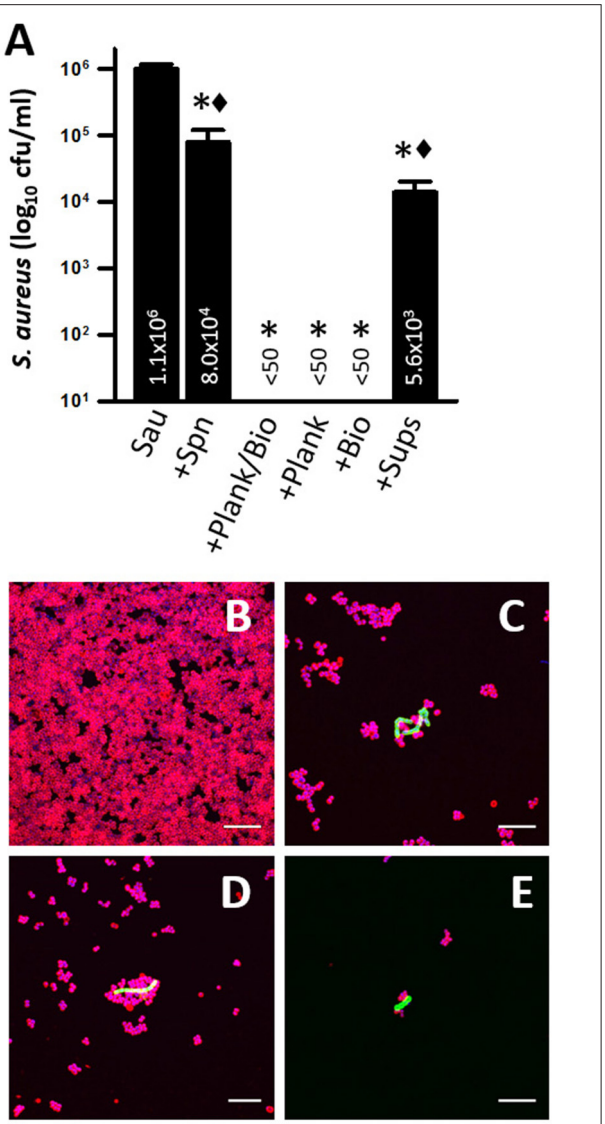

FIGURE 10 | Washed TIGR4 bacteria rapidly kill preformed Sau biofilms. (A) Sau was inoculated (Sau) in microtiter plates containing THY and incubated for 4 h, after which planktonic cells were removed and fresh THY medium was added. Another set of wells were inoculated with TIGR4 and incubated for 4 h at 37°C. Planktonic cells, biofilms, or supernatants from this TIGR4 4 h culture were separated as specified in Material and Methods. Preformed Sau biofilms were left uninoculated (Sau), or inoculated with ~1 × 10^6 cfu/ml of an early-log phase culture of planktonic TIGR4 cells (+Spn), or 4 h cultures of washed bacteria (+Plank/Bio), washed planktonic bacteria (+Plank), washed biofilms (+Bios) or supernatant (+Sup) and incubated for 2 h at 37°C. Cultures were harvested, serially diluted and plated onto salt mannitol agar plates to obtain Sau (cfu/ml). Error bars represent the standard errors of the means calculated using data from at least three independent experiments. Statistical significance in comparison to wells inoculated with (*, $p < 0.004$) Sau or (♦, $p < 0.001$) +Plank/Bio. **(B–E)** Sau was inoculated into an eight-well slide and incubated for 4 h at 37°C. Sau Biofilms were challenged with 4 h cultures of washed TIGR4 bacteria and incubated for 30 min **(B)**, 1 h **(C)**, 1.5 h **(D)**, and 2 h **(E)**. At the end of incubation, biofilms were fixed with 2% PFA and stained with an anti-Sau antibody followed by an Alexa 555-labeled anti-rabbit secondary antibody (red) and then an anti-Spn antibody labeled with Alexa 488 (green). DNA was stained with DAPI. Preparations were analyzed by confocal microscopy. A representative xy optical section is shown. Bar = 20 μm.

this work and others (Regev-Yochay et al., 2006), incubating with catalase was enough to inhibit killing of Sau by Spn. We further demonstrated in this study that the inhibitory effect of catalase was separate from its enzymatic activity against hydrogen peroxide, as incubating a TIGR4 isogenic *spx*B mutant, which does not produce H_2O_2, with catalase inhibited killing of Sau. Accordingly, Park et al. (2008), showed that catalase produced by Sau strains confers some degree of protection to a challenge with Spn; authors did not utilize, however, a hydrogen peroxide deficient-mutant to verify this protection was directly mediated by its enzymatic activity against H_2O_2, as shown in our studies (Park et al., 2008). We hypothesize that incubating Spn with catalase has downstream effects impacting a mechanism that seems to be more complex than originally thought. Future transcriptomic studies should help us to identify, if any, these changes. Changes in bacterial densities, affected by incubating with catalase (**Figure 5B**), can also be a factor, as bacterial density

ratios favoring the pneumococcus are required to eradicate Sau bacteria (discussed below).

Sau strains, including MRSA strains, were the second most common pathogen associated to nosocomial infections in 2011 in the USA accounting for 10.7% of all cases (Magill et al., 2014). In the study by Magill et al. (2014), conducted by the Centers for Disease Control and Prevention (CDC), it was estimated that there were ∼721,800 nosocomial infections in 2011. Biofilm-related, device-associated infections, (i.e., central-catheter–associated bloodstream infection, catheter-associated urinary tract infection, and ventilator-associated pneumonia), and surgical-site infections accounted for >47% of those cases (Magill et al., 2014). The majority of Sau nosocomial infections were related to formation of biofilms, i.e., catheter–associated bacteremia. Due to this, efforts are in place to eradicate Sau biofilms and thus decrease hospital-acquired infections and Sau biofilm-related disease.

A number of approaches, other than antibiotics, are now being tested to prevent, or once stablished to eradicate Sau biofilms. Prevention involves the development of new materials that prevent attachment, antibacterial coating, and vaccines (Bhattacharya et al., 2015). Treatment of established Sau biofilms includes matrix degrading enzymes, dispersal triggering agents, small-molecule inhibitors, targeting regulatory molecules, and surgical removal of the focus of infection. Although promising, no single treatment has proven effective to those suffering Sau biofilm disease. Whereas, comparisons were not made with the above mentioned approaches, studies within this work demonstrated complete removal of preformed Sau biofilms within 2 h of incubation with Spn strains TIGR4, A66.1 and GA13499. These observations certainly warrant further investigations and development.

Spn strains can produce two different quorum sensing pheromones, CSP1 and CSP2 (Pestova et al., 1996). The pheromones control competence for transformation (Håvarstein et al., 1995), biofilm formation (Vidal et al., 2013) and lysis of other pneumococci when incubated together, known as fratricide (Steinmoen et al., 2003; Guiral et al., 2005). As shown in our experiments, killing of Sau biofilms was not directly related to the production of a specific quorum sensing pheromone. The possibility exists, however, that a quorum sensing mediated mechanism regulates killing of Sau as our experiments with washed Spn bacteria, mid-log phase (4 h) cultures, killed more rapidly in comparison to early-log phase Spn cultures. Experiments are under way in our laboratories to address the potential role, if any, of quorum sensing in direct killing of Sau biofilms.

A mechanism mediated by the production and release of H_2O_2 has been demonstrated for planktonic cultures, and culture supernatants, of Sau strains (Regev-Yochay et al., 2006, 2008). Accordingly, in our study we also observed killing of Sau strains by culture supernatants of Spn (**Figure 10**), but this was not as efficient as killing of Sau by Spn bacteria. Hydrogen peroxide is a byproduct of the aerobic metabolism produced by pyruvate oxidase, SpxB. Production of H_2O_2 has been proposed as the main driver of the negative association between Spn and Sau, as observed in carriage studies (Regev-Yochay et al., 2006, 2008). There is, however, a significant proportion of cocolonization events observed in children (Chien et al., 2013; Dunne et al., 2013). Decreased Spn-mediated killing of some Sau strains was not a factor for the observed cocolonization events, as studies by Regev-Yochay et al. (2008) demonstrated similar bactericidal effect of Sau strains isolated from children co-colonized with pneumococcal strains vs. those only colonized by Sau (Regev-Yochay et al., 2008). Further studies using a neonatal rat model of colonization showed that Spn and Sau can cohabit the nasal passages (Margolis et al., 2010) and that Sau co-colonization rates with Spn TIGR4 wt were similar to those of its isogenic *spx*B mutant (Margolis, 2009). Perhaps levels of H_2O_2 in the animal model vs. those obtained in broth cultures are not comparable, which may explain the differences in cocolonization. To our knowledge, levels of H_2O_2 produced by Spn in the human nasopharynx or nasal passages in animal models have not been determined. Production of H_2O_2 by Spn appears not to be the factor allowing contact-mediated killing of Sau given that, in our study an isogenic spxB mutant was still able to eradicate Sau bacteria. Another streptococci, *S. gordonii*, produces levels of H_2O_2 comparable to TIGR4, but is unable to kill Sau (Regev-Yochay et al., 2006). Other lines of evidence indicate that H_2O_2 produced by streptococci induces Sau lethal prophages (Selva et al., 2009).

In our study with biofilms, and those conducted with planktonic cultures, killing of Sau required a minimum Spn inoculum of $\sim 1 \times 10^6$ cfu/ml to kill the same amount of inoculated Sau bacteria; a reduced Spn challenge, for example $\sim 1 \times 10^5$ cfu/ml, will not kill a density of $\sim 1 \times 10^6$ cfu/ml of Sau. Physical contact, which we observed in our studies was required for efficient killing, may be a limiting factor for the Spn-Sau required ratio. Another possibility is that a bacterial threshold is required to activate, i.e., by quorum sensing, an efficient killing mechanism which may include the production of enough H_2O_2. The need of a bacterial threshold observed in *in vitro* studies may provide an explanation for the cocolonization of Spn and Sau in animal models. For example, in the classic study by Margolis et al. (2010), authors demonstrated cocolonization of $<10^4$ cfu of both species, Spn and Sau, in the nasal passages of animals. Perhaps this limited amount of bacteria does not allow for both to reach physical interaction in the nasal microenvironment.

Studies in our laboratory have also recently investigated nasopharyngeal bacterial densities in Tanzanian children cocolonized, or not, with Spn and/or Sau. We, as others in previous studies, demonstrated a negative association for children colonized only with Spn vs. those colonized by both Spn and Sau. Moreover, our study also showed a statistically significant reduction ($p = 0.03$) of Sau density in those children cocolonized with Spn ($\sim 1.5 \times 10^4$ cfu/ml) vs. those colonized only by Sau ($\sim 5.2 \times 10^4$ cfu/ml). As per the *in vitro* situation shown in **Figures 2**, **6** of the current study, nasopharyngeal density of Spn strains in Tanzanian children did not change, whether or not the host was cocolonized with Sau, $\sim 1.5 \times 10^6$ cfu/ml vs. $\sim 1.7 \times 10^6$ cfu/ml, respectively (Chochua et al., unpublished data; Wu et al., unpublished data).

In conclusion, Spn rapidly eradicates preformed Sau biofilms, including those formed by MRSA strain USA300. The

mechanism requires physical contact and a bacterial threshold. Killing of Sau by Spn was not mediated by production of hydrogen peroxide, but it was inhibited by catalase through a mechanism independent of catalase's enzymatic activity against hydrogen peroxide.

AUTHOR CONTRIBUTIONS

JV, GM, and XW Wrote the paper, conceived research; FK, XW, GM, FS, and MK Performed experiments.

ACKNOWLEDGMENTS

We thank Dr. Sarah Satola from Emory University School of Medicine for providing *S. aureus* strain USA300 and Dr. Scott Chancey from the Centers for Disease Control and Prevention (CDC) for the gift of strain GA13499. The authors are grateful to professor Marc Lipsitch from Harvard T. H. Chan School of Public Health for his kind gift of strain TIGR4Δ*spx*B mutant. This study was supported by a grant from the National Institutes of Health (NIH; R21AI112768-01A1 to JV). The content is solely the responsibility of the authors and does not necessarily represent the official view of the National Institutes of Health. Confocal studies were in part supported by funds from the Integrated Cellular Imaging (ICI) pediatric core and the Emory+Children's Pediatric Research Center to JV. Authors appreciate the assistance of Dr. Neil Anthony, from Emory University School of Medicine, with confocal microscopy and David Watson from the Rollins School of Public Health for his reading and his thoughtful comments on this manuscript.

REFERENCES

Avery, O. T., Macleod, C. M., and McCarty, M. (1944). Studies on the chemical nature of the substance inducing transformation of pneumococcal types: induction of transformation by a desoxyribonucleic acid fraction isolated from Pneumococcus type iii. *J. Exp. Med.* 79, 137–158. doi: 10.1084/jem.79.2.137

Bakaletz, L. O. (2007). Bacterial biofilms in otitis media: evidence and relevance. *Pediatr. Infect. Dis. J.* 26, S17–S19. doi: 10.1097/inf.0b013e318154b273

Benton, K. A., Paton, J. C., and Briles, D. E. (1997). Differences in virulence for mice among *Streptococcus pneumoniae* strains of capsular types 2, 3, 4, 5, and 6 are not attributable to differences in pneumolysin production. *Infect. Immun.* 65, 1237–1244.

Bhattacharya, M., Wozniak, D. J., Stoodley, P., and Hall-Stoodley, L. (2015). Prevention and treatment of *Staphylococcus aureus* biofilms. *Expert Rev. Anti Infect. Ther.* 13, 1499–1516. doi: 10.1586/14787210.2015.1100533

Boake, W. C. (1956). Antistaphylocoagulase in experimental staphylococcal infections. *J. Immunol.* 76, 89–96.

Bogaert, D., Van Belkum, A., Sluijter, M., Luijendijk, A., De Groot, R., Rumke, H. C., et al. (2004). Colonisation by *Streptococcus pneumoniae* and *Staphylococcus aureus* in healthy children. *Lancet* 363, 1871–1872. doi: 10.1016/S0140-6736(04)16357-5

Centers for Disease Control and Prevention (2003). Methicillin-resistant *Staphylococcus aureus* infections among competitive sports participants–Colorado, Indiana, Pennsylvania, and Los Angeles County, 2000–2003. *MMWR Morb. Mortal. Wkly. Rep.* 52, 793–795.

Chao, Y., Marks, L. R., Pettigrew, M. M., and Hakansson, A. P. (2014). *Streptococcus pneumoniae* biofilm formation and dispersion during colonization and disease. *Front. Cell. Infect. Microbiol.* 4:194. doi: 10.3389/fcimb.2014.00194

Chien, Y. W., Vidal, J. E., Grijalva, C. G., Bozio, C., Edwards, K. M., Williams, J. V., et al. (2013). Density interactions among *Streptococcus pneumoniae*, Haemophilus influenzae and *Staphylococcus aureus* in the nasopharynx of young Peruvian children. *Pediatr. Infect. Dis. J.* 32, 72–77. doi: 10.1097/INF.0b013e318270d850

Costes, S. V., Daelemans, D., Cho, E. H., Dobbin, Z., Pavlakis, G., and Lockett, S. (2004). Automatic and quantitative measurement of protein-protein colocalization in live cells. *Biophys. J.* 86, 3993–4003. doi: 10.1529/biophysj.103.038422

Dunne, E. M., Smith-Vaughan, H. C., Robins-Browne, R. M., Mulholland, E. K., and Satzke, C. (2013). Nasopharyngeal microbial interactions in the era of pneumococcal conjugate vaccination. *Vaccine* 31, 2333–2342. doi: 10.1016/j.vaccine.2013.03.024

Gritzfeld, J. F., Cremers, A. J., Ferwerda, G., Ferreira, D. M., Kadioglu, A., Hermans, P. W., et al. (2014). Density and duration of experimental human pneumococcal carriage. *Clin. Microbiol. Infect.* 20, O1145–O1151. doi: 10.1111/1469-0691.12752

Guiral, S., Mitchell, T. J., Martin, B., and Claverys, J. P. (2005). Competence-programmed predation of noncompetent cells in the human pathogen *Streptococcus pneumoniae*: genetic requirements. *Proc. Natl. Acad. Sci. U.S.A.* 102, 8710–8715. doi: 10.1073/pnas.0500879102

Håvarstein, L. S., Coomaraswamy, G., and Morrison, D. A. (1995). An unmodified heptadecapeptide pheromone induces competence for genetic transformation in *Streptococcus pneumoniae*. *Proc. Natl. Acad. Sci. U.S.A.* 92, 11140–11144. doi: 10.1073/pnas.92.24.11140

Kiedrowski, M. R., and Horswill, A. R. (2011). New approaches for treating staphylococcal biofilm infections. *Ann. N. Y. Acad. Sci.* 1241, 104–121. doi: 10.1111/j.1749-6632.2011.06281.x

Lanie, J. A., Ng, W. L., Kazmierczak, K. M., Andrzejewski, T. M., Davidsen, T. M., Wayne, K. J., et al. (2007). Genome sequence of Avery's virulent serotype 2 strain D39 of *Streptococcus pneumoniae* and comparison with that of unencapsulated laboratory strain R6. *J. Bacteriol.* 189, 38–51. doi: 10.1128/JB.01148-06

Magill, S. S., Edwards, J. R., Bamberg, W., Beldavs, Z. G., Dumyati, G., Kainer, M. A., et al. (2014). Multistate point-prevalence survey of health care-associated infections. *N. Engl. J. Med.* 370, 1198–1208. doi: 10.1056/NEJMoa1306801

Margolis, E. (2009). Hydrogen peroxide-mediated interference competition by *Streptococcus pneumoniae* has no significant effect on *Staphylococcus aureus* nasal colonization of neonatal rats. *J. Bacteriol.* 191, 571–575. doi: 10.1128/JB.00950-08

Margolis, E., Yates, A., and Levin, B. R. (2010). The ecology of nasal colonization of *Streptococcus pneumoniae*, Haemophilus influenzae and *Staphylococcus aureus*: the role of competition and interactions with host's immune response. *BMC Microbiol.* 10:59. doi: 10.1186/1471-2180-10-59

Park, B., Nizet, V., and Liu, G. Y. (2008). Role of *Staphylococcus aureus* catalase in niche competition against *Streptococcus pneumoniae*. *J. Bacteriol.* 190, 2275–2278. doi: 10.1128/JB.00006-08

Pestova, E. V., Havarstein, L. S., and Morrison, D. A. (1996). Regulation of competence for genetic transformation in *Streptococcus pneumoniae* by an auto-induced peptide pheromone and a two-component regulatory system. *Mol. Microbiol.* 21, 853–862. doi: 10.1046/j.1365-2958.1996.501417.x

Regev-Yochay, G., Dagan, R., Raz, M., Carmeli, Y., Shainberg, B., Derazne, E., et al. (2004). Association between carriage of *Streptococcus pneumoniae* and *Staphylococcus aureus* in Children. *JAMA* 292, 716–720. doi: 10.1001/jama.292.6.716

Regev-Yochay, G., Malley, R., Rubinstein, E., Raz, M., Dagan, R., and Lipsitch, M. (2008). *In vitro* bactericidal activity of *Streptococcus pneumoniae* and bactericidal susceptibility of *Staphylococcus aureus* strains isolated from cocolonized versus noncocolonized children. *J. Clin. Microbiol.* 46, 747–749. doi: 10.1128/JCM.01781-07

Regev-Yochay, G., Trzcinski, K., Thompson, C. M., Malley, R., and Lipsitch, M. (2006). Interference between *Streptococcus pneumoniae* and *Staphylococcus aureus*: *in vitro* hydrogen peroxide-mediated killing by *Streptococcus pneumoniae*. *J. Bacteriol.* 188, 4996–5001. doi: 10.1128/JB.00317-06

Selva, L., Viana, D., Regev-Yochay, G., Trzcinski, K., Corpa, J. M., Lasa, I., et al. (2009). Killing niche competitors by remote-control bacteriophage induction. *Proc. Natl. Acad. Sci. U.S.A.* 106, 1234–1238. doi: 10.1073/pnas.0809600106

Shak, J. R., Cremers, A. J., Gritzfeld, J. F., De Jonge, M. I., Hermans, P. W., Vidal, J. E., et al. (2014). Impact of experimental human pneumococcal carriage on nasopharyngeal bacterial densities in healthy adults. *PLoS ONE* 9:e98829. doi: 10.1371/journal.pone.0098829

Shak, J. R., Vidal, J. E., and Klugman, K. P. (2013). Influence of bacterial interactions on pneumococcal colonization of the nasopharynx. *Trends Microbiol.* 21, 129–135. doi: 10.1016/j.tim.2012.11.005

Steinmoen, H., Teigen, A., and Havarstein, L. S. (2003). Competence-induced cells of *Streptococcus pneumoniae* lyse competence-deficient cells of the same strain during cocultivation. *J. Bacteriol.* 185, 7176–7183. doi: 10.1128/JB.185.24.7176-7183.2003

Tettelin, H., Nelson, K. E., Paulsen, I. T., Eisen, J. A., Read, T. D., Peterson, S., et al. (2001). Complete genome sequence of a virulent isolate of *Streptococcus pneumoniae*. *Science* 293, 498–506. doi: 10.1126/science.1061217

Vidal, J. E., Howery, K. E., Ludewick, H. P., Nava, P., and Klugman, K. P. (2013). Quorum-sensing systems LuxS/autoinducer 2 and Com regulate *Streptococcus pneumoniae* biofilms in a bioreactor with living cultures of human respiratory cells. *Infect. Immun.* 81, 1341–1353. doi: 10.1128/IAI.01096-12

Vidal, J. E., Ludewick, H. P., Kunkel, R. M., Zahner, D., and Klugman, K. P. (2011). The LuxS-dependent quorum-sensing system regulates early biofilm formation by *Streptococcus pneumoniae* strain D39. *Infect. Immun.* 79, 4050–4060. doi: 10.1128/IAI.05186-11

Yarwood, J. M., Bartels, D. J., Volper, E. M., and Greenberg, E. P. (2004). Quorum sensing in *Staphylococcus aureus* biofilms. *J. Bacteriol.* 186, 1838–1850. doi: 10.1128/JB.186.6.1838-1850.2004

Conflict of Interest Statement: The authors declare that the research was conducted in the absence of any commercial or financial relationships that could be construed as a potential conflict of interest.

frontiers in Cellular and Infection Microbiology

ORIGINAL RESEARCH
published: 16 November 2016
doi: 10.3389/fcimb.2016.00158

N-acetylglucosamine-Mediated Expression of *nagA* and *nagB* in *Streptococcus pneumoniae*

Muhammad Afzal[1,2], *Sulman Shafeeq*[3], *Irfan Manzoor*[1,2], *Birgitta Henriques-Normark*[3] *and Oscar P. Kuipers*[1]*

[1] Department of Molecular Genetics, Groningen Biomolecular Sciences and Biotechnology Institute, University of Groningen, Groningen, Netherlands, [2] Department of Bioinformatics and Biotechnology, Government College University, Faisalabad, Pakistan, [3] Department of Microbiology, Tumor and Cell Biology, Karolinska Institutet, Stockholm, Sweden

In this study, we have explored the transcriptomic response of *Streptococcus pneumoniae* D39 to N-acetylglucosamine (NAG). Transcriptome comparison of *S. pneumoniae* D39 wild-type grown in chemically defined medium (CDM) in the presence of 0.5% NAG to that grown in the presence of 0.5% glucose revealed elevated expression of many genes/operons, including *nagA*, *nagB*, *manLMN*, and *nanP*. We have further confirmed the NAG-dependent expression of *nagA*, *nagB*, *manLMN*, and *nanP* by β-galactosidase assays. *nagA*, *nagB* and *glmS* are putatively regulated by a transcriptional regulator NagR. We predicted the operator site of NagR (*dre* site) in P*nagA*, P*nagB,* and P*glmS*, which was further confirmed by mutating the predicted *dre* site in the respective promoters (*nagA*, *nagB,* and *glmS*). Growth comparison of Δ*nagA*, Δ*nagB,* and Δ*glmS* with the D39 wild-type demonstrates that *nagA* and *nagB* are essential for *S. pneumoniae* D39 to grow in the presence of NAG as a sole carbon source. Furthermore, deletion of *ccpA* shows that CcpA has no effect on the expression of *nagA*, *nagB,* and *glmS* in the presence of NAG in *S. pneumoniae*.

Keywords: N-acetylglucosamine, NAG, NagA, NagB, GlmS, pneumococcus, CcpA

OPEN ACCESS

Edited by:
Jorge Eugenio Vidal, Emory University, USA

Reviewed by:
Samantha J. King, Ohio State University, USA
Marco Rinaldo Oggioni, University of Leicester, UK
Zehava Eichenbaum, Georgia State University, USA

***Correspondence:**
Oscar P. Kuipers
o.p.kuipers@rug.nl

Received: *17 January 2016*
Accepted: *02 November 2016*
Published: *16 November 2016*

Citation:
Afzal M, Shafeeq S, Manzoor I, Henriques-Normark B and Kuipers OP (2016) N-acetylglucosamine-Mediated Expression of nagA and nagB in Streptococcus pneumoniae. Front. Cell. Infect. Microbiol. 6:158. doi: 10.3389/fcimb.2016.00158

INTRODUCTION

Pneumonia, sepsis, meningitis, otitis media, and conjunctivitis are a few of the diseases caused by the major human pathogen *Streptococcus pneumoniae* that results in over a million deaths each year worldwide (Ispahani et al., 2004; O'Brien et al., 2009). *S. pneumoniae* relies on several nutrient sources and virulence factors to colonize in the human nasopharynx (Phillips et al., 1990; Titgemeyer and Hillen, 2002; Carvalho et al., 2011). Regulatory mechanisms of a number of carbon and nitrogen sources important for the lifestyle and virulence of *S. pneumoniae* have already been studied (Kloosterman et al., 2006b; Carvalho et al., 2011; Kloosterman and Kuipers, 2011; Afzal et al., 2015c,d). *S. pneumoniae* has been shown to metabolize 32 carbohydrates including the three-carbon molecule glycerol, nine hexoses or hexose derivatives (ascorbate, fructose, galactose, glucosamine, glucose, mannose, N-acetylglucosamine, N-acetyl-mannosamine, and N-acetyl-neuraminic acid), three α-galactosides (melibiose, raffinose, and stachyose), two β-galactosides (lactose, and lactulose), four α-glucosides (maltose, maltotriose, sucrose, and trehalose), seven β-glucosides (amygdalin, arbutin, 1-O-methyl-β-glucoside, cellobiose, gentiobiose, aesculin, and salicin) and six polysaccharides (glycogen, hyaluronate, inulin, maltodextrin, pectin, and pullulan) (Bidossi et al., 2012).

The importance of carbon sources in the life-style of *S. pneumoniae* can be judged from the fact that over 30% of all the transporters in the genome are presumably involved in sugar uptake (Tettelin et al., 2001; Bidossi et al., 2012), a considerably larger number than that present in the other microorganisms inhabiting the same niche (Paulsen et al., 2000; Tettelin et al., 2001). The glycoproteins lining the epithelial surfaces in the human nasopharynx might be good carbon and energy sources for pneumococcal growth. Notably, *S. pneumoniae* has the ability to grow on mucin as a sole carbon source (Yesilkaya et al., 2008). Mucins are constituents of the mucus that span the epithelial surfaces (Rose and Voynow, 2006). These structures are largely O-glycosylated glycoproteins and are usually composed of N-acetylglucosamine (NAG), N-acetylgalactosamine, N-acetylneuraminic acid, galactose, fucose, and sulphated sugars connected to the protein core, mostly *via* an N-acetylgalactosamine moiety (Rose and Voynow, 2006; Terra et al., 2010). *S. pneumoniae* has several extracellular glycosidases with an extensive variety of substrates specificities and can make use of the other host glycans, such as N-glycans and glycosaminoglycans (Burnaugh et al., 2008; King, 2010; Marion et al., 2012). These enzymes produce a number of free sugars that potentially can be used by the pneumococcus. The deglycosylation activity of both exo- and endoglycosidades has previously been demonstrated in *S. pneumoniae* (King et al., 2006; Burnaugh et al., 2008; Jeong et al., 2009; Marion et al., 2009). The ability to utilize complex glycans present at the site of colonization contributes to the successful survival and virulence of *S. pneumoniae* in the host (Buckwalter and King, 2012; Linke et al., 2013). Besides, the role of these enzymes in *in vivo* fitness is demonstrated by the findings that glycosidase mutants show attenuated capacity to colonize and to cause disease in mouse models (Tong et al., 2000; Jeong et al., 2009; Marion et al., 2009; Terra et al., 2010).

NAG is an important amino-carbon source for several bacteria due to its role as an energy resource and in peptidoglycan synthesis (Dobrogosz, 1968; Mobley et al., 1982). Several studies highlighted the importance of NAG as a preferred carbon source in bacteria (Dobrogosz, 1968; Mobley et al., 1982). The involvement of NAG for both catabolic and anabolic purposes requires proper regulatory mechanisms for its utilization, as shown in model microorganisms, such as *Bacillus subtilis*, *Escherichia coli*, *Streptococcus mutans*, and *Streptomyces coelicolor* (Plumbridge, 2001; Nothaft et al., 2010; Bertram et al., 2011; Zeng and Burne, 2015). The NAG regulon consists of *nagA*, *nagB,* and *glmS* in *S. mutans*, and is regulated by a GntR-family transcriptional regulator NagR (Moye et al., 2014). NagA is an NAG-6-phosphate deacetylase, whereas NagB is a GlcN-6-P deaminase, and GlmS is a Fru-6-P amidotransferase. NagB was upregulated in the presence of NAG while GlmS expression decreased, signifying that the regulatory mode of these enzymes depends on the concentration of environmental NAG. A *glmS*-inactivated mutant could not grow in the absence of NAG, whereas the growth of *nagB*-inactivated mutant was decreased in the presence of NAG (Kawada-Matsuo et al., 2012). *nagB* inactivation led to a decrease in the expression of virulence factors, including cell-surface protein antigen and glucosyltransferase, and also impeded biofilm formation and saliva-induced aggregation in *S. mutans* (Kawada-Matsuo et al., 2012). NagA has been shown to be important for the growth of pneumococcus in the presence of NAG as a sole carbon source (Paixão et al., 2015).

Diverse bacterial groups including streptomycetes, firmicutes, and enterobacteriaceae universally use phosphotransferase systems (PTSs) for uptake and phosphorylation of NAG (Simoni et al., 1976; Mobley et al., 1982; Alice et al., 2003; Nothaft et al., 2003, 2010). ManLMN PTS has been shown to be a glucose and mannose PTS in *Streptococcus salivarius* (Vadeboncoeur, 1984) and was also responsible for uptake of fructose, and NAG (Lortie et al., 2000). ManLMN transports glucose and mannose, and also shows specificity for galactose, NAG, and glucosamine in *S. pneumoniae* (Bidossi et al., 2012). NagP (PTS EIIBC component) is the main transporter of NAG in *B. subtilis* and *S. mutans* (Reizer et al., 1999; Saier et al., 2002; Moye et al., 2014).

Here, we demonstrate the effect of NAG on the global gene expression of *S. pneumoniae* and NAG-dependent expression of *nagA*, *nagB*, *manLMN*, and *nanP*. We further hypothesize that a GntR-family transcriptional regulator, NagR, might be involved in the regulation of *nagA*, *nagB,* and *glmS* and predict a putative operator site for NagR (*dre* site). We also explored the global impact of *ccpA* deletion on the transcriptome of *S. pneumoniae* in the presence of NAG, showing that *ccpA* has no effect on the expression of *nagA*, *nagB,* and *glmS*. Furthermore, we show that *nagA* and *nagB* are essential for *S. pneumoniae* to grow on NAG validating the previous study, where essentiality of *nagA* in the growth of *S. pneumoniae* was demonstrated (Paixão et al., 2015).

MATERIALS AND METHODS

Bacterial Strains, Growth Conditions, and DNA Isolation and Manipulation

Bacterial strains and plasmids used in this study are listed in **Table 1**. *S. pneumoniae* D39 was grown as described previously (Kloosterman et al., 2006a; Afzal et al., 2014). For β-galactosidase assays, derivatives of *S. pneumoniae* D39 were grown in chemically defined medium (CDM) (Neves et al., 2002) supplemented either with 0.5% glucose or with 0.5% NAG. For selection on antibiotics, medium was supplemented with the following concentrations of antibiotics: 150 μg/ml spectinomycin, 15 μg/ml trimethoprim and 2.5 μg/ml tetracycline for *S. pneumoniae*; and 100 μg/ml ampicillin for *E. coli*. All bacterial strains used in this study were stored in 10% (v/v) glycerol at −80°C. For PCR amplification, chromosomal DNA of *S. pneumoniae* D39 (Lanie et al., 2007) was used. Primers used in this study are based on the sequence of the *S. pneumoniae* D39 genome and listed in **Table 2**.

Construction of *nagA*, *nagB,* and *glmS* Mutants

nagA and *nagB* deletion mutants were made by allelic replacement with trimethoprim- and spectinomycin-resistance cassettes, respectively. Briefly, primers nagA-1/nagA-2 and

TABLE 1 | List of strains and plasmids used in this study.

Strain/plasmid	Description*	Source
S. PNEUMONIAE		
D39	Serotype 2 strain	Laboratory of P. Hermans
MA700	D39 Δ*nagA*; Trm^R	This study
MA701	D39 Δ*nagB*; $Spec^R$	This study
MA702	D39 Δ*glmS*	This study
MA703	D39 Δ*bgaA*::P*nagA-lacZ*; Tet^R	This study
MA704	D39 Δ*bgaA*::P*nagB-lacZ*; Tet^R	This study
MA705	D39 Δ*bgaA*::P*glmS-lacZ*; Tet^R	This study
MA706	D39 Δ*bgaA*::P*manL-lacZ*; Tet^R	This study
MA707	D39 Δ*bgaA*::P*nagA-M-lacZ*; Tet^R	This study
MA708	D39 Δ*bgaA*::P*nagB-M-lacZ*; Tet^R	This study
MA709	D39 Δ*bgaA*::P*glmS1-M-lacZ*; Tet^R	This study
MA710	D39 Δ*bgaA*::P*glmS3-M-lacZ*; Tet^R	This study
MA203	D39 Δ*bgaA*::P*nanE-lacZ*; Tet^R	Afzal et al., 2015b
E. COLI		
EC1000		Laboratory collection
PLASMIDS		
pPP2	Amp^R Tet^R; promoter-less *lacZ*. For replacement of *bgaA* with promoter *lacZ* fusion. Derivative of pPP1	Halfmann et al., 2007
pORI280	Erm^R; *ori*$^+$ *repA*$^-$; deletion derivative of pWV01; constitutive *lacZ* expression from P32 promoter	Leenhouts et al., 1998
pMA700	pORI280 carrying *glmS* deletion	This study
pMA701	pPP2 P*nagA-lacZ*	This study
pMA702	pPP2 P*nagB-lacZ*	This study
pMA703	pPP2 P*glmS-lacZ*	This study
pMA704	pPP2 P*manL-lacZ*	This study
pMA705	pPP2 P*nagA-M-lacZ*	This study
pMA706	pPP2 P*nagB-M-lacZ*	This study
pMA707	pPP2 P*glmS1-M-lacZ*	This study
pMA708	pPP2 P*glmS3-M-lacZ*	This study

**Amp^R, $Spec^R$, Tet^R, and Trm^R confer ampicillin, spectinomycin, tetracycline and trimethoprim resistance gene, respectively.*

nagA-3/nagA-4 were used to generate PCR fragments of the left and right flanking regions of *nagA*. Similarly, primers nagB-1/nagB-2 and nagB3/nagB-4 were used to generate PCR fragments of the left and right flanking regions of *nagB*. PCR products of left and right flanking regions of *nagA* and *nagB* contain *AscI* and *NotI* restriction enzyme sites, respectively. The trimethoprim- and spectinomycin-resistance cassettes that are amplified by primers Spec-F/Spec-R and Trmp-F/Trmp-R, respectively from pORI38 and pKOT, also contain *AscI* and *NotI* restriction enzyme sites on their ends. Then, by restriction and ligation, the left and right flanking regions of *nagA* and *nagB* were fused to the trimethoprim- and spectinomycin-resistance genes, respectively. The resulting ligation products were transformed to *S. pneumoniae* D39 wild-type and selection of the mutant strains was done on appropriate concentrations of trimethoprim and spectinomycin.

A markerless *glmS* mutant (Δ*glmS*) was constructed in the *S. pneumoniae* D39 wild-type using the pORI280 plasmid, as described before (Kloosterman et al., 2006a). Primer pairs, glmS-1/glmS-2 and glmS-3/glmS-4, were used to generate PCR fragments of the left and right flanking regions of *glmS*, respectively. These PCR fragments were inserted into pORI280 using *XbaI* and *BglII* restriction sites, resulting in pMA700. All mutants were further confirmed by PCR and DNA sequencing.

Growth Analysis

For growth analysis of Δ*nagA*, Δ*nagB,* and Δ*glmS*, *S. pneumoniae* D39 wild-type and its isogenic mutants (Δ*nagA*, Δ*nagB,* and Δ*glmS*) were grown microaerobically at 37°C in 5 ml tubes containing 3 ml CDM supplemented either with 0.5% NAG or with 0.5% Glucose. Cultures were maintained at 37°C for 11 h and optical density at 600 nm was recorded with 1 h interval. CDM without inoculum was taken as blank. The growth of each strain was monitored from six biological replicates from at least two different days.

Construction of Promoter *lacZ*-fusions and β-Galactosidase Assays

Chromosomal transcriptional *lacZ*-fusions to the *nagA*, *nagB*, *glmS*, and *manL* promoters were constructed in the integration plasmid pPP2 (Halfmann et al., 2007) with primer pairs mentioned in **Table 2**, resulting in pMA701-04 respectively. Briefly, PCR products of *nagA*, *nagB*, *glmS*, and *manL* promoters were obtained using primers pairs mentioned in **Table 2**. These PCR fragments contain *EcoRI* and *BamHI* restriction sites at their ends. pPP2 also has *EcoRI* and *BamHI* restriction sites in its multiple cloning site (MCS). Then, by restriction and ligation, these PCR fragments were cloned into pPP2. pMA701-04 were further introduced into the *S. pneumoniae* D39 wild-type resulting in strains MA703-06, respectively. All plasmid constructs were checked by PCR and DNA sequencing. β-galactosidase assays were performed as described before (Israelsen et al., 1995; Kloosterman et al., 2006a) using cells that were grown in CDM with appropriate sugar mentioned in Results section and harvested in the mid-exponential phase of growth.

To study the functionality of *dre* site, the following promoter *lacZ*-fusions of *nagA*, *nagB,* and *glmS* with mutated *dre* sites were made in pPP2 (Halfmann et al., 2007) using the primer pairs mentioned in **Table 2**: P*nagA-M* (mutation in the *dre* site), P*nagB-M* (mutation in the *dre* site), P*glmS1-M* (mutation in the 1st *dre* site), and P*glmS3-M* (mutation in the 3rd *dre* site), resulting in plasmid pMA705-08, respectively. The mutations were incorporated into the primers used to amplify the target promoter regions containing the *dre* sites. These constructs were introduced into the *S. pneumoniae* D39 wild-type, resulting in strains MA707-10.

Microarray Analysis

For DNA microarray analysis in the presence of NAG, the transcriptome of *S. pneumoniae* D39 wild-type, grown in biological replicates in CDM with 0.5% NAG was compared to D39 wild-type grown in CDM with 0.5% glucose. Similarly, for DNA microarray analysis of Δ*ccpA*, the transcriptome of

TABLE 2 | List of primers used in this study.

Name	Nucleotide sequence (5′→3′)*	Restriction site
nagA-R	CATGGGATCCGTCCACAAGTTCCAAGTAACC	*BamHI*
nagA-F	CATGGAATTCGCAGACAGCTCAAGACAAGC	*EcoRI*
nagA-F-M	CATGGAATTCTATCTCCAAAAAATAGGTCGCTGTCATTTACAAAT	*EcoRI*
nagB-R	CATGGGATCCGCAACTTTTCCACCTTGAACTTGG	*BamHI*
nagB-F	CATGGAATTCGGGCAATCAATTCCTCTGGC	*EcoRI*
nagB-F-M	CATGGAATTCCGTTTTCACTTGACAAAAATTGGTCGCTGTCATATAATAA	*EcoRI*
glmS-R	CATGGGATCCCAACACCAACAATTCCACAC	*BamHI*
glmS-F	CATGGAATTCCGTCGTCTGAAGAAATCAGG	*EcoRI*
manL-F	CATGGAATTCCAGTAGAAGATGCTGTTG	*EcoRI*
manL-R	CATGGGATCCTGACTGATGAATACCC	*BamHI*
glmS1-F-M	CATGGAATTCACAGGAGCTTAATTTGAACGCTGTCAATTTTTACTC	*EcoRI*
glmS3-R-M	CATGGGATCCCACATAGTATATACGACACAGGCAAGCTGTGCTTTCTCCTT AAAATTGGGCGCGTCTAATTCA	*BamHI*
nagA-1	GACGGTGGTCATTGCGACTG	–
nagA-2	GCATAGGCGCGCCCCTCGACGAACTCCGTGTG	*AscI*
nagA-3	CGATTGCGGCCGCGGTAGCAACCTACCTAGATGG	*NotI*
nagA-4	CGTAGATATTCAGCCTGCATACC	–
nagB-1	GGGTGTCGTTCATGACAAGGG	–
nagB-2	GCATAGGCGCGCCGCTACTTCCTGTCGCAAGTCC	*AscI*
nagB-3	CGATTGCGGCCGCGCAGATGCTGAAGCGCTTAGC	*NotI*
nagB-4	CCATAGACAATGTCTAGTCTAAGC	–
glmS-1	TGCTCTAGAGGTCATCTTCGTGAACTTCACCG	*XbaI*
glmS-2	CCGCAGAATCATAGCCACGG	–
glmS-3	GCTATGATTCTGCGGCGACTGTACACCCTTACCTCTC	–
glmS-4	GAAGATCTCCAGGACAATCTCTGGGGC	*BglII*
Spec-R	GCTAAGCGGCCGCACTAAACGAAATAAACGC	*NotI*
Spec-F	GCTATGGCGCGCCCTAATCAAAATAGTGAGGAGG	*AscI*
Trmp-R	GCATGCGGCCGCGTTACGACGCGCATAGACGG	*AscI*
Trmp-F	GCATGGCGCGCCGGATTTTTGTGAGCTTGGA	*NotI*

**The underlined sequences represent the respective restriction sites.*

S. pneumoniae D39 wild-type was compared to D39 Δ*ccpA*, grown in biological replicates in CDM with 0.5% NAG. The cells were harvested at their respective mid-exponential growth phases. All other procedures regarding the DNA microarray experiment and data analysis were performed as previously described (Afzal et al., 2015a; Shafeeq et al., 2015). For the identification of differentially expressed genes a Bayesian $p < 0.001$ and a fold change cut-off ≥ 2 was applied. Microarray data have been submitted to GEO (Gene Expression Omnibus) database under the accession number GSE89589 and GSE89590.

RESULTS

The Putative NAG Regulon in *S. pneumoniae*

The NAG regulon consists of *nagA*, *nagB,* and *glmS* in *S. mutans* and is regulated by a GntR-family transcriptional regulator NagR (Moye et al., 2014). NagA is an NAG-6-phosphate deacetylase, whereas NagB is a GlcN-6-P deaminase, and GlmS is a Fru-6-P amidotransferase. *S. pneumoniae* D39 also possess the genes that encode proteins putatively involved in the transport and utilization of NAG. These genes are *nagA*, *nagB*, *manLMN*, *nanP*, and *glmS*. In *S. pneumoniae*, it appears that NAG enters the cell through NanP PTS (SPD-1496) and/or ManLMN (SPD-0262-64) and is subsequently phosphorylated (Kanehisa et al., 2014). NanP (PTS) is encoded by the gene that is part of *nan* operon-I (*spd_1488-97*) of the *nan* gene cluster and is proposed to transport amino sugars (Bidossi et al., 2012; Afzal et al., 2015b). *nanP* codes for EIIBC components of the PTS and therefore, needs EIIA component of another PTS to phosphorylate the incoming NAG. The phosphorylated NAG is deacetylated to glucosamine-6-P by NagA (Kanehisa et al., 2014). NagB converts glucosamine-6-P to fructose-6-P, whereas GlmS converts fructose-6-P to glucosamine-6-P. The role of NAG on the gene expression of *S. pneumoniae* has not been investigated before. Therefore, we decided to explore the effect of NAG on the whole transcriptome of *S. pneumoniae*.

NAG-Dependent Gene Expression in *S. pneumoniae*

To study the transcriptomic response of *S. pneumoniae* D39 to NAG, microarray comparison of *S. pneumoniae* D39 wild-type grown in CDM with 0.5% NAG to that grown in CDM with

0.5% glucose was performed. Presence of NAG in the medium resulted in altered expression of a number of genes/operons after applying the criteria of ≥2.0-fold and $p < 0.001$ (Table S1). **Table 3** summarizes the transcriptome changes incurred in *S. pneumoniae* in the presence of NAG and lists the fold-change in the expression of the putative NAG transport and utilization genes.

The glutamine regulon was downregulated around 4-fold in the presence of NAG. This regulon consists of genes involved in glutamine synthesis and uptake (*glnA* and *glnPQ*), glutamate synthesis (*gdhA*), and the gene coding for the pentose phosphate pathway enzyme Zwf, which forms an operon with *glnPQ* (Kloosterman et al., 2006b). The glutamine regulon is shown to be repressed in the presence of a nitrogen source (Kloosterman et al., 2006b). The presence of nitrogen in NAG might be the reason of down-regulation of the glutamine regulon. A putative operon *spd_1969-72* was highly upregulated in the presence of NAG. This operon encodes proteins that are putatively involved in the utilization of carbohydrates. *spd_1970* codes for a ROK-family protein (RokD), but it lacks an HTH (helix-turn-helix) domain making it a less probable candidate as a transcriptional regulator of this operon (Shafeeq et al., 2012). ROK-family proteins are a class of transcriptional regulators involved in carbohydrate-dependent transcriptional control (repressor, ORF and kinase). They also contain sugar kinases and many functionally uncharacterized proteins (Titgemeyer et al., 1994). This operon was also upregulated in the presence of cellobiose (Shafeeq et al., 2013) and some other sugars making it a candidate for the utilization of multiple sugars. *strH* is another gene that was highly upregulated in the presence of NAG. StrH is a β-N-acetylhexosaminidase and is an important virulence factor of *S. pneumoniae*. StrH is a cell-surface attached β-N-acetylglucosaminidase that is used by *S. pneumoniae* to process the termini of host complex N-linked glycans (Pluvinage et al., 2013). StrH and SPD-1969 are also possibly being involved in the conversion of chitobiose into NAG based presumably on bioinformatics (Kanehisa et al., 2014). Similarly, *spd_1973-74* was also upregulated in our microarray analysis. Both these genes are annotated to be involved in carbohydrate metabolism, where SPD-1973 is a putative α-1,2-mannosidase and SPD-1974 is a hypothetical protein.

cel gene cluster (*spd-0277-0283*) putatively involved in the utilization of cellobiose is upregulated in the presence of NAG. This gene cluster is shown to be activated by transcriptional regulator CelR in the presence of cellobiose (Shafeeq et al., 2011). Tagatose pathways (*lac* gene cluster) and Leloir pathway genes (*galK* and *galT*) involved in the utilization of lactose and galactose (Afzal et al., 2014, 2015e) are significantly upregulated in the presence of NAG. *lac* gene cluster comprises of two operons in *S. pneumoniae*, i.e., *lac* operon-I (*lacABCD*) and *lac* operon-II (*lacFEG*) (Afzal et al., 2014). LacR, a DeoR-type regulator acts as a transcriptional repressor of *lac* operon-I in the absence of lactose/galactose (Afzal et al., 2014). Whereas, BglG-family transcriptional antiterminator LacT acts as a transcriptional activator of the *lac* operon-II in the presence of lactose (Afzal et al., 2014). Putative Raffinose uptake genes

TABLE 3 | Summary of data from Table S1 showing transcriptome comparison of *S. pneumoniae* D39 wild-type grown in CDM with 0.5% NAG to that grown in CDM with 0.5% glucose.

D39 tag[a]	Function[b]	Ratio[c]
spd_1971	Glycosyl hydrolase-related protein	22.8
spd_0063	β-N-acetylhexosaminidase, StrH	14.2
spd_1970	ROK family protein	13.9
spd_1050	Tagatose 1,6-diphosphate aldolase, LacD	13.7
spd_1972	hypothetical protein	13.6
spd_0277	6-phospho-β-glucosidase	13.1
spd_1969	Glycosyl hydrolase-related protein	11.9
spd_1051	Tagatose-6-phosphate kinase, LacC	11.0
spd_1052	Galactose-6-phosphate isomerase, LacB	10.7
spd_1053	Galactose-6-phosphate isomerase, LacA	9.9
spd_0280	Transcriptional regulator, CelR	7.7
spd_1677	Sugar ABC transporter, RafE	7.4
spd_1676	Sugar ABC transporter, RafF	6.6
spd_1634	Galactokinase, GalK	6.5
spd_1633	Galactose-1-phosphate uridylyltransferase, GalT	6.3
spd_1675	Sugar ABC transporter, RafG	5.6
spd_1047	PTS system, lactose-specific IIBC components, LacE	5.4
spd_0283	PTS system, IIC component	5.2
spd_1974	Hypothetical protein	4.8
spd_1046	6-phospho-β-galactosidase, LacG	4.4
spd_1049	Transcription antiterminator, LacT	4.4
spd_0282	Hypothetical protein	4.4
spd_0281	PTS system, IIA component	4.2
spd_1664	PTS system, trehalose-specific IIABC components	4.2
spd_1663	α-phosphotrehalase, TreC	4.0
spd_0279	PTS system, IIB component	3.9
spd_1495	Sugar ABC transporter, sugar-binding protein	3.7
spd_1973	α-1,2-mannosidase, putative	3.6
spd_1496	PTS system, IIBC components	3.4
spd_0263	PTS system, mannose-specific IIC component, ManM	3.2
spd_0262	PTS system, mannose/fructose/sorbose family protein, IID component	3.0
spd_1494	Sugar ABC transporter, permease protein	2.7
spd_1493	Sugar ABC transporter, permease protein	2.4
spd_1866	N-acetylglucosamine-6-phosphate deacetylase, NagA	2.4
spd_1846	PTS system, IIB component	2.3
spd_1246	glucosamine-6-phosphate isomerase, NagB	2.3
spd_0264	PTS system, mannose-specific IIAB components, ManL	2.1
spd_1492	Hypothetical protein	2.0
spd_1491	Hypothetical protein	2.0
spd_1100	Glucose-6-phosphate 1-dehydrogenase, Zwf	−2.2
spd_0448	Glutamine synthetase, GlnA	−3.3
spd_1099	Amino acid ABC transporter, ATP-binding protein	−3.3
spd_0447	Transcriptional regulator, GlnR	−3.7
spd_1098	Amino acid ABC transporter, amino acid-binding protein	−4.4

[a] *Gene numbers refer to D39 locus tags.*
[b] *D39 annotation (Lanie et al., 2007).*
[c] *Ratio represents the fold increase/decrease in the expression of genes in the presence of 0.5% NAG compared to 0.5% glucose.*

rafEFG (*spd-1675-77*) are highly upregulated in the presence of NAG. Glucose and sucrose are shown to inhibit raffinose uptake (Tyx et al., 2011). A putative trehalose system (*spd-1663-64*) is highly expressed under our tested conditions. Upregulation of these different sugar systems under our tested conditions might be due to absence of CCR in the presence of NAG as a sole carbon source and further experiments are required to explore the role of these genes in the utilization of NAG.

Expression of genes that are putatively part of NAG utilization and transport pathway was also altered in our transcriptome analysis (**Table 3**). Expression of *manLMN* is upregulated around 3-fold in the presence of NAG. We observed upregulation of the *nan* operon-I, which is involved in the transport and utilization of sialic acid (an amino carbon source) (Marion et al., 2011). Moreover, expression of *nagA* and *nagB* was upregulated more than two folds in the presence of NAG (**Table 3**). No change in the expression of *glmS* is observed in our transcriptome in the presence of NAG. Upregulation of *nanP*, *manLMN*, *nagA*, and *nagB* in our transcriptome supports that these genes are important in NAG utilization in *S. pneumoniae* and strengthens the notion that NanP and ManLMN might be very important for NAG transport. Therefore, we decided to further explore the regulation of these genes in the presence of NAG.

NAG Induces the Expression of the Genes Involved in the Putative Transport and Utilization of Amino Sugars

In order to investigate in more detail the transcriptional regulation of *nanP*, *manLMN*, *nagA*, and *nagB* in the presence of NAG and to confirm our microarray results, we made ectopic transcriptional *lacZ*-fusions of *nanE*, *manL*, *nagA*, and *nagB* promoters (P*nagA-lacZ*, P*nagB-lacZ*, P*nanE-lacZ*, and P*manL-lacZ*) and performed β-galactosidase assays (**Figure 1**). Our β-galactosidase assays data revealed that the expression of P*nagA-lacZ*, P*nagB-lacZ*, P*nanE-lacZ*, and P*manL-lacZ* was strikingly higher in the presence of NAG compared to glucose in CDM (**Figure 1**). These data further confirm our microarray data mentioned above. We did not observe any change in the expression of *glmS* in our microarray analysis in the presence of NAG. To further study the expression of *glmS* in the presence of NAG and confirm our microarray analysis, we constructed ectopic transcriptional *lacZ*-fusion of *glmS* promoter (P*glmS-lacZ*) and performed β-galactosidase assays. We could not see any significant change in the expression of P*glmS-lacZ* under our tested conditions.

Predication and Confirmation of the *dre* Sites in the Promoter Regions of *glmS*, *nagA,* and *nagB*

Recently, NagR was characterized as a transcriptional repressor and shown to bind with specific DNA sequences named as *dre* sites, present in the promoter regions of the *nagAB* and *glmS* genes in *S. mutans* (Zeng and Burne, 2015). Blast search in *S. pneumoniae* D39 for NagR revealed the presence of a putative GntR-family transcriptional regulator NagR (SPD-1275)

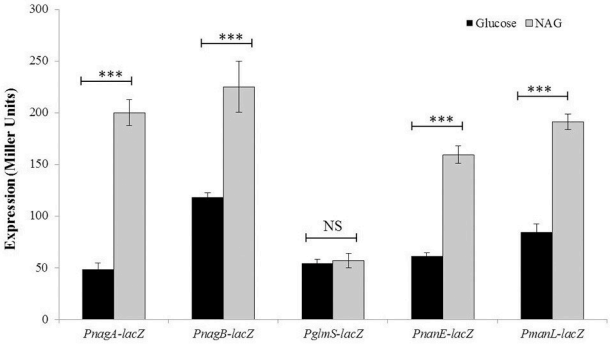

FIGURE 1 | Expression levels (in Miller units) of P*nagA-lacZ*, P*nagB-lacZ*, P*glmS-lacZ*, P*nanE-lacZ*, and P*manL-lacZ* in *S. pneumoniae* D39 wild-type grown in CDM either with 0.5% glucose or with 0.5% NAG. Standard deviations of three independent experiments are indicated in bars. Statistical significance of the differences in the expression levels was determined by one-way ANOVA (NS, not significant and $^{***}P < 0.0001$).

in *S. pneumoniae* D39. Presence of a NagR ortholog in *S. pneumoniae* might suggest its role in the regulation of the *glmS*, *nagA,* and *nagB*. We decided to delete *nagR* in *S. pneumoniae* D39 and study its role. However, we could not delete *nagR* in *S. pneumoniae* D39, suggesting the essentiality of NagR in the lifestyle of *S. pneumoniae*.

To explore the NagR regulated genes in *S. pneumoniae* D39, we decided to explore the genome of *S. pneumoniae* D39 for *dre* sites by using the Genome2D tool (Baerends et al., 2004) and a MEME motif sampler search (Bailey and Elkan, 1994). A 20-bp consensus sequence was found upstream of *nagA* (5′-AAATAGGTCTATACCATTTA-3′) and *nagB* (5′- AAATTGGTCTATACCATATA-3′) in *S. pneumoniae* D39 (Figure S1). We also found three *dre* sites in the promoter region of *glmS* (5′-AATTTGAACTATACCAATTT-3′, 5′-AAACAAGTATATACTGTTTT-3′ and 5′-GAATTAGACT ATACCAATTT-3′). These DNA stretches may serve as *dre* sites in *S. pneumoniae*. We further checked the conservation of this *dre* site in other streptococcal species (*Streptococcus mitis*, *Streptococcus agalactiae*, *Streptococcus dysgalactiae*, *Streptococcus equi*, *S. mutans*, *Streptococcus pyogenes*, *Streptococcus sanguinis*, *Streptococcus gallolyticus*, *Streptococcus suis,* and *Streptococcus uberis*) and constructed weight matrix of the putative *dre* sites presents in different streptococci (Figure S2). We found that the *dre* sequence is highly conserved in the promoter regions of *nagA*, *nagB* and *glmS* in these streptococci as well (Figure S1).

To determine if the located stretch of DNA mediates the NagR-dependent transcriptional control of the *glmS*, *nagA,* and *nagB*, we made a number of transcriptional *lacZ*-fusions, where conserved bases in the putative *dre* sites were mutated in P*nagA* (5′-AAATAGGTCTATACCATTTA-3′ to 5′-AAATAGGTC**GCTGT**CATTTA-3′), P*nagB* (5′-AAATTGGTC TATACCATATA-3′ to 5′-AAATTGGTC**GCTGT**CATATA-3′) and P*glmS* (first site: 5′-AATTTGAACTATACCAATTT-3′ to 5′-AATTTGAAC**GCTGT**CAATTT-3′ and third site: 5′-GAATTAGACTATACCAATTT-3′ to 5′-GAATTAGAC

GCGCCCAATTT-3′). We could not mutate the second *dre* site in P*glmS* as it overlaps with core promoter sequence. The expression of P*nagA-M-lacZ* and P*nagB-M-lacZ* (few conserved bases of the *dre* sites were mutated) compared to that of the promoters with the intact *dre* sites (P*nagA-lacZ* and P*nagB-lacZ*) was considerably higher in the presence of glucose and NAG (**Figures 2A,B**). A derepression of the expression of P*glmS* was observed when either of the putative *dre* sites in P*glmS* (*dre* site 1 and 3) was mutated. These results suggest that *dre* sites present in P*glmS*, P*nagA* and P*nagB* are active and may act as an operator site for NagR in *S. pneumoniae*.

nagA and *nagB* Are Essential for *S. pneumoniae* D39 to Grow in the Presence of NAG as a Sole Carbon Source

nagA, *nagB,* and *glmS* encode important enzymes for the metabolism of NAG in bacteria. To elucidate the significance of these genes on the growth of *S. pneumoniae*, we made knockout mutants of these genes (Δ*nagA*, Δ*nagB,* and Δ*glmS*), and explored the impact of mutation of these genes on the growth of *S. pneumoniae* D39 in the presence of 0.5% NAG or glucose in CDM. The genetic organization and PCR confirmation of *nagA*, *nagB,* and *glmS* mutants are given in the **Figure 3** and Figure S3, respectively. All three mutants (Δ*nagA*, Δ*nagB,* and Δ*glmS*) had approximately the same growth as D39 wild-type in the presence of glucose in the medium (**Figure 4**). Δ*glmS* also showed the same growth pattern as the D39 wild-type in the presence of NAG. However, in contrast to D39 wild-type, Δ*nagA* and Δ*nagB* were not able to grow in the presence of NAG (**Figure 4**). These results suggest that *nagA* and *nagB* are necessary for *S. pneumoniae* to grow in the presence of NAG. These results are also in accordance with recently published data, where they showed that a mutant of *nagA* did not grow in the presence of NAG as a sole carbon source (a phenotype that could be complemented) (Paixão et al., 2015).

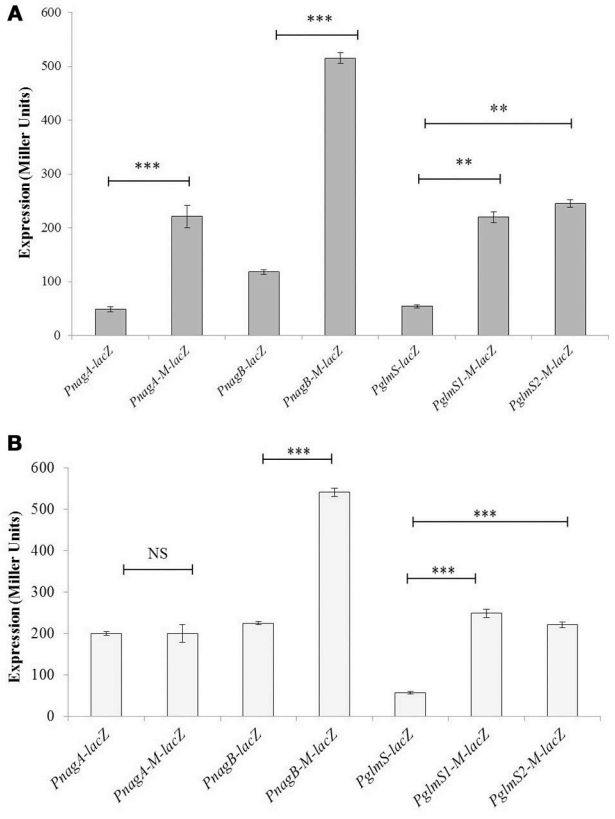

FIGURE 2 | Verification of *dre* sites in P*nagA*, P*nagB,* and P*glmS*. Expression levels (in Miller units) of P*nagA-lacZ*, P*nagB-lacZ*, P*glmS-lacZ*, P*nagA-M-lacZ*, P*nagB-M-lacZ*, P*glmS1-M-lacZ*, and P*glmS3-M-lacZ* in *S. pneumoniae* D39 wild-type grown in CDM with 0.5% glucose **(A)** and 0.5% NAG **(B)**. P*nagA-M-lacZ* and P*nagB-M-lacZ* represent promoter *lacZ*-fusions of *nagA* and *nagB* with mutated *dre* sites, whereas P*glmS1-M-lacZ* and P*glmS3-M-lacZ* represents promoter-*lacZ*-fusions with mutated *dre* site 1 and 3, respectively in P*glmS*. Standard deviations of three independent experiments are indicated in bars. Statistical significance of the differences in the expression levels was determined by one-way ANOVA (NS, not significant, $^{**}P < 0.001$, and $^{***}P < 0.0001$).

Role of CcpA in Regulation of *nagA*, *nagB*, *nanP*, *glmS*, and *manL*

CcpA is the master transcriptional regulator in *S. pneumoniae* that represses the expression of genes involved in the utilization of non-preferred sugars in the presence of a preferred one. To explore the effect of *ccpA* deletion on the transcriptome of *S. pneumoniae* and in NAG-dependent regulation of NAG utilization and transport genes, we performed transcriptome comparison of D39 Δ*ccpA* to D39 wild-type in CDM with 0.5% NAG. Expression of a number of genes was altered significantly (Table S1). These genes have been categorized according to their protein function in COG categories (**Table 4**). We did not observe any significant change in the expression of *nagA*, *nagB,* or *glmS*, suggesting CcpA independent expression of these genes. However, expression of *manLMN* and *nan* operon-I was upregulated in Δ*ccpA*, which might suggest a putative role of CcpA in regulation of the *manLMN* and *nan* operon-I. *nan* operon-I was already shown to be regulated by CcpA and to have a *cre* box (Afzal et al., 2015b). Therefore, upregulation of *nan* operon-I in the absence of *ccpA* strengthens the previous observation (Afzal et al., 2015b).

To further confirm the role of CcpA in the regulation of *nagA*, *nagB*, *glmS*, and *manL*, we analyzed the promoter regions of these genes for the presence of *cre* boxes. We could not find a *cre* box in the promoter regions of *nagA*, *nagB,* and *glmS*, which might confirm the CcpA-independent regulation of the *nagA*, *nagB,* and *glmS* by transcriptional regulator NagR. However, we found a putative *cre* box (5′-ATGAAAACGGTTTATA-3′) in the promoter regions of *manL*, further confirming the role of CcpA in the regulation of *manLMN*.

DISCUSSION AND CONCLUSIONS

The existence of well-developed sugar transport mechanisms in the opportunistic respiratory human pathogen, *S. pneumoniae*, emphasizes the importance of carbohydrates in the lifestyle of pneumococcus and confers an extra advantage to survive in a

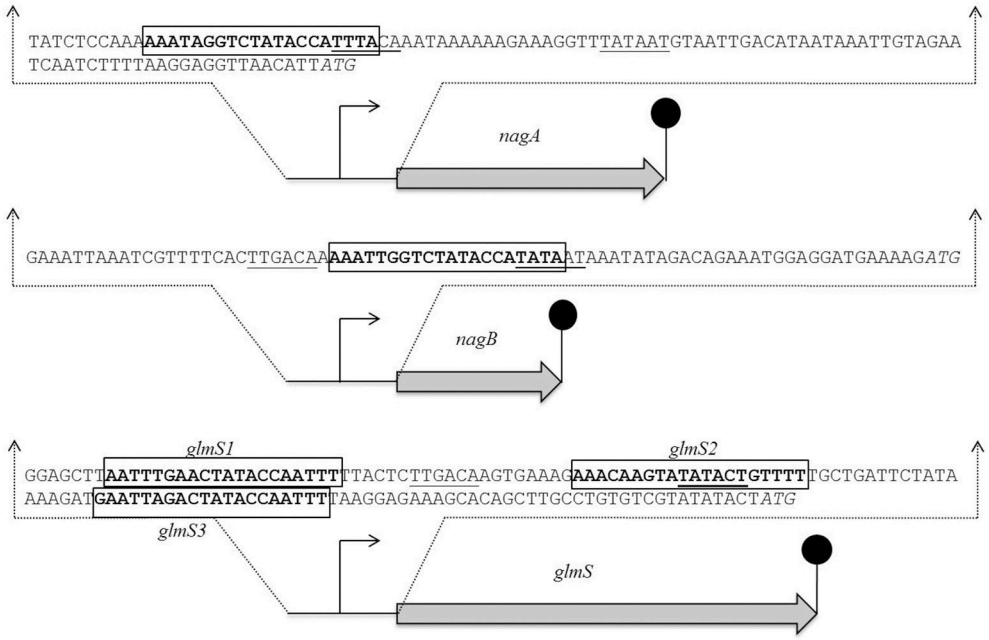

FIGURE 3 | Identification of the *dre* site in the promoter regions of *nagA*, *nagB,* and *glmS* in *S. pneumoniae* D39 wild-type. Translational start sites are italicized and putative *dre* sites are bold and rectangle. Core promoter sequences are underlined.

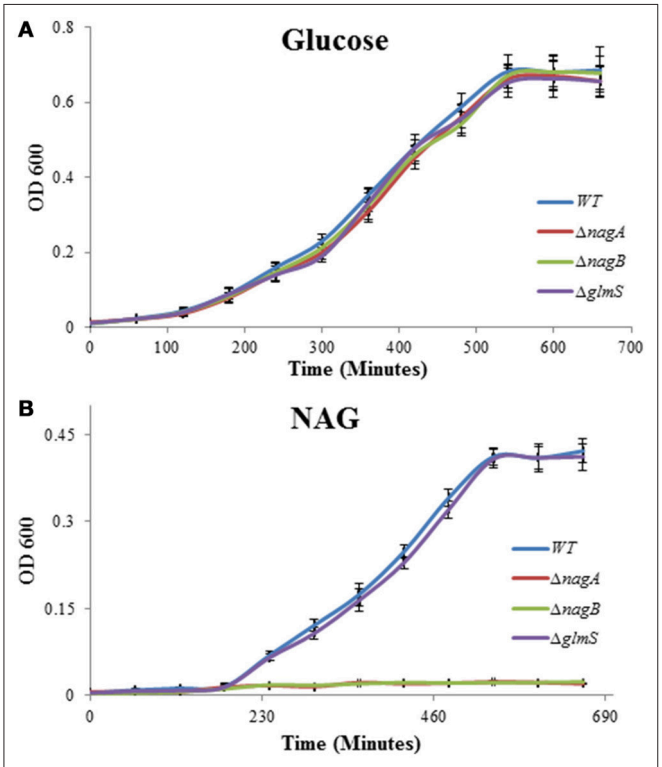

FIGURE 4 | Growth of *S. pneumoniae* D39 wild-type and its isogenic mutants Δ*nagA*, Δ*nagB,* and Δ*glmS* grown in CDM with 0.5% glucose (A) and 0.5% NAG **(B)**.

changing nutritional environment (Tettelin et al., 2001). Glucose is the most preferred carbon source for *S. pneumoniae* but the presence of several other sugar-specific systems in *S. pneumoniae* indicates its ability to use other available sugars (Hoskins et al., 2001; Lanie et al., 2007; Bidossi et al., 2012). Extensive studies have been performed regarding regulatory mechanisms of different dedicated systems for sugars, including maltose, raffinose, cellobiose, sialic acid, and others in *S. pneumoniae* (Tyx et al., 2011; Shafeeq et al., 2013; Afzal et al., 2015b,f). Lack of free carbohydrates in the human airway makes modification and import of complex glycans much more critical for pneumococci to obtain the necessary carbon (Buckwalter and King, 2012). At least nine surface-associated glycosidases have been shown to modify host glycans in pneumococci, which makes bacterial survival better in the host (King et al., 2006; Burnaugh et al., 2008; Dalia et al., 2010). Data suggests that NAG may be an important carbohydrate for pneumococci (Bidossi et al., 2012). The regulatory mechanisms of genes putatively involved in NAG utilization have not been explored in *S. pneumoniae*. The current study sheds light on the regulatory mechanism of the *nagA*, *nagB,* and *glmS* in *S. pneumoniae*.

nagA, *nagB,* and *glmS* are annotated as a part of the amino sugar metabolism pathways in *S. pneumoniae* (Kanehisa et al., 2014). In our transcriptome comparison of *S. pneumoniae* D39 grown in CDM with 0.5% NAG to that grown in CDM with 0.5% glucose revealed increased expression of *nagA*, *nagB*, *manLMN*, and *nanP*. In *S. mutans*, expression of *glmS* is repressed in the presence of NAG compared to glucose (Zeng and Burne, 2015). This repression of *glmS* in the presence of NAG was relieved

TABLE 4 | Number of genes significantly affected in *S. pneumoniae* D39 Δ*ccpA* compared to the D39 wild-type grown in CDM with 0.5% NAG.

Functional categories	Total	Up	Down
C: Energy production and conversion	10	4	6
D: Cell cycle control, cell division, chromosome partitioning	2	0	2
E: Amino acid transport and metabolism	4	3	1
F: Nucleotide transport and metabolism	1	0	1
G: Carbohydrate transport and metabolism	19	17	2
H: Coenzyme transport and metabolism	1	0	1
I: Lipid transport and metabolism	3	0	3
J: Translation, ribosomal structure and biogenesis	15	3	12
K: Transcription	3	2	1
L: Replication, recombination and repair	3	2	1
M: Cell wall/membrane/envelope biogenesis	6	2	4
O: Posttranslational modification, protein turnover, chaperones	3	3	0
P: Inorganic ion transport and metabolism	3	1	2
Q: Secondary metabolites biosynthesis, transport and catabolism	2	1	1
R: General function prediction only	5	3	2
S: Function unknown	42	22	20
T: Signal transduction mechanisms	3	3	0
U: Intracellular trafficking, secretion, and vesicular transport	2	2	0
V: Defense mechanisms	8	7	1
Others	34	19	15
Total number of genes	169	94	75

Genes affected with more than 2-fold in D39 ΔccpA compared to the D39 wild-type are shown in COG functional categories.

in *nagR* mutant (Zeng and Burne, 2015). However, no change in the expression of *glmS* is observed in our NAG-dependent transcriptome and no effect of *ccpA* deletion on the expression of *glmS* is observed. Mutating *dre* site 1 or 3 in the P*glmS* led to increase in expression of *PglmS* in the presence of glucose and NAG. This might indicate that NagR represses the expression of *glmS* in the presence of glucose and NAG.

The transport of amino-sugars has been attributed to a PTS (NanP) and *manLMN* in *S. mutans* (Moye et al., 2014). Similarly, a NAG-specific PTS (NagE) and a mannose-specific PTS ManXYZ have been shown to be involved in the NAG transport in *E. coli* (White, 1970; Alvarez-Añorve et al., 2009). *manLMN* has also been proposed to be involved in NAG transport in *S. pneumoniae* (Bidossi et al., 2012). Similarly, a PTS present in *nan* operon-I (putatively called *nanP*) has been suggested to play a part in the transport of glucosamine in *S. pneumoniae* (Kanehisa et al., 2014). *manLMN* and *nanP* are upregulated in our NAG-dependent transcriptome analysis, which is further confirmed by β-galactosidase assays. These observations confirm the findings of the previous studies and strengthen the involvement of *nanP* and *manLMN* in the transport of NAG.

NagA, NagB, and GlmS are very important for the metabolism of NAG and these three factors are associated with the synthesis of GlcN-6-P, a precursor for cell wall peptidoglycan synthesis in *E. coli* (Plumbridge et al., 1993; Plumbridge and Vimr, 1999). Here, we have studied the impact of *nagA*, *nagB,* and *glmS* deletions on the growth of *S. pneumoniae* in the presence of NAG. Our studies suggest that *nagA* and *nagB* are important for pneumococcus to grow on NAG as their deletion mutants failed to grow in the presence of NAG in the medium as a sole carbon source. NagA has also been shown to be essential for growth in the presence of NAG as a sole carbon source (Paixão et al., 2015). However, no impact of *glmS* deletion on the growth of *S. pneumoniae* was observed. In *B. subtilis*, *nagB* has been shown to be essential for growth in the presence of NAG (Gaugué et al., 2013). NagB and GlmS have been shown to be involved in virulence in *S. mutans* (Kawada-Matsuo et al., 2012). Inactivation of *nagB* led to a decrease in the expression of virulence factors, including cell-surface protein antigen and glucosyltransferase, and also impeded biofilm formation and saliva-induced aggregation in *S. mutans* (Kawada-Matsuo et al., 2012). Pneumococcal *nagA* mutant was tested in mouse model of colonization and of model of bronchopneumonia with bacteremia, and no difference in virulence was observed (Paixão et al., 2015). It might be still interesting to further explore the role of the *nagB* and *glmS* in virulence of *S. pneumoniae*.

In *E. coli,* a ROK-family protein (NagC) acts as a transcriptional repressor of the NAG regulon (*nagE* and *nagBACD*), which encodes genes that are involved in the uptake and metabolism of NAG. Furthermore, it has been shown that NAG binds to NagC to relieve the repression caused by NagC (Plumbridge, 1991; Titgemeyer et al., 1994). Similarly, a GntR family transcriptional regulator NagR has been shown to act as a transcriptional regulator of the genes involved in NAG utilization in *B. subtilis*, *S. mutans* and in some other bacteria

(Bertram et al., 2011; Moye et al., 2014). In *S. mutans*, NagR has been shown to regulate the expression of *glmS* and *nagAB* by binding to the NagR operator sites called *dre* sites (Zeng and Burne, 2015). Our study suggests that NagR is present in *S. pneumoniae* and might regulate the expression of the *nagA*, *nagB,* and *glmS* by binding to the *dre* sites present in the promoter regions of these genes. We could not delete *nagR*, which might indicate about its essentiality or its involvement in some important cell process directly or indirectly. However, we mutated the conserved bases in the *dre* sites present in the promoter regions of *nagA*, *nagB,* and *glmS* which might suggest the importance of these bases in the regulation of these genes. To explore more putative *dre* sites in the D39 genome, we conducted a genome-wide search for putative pneumococcal *dre* sites. A *dre* site was only found in the promoter regions of *nagA* and *nagB*, and three *dre* sites were found in the promoter region of *glmS*. This predicted *dre* site was also found to be highly conserved in other streptococcal species as well (Novichkov et al., 2010), suggesting a similar function of NagR in these organisms.

The master transcriptional regulator, CcpA (Carbon catabolite protein A), was shown to be involved in the repression of non-preferred sugar metabolism genes in the presence of a preferred carbon source, and has a role in pneumococcal pathogenesis (Lulko et al., 2007; Zomer et al., 2007; Carvalho et al., 2011). A number of non-preferred sugar systems have also been shown to be regulated independently of CcpA by other transcriptional regulators, like the *cel* gene cluster activated by CelR in *S. pneumoniae* (Shafeeq et al., 2011). In this study, we elucidated the role of CcpA in the regulation of *nagA*, *nagB*, *glmS*, *manLMN*, and the *nan* operon-I by elaborating the impact of a *ccpA* deletion on the whole transcriptome of *S. pneumoniae* in the presence of NAG as a sole carbon source in CDM. Our transcriptome data demonstrated the CcpA-independent expression of *nagA*, *nagB,* and *glmS*, and CcpA-dependent expression of *manLMN* and the *nan* operon-I. We further analyzed the promoter regions of these genes for the presence of a *cre* box and found *cre* boxes only in the promoter regions of *manLMN* and the *nan* operon-I. The absence of *cre* boxes in the promoter regions of *nagA*, *nagB,* and *glmS* confirms that CcpA may not have a role in the regulation of *nagA*, *nagB,* and *glmS*. However, the presence of a *cre* box in the promoter regions of *manLMN* and the *nan* operon-I further supports the role of CcpA in the regulation of *manLMN* and the *nan* operon-I.

AUTHOR CONTRIBUTIONS

Substantial contributions to the conception or design of the work; or the acquisition, analysis, or interpretation of data for the work: MA, SS, IM, BHN, and OPK. Drafting the work or revising it critically for important intellectual content: MA, SS, IM, BHN, and OPK. Final approval of the version to be published: MA, SS, IM, BHN, and OPK. Agreement to be accountable for all aspects of the work in ensuring that questions related to the accuracy or integrity of any part of the work are appropriately investigated and resolved: MA, SS, IM, BHN, and OPK.

ACKNOWLEDGMENTS

MA and IM are supported by Government College University, Faisalabad, Pakistan under faculty development program of HEC Pakistan.

SUPPLEMENTARY MATERIAL

The Supplementary Material for this article can be found online at: http://journal.frontiersin.org/article/10.3389/fcimb.2016.00158/full#supplementary-material

REFERENCES

Afzal, M., Manzoor, I., and Kuipers, O. P. (2015a). A fast and reliable pipeline for bacterial transcriptome analysis case study: serine-dependent gene regulation in *Streptococcus pneumoniae*. *J. Vis. Exp. JoVE.* e52649. doi: 10.3791/52649

Afzal, M., Shafeeq, S., Ahmed, H., and Kuipers, O. P. (2015b). Sialic acid-mediated gene expression in *Streptococcus pneumoniae* and role of NanR as a transcriptional activator of the *nan* gene cluster. *Appl. Environ. Microbiol.* 81, 3121–3131. doi: 10.1128/AEM.00499-15

Afzal, M., Shafeeq, S., Henriques-Normark, B., and Kuipers, O. P. (2015c). UlaR activates expression of the *ula* operon in *Streptococcus pneumoniae* in the presence of ascorbic acid. *Microbiol. Read. Engl.* 161, 41–49. doi: 10.1099/mic.0.083899-0

Afzal, M., Shafeeq, S., and Kuipers, O. P. (2014). LacR is a repressor of *lacABCD* and LacT is an activator of *lacTFEG*, constituting the *lac*-gene cluster in *Streptococcus pneumoniae*. *Appl. Environ. Microbiol.* 80, 5349–5358. doi: 10.1128/AEM.01370-14

Afzal, M., Shafeeq, S., and Kuipers, O. P. (2015d). Ascorbic acid-dependent gene expression in *Streptococcus pneumoniae* and the activator function of the transcriptional regulator UlaR2. *Front. Microbiol.* 6:72. doi: 10.3389/fmicb.2015.00072

Afzal, M., Shafeeq, S., Manzoor, I., and Kuipers, O. P. (2015e). GalR acts as a transcriptional activator of *galKT* in the presence of galactose in *Streptococcus pneumoniae*. *J. Mol. Microbiol. Biotechnol.* 25, 363–371. doi: 10.1159/000439429

Afzal, M., Shafeeq, S., Manzoor, I., and Kuipers, O. P. (2015f). Maltose-dependent transcriptional regulation of the *mal* regulon by MalR in *Streptococcus pneumoniae*. *PLoS ONE* 10:e0127579. doi: 10.1371/journal.pone.0127579

Alice, A. F., Pérez-Martínez, G., and Sánchez-Rivas, C. (2003). Phosphoenolpyruvate phosphotransferase system and N-acetylglucosamine metabolism in Bacillus sphaericus. *Microbiol. Read. Engl.* 149, 1687–1698. doi: 10.1099/mic.0.26231-0

Alvarez-Añorve, L. I., Bustos-Jaimes, I., Calcagno, M. L., and Plumbridge, J. (2009). Allosteric regulation of glucosamine-6-phosphate deaminase (NagB) and growth of *Escherichia coli* on glucosamine. *J. Bacteriol.* 191, 6401–6407. doi: 10.1128/JB.00633-09

Baerends, R. J. S., Smits, W. K., de Jong, A., Hamoen, L. W., Kok, J., and Kuipers, O. P. (2004). Genome2D: a visualization tool for the rapid analysis of bacterial transcriptome data. *Genome Biol.* 5:R37. doi: 10.1186/gb-2004-5-5-r37

Bailey, T. L., and Elkan, C. (1994). Fitting a mixture model by expectation maximization to discover motifs in biopolymers. *Proc. Int. Conf. Intell. Syst. Mol. Biol. ISMB Int. Conf. Intell. Syst. Mol. Biol.* 2, 28–36.

Bertram, R., Rigali, S., Wood, N., Lulko, A. T., Kuipers, O. P., and Titgemeyer, F. (2011). Regulon of the N-acetylglucosamine utilization regulator NagR in *Bacillus subtilis*. *J. Bacteriol.* 193, 3525–3536. doi: 10.1128/JB.00264-11

Bidossi, A., Mulas, L., Decorosi, F., Colomba, L., Ricci, S., Pozzi, G., et al. (2012). A functional genomics approach to establish the complement of carbohydrate transporters in *Streptococcus pneumoniae*. *PLoS ONE* 7:e33320. doi: 10.1371/journal.pone.0033320

Buckwalter, C. M., and King, S. J. (2012). Pneumococcal carbohydrate transport: food for thought. *Trends Microbiol.* 20, 517–522. doi: 10.1016/j.tim.2012.08.008

Burnaugh, A. M., Frantz, L. J., and King, S. J. (2008). Growth of *Streptococcus pneumoniae* on human glycoconjugates is dependent upon the sequential activity of bacterial exoglycosidases. *J. Bacteriol.* 190, 221–230. doi: 10.1128/JB.01251-07

Carvalho, S. M., Kloosterman, T. G., Kuipers, O. P., and Neves, A. R. (2011). CcpA ensures optimal metabolic fitness of *Streptococcus pneumoniae*. *PLoS ONE* 6:e26707. doi: 10.1371/journal.pone.0026707

Dalia, A. B., Standish, A. J., and Weiser, J. N. (2010). Three surface exoglycosidases from *Streptococcus pneumoniae*, NanA, BgaA, and StrH, promote resistance to opsonophagocytic killing by human neutrophils. *Infect. Immun.* 78, 2108–2116. doi: 10.1128/IAI.01125-09

Dobrogosz, W. J. (1968). Effect of amino sugars on catabolite repression in *Escherichia coli*. *J. Bacteriol.* 95, 578–584.

Gaugué, I., Oberto, J., Putzer, H., and Plumbridge, J. (2013). The use of amino sugars by *Bacillus subtilis*: presence of a unique operon for the catabolism of glucosamine. *PLoS ONE* 8:e63025. doi: 10.1371/journal.pone.0063025

Halfmann, A., Hakenbeck, R., and Bruckner, R. (2007). A new integrative reporter plasmid for *Streptococcus pneumoniae*. *FEMS Microbiol. Lett.* 268, 217–224. doi: 10.1111/j.1574-6968.2006.00584.x

Hoskins, J., Alborn, W. E. Jr., Arnold, J., Blaszczak, L. C., Burgett, S., DeHoff, B. S., et al. (2001). Genome of the bacterium *Streptococcus pneumoniae* strain R6. *J. Bacteriol.* 183, 5709–5717. doi: 10.1128/JB.183.19.5709-5717.2001

Ispahani, P., Slack, R. C. B., Donald, F. E., Weston, V. C., and Rutter, N. (2004). Twenty year surveillance of invasive pneumococcal disease in Nottingham: serogroups responsible and implications for immunisation. *Arch. Dis. Child.* 89, 757–762. doi: 10.1136/adc.2003.036921

Israelsen, H., Madsen, S. M., Vrang, A., Hansen, E. B., and Johansen, E. (1995). Cloning and partial characterization of regulated promoters from *Lactococcus lactis* Tn917-lacZ integrants with the new promoter probe vector, pAK80. *Appl. Environ. Microbiol.* 61, 2540–2547.

Jeong, J. K., Kwon, O., Lee, Y. M., Oh, D. B., Lee, J. M., Kim, S., et al. (2009). Characterization of the *Streptococcus pneumoniae* BgaC protein as a novel surface beta-galactosidase with specific hydrolysis activity for the Galbeta1-3GlcNAc moiety of oligosaccharides. *J. Bacteriol.* 191, 3011–3023. doi: 10.1128/JB.01601-08

Kanehisa, M., Goto, S., Sato, Y., Kawashima, M., Furumichi, M., and Tanabe, M. (2014). Data, information, knowledge and principle: back to metabolism in KEGG. *Nucleic Acids Res.* 42, D199–D205. doi: 10.1093/nar/gkt1076

Kawada-Matsuo, M., Mazda, Y., Oogai, Y., Kajiya, M., Kawai, T., Yamada, S., et al. (2012). GlmS and NagB regulate amino sugar metabolism in opposing directions and affect *Streptococcus mutans* virulence. *PLoS ONE* 7:e33382. doi: 10.1371/journal.pone.0033382

King, S. J. (2010). Pneumococcal modification of host sugars: a major contributor to colonization of the human airway? *Mol. Oral Microbiol.* 25, 15–24. doi: 10.1111/j.2041-1014.2009.00564.x

King, S. J., Hippe, K. R., and Weiser, J. N. (2006). Deglycosylation of human glycoconjugates by the sequential activities of exoglycosidases expressed by *Streptococcus pneumoniae*. *Mol. Microbiol.* 59, 961–974. doi: 10.1111/j.1365-2958.2005.04984.x

Kloosterman, T. G., Bijlsma, J. J. E., Kok, J., and Kuipers, O. P. (2006a). To have neighbour's fare: extending the molecular toolbox for *Streptococcus pneumoniae*. *Microbiol. Read. Engl.* 152, 351–359. doi: 10.1099/mic.0.28521-0

Kloosterman, T. G., Hendriksen, W. T., Bijlsma, J. J., Bootsma, H. J., van Hijum, S. A., Kok, J., et al. (2006b). Regulation of glutamine and glutamate metabolism by GlnR and GlnA in *Streptococcus pneumoniae*. *J. Biol. Chem.* 281, 25097–25109. doi: 10.1074/jbc.M601661200

Kloosterman, T. G., and Kuipers, O. P. (2011). Regulation of arginine acquisition and virulence gene expression in the human pathogen *Streptococcus pneumoniae* by transcription regulators ArgR1 and AhrC. *J. Biol. Chem.* 286, 44594–44605. doi: 10.1074/jbc.M111.295832

Lanie, J. A., Ng, W. L., Kazmierczak, K. M., Andrzejewski, T. M., Davidsen, T. M., Wayne, K. J., et al. (2007). Genome sequence of Avery's virulent serotype 2 strain D39 of *Streptococcus pneumoniae* and comparison with that of unencapsulated laboratory strain R6. *J. Bacteriol.* 189, 38–51. doi: 10.1128/JB.01148-06

Leenhouts, K., Venema, G., and Kok, J. (1998). A lactococcal pWV01 based integration toolbox for bacteria. *Methods Cell Sci.* 20, 35–50. doi: 10.1023/A:1009862119114

Linke, C. M., Woodiga, S. A., Meyers, D. J., Buckwalter, C. M., Salhi, H. E., and King, S. J. (2013). The ABC transporter encoded at the pneumococcal fructooligosaccharide utilization locus determines the ability to utilize long- and short-chain fructooligosaccharides. *J. Bacteriol.* 195, 1031–1041. doi: 10.1128/JB.01560-12

Lortie, L. A., Pelletier, M., Vadeboncoeur, C., and Frenette, M. (2000). The gene encoding IIAB(Man)L in *Streptococcus salivarius* is part of a tetracistronic operon encoding a phosphoenolpyruvate: mannose/glucose phosphotransferase system. *Microbiol. Read. Engl.* 146(Pt 3), 677–685. doi: 10.1099/00221287-146-3-677

Lulko, A. T., Buist, G., Kok, J., and Kuipers, O. P. (2007). Transcriptome analysis of temporal regulation of carbon metabolism by CcpA in *Bacillus subtilis* reveals additional target genes. *J. Mol. Microbiol. Biotechnol.* 12, 82–95. doi: 10.1159/000096463

Marion, C., Burnaugh, A. M., Woodiga, S. A., and King, S. J. (2011). Sialic acid transport contributes to pneumococcal colonization. *Infect. Immun.* 79, 1262–1269. doi: 10.1128/IAI.00832-10

Marion, C., Limoli, D. H., Bobulsky, G. S., Abraham, J. L., Burnaugh, A. M., and King, S. J. (2009). Identification of a pneumococcal glycosidase that modifies O-linked glycans. *Infect. Immun.* 77, 1389–1396. doi: 10.1128/IAI.01215-08

Marion, C., Stewart, J. M., Tazi, M. F., Burnaugh, A. M., Linke, C. M., Woodiga, S. A., et al. (2012). *Streptococcus pneumoniae* can utilize multiple sources of hyaluronic acid for growth. *Infect. Immun.* 80, 1390–1398. doi: 10.1128/IAI.05756-11

Mobley, H. L., Doyle, R. J., Streips, U. N., and Langemeier, S. O. (1982). Transport and incorporation of N-acetyl-D-glucosamine in *Bacillus subtilis*. *J. Bacteriol.* 150, 8–15.

Moye, Z. D., Burne, R. A., and Zeng, L. (2014). Uptake and metabolism of N-acetylglucosamine and glucosamine by *Streptococcus mutans*. *Appl. Environ. Microbiol.* 80, 5053–5067. doi: 10.1128/AEM.00820-14

Neves, A. R., Ventura, R., Mansour, N., Shearman, C., Gasson, M. J., Maycock, C., et al. (2002). Is the glycolytic flux in *Lactococcus lactis* primarily controlled by the redox charge? Kinetics of NAD(+) and NADH pools determined *in vivo* by 13C NMR. *J. Biol. Chem.* 277, 28088–28098. doi: 10.1074/jbc.M202573200

Nothaft, H., Dresel, D., Willimek, A., Mahr, K., Niederweis, M., and Titgemeyer, F. (2003). The phosphotransferase system of *Streptomyces coelicolor* is biased for N-acetylglucosamine metabolism. *J. Bacteriol.* 185, 7019–7023. doi: 10.1128/JB.185.23.7019-7023.2003

Nothaft, H., Rigali, S., Boomsma, B., Swiatek, M., McDowall, K. J., van Wezel, G. P., et al. (2010). The permease gene nagE2 is the key to N-acetylglucosamine sensing and utilization in *Streptomyces coelicolor* and is subject to multi-level control. *Mol. Microbiol.* 75, 1133–1144. doi: 10.1111/j.1365-2958.2009.07020.x

Novichkov, P. S., Laikova, O. N., Novichkova, E. S., Gelfand, M. S., Arkin, A. P., Dubchak, I., et al. (2010). RegPrecise: a database of curated genomic inferences of transcriptional regulatory interactions in prokaryotes. *Nucleic Acids Res.* 38, D111–D118. doi: 10.1093/nar/gkp894

O'Brien, K. L., Wolfson, L. J., Watt, J. P., Henkle, E., Deloria-Knoll, M., McCall, N., et al. (2009). Burden of disease caused by *Streptococcus pneumoniae* in children younger than 5 years: global estimates. *Lancet* 374, 893–902. doi: 10.1016/S0140-6736(09)61204-6

Paixão, L., Oliveira, J., Veríssimo, A., Vinga, S., Lourenço, E. C., Ventura, M. R., et al. (2015). Host glycan sugar-specific pathways in *Streptococcus pneumoniae*: galactose as a key sugar in colonisation and infection [corrected]. *PLoS ONE* 10:e0121042. doi: 10.1371/journal.pone.0121042

Paulsen, I. T., Nguyen, L., Sliwinski, M. K., Rabus, R., and Saier, M. H. (2000). Microbial genome analyses: comparative transport capabilities in eighteen prokaryotes. *J. Mol. Biol.* 301, 75–100. doi: 10.1006/jmbi.2000.3961

Phillips, N. J., John, C. M., Reinders, L. G., Gibson, B. W., Apicella, M. A., and Griffiss, J. M. (1990). Structural models for the cell surface lipooligosaccharides of *Neisseria gonorrhoeae* and *Haemophilus influenzae*. *Biomed. Environ. Mass Spectrom.* 19, 731–745. doi: 10.1002/bms.1200191112

Plumbridge, J. (2001). Regulation of PTS gene expression by the homologous transcriptional regulators, Mlc and NagC, in *Escherichia coli* (or how two similar repressors can behave differently). *J. Mol. Microbiol. Biotechnol.* 3, 371–380.

Plumbridge, J. A. (1991). Repression and induction of the nag regulon of *Escherichia coli* K-12: the roles of nagC and nagA in maintenance of the uninduced state. *Mol. Microbiol.* 5, 2053–2062. doi: 10.1111/j.1365-2958.1991.tb00828.x

Plumbridge, J. A., Cochet, O., Souza, J. M., Altamirano, M. M., Calcagno, M. L., and Badet, B. (1993). Coordinated regulation of amino sugar-synthesizing and -degrading enzymes in *Escherichia coli* K-12. *J. Bacteriol.* 175, 4951–4956.

Plumbridge, J., and Vimr, E. (1999). Convergent pathways for utilization of the amino sugars N-acetylglucosamine, N-acetylmannosamine, and N-acetylneuraminic acid by *Escherichia coli*. *J. Bacteriol.* 181, 47–54.

Pluvinage, B., Stubbs, K. A., Hattie, M., Vocadlo, D. J., and Boraston, A. B. (2013). Inhibition of the family 20 glycoside hydrolase catalytic modules in the *Streptococcus pneumoniae* exo-β-D-N-acetylglucosaminidase, StrH. *Org. Biomol. Chem.* 11, 7907–7915. doi: 10.1039/c3ob41579a

Reizer, J., Bachem, S., Reizer, A., Arnaud, M., Saier, M. H. Jr., and Stulke, J. (1999). Novel phosphotransferase system genes revealed by genome analysis - the complete complement of PTS proteins encoded within the genome of *Bacillus subtilis*. *Microbiol. Read. Engl.* 145(Pt 12), 3419–3429. doi: 10.1099/00221287-145-12-3419

Rose, M. C., and Voynow, J. A. (2006). Respiratory tract mucin genes and mucin glycoproteins in health and disease. *Physiol. Rev.* 86, 245–278. doi: 10.1152/physrev.00010.2005

Saier, M. H., Goldman, S. R., Maile, R. R., Moreno, M. S., Weyler, W., Yang, N., et al. (2002). Transport capabilities encoded within the *Bacillus subtilis* genome. *J. Mol. Microbiol. Biotechnol.* 4, 37–67.

Shafeeq, S., Afzal, M., Henriques-Normark, B., and Kuipers, O. P. (2015). Transcriptional profiling of UlaR-regulated genes in *Streptococcus pneumoniae*. *Genomics Data* 4, 57–59. doi: 10.1016/j.gdata.2015.02.004

Shafeeq, S., Kloosterman, T. G., and Kuipers, O. P. (2011). CelR-mediated activation of the cellobiose-utilization gene cluster in *Streptococcus pneumoniae*. *Microbiol. Read. Engl.* 157, 2854–2861. doi: 10.1099/mic.0.051359-0

Shafeeq, S., Kloosterman, T. G., Rajendran, V., and Kuipers, O. P. (2012). Characterization of the ROK-family transcriptional regulator RokA of *Streptococcus pneumoniae* D39. *Microbiol. Read. Engl.* 158, 2917–2926. doi: 10.1099/mic.0.062919-0

Shafeeq, S., Kuipers, O. P., and Kloosterman, T. G. (2013). Cellobiose-mediated gene expression in *Streptococcus pneumoniae*: a repressor function of the novel GntR-type regulator BguR. *PLoS ONE* 8:e57586. doi: 10.1371/journal.pone.0057586

Simoni, R. D., Roseman, S., and Saier, M. H. (1976). Sugar transport. Properties of mutant bacteria defective in proteins of the phosphoenolpyruvate: sugar phosphotransferase system. *J. Biol. Chem.* 251, 6584–6597.

Terra, V. S., Homer, K. A., Rao, S. G., Andrew, P. W., and Yesilkaya, H. (2010). Characterization of novel beta-galactosidase activity that contributes to glycoprotein degradation and virulence in *Streptococcus pneumoniae*. *Infect. Immun.* 78, 348–357. doi: 10.1128/IAI.00721-09

Tettelin, H., Nelson, K. E., Paulsen, I. T., Eisen, J. A., Read, T. D., Peterson, S., et al. (2001). Complete genome sequence of a virulent isolate of *Streptococcus pneumoniae*. *Science* 293, 498–506. doi: 10.1126/science.1061217

Titgemeyer, F., and Hillen, W. (2002). Global control of sugar metabolism: a gram-positive solution. *Antonie Van Leeuwenhoek* 82, 59–71. doi: 10.1023/A:1020628909429

Titgemeyer, F., Reizer, J., Reizer, A., and Saier, M. H. Jr. (1994). Evolutionary relationships between sugar kinases and transcriptional repressors in bacteria. *Microbiol. Read. Engl.* 140(Pt 9), 2349–2354. doi: 10.1099/13500872-140-9-2349

Tong, H. H., Blue, L. E., James, M. A., and DeMaria, T. F. (2000). Evaluation of the virulence of a *Streptococcus pneumoniae* neuraminidase-deficient mutant in nasopharyngeal colonization and development of otitis media in the chinchilla model. *Infect. Immun.* 68, 921–924. doi: 10.1128/IAI.68.2.921-924.2000

Tyx, R. E., Roche-Hakansson, H., and Hakansson, A. P. (2011). Role of dihydrolipoamide dehydrogenase in regulation of raffinose transport in *Streptococcus pneumoniae*. *J. Bacteriol.* 193, 3512–3524. doi: 10.1128/JB.01410-10

Vadeboncoeur, C. (1984). Structure and properties of the phosphoenolpyruvate: glucose phosphotransferase system of oral streptococci. *Can. J. Microbiol.* 30, 495–502. doi: 10.1139/m84-073

White, R. J. (1970). The role of the phosphoenolpyruvate phosphotransferase system in the transport of N-acetyl-D-glucosamine by *Escherichia coli*. *Biochem. J.* 118, 89–92. doi: 10.1042/bj1180089

Yesilkaya, H., Manco, S., Kadioglu, A., Terra, V. S., and Andrew, P. W. (2008). The ability to utilize mucin affects the regulation of virulence gene expression in *Streptococcus pneumoniae*. *FEMS Microbiol. Lett.* 278, 231–235. doi: 10.1111/j.1574-6968.2007.01003.x

Zeng, L., and Burne, R. A. (2015). NagR differentially regulates the expression of the glmS and nagAB genes required for amino sugar metabolism by *Streptococcus mutans*. *J. Bacteriol.* 197, 3533–3544. doi: 10.1128/JB.00606-15

Zomer, A. L., Buist, G., Larsen, R., Kok, J., and Kuipers, O. P. (2007). Time-resolved determination of the CcpA regulon of *Lactococcus lactis* subsp. cremoris MG1363. *J. Bacteriol.* 189, 1366–1381. doi: 10.1128/JB.01013-06

Conflict of Interest Statement: The authors declare that the research was conducted in the absence of any commercial or financial relationships that could be construed as a potential conflict of interest.

frontiers in Cellular and Infection Microbiology

ORIGINAL RESEARCH
published: 23 March 2022
doi: 10.3389/fcimb.2022.849224

The Age-Driven Decline in Neutrophil Function Contributes to the Reduced Efficacy of the Pneumococcal Conjugate Vaccine in Old Hosts

Shaunna R. Simmons, Essi Y. I. Tchalla, Manmeet Bhalla and Elsa N. Bou Ghanem *

Department of Microbiology and Immunology, University at Buffalo School of Medicine, Buffalo, NY, United States

Despite the availability of vaccines, *Streptococcus pneumoniae* (pneumococcus) remains a serious cause of infections in the elderly. The efficacy of anti-pneumococcal vaccines declines with age. While age-driven changes in antibody responses are well defined, less is known about the role of innate immune cells such as polymorphonuclear leukocytes (PMNs) in the reduced vaccine protection seen in aging. Here we explored the role of PMNs in protection against *S. pneumoniae* in vaccinated hosts. We found that depletion of PMNs in pneumococcal conjugate vaccine (PCV) treated young mice prior to pulmonary challenge with *S. pneumoniae* resulted in dramatic loss of host protection against infection. Immunization boosted the ability of PMNs to kill *S. pneumoniae* and this was dependent on bacterial opsonization by antibodies. Bacterial opsonization with immune sera increased several PMN anti-microbial activities including bacterial uptake, degranulation and ROS production. As expected, PCV failed to protect old mice against *S. pneumoniae*. In probing the role of PMNs in this impaired protection, we found that aging was accompanied by an intrinsic decline in PMN function. PMNs from old mice failed to effectively kill *S. pneumoniae* even when the bacteria were opsonized with immune sera from young controls. In exploring mechanisms, we found that PMNs from old mice produced less of the antimicrobial peptide CRAMP and failed to efficiently kill engulfed pneumococci. Importantly, adoptive transfer of PMNs from young mice reversed the susceptibility of vaccinated old mice to pneumococcal infection. Overall, this study demonstrates that the age-driven decline in PMN function impairs vaccine-mediated protection against *Streptococcus pneumoniae*.

Keywords: neutrophils, vaccines, *S. pneumoniae*, immunosenescence, antimicrobial activity

OPEN ACCESS

Edited by:
Matthew B. Lawrenz, University of Louisville, United States

Reviewed by:
Lee-Ann H. Allen, University of Missouri, United States
Lance Edward Keller, University of Mississippi Medical Center, United States

***Correspondence:**
Elsa N. Bou Ghanem
elsaboug@buffalo.edu

Specialty section:
This article was submitted to Molecular Bacterial Pathogenesis, a section of the journal Frontiers in Cellular and Infection Microbiology

Received: *05 January 2022*
Accepted: *28 February 2022*
Published: *23 March 2022*

Citation:
Simmons SR, Tchalla EYI, Bhalla M and Bou Ghanem EN (2022) The Age-Driven Decline in Neutrophil Function Contributes to the Reduced Efficacy of the Pneumococcal Conjugate Vaccine in Old Hosts. Front. Cell. Infect. Microbiol. 12:849224. doi: 10.3389/fcimb.2022.849224

INTRODUCTION

Streptococcus pneumoniae (pneumococcus) infections are responsible for an estimated 1.6 million deaths globally each year (WHO., 2014). Pneumococcal infections occur most frequently in young children and older adults (Grudzinska et al., 2020). In fact, *S. pneumoniae* remain the leading cause of community acquired bacterial pneumonia in people over the age of 65 years old (CDC., 2018 2018; Grudzinska et al., 2020). This is despite the availability of two pneumococcal vaccines, the

pneumococcal polysaccharide vaccine (PPSV) which is recommended for older adults and the pneumococcal conjugate vaccine (PCV) which is recommended for the most vulnerable elderly in the USA (Matanock A et al., 2019). However, both vaccines have shown reduced protection in elderly individuals (Simell et al., 2011; Gonçalves et al., 2016; Matanock A et al., 2019). This is in part, due to immunosenescence, defined as the age-related decline in immune system function (Simell et al., 2011), that leads to reduced antibody levels and function following vaccination (Simell et al., 2011; Jackson et al., 2013).

Polymorphonuclear leukocytes (PMNs) are innate immune cells required for host defense against *S. pneumoniae* infection. These cells are the first to influx to the site of pneumococcal infection and are essential for bacterial clearance (Hahn et al., 2011; Kolaczkowska and Kubes, 2013; Bou Ghanem et al., 2015; Gonçalves et al., 2016). PMNs can kill bacteria through several antimicrobial effector functions. PMNs kill extracellular bacteria *via* the release of reactive oxygen species (ROS), neutrophil extracellular traps (NETs), and by degranulation of preformed granules that contain antimicrobial compounds (Kolaczkowska and Kubes, 2013; Naegelen et al., 2015; El-Benna et al., 2016; Nguyen et al., 2017; Yin and Heit, 2018). PMNs also engulf *S. pneumoniae* through the process of phagocytosis (Kolaczkowska and Kubes, 2013). Once engulfed, the bacteria are contained within phagosomes where they are killed intracellularly through ROS production, acidification of the phagosome, and primarily by fusion of antimicrobial granules with the phagosome membrane (Nordenfelt and Tapper, 2011; Monfregola et al., 2012; Johnson and Criss, 2013; Yin and Heit, 2018). The importance of these cells in bacterial killing and defense of naïve hosts against pneumococcal infection is well established (Garvy and Harmsen, 1996; Hahn et al., 2011; Bou Ghanem et al., 2015). However, whether these innate immune cells also play a critical role in protection of vaccinated hosts against *S. pneumoniae* challenge is not fully explored.

Despite different methods of bacterial killing utilized by PMNs, *S. pneumoniae* express several factors to evade PMN-mediated killing, one of which is the expression of a polysaccharide capsule (Shenoy and Orihuela, 2016). This capsule helps the bacteria resist phagocytic killing (Hyams et al., 2010). The presence of an opsonin, in the form of complement or antibody, deposited on the surface of the bacteria helps overcome this resistance and mediates clearance through activation of complement and Fc receptors on PMNs (Kadioglu et al., 2008; Shenoy and Orihuela, 2016). Activation of these receptors triggers distinct signaling pathways in PMNs (García-García and Rosales, 2002; Kobayashi et al., 2002; Nguyen et al., 2017). Previous studies using coated beads found that signaling *via* Fc and complement receptors resulted in differences in phagocytosis, ROS production as well as receptor specific changes in gene expression (García-García and Rosales, 2002; Kobayashi et al., 2002). Thus, in a vaccinated host, antibodies may enhance host protection against infection by binding pneumococci and promoting their uptake and killing by PMNs (Dalia and Weiser, 2011).

Aging is accompanied by a decline in levels and opsonic capacity of antibodies (Simell et al., 2011; Jackson et al., 2013; Adler et al., 2017) in response to immunization, which blunts the effectiveness of vaccines in protecting the host against infection. However, there is also impaired intrinsic PMN function in elderly subjects (Simell et al., 2011). When compared to young donors, PMNs from elderly human donors display reduced killing of *S. pneumoniae* even when the bacteria were opsonized with sera from young PPSV immunized hosts (Simell et al., 2011). This suggests that antibody-mediated responses by PMNs are impaired with age. Similar studies, however, are lacking for PCV. Further, the contribution of PMNs to the age-driven decline in vaccine protectiveness is unclear.

In this study, using a murine model of infection, we asked if the decline in PMN function contributes to the reduced efficacy of the pneumococcal conjugate vaccine in aged hosts. We found that following PCV vaccination, PMNs are necessary for protection of young hosts against infection with *S. pneumoniae*. Aged mice were not protected by PCV vaccination. This was associated with an age-related intrinsic decline in PMN function, specifically in intracellular killing of engulfed bacteria following antibody-mediated uptake. Importantly, adoptive transfer of PMNs from young hosts into vaccinated, aged mice, rescued their ability to fight infection. These findings indicate that enhancing PMN function in aged hosts, may boost overall vaccine protectiveness.

MATERIALS AND METHODS

Ethics Statement

All animal studies were performed in accordance with the recommendations in the Guide for the Care and Use of Laboratory Animals. Procedures were reviewed and approved by the University at Buffalo Institutional Animal Care and Use Committee (approval number AR202100089).

Mice

Young (2 months) and old (18-22 months) C57BL/6 mice were obtained from the National Institute on Aging colonies or purchased from Jackson Laboratories (Bar Harbor, ME). All mice were housed in a specific-pathogen free facility at the University at Buffalo for four weeks prior to starting experiments. Due to mice availability, all experiments were performed in male mice, however the role of PMNs in vaccinated hosts was also confirmed in young female C57BL/6 mice (**Figure 1**).

Bacteria

Wildtype (WT) *Streptococcus pneumoniae* TIGR4 strain and a pneumolysin deletion mutant (*Δply*) were a kind gift from Andrew Camilli (Greene et al., 2015). GFP-expressing *Streptococcus pneumoniae* TIGR4 was a kind gift from Sarah Roggensack (Bhalla et al., 2020). Bacteria were grown to mid-exponential phase at 37°C at 5% CO_2 in Todd Hewitt broth

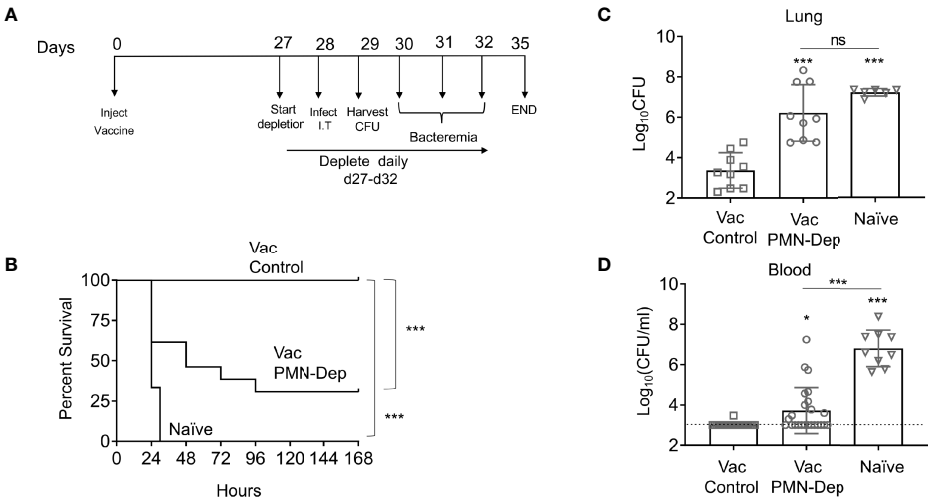

FIGURE 1 | PMNs are required for protection of PCV immunized young hosts at the time of bacterial challenge. Young C57BL/6 female mice were mock treated (naïve) or administered 50µl of Prevnar-13 *via* intramuscular injections to the hind legs (vaccinated). Four weeks following vaccination mice were challenged i.t. with $1x10^7$ CFU *S. pneumoniae* TIGR4. To deplete PMNs prior to infection, mice were injected i.p. with anti-Ly6G antibodies (IA8) or isotype control at days -1, 0, and +1 to +4 with respect to infection as outlined in **(A)**. **(B)** Mice were then monitored for survival. **(B)** Data were pooled from three experiments with 14 mice per group. Significant differences were determined using the Log-Rank (Mantel-Cox) test. Bacterial burden in the lung **(C)** and blood **(D)** were also assessed 1 day post infection. **(C, D)** Data were pooled from three separate experiments with n = 9 mice per group. Each square indicates an individual mouse. *, denotes significant differences by One-way ANOVA followed by Tukey's multiple comparisons test. ** denotes $p < 0.05$ and *** denotes $p < 0.001$*. ns denotes not significant.

supplemented with 0.5% yeast extract and oxyrase as previously described (Siwapornchai et al., 2020).

PMN Isolation

Bone marrow cells were collected by flushing the femurs and tibias harvested from uninfected mice with RPMI supplemented with 10% FBS and 2mM EDTA. Red blood cells were then lysed, and remaining cells were washed, and resuspended in PBS. PMNs were separated *via* density centrifugation using histopaque 1119 and 1077 (Sigma) as previously described (Swamydas and Lionakis, 2013; Bhalla et al., 2020; Siwapornchai et al., 2020; Tchalla et al., 2020). The PMNs were then resuspended at the desired concentration in Hank's Balanced Salt Solution/ 0.1% gelatin with no Ca^{2+} or Mg^{2+}. The purity of PMNs was confirmed using flow cytometry and 85-90% of enriched cells were positive for Ly6G and CD11b.

Mouse Infections

Mice were anesthetized with isoflurane and infected intratracheally (i.t.) with 50ul of the indicated concentrations of WT *Streptococcus pneumoniae* TIGR4 pipetted directly into the trachea with the tongue pulled out to ensure delivery of bacteria directly into the lungs. Following infection, mice were monitored for signs of disease including activity, weight loss, posture, breathing, and blindly scored from 0 (healthy) to 21 (severe disease) as previously described (Tchalla et al., 2020). Lungs were harvested and homogenized in sterile PBS. Blood was collected from the tail vein to follow bacteremia. Samples were diluted in sterile PBS and plated on blood agar plates to enumerate bacterial numbers.

Generation of Immune Sera

To generate immune sera, mice were immunized intramuscularly *via* injection of 50ul of the pneumococcal conjugate vaccine (PCV) Prevnar-13® (Wyeth pharmaceuticals) into the caudal thigh muscle. Mice were euthanized four weeks following vaccination and blood was collected by cardiac puncture into microtainer tubes (BD) and centrifuged at 9000 rpm to collect sera. Sera were stored at -80°C until use. To heat inactivate the sera, samples were incubated at 56°C for 40 minutes as previously described (Fante et al., 2021).

Opsonophagocytic Killing Assay

The ability of PMNs to kill *S. pneumoniae* was determined as previously described (Lysenko et al., 2007; Bou Ghanem et al., 2015). 10^5 PMNs were infected with $2x10^5$ CFU (at a multiplicity of infection (MOI) of 2) of *S. pneumoniae* TIGR4 pre-opsonized with 3% naïve, immune, or heat inactivated (Hi) immune sera as indicated. PMNs were infected for 40 minutes at 37°C, reactions were then stopped on ice for 2 minutes. Reactions were then plated on blood agar and killing percentage was determined with respect to no PMN control wells under the same treatment conditions.

MPO and CRAMP ELISAs

PMNs were infected at a MOI of 2 with *S. pneumoniae* TIGR4 pre-opsonized with 3% naïve or heat inactivated immune sera. Control wells were mock infected with 3% sera only. PMNs were infected for 40 minutes at 37°C. Cells were then centrifuged to collect the supernatants and pellets. Pellets were lysed with RIPA lysis buffer with 0.1% Tx-100 and both, supernatants and pellets

were analyzed for MPO (MPO ELISA, Invitrogen) and the Cathelicidin antimicrobial peptide (CAMP ELISA kit, mybiosource) as per manufacturer's instructions.

Measurement of ROS

Intracellular and extracellular ROS production was measured as previously described (Siwapornchai et al., 2020). PMNs were re-suspended in HBSS (Ca^{2+} and Mg^{2+} free) and acclimated at room temperature for one hour. The cells were then spun down and re-suspended in KRP buffer (Phosphate buffered saline with 5mM glucose, 1mM $CaCl_2$ and 1mM $MgSO_4$) and equilibrated at room temperature for 30 minutes. $5x10^5$ PMNs were then seeded per well in 96-well white LUMITRAC™ plates (Greiner Bio-One). Wells were infected with TIGR4 *S. pneumoniae* pre-opsonized with naïve or heat inactivated immune sera. Control wells were mock infected with PBS and 3% sera only. Phorbol 12-myristate 13-acetate (PMA) (Sigma) (100nM) was used as a positive control. For detection of extracellular ROS, 50μM Isoluminol (Sigma) plus 10U/ml HRP (Sigma) were added to the wells and for detection of intracellular ROS, 50μM Luminol (Sigma) was added to the wells as previously described (Dahlgren et al., 1989; Dahlgren and Karlsson, 1999; Martner et al., 2008; Rajecky et al., 2012). Luminescence was immediately read (following infection) over a period of one hour at 37°C in a pre-warmed Biotek Plate reader. Wells containing buffer and Isoluminol plus HRP or Luminol alone were used as blanks.

Gentamicin Protection Assay

PMNs were infected at MOI 25 with *Δply S. pneumoniae* pre-opsonized with 3% naïve or heat inactivated immune sera for 15 minutes at 37°C. Gentamicin was then added at 100μg/ml for 30 minutes to kill the extracellular bacteria. To determine initial bacterial uptake, reactions were washed with HBSS and resuspended in HBSS/0.1% gelatin, reactions were then diluted and plated on blood agar. To determine intracellular killing, reactions continued at 37°C for an additional 30 minutes. The reactions were then diluted and plated on blood agar plates. The percentage of the engulfed inoculum (at 15 minutes) that was killed was then calculated.

Bacterial Uptake Assay

Bacterial uptake was determined using inside-out staining as previously described (Bhalla et al., 2020). PMNs were infected with GFP-expressing *S. pneumoniae* at a MOI of 2. Reactions were incubated rotating for the indicated times at 37°C. Cells were washed and resuspend in FACS buffer. To differentiate between associated vs. engulfed bacteria, the cells were stained with rabbit polyclonal anti-pneumococcal serotype 4 capsular antibodies (Cederlane) followed by a PE-conjugated secondary anti-Rabbit IgG antibody (12473981; Invitrogen). Flow cytometry was used to determine the percentage of PMNs that associated with bacteria (GFP^+ PMNs). GFP^+ PMNs were analyzed for a PE signal and the percentage of engulfed bacteria (GFP^+/PE^-) vs. extracellular bacteria (GFP^+PE^+) was determined. To assess the amounts of engulfed bacteria, we gated on GFP^+/PE^- PMNs and measured the mean fluorescent intensity of GFP within that gate.

Adoptive Transfer of PMNs

PMNs were adoptively transferred as previously described (Bhalla et al., 2020; Siwapornchai et al., 2020). Briefly, PMNs were isolated from the bone marrow of young and old naïve (unvaccinated), uninfected mice and resuspended in PBS. $2.5x10^6$ PMNs were then transferred into old PCV vaccinated mice by intraperitoneal (i.p) injection. This method allows delivery of PMNs into the circulation as we previously described (Siwapornchai et al., 2020). One hour following transfer, mice were infected i.t with $1x10^6$ Colony Forming Units (CFU) *S. pneumoniae* TIGR4. At 18 hours post infection, the mice were scored for clinical signs of disease. Mice were euthanized and the lung and blood collected and plated on blood agar plates for enumeration of bacterial CFU.

Measurement of Extracellular DNA

PMNs were infected at a MOI of 2 with *S. pneumoniae* TIGR4 pre-opsonized with 3% naïve or heat inactivated immune sera for 40 minutes at 37°C. Control wells were mock infected with 3% sera only. Cells were then centrifuged to collect the supernatants. Supernatant samples were then stained for DNA with SYTOX Green (Invitrogen) and DNA was measured using a Biotek plate reader.

Antibody ELISA

Antibody levels against heat-killed *S. pneumoniae* TIGR4 were measured by ELISA as previously described (Bou Ghanem et al., 2018; Tchalla et al., 2020; Bhalla et al., 2021).

Antibody Binding to Bacterial Surfaces

WT and capsule deletion mutant (Δcps) *S. pneumoniae* TIGR4 bacteria were opsonized with 3% heat inactivated immune, immune, or naïve sera at 37°C for 30 minutes. Cells were washed, pelleted and stained for IgG antibodies with APC conjugated IgG (H+L) F(ab ft.) Goat anti-Mouse (17-4010-82; eBioscience). Flow cytometry was used to measure the MFI of antibody bound to the surface of bacteria.

Complement Deposition Assay

WT *S. pneumoniae* TIGR4 bacteria were opsonized at 37°C for 30 minutes with 3% naïve, heat inactivated naïve, immune, or heat inactivated immune sera as indicated. Following opsonization, cells were washed, pelleted, and stained for complement with FITC conjugated Goat anti-mouse C3 (Catalogue number GC3-90F-Z; purchased from ICL). Flow cytometry was used to measure the MFI of complement bound to the surface of bacteria.

Neutrophil Depletion

Neutrophils were depleted by intraperitoneal injection of 50ug of anti Ly6G antibody (clone IA8) or isotype IgG control (BD Pharmingen) following the timeline outlined in **Figure 1A** (Tchalla et al., 2020).

Flow Cytometry

Fluorescence intensities were measured on a BD Fortessa and at least 20,000 events were analyzed using FlowJo.

Statistics

Statistical analysis was performed using Prism 9 (Graph Pad). CFU data were log-transformed to normalize distribution. Bar graphs represent the mean values +/- SD. Significant differences were determined by Student's t-test, one-way ANOVA followed by Dunnet's or Tukey's multiple comparisons test or 2-way ANOVA followed by Sidak's multiple comparisons test as appropriate (indicated in the legends). Differences between fractions were determined by Fisher's exact test. Survival analyses were performed using the log-rank (Mantel-Cox) test. All *p* values less than 0.05 were considered significant (as indicated by asterisks). * denotes *p<0.05, ** denotes p<0.01, and *** denotes p<0.001.*

RESULTS

PMNs Are Required for Protection in PCV Vaccinated Young Hosts Following Bacterial Infection

PMNs are required for innate resistance of naïve hosts against *S. pneumoniae* infection, however, the role of neutrophils in anti-bacterial defense in vaccinated hosts is unclear. To determine the role of PMNs in response to *S. pneumoniae* in vaccinated hosts, young, C57BL/6 female mice were immunized with pneumococcal conjugate vaccine (PCV). Four weeks later, immunized mice were treated with isotype controls or anti-Ly6G Ab IA8 to deplete PMNs one day prior to and daily throughout the first 4 days following *S. pneumoniae* pulmonary infection (**Figure 1A**). Depletion of PMNs prior to intratracheal challenge with *S. pneumoniae* and throughout the course of infection resulted in loss of vaccine-mediated protection (**Figure 1**). While 100% of PMN sufficient vaccinated controls survived a challenge dose that is lethal in naïve mice, only 25% of PMN depleted vaccinated mice survived the infection (**Figure 1B**). As biological sex can influence immune responses, and our studies in old mice are limited to males due to availability, we tested the role of PMNs in young vaccinated male mice. Similar to what we found in females, PMN depletion of vaccinated young male mice resulted in a significant decrease in survival and loss of vaccine-mediated protection (**Figure S1**). These data show that PMNs are required for PCV-mediated protection against *S. pneumoniae* infection in young hosts.

The Presence of Immune Sera Enhances Opsonophagocytic Killing in Vaccinated Young Hosts

To investigate the role of PMN conferred protection in vaccinated hosts, we compared the ability of PMNs from immunized and naïve mice to kill *S. pneumoniae ex vivo* using established opsonophagocytic killing assays (Lysenko et al., 2007; Bou Ghanem et al., 2015). We found that PMNs from immunized mice killed *S. pneumoniae* significantly better than those isolated from naïve mice (**Figure 2**). This enhanced killing was a result of the presence of anti-pneumococcal antibodies in sera and not intrinsic to the PMNs themselves. When exposed to bacteria opsonized with naïve sera, the ability of PMNs from vaccinated mice to kill *S. pneumoniae* was comparable to that of naïve hosts (**Figure 2**).

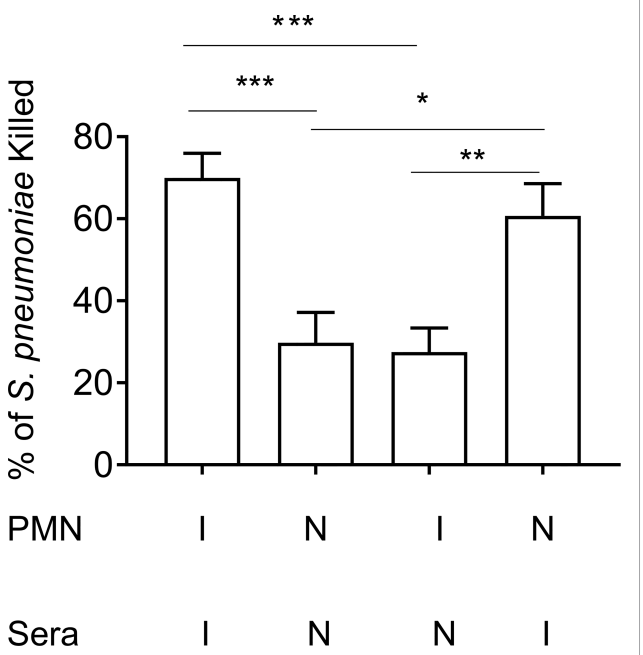

FIGURE 2 | Enhanced opsonophagocytic bacterial killing by PMNs from vaccinated mice is dependent on opsonization by immune sera. PMNs were isolated from the bone marrow of young male C57BL/6 naïve (N) or Prevnar-13 immunized mice (I) and infected with *S. pneumoniae* pre-opsonized with either naïve or immune sera. The percentage of bacteria killed was then calculated with respect to a no PMN control under the same treatment conditions. Data shown are pooled from three separate experiments (n = 3 biological replicates) where each condition was tested in triplicate (n = 3 technical replicates) per experiment. *, denotes significance as calculated by One-way ANOVA followed by Tukey's multiple comparisons test. ** denotes p < 0.05, ** denotes p < 0.01, and *** denotes p < 0.001.*

Similarly, the ability of PMNs from naïve mice to kill *S. pneumoniae* pre-opsonized with immune sera was significantly boosted (**Figure 2**). Sera isolated from immune mice contained significantly higher levels of IgG antibodies compared to naïve controls (**Figure S2A**). These antibodies bound to the surface of *S. pneumoniae* and were specific to the pneumococcal capsule (**Figure S2B**). These findings suggested that PMNs promote clearance of antibody opsonized bacteria. In fact, when we compared bacterial burdens in vaccinated mice following pulmonary challenge with *S. pneumoniae*, we found that the vaccinated PMN depleted hosts had a 100-fold higher bacterial burden in the lungs (**Figure 1C**) compared to vaccinated PMN sufficient controls. The vaccinated PMN depleted hosts also had systemic spread of the infection, where half of the mice became bacteremic compared to only 10% of the vaccinated isotype treated controls (**Figure 1D**). Overall, these findings suggest that following vaccination, PMNs act as effectors that promote clearance of antibody opsonized bacteria enhancing host resistance to infection.

Anti-Pneumococcal Antibodies Enhance PMN Anti-Microbial Responses

PMNs can kill bacteria through several antimicrobial functions. To determine the mechanisms by which immune sera enhances

PMN activity, we analyzed several PMN functions in response to *S. pneumoniae* opsonized with naïve, or heat inactivated (Hi) immune sera. Heat inactivated immune sera was used to denature complement proteins and isolate the role of antibodies as an opsonin. We confirmed that heat inactivation of sera had no effect on antibody binding to the pneumococcal capsule when compared to full immune sera (**Figure S2B**). We also confirmed that heat inactivation of sera prevented complement deposition on the surface of bacteria (**Figure S2C**). To probe mechanisms, we assessed phagocytosis, degranulation and ROS production, which have all been shown to be important for the ability of PMNs to kill *S. pneumoniae* (Domon and Terao, 2021). We first measured phagocytosis of *S. pneumoniae* by PMNs using GFP-tagged bacteria and a flow-cytometry based assay we had previously established (Bhalla et al., 2020) and found that significantly more bacteria are taken in by PMNs when opsonized with Hi immune sera compared to when opsonized with naïve sera (**Figure 3B**). As the ~ 1.7-fold increase in the amount of engulfed bacteria did not fully account for the overall increase in killing capacity, we also assessed other antimicrobial activities. We measured the amount of Myeloperoxidase (MPO) released by PMNs into the supernatants in response to infection as a proxy for mobilization of primary granules (Armstrong et al., 2016; Miralda et al., 2020). We found that PMNs released 7-fold more MPO upon infection with *S. pneumoniae* opsonized with heat inactivated immune sera compared to bacteria opsonized with naïve sera (**Figure 3A**). Finally, we measured production of intracellular and extracellular reactive oxygen species (ROS) by PMNs using chemiluminescent assays. We found that when infected with *S. pneumoniae* opsonized with heat inactivated immune sera, both intracellular (**Figure 3C**) and extracellular (**Figure 3D**) ROS production by PMNs significantly increases when compared to infection by naïve sera opsonized bacteria. These data show that the presence of anti-pneumococcal antibodies in a PCV vaccinated host enhance PMN antimicrobial effector functions in response to *S. pneumoniae*.

PCV Fails to Protect Old Mice Following *S. pneumoniae* Infection

The findings above indicate that following vaccination, enhanced PMN antimicrobial function protects young hosts from pneumococcal infection, however, it is known that vaccine efficacy declines with age. To determine the efficacy of PCV vaccination using an aged murine model, young (2-3 months) and old (18-22 months) male C57BL/6 mice were vaccinated with PCV and four weeks following vaccination the mice were infected intratracheally with *S. pneumoniae* and monitored for survival. We found that while vaccinated young mice were fully protected, PCV immunization induced protection in less than half of the old mice, where only 37% survived the pulmonary challenge (**Figure 4**). These data show that PCV-mediated protection declines in aged hosts.

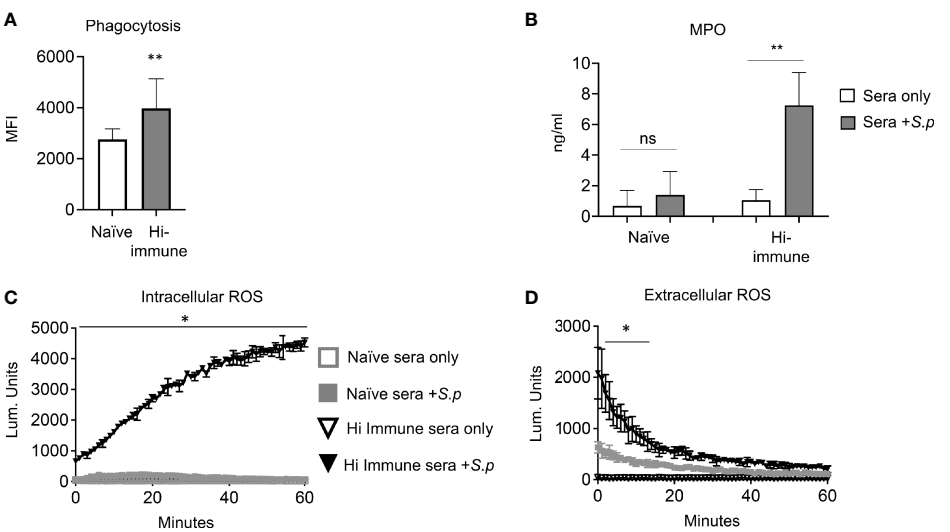

FIGURE 3 | PMN anti-bacterial responses are enhanced in the presence of specific anti-pneumococcal antibodies. **(A)** PMNs were isolated from the bone marrow of young male C57BL/6 naïve mice and infected for 10 minutes with GFP tagged *S. pneumoniae* TIGR4 preopsonized with naïve or heat inactivated immune sera. The amount of GFP positive bacteria (MFI) inside each cell was determined *via* flow cytometry using inside-out staining. Data are pooled from three separate experiments where each condition was tested in triplicate (n = 3). Significant differences ($p < 0.05$, indicated by *) were determined by unpaired Student's t test. **(B–D)** PMNs isolated from the bone marrow of young male C57BL/6 naïve mice were infected with *S. pneumoniae* pre-opsonized with naïve or heat inactivated (Hi-) immune sera or mock treated with sera alone as indicated. **(B)** The supernatants were t collected and myeloperoxidase (MPO) levels measured by ELISA. *, denotes significant difference compared to uninfected controls as determined by unpaired Student's t test. Data are pooled from 3 separate experiments with n = 3 mice per group. **(C)** Production of intracellular ROS over time was measured by chemiluminescence of luminol. **(D)** Production of extracellular ROS over time was measured by chemiluminescence of isoluminol in the presence of HRP. **(C, D)** Data are representative of one of three separate experiments where each condition was tested in triplicate (n = 3 technical replicates) per experiment. Significant differences ($p < 0.05$, indicated by *) were determined by 2-way ANOVA followed by Sidak's multiple comparisons test. ** denotes $p < 0.05$, and ** denotes $p < 0.01$.*

Intrinsic PMN Function Declines With Age

Given the decline in protection with age and the essential role of PMNs in vaccinated young hosts, we next looked at how PMN function changes with age upon vaccination. Using an opsonophagocytic killing assay, PMNs were isolated from young and old mice and exposed to *S. pneumoniae* opsonized with matching immune sera. We found that PMNs from vaccinated old mice kill pneumococci significantly worse than those isolated from young counterparts (**Figure 5**). It is well known that antibody levels and function following vaccination decline with age (Simell et al., 2011; Jackson et al., 2013). Therefore, to parse out the effect of the sera vs PMN intrinsic function, we mixed and matched sera and found that bacterial opsonization with immune sera from young controls failed to boost the antimicrobial activity of PMNs from old mice (**Figure 5**). This indicates that the decline in neutrophil function observed here is not solely due to the well-established age-related decline in anti-pneumococcal antibodies, but that there is an intrinsic decline in PMN function with age. Strikingly, when the immune sera from young mice were heat inactivated, PMNs from old mice completely failed to kill pneumococci and in fact bacterial growth occurred (**Figure 5**). This occurred only in the presence of PMNs from aged hosts as pre-opsonization with heat-inactivated immune sera still induced significant killing by PMNs from young mice (**Figure 5**), indicating there is an age-related decline in PMN killing of antibody opsonized *S. pneumoniae*. These data show that unlike in young hosts, immunization of old mice fails to boost PMN antimicrobial activity.

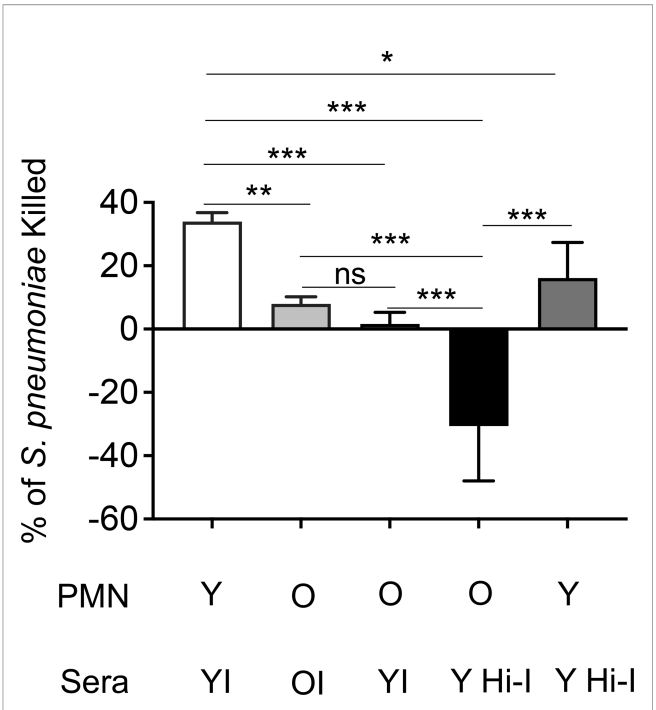

FIGURE 5 | The intrinsic antibacterial function of PMNs declines with age. PMNs were isolated from the bone marrow of naïve young and old male C57BL/6 mice and infected with *S. pneumoniae* pre-opsonized with young immune (YI), old immune (OI), or young heat inactivated immune (Y Hi-I) sera. The percentage of bacteria killed was then calculated in comparison to a no PMN control under the same treatment conditions. Data are pooled from four separate experiments (n=4 biological replicates) where each condition was tested in triplicate (n=3 technical replicates) per experiment. *, denotes significant differences as determined by One-way ANOVA followed by Tukey's multiple comparisons test. ** denotes $p < 0.05$, ** denotes $p < 0.01$, and *** denotes $p < 0.001$*. ns denotes not significant.

Intracellular Killing of Engulfed *S. pneumoniae* Is Impaired With Age

To determine the mechanism of the intrinsic decline in PMN function observed with age, we compared the antimicrobial effector functions of PMNs isolated from young and old mice in response to *S. pneumoniae* opsonized with heat inactivated immune sera from young controls. We found that when comparing extracellular anti-microbial activities such as MPO release, extracellular ROS production, and extracellular DNA released as a marker of NETosis (Linnemann et al., 2020), there was no difference with age (**Figures S3A, C, E**). Additionally, we found no age-related difference in the amount of intracellular MPO levels or the amount of intracellular ROS produced (**Figures S3B, D**). As phagocytosis is required for the ability of PMNs to efficiently kill *S. pneumoniae* (Standish and Weiser, 2009) we next compared pneumococcal uptake by PMNs from young and old mice. We found no age-related difference in phagocytosis of bacteria opsonized with heat inactivated immune sera (**Figure S3F**). However, when we compared killing of engulfed bacteria using a gentamicin-protection assay we had previously established (Bhalla et al., 2020), we found a significant decline in the ability of PMNs from old mice to intracellularly kill *S. pneumoniae* opsonized with heat inactivated immune sera compared to PMNs from young mice (**Figure 6A**). An important mediator of pneumococcal intracellular killing by PMNs are antimicrobial enzymes and peptides packaged in intracellular

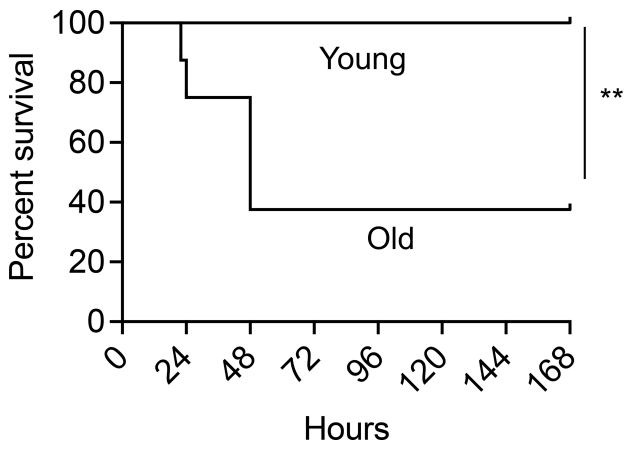

FIGURE 4 | PCV administration fails to protect old mice against *S. pneumoniae* pulmonary infection. Young and old male C57BL/6 mice were vaccinated with Prevnar-13. Four weeks following vaccination, mice were infected intra-tracheally (i.t.) with 10^6 CFU *S. pneumoniae* and monitored for survival. Data are pooled from 2 separate experiments with n = 8 mice per group. Significant differences were determined by Log-Rank (Mantel-Cox) test. *** denotes $p < 0.01$*.

granules within the cell (Yin and Heit, 2018). As we previously found no age-related difference in the intracellular concentration of the primary granule enzyme MPO (**Figure S3B**), we then analyzed the intracellular concentration of Cathelicidin-related antimicrobial peptide (CRAMP), a peptide that is able to kill pneumococci (Habets et al., 2012) and is found in PMN secondary granules (Borregaard et al., 2007). We found that at baseline, PMNs from old mice expressed significantly lower concentrations of CRAMP when compared to PMNs from young controls (**Figure 6B**). Following infection with *S. pneumoniae* opsonized with heat inactivated young immune sera, while both PMNs from young and old mice had increased levels of CRAMP, overall amounts were still significantly lower in aged hosts (**Figure 6B**). These data suggest that following antibody-mediated uptake, there is an age-related decline in the ability of PMNs to kill pneumococcus intracellularly, and this deficit in intracellular killing may be due to a decrease in intracellular CRAMP levels.

Adoptive Transfer of PMNs From Young Mice Rescues the Age-Related Susceptibility of Vaccinated Old Mice to *S. pneumoniae* Infection

Aged mice are not protected following PCV vaccination and we have found that PMNs from aged mice fail to efficiently kill *S. pneumoniae* following antibody-mediated uptake. To determine if PMNs from young mice could boost the resistance of old PCV vaccinated mice to *S. pneumoniae* infection, we adoptively transferred $2.5x10^6$ PMNs isolated from the bone marrow of naïve young or old mice into four-week PCV vaccinated old mice. Following transfer of PMNs, mice were infected intratracheally with *S. pneumoniae*, and 18 hours post infection we analyzed the clinical score where a higher score corresponds to worse disease severity. We found that old PCV vaccinated mice that received PMNs from young controls had significantly lower clinical score compared to the old mice that received age matched PMNs (**Figure 7A**). The lower clinical score in the young PMN transfer group was accompanied by lower incidences of bacteremia with 50% of mice in this group becoming bacteremic compared with 90% of the mice in the aged matched transfer group (**Figure 7B**). Additionally, the old vaccinated mice that received PMNs from young controls also had significantly less bacterial burden in the lung compared to the age matched controls (**Figure 7C**). Taken together these data show that the presence of young, functional PMNs in an old vaccinated host reduces clinical disease presentation, and also reduces lung infection and systemic spread of the bacteria. These results indicate that enhancing PMN function in aged hosts improves anti-pneumococcal vaccine-mediated protection.

DISCUSSION

The role of PMNs in innate immunity and their interactions with *S. pneumoniae* have been well characterized (Kolaczkowska and Kubes, 2013; Simmons et al., 2021). However, many studies have been performed using un-opsonized bacteria, naïve sera (Standish and Weiser, 2009; Dalia et al., 2010; Bou Ghanem et al., 2015; Siwapornchai et al., 2020) or complement (Standish and Weiser, 2009; Bou Ghanem et al., 2017), while the interactions of PMNs with antibody-opsonized *S. pneumoniae* which have major implications on vaccine effectiveness are less explored (Fulop et al., 1985; Esposito et al., 1990; Butcher et al., 2001; Simell et al., 2011). This is of particular importance in hosts where immune responses to vaccination are sub-par as is the case in older individuals. The efficacy of pneumococcal vaccines is known to decline with age (Simell et al., 2011; Gonçalves et al., 2016; Matanock A et al., 2019) and while several aspects of the age-driven decline in adaptive immunity that result in reduced antibody production and function in response to immunization have been elucidated, the importance of PMNs in the decline of vaccine-mediated protection during aging remains under explored. In this study, we found that following PCV vaccination, PMNs are necessary for the protection of young

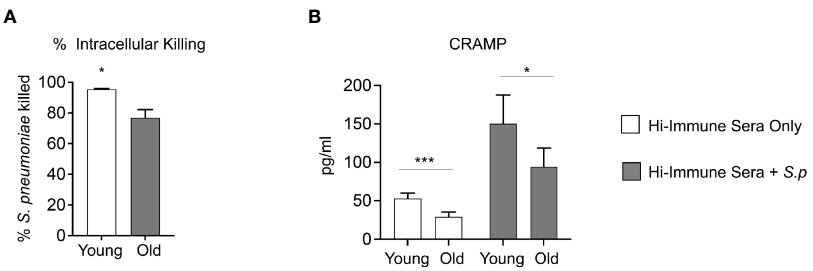

FIGURE 6 | Aging impairs intracellular killing of engulfed *S. pneumoniae*. **(A)** PMNs were isolated from the bone marrow of naïve young and old male C57BL/6 mice and infected with *S. pneumoniae* pre-opsonized with young heat inactivated immune sera for 15 minutes at 37°C. Gentamicin (100μg/ml) was then added for 30 minutes to kill extracellular bacteria. PMNs were then washed and one set immediately plated on blood agar plates to determine the amounts of engulfed bacteria. The other sets of PMNs were incubated for 30 more minutes and then plated to enumerate remaining viable bacteria. The % of engulfed bacteria that was killed was then calculated. **(B)** PMNs from young and old naive mice were infected with *S. pneumoniae* pre-opsonized with young heat inactivated immune sera for 40 minutes. The cells were then lysed and assayed for CRAMP levels using ELISA. Data are pooled from **(A)** three separate experiments (n=3 biological replicates) where each condition was tested in triplicate (n=3 technical replicates) per experiment and **(B)** four separate experiments (n=4 biological replicates). *, denotes significant differences as determined by unpaired Student's t test. * *denotes* $p < 0.05$, *and* *** *denotes* $p < 0.001$. ns denotes not significant.

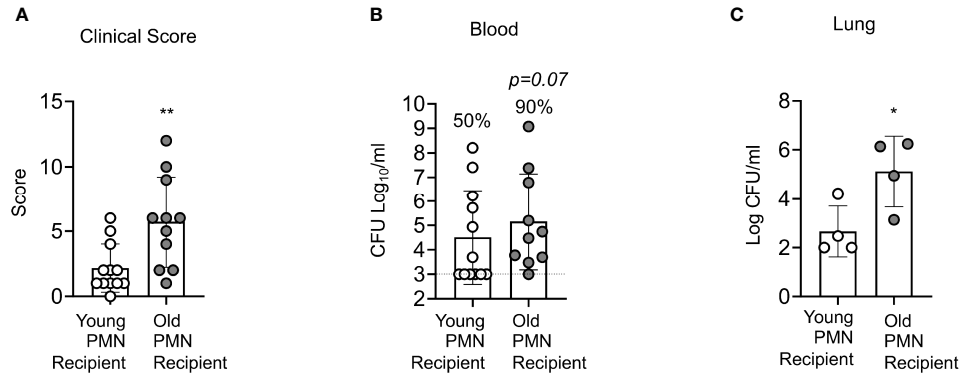

FIGURE 7 | Adoptive transfer of PMNs from young mice at the time of challenge rescues the susceptibility of vaccinated old mice to *S. pneumoniae*. Old male C57BL/6 mice were vaccinated with Prevnar-13, four weeks post vaccination mice were adoptively transferred $2.5x10^6$ PMNs from either naïve young or naïve old mice. One hour post transfer, mice were infected i.t. with $1x10^6$ CFU of *S. pneumoniae* and clinical score **(A)** as well as bacterial numbers in the blood **(B)**, and lung **(C)** were determined 18 hours post infection. **(B)** Fractions indicate the percent of mice that were bacteremic. Asterisks indicate significant differences calculated by unpaired Student's test **(A, C)** and Fisher's exact test **(B)**. Data pooled from n=11 mice per group **(A, B)** or n=4 **(C)** mice per group are shown. * *denotes* $p < 0.05$, *and* ** *denotes* $p < 0.01$.

hosts upon infection with *S. pneumoniae*. The binding of specific anti-capsular antibodies on the surface of the bacteria were shown to enhance several antimicrobial activities and overall pneumococcal killing by PMNs from young mice. However, aged mice were not protected by PCV vaccination and this decline in vaccine protection was associated with an age-related intrinsic decline in PMN function, specifically in antibody-mediated bacterial killing. Importantly, adoptive transfer of PMNs from young mice into aged hosts, rescued the ability of PCV to confer protection against infection. This work highlights both the importance of PMNs in protection of vaccinated hosts and that PMNs may be a potential target to boost vaccine-mediated protection in aged hosts that otherwise remain susceptible to *S. pneumoniae* infection.

S. pneumoniae have evolved several mechanisms to evade phagocytic uptake and clearance including the expression of capsule on their surface (Hyams et al., 2010; Shenoy and Orihuela, 2016). Therefore, opsonization of *Streptococcus pneumoniae* by complement and/or antibodies is important for bacterial uptake and clearance by PMNs (Kadioglu et al., 2008; Shenoy and Orihuela, 2016). Activation of complement receptors (CR) or Fc Receptors (FcR) on the PMN surface trigger distinct signaling pathways. It has been shown previously that activation of PMNs from young hosts and their resulting antimicrobial response is dependent on the receptor triggered (Kobayashi et al., 2002). When PMNs isolated from healthy, young, human donors were exposed to latex beads coated with IgG, serum complement, or both, phagocytosis and ROS production were affected based on the opsonin used (Kobayashi et al., 2002). IgG-coated beads induced faster phagocytosis and greater ROS production than beads coated with complement. In the case of ROS production the combined activation of both CRs and FcRs produced the highest amounts of ROS (Kobayashi et al., 2002). Additional studies using antibody or complement coated surfaces have shown that CRs alone do not initiate a strong ROS response but FcR-mediated activation or combined FcR and CR activation produce higher amounts of ROS (Zhou and Brown, 1994). PMN ROS response through the NADPH complex can also activate additional antimicrobial responses, such as NETosis and the production of proinflammatory cytokines (Nguyen et al., 2017). These data indicate that activation of antimicrobial effector functions by PMNs *via* CRs or FcRs proceed by distinct signaling pathways (Nguyen et al., 2017). In this study we used live bacteria to show that, similar to previous reports, PMNs isolated from young mice display increased antimicrobial effector functions when *S. pneumoniae* is opsonized with specific antibodies. When compared to opsonization with complement, opsonization of *S. pneumoniae* with antibodies alone resulted in a significant increase in overall pneumococcal killing and an increase in phagocytosis, ROS production, as well as MPO release.

Our work also shows an age-related decline in antibody-mediated bacterial killing by PMNs in mice immunized with the pneumococcal conjugate vaccine. This is in line with previous work in humans vaccinated with PCV, where PMNs isolated from the blood of elderly donors displayed a significant decline in opsonophagocytic killing when compared to PMNs isolated from young donors (Simell et al., 2011). This decline in opsonophagocytic killing with age was also accompanied by a significant decline in the opsonic titer of antibodies to multiple pneumococcal serotypes and there was an increase in the amounts of antibodies needed for functional bacterial killing to occur, however, complement activity was found to be higher with age (Simell et al., 2011). We showed here that when PMNs isolated from aged mice are exposed to *S. pneumoniae* opsonized with sera from immunized young donors, there was an age-related decline in pneumococcal killing. This impairment was even more pronounced when complement was deactivated, despite the presence of functional antibodies, suggesting that there is an intrinsic decline in select FcR-mediated antimicrobial

responses with age. Indeed, pneumococci pre-opsonized with heat-inactivated sera were able to replicate in the presence of PMNs from aged mice. This is in line with our previous findings using these opsonophagocytic killing assays, where when PMNs fail to kill bacteria, we observe bacterial growth instead (Siwapornchai et al., 2020). It is known that *S. pneumoniae* express several exoglycosidases that can cleave terminal sugars off of glycoconjugates (King et al., 2006) and use those for growth (Burnaugh et al., 2008). Therefore, it is possible that *S. pneumoniae* are using factors expressed or released by PMNs such as glycoconjugates as a nutrient source, aiding bacterial replication.

We sought to determine the reason for this age-related decline, and found that in aged mice, following antibody-mediated uptake, PMNs have a decline in intracellular pneumococcal killing. To explore the mechanisms of this age-related decline in antibody-mediated intracellular killing we analyzed the intracellular levels of antimicrobial peptide CRAMP, a component of PMN secondary granules (Borregaard et al., 2007). In PMNs, secondary (also known as specific) granules, are released prior to the release of primary granules and play a role in the killing of pathogens (Yin and Heit, 2018). *S. pneumoniae* were shown to be susceptible to CRAMP and the human homologue LL-37 and clinical isolates of several different serotypes are killed upon exposure to LL-37 *in vitro* (Habets et al., 2012). CRAMP deficiency in CRAMP knockout mice was also shown to increase mortality in mice with pneumococcal meningitis (Merres et al., 2014). These data indicate that CRAMP is an antimicrobial product that is important for killing of *S. pneumoniae*. Our study shows that with age there is a decline in the intracellular levels of the antimicrobial peptide CRAMP in PMNs. This decline was both in resting PMNs and in response to infection suggesting less of this antimicrobial product is pre-made within PMNs and production of new CRAMP in response to infection is also impaired with aging. Interestingly, aged mice were also reported to display a decline in CRAMP expression in the epithelium of the upper respiratory tract, which was associated with a decline in pneumococcal clearance (Krone et al., 2013). Reduction in CRAMP abundance may partially account for the age-related decline in intracellular killing of bacteria by PMNs; however, as CRAMP production is reduced but not abolished, additional factors such as overall levels of granules, composition of the granular components, and their trafficking towards the bacteria containing phagosome in PMNs from aged hosts may also play a role and need to be investigated in the future.

With age there is a functional decline in antibody opsonic capacity and a decline in the number of antibodies produced in response to vaccination (Simell et al., 2011; Jackson et al., 2013). However, we found that introduction of PMNs from young hosts to aged vaccinated hosts was able to enhance host protection, despite the well-established decline in antibody number and function. These data indicate that in an immune aged host, despite a decline in adaptive immunity, the presence of functional PMNs is critical for protection against pneumococcal infection. This further suggests that the age-driven decline in PMN function also impairs vaccine-mediated protection against *Streptococcus pneumoniae*. As PMNs are crucial for host defense against a plethora of pathogens and their overall anti-microbial function declines with age (Butcher et al., 2000; Simmons et al., 2021), our findings have far-reaching implications to other infections in the elderly. Therefore, targeting PMN responses may be a potential future avenue for boosting overall vaccine efficacy in aged hosts.

DATA AVAILABILITY STATEMENT

The original contributions presented in the study are included in the article/**Supplementary Material**. Further inquiries can be directed to the corresponding author.

ETHICS STATEMENT

The animal study was reviewed and approved by University at Buffalo Institutional Animal Care and Use Committee.

AUTHOR CONTRIBUTIONS

SS conducted research, analyzed data and wrote paper. ET and MB conducted research and analyzed data. ENBG designed research, wrote the paper and had responsibility for final content. All authors read and approved the final manuscript.

FUNDING

This work supported by National Institute of Health grant R01AG068568-01A1 to ENBG. This work was also supported by American Heart Association Grant number 827322 to MB.

ACKNOWLEDGMENTS

We would like to thank Dr. Beth Wohlfert for her critical feedback on the manuscript.

SUPPLEMENTARY MATERIAL

The Supplementary Material for this article can be found online at: https://www.frontiersin.org/articles/10.3389/fcimb.2022.849224/full#supplementary-material

Supplementary Figure 1 | PMNs are required for protection of PCV immunized young male hosts at the time of bacterial challenge. Young (2 months old) C57BL/6 male mice were mock treated (naïve) or administered 50µl of Prevnar-13 *via* intramuscular injections to the hind legs (vaccinated). Four weeks following vaccination mice were challenged i.t. with $1x10^6$ CFU *S. pneumoniae* TIGR4. To deplete PMNs prior to infection, mice were injected i.p. with anti-Ly6G antibodies (IA8) or isotype control at days -1, 0, and +1 to +4 with respect to infection as outlined in **Figure 1A**. Mice were then monitored for survival. Data were pooled from two experiments with 6 mice per group. Significant differences were

determined using the Log-Rank (Mantel-Cox) test. * *denotes p<0.05, ** denotes p<0.01, and *** denotes p<0.001.*

Supplementary Figure 2 | Production of anti-pneumococcal IgG in the sera following PCV administration. **(A)** Young C57BL/6 mice were mock treated (naïve) or vaccinated with Prevnar-13 and blood was collected at two and four weeks following vaccination. IgG levels against heat-killed *S. pneumoniae* TIGR4 were measured by ELISA. Antibody (Ab) units were calculated based on a hyperimmune standard included in each ELISA. Asterisks indicate significant differences with respect to vaccinated mice as determined by unpaired Student t-test. Data were pooled from two separate experiments with n=6 mice per group and presented as means +/- SD. **(B)** Sera was collected from four-week immunized or naïve male mice as indicated and used to opsonize *S. pneumoniae* TIGR4 (WT) or a capsular deletion mutant (*Δcps*) for 30 minutes. The cells were then washed and stained with fluorescently-labeled anti-mouse IgG. The amount (mean fluorescent intensity or MFI) of Abs bound to the bacterial surface was determined by flow cytometry. Representative data from one of three separate experiments (n=3 biological replicates) are shown where each condition was tested in triplicate (n=3 technical replicates) per experiment. *, denotes significant differences from WT bacteria opsonized with immune sera by One-way ANOVA followed by Dunnett's multiple comparisons test. **(C)** Sera was collected from PCV immunized or naïve mice and heat inactivated at 56°C for 40 minutes as indicated. *S.pneumoniae* TIGR4 was opsonized with the sera for 30 minutes. Cells were labeled with fluorescently tagged anti-mouse C3 antibody and the amount (MFI) of antibody bound to complement was determined by flow cytometry. Data are pooled from n=3 separate experiments with each condition tested in triplicate (n=3). *, indicates significant difference by One-way ANOVA followed by Dunnett's multiple comparisons test. * *denotes p<0.05, ** denotes p<0.01, and *** denotes p<0.001.*

Supplementary Figure 3 | Aging does not affect production of ROS, MPO, release of extracellular DNA or bacterial uptake by PMNs in response to antibody-opsonized *S. pneumoniae.* PMNs were isolated from the bone marrow of naïve young and old male C57BL/6 mice and infected with *S. pneumoniae* pre-opsonized with heat inactivated immune sera from young mice (+*S.p*) or mock infected with heat inactivated immune sera alone (uninfected) as indicated. **(A, B)** Forty minutes post-infection, MPO concentrations present in the pellets or released in the supernatants were measured using ELISA. Data are pooled from three separate experiments. **(C)** The levels of extracellular DNA released in the supernatants were also measured by SYTOX Green. Data are pooled from three separate experiments (n=3 biological replicates per group). **(D, E)** Production of intracellular and extracellular ROS over time following infection was measured by chemiluminescence of luminol and isoluminol plus HRP respectively. Data are representative of one of three separate experiments where each condition was tested in triplicate (n=3 technical replicates) per experiment. **(F)** PMNs were infected for 15 minutes with GFP tagged *S. pneumoniae* pre-opsonized with heat-inactivated immune sera. The amount (MFI) of intracellular bacteria was determined be flow cytometry using inside-out staining. Data are pooled from three separate experiments (n=3 biological replicates per group).

REFERENCES

Adler, H., Ferreira, D. M., Gordon, S. B., and Rylance, J. (2017). Pneumococcal Capsular Polysaccharide Immunity in the Elderly. *Clin. Vaccine Immunol.* 24 (6). doi: 10.1128/CVI.00004-17

Armstrong, C. L., Miralda, I., Neff, A. C., Tian, S., Vashishta, A., Perez, L., et al. (2016). Filifactor Alocis Promotes Neutrophil Degranulation and Chemotactic Activity. *Infect. Immun.* 84 (12), 3423–3433. doi: 10.1128/IAI.00496-16

Bhalla, M., Nayerhoda, R., Tchalla, E. Y. I., Abamonte, A., Park, D., Simmons, S. R., et al. (2021). Liposomal Encapsulation of Polysaccharides (LEPS) as an Effective Vaccine Strategy to Protect Aged Hosts Againsts. Pneumoniae Infection. *Front. Aging* 2. doi: 10.3389/fragi.2021.798868

Bhalla, M., Simmons, S. R., Abamonte, A., Herring, S. E., Roggensack, S. E., and Bou Ghanem, E. N. (2020). Extracellular Adenosine Signaling Reverses the Age-Driven Decline in the Ability of Neutrophils to Kill Streptococcus Pneumoniae. *Aging Cell* 19, e13218. doi: 10.1111/acel.13218

Borregaard, N., Sørensen, O. E., and Theilgaard-Mönch, K. (2007). Neutrophil Granules: A Library of Innate Immunity Proteins. *Trends Immunol.* 28 (8), 340–345. doi: 10.1016/j.it.2007.06.002

Bou Ghanem, E. N., Clark, S., Roggensack, S. E., McIver, S. R., Alcaide, P., Haydon , P. G., et al. (2015). Extracellular Adenosine Protects Against Streptococcus Pneumoniae Lung Infection by Regulating Pulmonary Neutrophil Recruitment. *PloS Pathog.* 11 (8), e1005126. doi: 10.1371/journal.ppat.1005126

Bou Ghanem, E. N., Lee, J. N., Joma, B. H., Meydani, S. N., Leong, J. M., and Panda, A. (2017). The Alpha-Tocopherol Form of Vitamin E Boosts Elastase Activity of Human Pmns and Their Ability to Kill Streptococcus Pneumoniae. *Front. Cell Infect. Microbiol.* 7, 161. doi: 10.3389/fcimb.2017.00161

Bou Ghanem, E. N., Maung, N. H. T., Siwapornchai, N., Goodwin, A. E., Clark, S., Munoz-Elias, E. J., et al. (2018). Nasopharyngeal Exposure to Streptococcus Pneumoniae Induces Extended Age-Dependent Protection Against Pulmonary Infection Mediated by Antibodies and CD138(+) Cells. *J. Immunol.* 200 (11), 3739–3751. doi: 10.4049/jimmunol.1701065

Burnaugh, A. M., Frantz, L. J., and King, S. J. (2008). Growth of Streptococcus Pneumoniae on Human Glycoconjugates Is Dependent Upon the Sequential Activity of Bacterial Exoglycosidases. *J. Bacteriol* 190 (1), 221–230. doi: 10.1128/JB.01251-07

Butcher, S. K., Chahal, H., Nayak, L., Sinclair, A., Henriquez, N. V., Sapey, E., et al. (2001). Senescence in Innate Immune Responses: Reduced Neutrophil Phagocytic Capacity and CD16 Expression in Elderly Humans. *J. Leukoc. Biol.* 70 (6), 881–886. doi: 10.1189/jlb.70.6.881

Butcher, S., Chahel, H., and Lord, J. M. (2000). Review Article: Ageing and the Neutrophil: No Appetite for Killing? *Immunology* 100 (4), 411–416. doi: 10.1046/j.1365-2567.2000.00079.x

CDC. (2018) *Pneumococcal Disease Global Pneumococcal Disease and Vaccine CDC: Centers for Disease Control and Prevention*. Available at: https://www.cdc.gov/pneumococcal/global.html.

Dahlgren, C., Follin, P., Johansson, A., Lock, R., and Orselius, K. (1989). Localization of the Luminol-Dependent Chemiluminescence Reaction in Human Granulocytes. *J. Biolumin Chemilumin* 4 (1), 263–266. doi: 10.1002/bio.1170040137

Dahlgren, C., and Karlsson, A. (1999). Respiratory Burst in Human Neutrophils. *J. Immunol. Methods* 232 (1-2), 3–14. doi: 10.1016/S0022-1759(99)00146-5

Dalia, A. B., Standish, A. J., and Weiser, J. N. (2010). Three Surface Exoglycosidases From Streptococcus Pneumoniae, Nana, Bgaa, and Strh, Promote Resistance to Opsonophagocytic Killing by Human Neutrophils. *Infect. Immun.* 78 (5), 2108–2116. doi: 10.1128/IAI.01125-09

Dalia, A. B., and Weiser, J. N. (2011). Minimization of Bacterial Size Allows for Complement Evasion and Is Overcome by the Agglutinating Effect of Antibody. *Cell Host Microbe* 10 (5), 486–496. doi: 10.1016/j.chom.2011.09.009

Domon, H., and Terao, Y. (2021). The Role of Neutrophils and Neutrophil Elastase in Pneumococcal Pneumonia. *Front. Cell. Infect. Microbiol.* 11 (214). doi: 10.3389/fcimb.2021.615959

El-Benna, J., Hurtado-Nedelec, M., Marzaioli, V., Marie, J. C., Gougerot-Pocidalo, M. A., and Dang, P. M. (2016). Priming of the Neutrophil Respiratory Burst: Role in Host Defense and Inflammation. *Immunol. Rev.* 273 (1), 180–193. doi: 10.1111/imr.12447

Esposito, A. L., Clark, C. A., and Poirier, W. J. (1990). An Assessment of the Factors Contributing to the Killing of Type 3 Streptococcus Pneumoniae by Human Polymorphonuclear Leukocytes *In Vitro*. *APMIS: Acta Pathologica Microbiologica Immunologica Scandinavica* 98 (2), 111–121. doi: 10.1111/j.1699-0463.1990.tb01009.x

Fante, M. A., Decking, S. M., Bruss, C., Schreml, S., Siska, P. J., Kreutz, M., et al. (2021). Heat-Inactivation of Human Serum Destroys C1 Inhibitor, Pro-Motes Immune Complex Formation, and Improves Human T Cell Function. *Int. J. Mol. Sci.* 22 (5). doi: 10.3390/ijms22052646

Fulop, T.Jr., Foris, G., Worum, I., and Leovey, A. (1985). Age-Dependent Alterations of Fc Gamma Receptor-Mediated Effector Functions of Human Polymorphonuclear Leucocytes. *Clin. Exp. Immunol.* 61 (2), 425–432.

García-García, E., and Rosales, C. (2002). Signal Transduction During Fc Receptor-Mediated Phagocytosis. *J. Leukoc. Biol.* 72 (6), 1092–1108. doi: 10.1189/jlb.72.6.1092

Garvy, B. A., and Harmsen, A. G. (1996). The Importance of Neutrophils in Resistance to Pneumococcal Pneumonia in Adult and Neonatal Mice. *Inflammation* 20 (5), 499–512. doi: 10.1007/BF01487042

Gonçalves, M. T., Mitchell, T. J., and Lord, J. M. (2016). Immune Ageing and Susceptibility to Streptococcus Pneumoniae. *Biogerontology* 17 (3), 449–465. doi: 10.1007/s10522-015-9614-8

Greene, N. G., Narciso, A. R., Filipe, S. R., and Camilli, A. (2015). Peptidoglycan Branched Stem Peptides Contribute to Streptococcus Pneumoniae Virulence by Inhibiting Pneumolysin Release. *PloS Pathog.* 11 (6), e1004996. doi: 10.1371/journal.ppat.1004996

Grudzinska, F. S., Brodlie, M., Scholefield, B. R., Jackson, T., Scott, A., Thickett, D. R., et al. (2020). Neutrophils in Community-Acquired Pneumonia: Parallels in Dysfunction at the Extremes of Age. *Thorax* 75 (2), 164–171. doi: 10.1136/thoraxjnl-2018-212826

Habets, M. G., Rozen, D. E., and Brockhurst, M. A. (2012). Variation in Streptococcus Pneumoniae Susceptibility to Human Antimicrobial Peptides may Mediate Intraspecific Competition. *Proc. Biol. Sci.* 279 (1743), 3803–3811. doi: 10.1098/rspb.2012.1118

Hahn, I., Klaus, A., Janze, A. K., Steinwede, K., Ding, N., Bohling, J., et al. (2011). Cathepsin G and Neutrophil Elastase Play Critical and Nonredundant Roles in Lung-Protective Immunity Against Streptococcus Pneumoniae in Mice. *Infect. Immun.* 79 (12), 4893–4901. doi: 10.1128/IAI.05593-11

Hyams, C., Camberlein, E., Cohen, J. M., Bax, K., and Brown, J. S. (2010). The Streptococcus Pneumoniae Capsule Inhibits Complement Activity and Neutrophil Phagocytosis by Multiple Mechanisms. *Infect. Immun.* 78 (2), 704–715. doi: 10.1128/IAI.00881-09

Jackson, L. A., Gurtman, A., van Cleeff, M., Frenck, R. W., Treanor, J., Jansen, K. U., et al. (2013). Influence of Initial Vaccination With 13-Valent Pneumococcal Conjugate Vaccine or 23-Valent Pneumococcal Polysaccharide Vaccine on Anti-Pneumococcal Responses Following Subsequent Pneumococcal Vaccination in Adults 50 Years and Older. *Vaccine* 31 (35), 3594–3602. doi: 10.1016/j.vaccine.2013.04.084

Johnson, M. B., and Criss, A. K. (2013). Neisseria Gonorrhoeae Phagosomes Delay Fusion With Primary Granules to Enhance Bacterial Survival Inside Human Neutrophils. *Cell Microbiol.* 15 (8), 1323–1340. doi: 10.1111/cmi.12117

Kadioglu, A., Weiser, J. N., Paton, J. C., and Andrew, P. W. (2008). The Role of Streptococcus Pneumoniae Virulence Factors in Host Respiratory Colonization and Disease. *Nat. Rev. Microbiol.* 6 (4), 288–301. doi: 10.1038/nrmicro1871

King, S. J., Hippe, K. R., and Weiser, J. N. (2006). Deglycosylation of Human Glycoconjugates by the Sequential Activities of Exoglycosidases Expressed by Streptococcus Pneumoniae. *Mol. Microbiol.* 59 (3), 961–974. doi: 10.1111/j.1365-2958.2005.04984.x

Kobayashi, S. D., Voyich, J. M., Buhl, C. L., Stahl, R. M., and DeLeo, F. R. (2002). Global Changes in Gene Expression by Human Polymorphonuclear Leukocytes During Receptor-Mediated Phagocytosis: Cell Fate is Regulated at the Level of Gene Expression. *Proc. Natl. Acad. Sci. U.S.A.* 99 (10), 6901–6906. doi: 10.1073/pnas.092148299

Kolaczkowska, E., and Kubes, P. (2013). Neutrophil Recruitment and Function in Health and Inflammation. *Nat. Rev. Immunol.* 13 (3), 159–175. doi: 10.1038/nri3399

Krone, C. L., Trzcinski, K., Zborowski, T., Sanders, E. A., and Bogaert, D. (2013). Impaired Innate Mucosal Immunity in Aged Mice Permits Prolonged Streptococcus Pneumoniae Colonization. *Infect. Immun.* 81 (12), 4615–4625. doi: 10.1128/IAI.00618-13

Linnemann, C., Venturelli, S., Konrad, F., Nussler, A. K., and Ehnert, S. (2020). Bio-Impedance Measurement Allows Displaying the Early Stages of Neutrophil Extracellular Traps. *Excli J.* 19, 1481–1495. doi: 10.17179/excli2020-2868

Lysenko, E. S., Clarke, T. B., Shchepetov, M., Ratner, A. J., Roper, D. I., Dowson, C. G., et al. (2007). Nod1 Signaling Overcomes Resistance of S. Pneumoniae to Opsonophagocytic Killing. *PloS Pathog.* 3 (8), e118. doi: 10.1371/journal.ppat.0030118

Martner, A., Dahlgren, C., Paton, J. C., and Wold, A. E. (2008). Pneumolysin Released During Streptococcus Pneumoniae Autolysis Is a Potent Activator of Intracellular Oxygen Radical Production in Neutrophils. *Infect. Immun.* 76 (9), 4079–4087. doi: 10.1128/IAI.01747-07

Matanock A, L. G., Gierke, R., Kobayashi, M., Leidner, A., and Pilishvili, T. (2019). Use of 13-Valent Pneumococcal Conjugate Vaccine and 23-Valent Pneumococcal Polysaccharide Vaccine Among Adults Aged ≥65 Years: Updated Recommendations of the Advisory Committee on Immunization Practices. *MMWR Morb. Mortal. Wkly. Rep.* 68, 1069–1075. CDC; 2019. doi: 10.15585/mmwr.mm6846a5

Merres, J., Hoss, J., Albrecht, L. J., Kress, E., Soehnlein, O., Jansen, S., et al. (2014). Role of the Cathelicidin-Related Antimicrobial Peptide in Inflammation and Mortality in a Mouse Model of Bacterial Meningitis. *J. Innate Immun.* 6 (2), 205–218. doi: 10.1159/000353645

Miralda, I., Klaes, C. K., Graham, J. E., and Uriarte, S. M. (2020). Human Neutrophil Granule Exocytosis in Response to Mycobacterium Smegmatis. *Pathogens* 9 (2). doi: 10.3390/pathogens9020123

Monfregola, J., Johnson, J. L., Meijler, M. M., Napolitano, G., and Catz, S. D. (2012). MUNC13-4 Protein Regulates the Oxidative Response and Is Essential for Phagosomal Maturation and Bacterial Killing in Neutrophils. *J. Biol. Chem.* 287 (53), 44603–44618. doi: 10.1074/jbc.M112.414029

Naegelen, I., Beaume, N., Plançon, S., Schenten, V., Tschirhart, E. J., and Bréchard, S. (2015). Regulation of Neutrophil Degranulation and Cytokine Secretion: A Novel Model Approach Based on Linear Fitting. *J. Immunol. Res.* 2015, 817038. doi: 10.1155/2015/817038

Nguyen, G. T., Green, E. R., and Mecsas, J. (2017). Neutrophils to the Roscue: Mechanisms of NADPH Oxidase Activation and Bacterial Resistance. *Front. Cell Infect. Microbiol.* 7, 373. doi: 10.3389/fcimb.2017.00373

Nordenfelt, P., and Tapper, H. (2011). Phagosome Dynamics During Phagocytosis by Neutrophils. *J. Leukoc. Biol.* 90 (2), 271–284. doi: 10.1189/jlb.0810457

Rajecky, M., Lojek, A., and Ciz, M. (2012). Differentiating Between Intra- and Extracellular Chemiluminescence in Diluted Whole-Blood Samples. *Int. J. Lab. Hematol.* 34 (2), 136–142. doi: 10.1111/j.1751-553X.2011.01370.x

Shenoy, A. T., and Orihuela, C. J. (2016). Anatomical Site-Specific Contributions of Pneumococcal Virulence Determinants. *Pneumonia (Nathan)* 8. doi: 10.1186/s41479-016-0007-9

Simell, B., Vuorela, A., Ekstrom, N., Palmu, A., Reunanen, A., Meri, S., et al. (2011). Aging Reduces the Functionality of Anti-Pneumococcal Antibodies and the Killing of Streptococcus Pneumoniae by Neutrophil Phagocytosis. *Vaccine* 29 (10), 1929–1934. doi: 10.1016/j.vaccine.2010.12.121

Simmons, S. R., Bhalla, M., Herring, S. E., Tchalla, E. Y. I., and Bou Ghanem, E. N. (2021). Older But Not Wiser: The Age-Driven Changes in Neutrophil Responses During Pulmonary Infections. *Infect. Immun.* 89 (4). doi: 10.1128/IAI.00653-20

Siwapornchai, N., Lee, J. N., Tchalla, E. Y. I., Bhalla, M., Yeoh, J. H., Roggensack, S. E., et al. (2020). Extracellular Adenosine Enhances the Ability of Pmns to Kill Streptococcus Pneumoniae by Inhibiting IL-10 Production. *J. Leukoc. Biol.* 108, 867–882. doi: 10.1002/JLB.4MA0120-115RR

Standish, A. J., and Weiser, J. N. (2009). Human Neutrophils Kill Streptococcus Pneumoniae *via* Serine Proteases. *J. Immunol.* 183 (4), 2602–2609. doi: 10.4049/jimmunol.0900688

Swamydas, M., and Lionakis, M. S. (2013). Isolation, Purification and Labeling of Mouse Bone Marrow Neutrophils for Functional Studies and Adoptive Transfer Experiments. *J. Vis. Exp.* 2013 (77), e50586. doi: 10.3791/50586

Tchalla, E. Y. I., Bhalla, M., Wohlfert, E. A., and Bou Ghanem, E. N. (2020). Neutrophils are Required During Immunization With the Pneumococcal Conjugate Vaccine for Protective Antibody Responses and Host Defense Against Infection. *J. Infect. Dis.* 222, 1363–1370. doi: 10.1093/infdis/jiaa242

WHO. (2014). *Pneumococcal Disease* (Geneva: World Health Organization).

Yin, C., and Heit, B. (2018). Armed for Destruction: Formation, Function and Trafficking of Neutrophil Granules. *Cell Tissue Res.* 371 (3), 455–471. doi: 10.1007/s00441-017-2731-8

Zhou, M. J., and Brown, E. J. (1994). CR3 (Mac-1, Alpha M Beta 2, CD11b/CD18) and Fc Gamma RIII Cooperate in Generation of a Neutrophil Respiratory Burst: Requirement for Fc Gamma RIII and Tyrosine Phosphorylation. *J. Cell Biol.* 125 (6), 1407–1416. doi: 10.1083/jcb.125.6.1407

Author Disclaimer: The content is solely the responsibility of the authors and does not necessarily represent the official views of the National Institutes of Health.

Conflict of Interest: The authors declare that the research was conducted in the absence of any commercial or financial relationships that could be construed as a potential conflict of interest.

Publisher's Note: All claims expressed in this article are solely those of the authors and do not necessarily represent those of their affiliated organizations, or those of the publisher, the editors and the reviewers. Any product that may be evaluated in this article, or claim that may be made by its manufacturer, is not guaranteed or endorsed by the publisher.

Advantages of publishing in Frontiers

OPEN ACCESS
Articles are free to read for greatest visibility and readership

FAST PUBLICATION
Around 90 days from submission to decision

HIGH QUALITY PEER-REVIEW
Rigorous, collaborative, and constructive peer-review

TRANSPARENT PEER-REVIEW
Editors and reviewers acknowledged by name on published articles

Frontiers
Avenue du Tribunal-Fédéral 34
1005 Lausanne | Switzerland

Visit us: www.frontiersin.org
Contact us: frontiersin.org/about/contact

REPRODUCIBILITY OF RESEARCH
Support open data and methods to enhance research reproducibility

DIGITAL PUBLISHING
Articles designed for optimal readership across devices

FOLLOW US
@frontiersin

IMPACT METRICS
Advanced article metrics track visibility across digital media

EXTENSIVE PROMOTION
Marketing and promotion of impactful research

LOOP RESEARCH NETWORK
Our network increases your article's readership